OLLSCOIL NA GAILLIMHE
UNIVERSITY OF GALWAY

The role of microRNAs in muscle wasting during ageing and disease

Anthony J Sannicandro

A thesis submitted to the University of Galway as fulfilment of the requirement for the degree of Doctor of Philosophy

Supervisor: Dr Kasia Goljanek-Whysall
Co-Supervisor: Dr Brian McDonagh

Department of Physiology
School of Medicine
College of Medicine, Nursing & Health Sciences
University of Galway
January 2023

Table of Contents

Table of Contents i

List of Figures xi

List of Tables xv

Abbreviations xvi

Acknowledgements xxiv

Declaration xxvi

Abstract xxvii

1 Introduction 1

1.1 Skeletal muscle overview 1

1.2 Mechanism of muscle contraction 4

1.2.1 Control of the skeletal muscle contraction system 7

1.3 Skeletal muscle fibre types 10

1.4 Development of skeletal muscle 13

1.5 Molecular mechanisms of muscle maintenance 15

1.6 Hypertrophy, atrophy, and regeneration of muscle 18

1.6.1 Muscle fibre hypertrophy 18

1.6.2 Muscle fibre atrophy 18

1.6.3 Muscle fibre regeneration 20

1.7 Mitochondrial homeostasis in skeletal muscle 23

1.8 The role of ER stress signalling in skeletal muscle 24

1.9 Skeletal muscle in disease 27

1.9.1 Sarcopenia 27

1.10 Mechanisms of muscle atrophy 27

1.10.1 Muscle protein homeostasis 27

1.10.2 Senescence 28
1.10.3 Muscle regeneration 28
1.10.4 Fibro-adipogenic progenitor cells 29
1.11 microRNA as regulators of molecular mechanisms of muscle 30
1.11.1 miR biogenesis: canonical pathway 30
1.11.2 miR biogenesis: non-canonical pathways 32
1.11.3 miR-mediated gene regulation 33
1.12 Skeletal muscle and the role of miRs 35
1.12.1 miRs in muscle development and regeneration 36
1.12.2 miRs regulating muscle hypertrophy and atrophy 36
1.12.3 miRs and neuromuscular communication 37
1.12.4 miRs and cellular senescence 38
1.12.5 miR involvement in regulation of mitochondrial dynamics 39
1.12.6 miRs and Fibro-Adipogenic progenitors 39
1.13 miRs as potential therapeutics 40
1.14 Hypothesis 42
1.14.1 Objectives 43
2 Materials and methods 45
2.1 List of materials, equipment, and reagents used in this project 45
2.2 C2C12 and NSC-34 immortalised mouse myoblasts 48
2.2.1 C2C12 49
2.2.2 NSC-34 49
2.3 Human primary myoblasts 50
2.4 Cell culture media 50
2.4.1 C2C12 proliferation and differentiation 50

2.4.2 NSC-34 growth and differentiation 50
2.4.3 Human primary myoblast culture medium 50
2.5 Cell culture 51
2.5.1 Cell expansion 52
2.5.2 Laminin coating for human myoblast cultures 52
2.5.3 Cell differentiation 53
2.5.4 Cryopreservation and thawing of cells 53
2.6 Treatment of cells with miR mimics or antagomiRs 54
2.6.1 Sequences of miR and antagomiR mimics 54
2.7 Immunostaining of cells *in vitro* following miR transfection 55
2.7.1 Antibodies and stains used for all immunostaining 55
2.7.2 Immunostaining general protocol 56
2.7.3 MF20 immunostaining 57
2.7.4 MitoTracker Green staining to assess mitochondria 58
2.7.5 Tubulin staining of NSC-34 differentiated cells 59
2.8 Immunostaining of muscle tissues 59
2.8.1 Wheat Germ Agglutinin (WGA) fibre staining 59
2.8.2 Neuromuscular junction (NMJ) staining of longitudinal muscle sections 60
2.9 RNA isolation 60
2.9.1 RNA isolation from cells using TRIzol/chloroform method: 61
2.9.2 RNA isolation protocol using miRvana kit 61
2.9.3 NanoDrop2000 assessment of RNA quality 62
2.10 cDNA synthesis from isolated RNA 63
2.10.1 cDNA synthesis for mRNA cDNA: 63

2.10.2 cDNA synthesis for miRCURY miR cDNA 63
2.11 Real-time quantitative PCR (RT-qPCR)..... 64
2.11.1 Standard RT-qPCR procedure 66
2.11.2 qPCR protocol for miRs using miRCURY kit..... 67
2.11.3 Visualisation of PCR products using gel electrophoresis..... 68
2.12 Muscle tissue processing *in vivo*..... 69
2.12.1 Processing of frozen muscle 69
2.12.2 RNA isolation from muscle using TRIzol 70
(246)..... **Error! Bookmark not defined.**
2.13 Protein Isolation..... 71
2.13.1 Basic procedure for protein isolation of cells and tissues..... 71
2.13.2 Protein quantification assay (Bradford)..... 71
2.14 Western blot..... 73
2.14.1 Western blot reagents: 73
2.14.2 Gel preparation for western blot applications:..... 77
2.14.3 Gel transfer (semi-dry) and blotting procedure: 77
2.14.4 Imaging blots using LI-COR and Image Studio Lite..... 79
2.15 Procedures and methods for *in vivo* experiments 79
2.15.1 Animals used for experiments 79
2.15.2 Dissection and tissue collection..... 80
2.15.3 The role of miR-199a in NMJ homeostasis *in vivo* 80
2.15.4 Intravenous (IV) injections *in vivo* 80
2.15.5 Assessment of tissues following miR delivery *in vivo*. 81
2.15.6 Cryosectioning of muscle tissue 82
2.16 Target selection of miRs..... 83

2.17 Statistical analysis 83
2.18 Microscopic Imaging 84
2.18.1 Immunostaining microscopy 84
2.18.2 Western blot 84
3 Changes to miR-199a-5p expression levels in ageing 86
3.1 Introduction 86
3.2 Materials and methods 88
3.2.1 Human samples 88
3.2.2 Muscle digestion 89
3.2.3 Primary cell culture 89
3.2.4 RNA isolation and small RNA-seq 89
3.2.5 cDNA synthesis and RT-qPCR 91
3.2.6 Identification of miR-199a-5p predicted targets and pathways 91
3.3 Results 92
3.3.1 miR-199a-5p is upregulated during ageing in humans 92
3.3.2 miR-199a-5p targets genes associated with ER stress, mitochondria, and neuronal regulation. 95
3.3.3 miR-199a-5p predicted target genes are associated with neuronal homeostasis and Wnt signalling. 97
3.3.4 miR-199a-5p is upregulated in skeletal muscle during ageing in mice, and its targets are differentially expressed in ageing. 102
3.4 Discussion 105
3.4.1 miR-199a-5p is upregulated in ageing in humans 105
3.4.2 miR-199a-5p targets genes associated with ER stress, mitochondria, and neuronal regulation 106

3.4.3 miR-199a-5p predicted target genes are associated with neuronal homeostasis and Wnt signalling. 106

3.4.4 miR-199a-5p is upregulated in skeletal muscle during ageing in mice. 107

4 The role of miR-199a-5p in muscle and neuronal homeostasis *in vitro* 110

4.1 Introduction 110

4.2 miR-199a-5p *in vitro* materials and methods 113

4.2.1 Cells and cell culture 113

4.2.2 miR-199a-5p mimic and inhibitor sequences 113

4.2.3 Cell Counting Kit-8 assay 114

4.2.4 ER stress assay 114

4.2.5 *In vitro* immunostaining 115

4.2.6 RNA isolation 115

4.2.7 cDNA synthesis and RT-qPCR 115

4.2.8 Protein isolation from C2C12 cells 116

4.2.9 Protein quantification and Western blot 116

4.2.10 Luciferase assay and reporter constructs 116

4.2.11 Image analysis 117

4.2.12 Statistical analysis 117

4.3 Results 117

4.3.1 miR-199a-5p regulates myogenesis *in vitro* in C2C12 mouse myoblasts 117

4.3.2 miR-199a-5p inhibition reduces C2C12 cell number 121

4.3.3 miR-199a-5p regulated the expression of ER stress marker, Grp78, in C2C12 cells 121

4.3.4 miR-199a-5p inhibition significantly ameliorates the effects of tunicamycin on C2C12 myotubes 124
4.3.5 miR-199a-5p did not signifcantly regulate mitochondrial biogenesis 126
4.3.6 miR-199a-5p regulates expression of NMJ-related gene *Gap43 in vitro* 130
4.3.7 miR-199a-5p directly binds to GAP43 3'UTR region 131
4.4 Discussion 132
4.4.1 miR-199a-5p regulates myogenesis *in vitro* in C2C12 mouse myoblasts 133
4.4.2 miR-199a-5p inhibition reduces C2C12 cell number 135
4.4.3 miR-199a-5p inhibition significantly ameliorates effect of tunicamycin induced myotube atrophy 135
4.4.4 miR-199a-5p is predicted to regulate Grp78 associated with ER stress 137
4.4.5 miR-199a-5p did not significantly regulate mitochondrial biogenesis 138
4.4.6 miR-199a-5p regulates expression of NMJ-related gene *Gap43 in vitro* 140
4.4.7 miR-199a-5p directly binds to GAP43 3'UTR 140
5 The role of miR-199a-5p in maintaining neuronal homeostasis *in vitro* in NSC-34 neuron-like cells 143
5.1 Introduction 143
5.2 Materials and methods 144
5.2.1 Cells and cell culture 144
5.2.2 NSC-34 cell differentiation 144
5.2.3 Cell Counting Kit-8 assay 145
5.2.4 miR-199a-5p transfection 145

5.2.5 Immunostaining of NSC-34 cells 145
5.2.6 RNA collection from NSC-34 cells 146
5.2.7 cDNA synthesis and RT-qPCR from NSC-34 cells 146
5.2.8 Protein isolation from NSC-34 cells 146
5.2.9 Protein quantification and Western blot 146
5.2.10 Image analysis 147
5.2.11 Statistical analysis 147
5.3 Results 147
5.3.1 miR-199a-5p does not regulate neurite growth in NSC-34 cells 147
5.3.2 miR-199a-5p affects the expression of genes associated with ER stress response in NSC-34 cells 149
5.3.3 miR-199a-5p regulates the expression of GAP43 *in vitro* in NSC-34 cells. 151
5.3.4 miR-199a-5p regulates the expression of mitochondria-and-autophagy-associated genes in NSC-34 cells. 152
5.4 Discussion 154
5.4.1 miR-199a-5p overexpression or inhibition affects differentiated neurites in NSC-34 cells 155
5.4.2 miR-199a-5p affects the levels of ER stress-related proteins in NSC-34 cells 155
5.4.3 miR-199a-5p effects GAP43 in NSC-34 cells 156
5.4.4 miR-199a-5p regulates the expression of mitochondrial-, oxidative stress-, and autophagy-associated genes in NSC-34 cells 158
6 The role of miR-199 in muscle and neuronal homeostasis *in vivo* 162
6.1 Introduction 162
6.2 Materials and methods 163

6.2.1 Animals....163
6.2.2 Mimic and inhibitor sequences used *in vivo*....164
6.2.3 Muscle histology 165
6.2.4 Muscle function analysis 165
6.2.5 RNA isolation and cDNA synthesis 166
6.2.6 Real-time qPCR and PCR 166
6.2.7 Protein isolation and Western blot 166
6.2.8 Barium chloride injections for muscle regeneration *in vivo*....167
6.2.9 Image analysis 167
6.2.10 Statistical analysis....168
6.3 Results....168
6.3.1 miR-199 has little effect on myofibre size *in vivo* 168
6.3.2 miR-199a-5p inhibition leads to increased specific and maximum EDL force *in vivo*.....173
6.3.3 miR-199a-5p disrupts NMJ morphology *in vivo*.....174
6.3.4 miR-199a-5p regulates expression of genes associated with ER stress *in vivo*. 177
6.3.5 miR-199a-5p does not regulate mitochondrial biogenesis but regulates autophagy *in vivo.* 180
6.3.6 miR-199a-5p regulates the expression of GAP43 *in vivo.* 183
6.3.7 miR-199a-5p does not affect muscle regeneration *in vivo*. 186
6.3.8 Age changes the expression of some NMJ-related genes *in vivo* in sciatic nerve.....191
6.4 Discussion....192
6.4.1 miR-199a-5p had little effect on myofibre size *in vivo.*....193

6.4.2 miR-199a-5p inhibition leads to increased specific and maximum EDL force *in vivo.* 194

6.4.3 miR-199a-5p disrupts NMJ morphology *in vivo* 195

6.4.4 miR-199a-5p may regulate the expression of genes associated with ER stress *in vivo.* 196

6.4.5 miR-199a-5p does not regulate mitochondrial biogenesis but regulates autophagy *in vivo*. 198

6.4.6 miR-199a-5p regulates the expression of GAP43 *in vivo*. 200

6.4.7 miR-199a-5p does not affect muscle regeneration *in vivo*. 201

6.4.8 Age changes the expression of some NMJ-related genes *in vivo* in sciatic nerves. 202

7 Discussion 204

7.1 Strengths and weaknesses 209

8 References 213

Appendices 277

List of Figures

Figure 1.1.1 The structure of skeletal muscle is highly organised 3
Figure 1.1.2 The sarcomere is the functional unit of contraction 4
Figure 1.2.1 Sliding filament model of contraction 6
Figure 1.2.2 Gross skeletal muscle cross-section highlighting the NMJ. 8
Figure 1.2.3. Cross section of the NMJ 9
Figure 1.4.1 Progression of myogenesis. 14
Figure 1.5.1. Autophagy involves a step-by-step sequence of events to degrade cellular debris 17
Figure 1.6.1 Hypertrophy and atrophy signalling pathways 20
Figure 1.6.2 Satellite cell activation and differentiation 22
Figure 1.6.3. The main phases of muscle regeneration following injury 23
Figure 1.8.1. The ER stress response initiates the UPR *via* three transmembrane proteins. 26
Figure 1.11.1. miR biogenesis 32
Figure 1.11.2. miR mechanisms of mRNA target interactions. 34
Figure 2.2.1. C2C12 and NSC-34 are capable of differentiation. 49
Figure 2.12.1. Processing of frozen muscle tissue using handheld method 69
Figure 2.13.1 Representative image of BSA standard 73
Figure 2.14.1. Gel percentages and molecular weight guide 76
Figure 2.14.2 ‘Sandwich’ layout for semi-dry gel transfer 78
Figure 2.15.1. Cross section of mouse tail highlighting lateral tail veins for IV injection. 81
Figure 2.15.2 Section examples of muscle tissue. 82
Figure 3.3.1. Heatmap of differentially expressed miRs in adult and old skeletal muscle 94
Figure 3.3.2. miR-199a-5p predicted targets are associated with activin receptor complex formation, kinase activity, and Wnt signalling 99
Figure 3.3.3. Pathway analysis of predicted miR-199a-5p target genes 100

Figure 3.3.4. Combined database pathway analyses show miR-199a-5p is predicted to regulate genes involved in mTOR signalling, phosphorylation, and nervous system. 101
Figure 3.3.5. miR-199a-5p expression is increased in skeletal muscle of old mice, but not the sciatic nerve. 102
Figure 3.3.6. Nd1, miR-199a-5p predicted target, was differentially expressed in aged skeletal muscle 104
Figure 3.3.7. Hdac9, associated with NMJ, was differentially expressed in aged sciatic nerve 105
Figure 4.3.1. Treatment of C2C12 myoblasts with miR-199a-5p mimic or AM-199 results in upregulated and downregulated levels of miR-199a-5p, respectively, as compared to Scr control. 118
Figure 4.3.2. miR-199a-5p regulates myogenesis in C2C12 mouse myoblasts. 119
Figure 4.3.3. miR-199a-5p negatively regulates myotube growth 120
Figure 4.3.4. miR-199a-5p does not affect cell number in the presence of H2O2 but reduces proliferation in growth conditions. 121
Figure 4.3.5. Overexpression of miR-199 led to increased expression of ER stress-related protein, GRP78 123
Figure 4.3.6. Overexpression of miR-199a-5p in C2C12 cells results in an increased number of CHOP-positive cells 124
Figure 4.3.7. Inhibition of miR-199a-5p in C2C12 myotubes significantly ameliorated the effect of tunicamycin on diameter 125
Figure 4.3.8. miR-199 affects mitochondrial activity in C2C12 myoblasts 127
Figure 4.3.9. Inhibition of miR-199a-5p has a positive effect on mitochondrial respiration 128
Figure 4.3.10. The expression of mitochondrial biogenesis target, Pgc-1α, was not regulated by miR-199a-5p. 129
Figure 4.3.11. miR-199 regulates the expression of Gap43 *in vitro*. 131
Figure 4.3.12. miR-199a-5p directly binds to its target sites within 3'UTRs of Gap43 and Grp78 132

Figure 5.3.1. Treatment of NSC-34 cells with miR-199a-5p mimic results in upregulated level of miR-199a-5p as compared to Scr control. 148
Figure 5.3.2 NSC-34 neurite length and number are affected by miR-199a-5p overexpression. 149
Figure 5.3.3. miR-199a-5p inhibition increases number of NSC-34 cells in the presence of H_2O_2. 150
Figure 5.3.4. miR-199a-5p affects the expression of genes associated with ER stress in NSC-34 cells 151
Figure 5.3.5. miR-199a-5p affects NMJ-related protein GAP43 in NSC-34 cells 152
Figure 5.3.6. miR-199a-5p regulates the expression of mitochondrial and autophagy-associated genes in NSC-34 cells 153
Figure 6.3.1. miR-199a-5p mimic and inhibitor delivery to muscle 169
Figure 6.3.2. miR-199a-5p overexpression does not regulate muscle weight *in vivo in* young mice, but increased weight in old mice. 170
Figure 6.3.3. miR-199a-5p has a minimal effect on muscle weight *in vivo* 170
Figure 6.3.4. miR-199a-5p has a minimal effect on muscle weight *in vivo* when bodyweight is considered 171
Figure 6.3.5. miR-199a-5p has little effect on myofibre size *in vivo*. 172
Figure 6.3.6. miR-199a-5p inhibition improves maximum and specific force *in vivo* in EDL of old mice 173
Figure 6.3.7. miR-199a-5p regulates neuromuscular morphology *in vivo*. 175
Figure 6.3.8. miR-199a-5p regulates NMJ morphology *in vivo* 176
Figure 6.3.9. Quantification of NMJ morphology shows miR-199a-5p contributes to abnormal morphology. 177
Figure 6.3.10. miR-199a-5p regulates some ER stress genes *in vivo* 179
Figure 6.3.11. miR-199a-5p does not regulate the expression of mitochondrial-associated genes *in vivo*. 182
Figure 6.3.12. miR-199a-5p regulates the expression of autophagy-associated proteins *in vivo* 183
Figure 6.3.13. miR-199a-5p regulates the expression of GAP43 *in vivo* 185

Figure 6.3.14. miR-199a-5p does not significantly affect bodyweight or muscle weight during regeneration 187
Figure 6.3.15. miR-199a-5p has a minimal effect on muscle weight *in vivo* during muscle regeneration when bodyweight is considered 188
Figure 6.3.16. miR-199a-5p has no effect on myofibre size during muscle regeneration *in vivo* 189
Figure 6.3.17. Maximum and specific forces were not affected by miR-199a-5p during muscle regeneration *in vivo* 189
Figure 6.3.18. miR-199a-5pa-5p does not significantly affect muscle regeneration *in vivo* 190
Figure 6.3.19. miR-199a-5p expression in sciatic nerve *in vivo*. Delivery of miRs in young and old mice did not result in increased expression of miR-199a-5p in the sciatic nerve as quantified by RT-qPCR 191
Figure 6.3.20. Age changes the expression of some NMJ-related genes *in vivo* in sciatic nerves 192

List of Tables

Table 1.3.1 MyHC isoforms in skeletal muscle 11
Table 1.3.2. Summary of skeletal muscle fibre types..... 13
Table 2.5.1. Experiment layout for miR transfections 52
Table 2.5.2 Culture dish sizes and volume of laminin 53
Table 2.11.1. List of primer sequences used for qPCR..... 65
Table 2.14.1. Volumes of gel reagents for two gels by gel percentage..... 75
Table 3.2.1. Muscle sample donor information..... 88
Table 3.3.1 Downregulated miRs in old human primary myoblasts. 93
Table 3.3.2 Upregulated miRs in old human primary myoblasts..... 93
Table 3.3.3. miRtarbase validated miR-199a-5p targets 96
Table 3.3.4. Predicted target genes of miR-199a-5p 97

Abbreviations

3’UTR 3’-untranslated region

5’UTR 5’-untranslated region

Ach acetylcholine

Achr acetylcholine receptor

ADP adenosine diphosphate

AGO argonaute

AMP adenosine monophosphate

AMPK AMP-activated protein kinase

ANOVA analysis of variance

AS alternative splicing

AST autophagy-senescence transition

ATF6 activating transcription factor 6

ATG autophagy-related gene

ATP adenosine triphosphate

ATP2C1 ATPase secretory pathway Ca2+ transporting 1

B2M β-2-microglobulin

$BaCl_2$ barium chloride

BSA bovine serum albumin

$CaCl_2$ calcium chloride

CD34 cluster of differentiation 34

CDKNs cyclin-dependent kinases inhibitors

cDNA complementary DNA

COX1 Cytochrome c oxidase 1

CP creatine phosphate

CSA cross sectional area

Ct copy threshold

CXCR4 C-X-C chemokine receptor type 4

DAPI 4',6-Diamidino-2-Phenylindole, Dihydrochloride

DGCR8 DiGeorge Syndrome Critical Region 8

Dicer endoribonuclease Dicer or helicase with RNase motif

DM differentiation medium

DMEM Dulbecco’s Modified Eagle’s Medium

DMSO dimethyl sulfoxide

DPBS Dulbecco's phosphate-buffered saline

DRP1 dynamin-related protein 1

ECM extracellular matrix

EDL extensor digitorum longus

eIF2b eukaryotic Initiation Factor 2b

ETS electron transport system

F-12 media Ham's F-12 Nutrient Mix

FAD flavin adenine dinucleotide (oxidised form)

FADH flavin adenine dinucleotide

FADH2 flavin adenine dinucleotide (reduced form)

FAPs fibro-adipogenic progenitors

FBS foetal bovine serum

FGF fibroblast growth factor

FGF-b recombinant human fibroblast growth factor-basic

FIS1 mitochondrial fission 1 protein

FoxO forkhead box O

GAP43 growth associated protein 43

GAS gastrocnemius

GM growth medium

GO gene ontology

GPX glutathione peroxidase

GRP78 78 kDa glucose-regulated protein/ heat shock 70 kDa protein 5

GS glycogen synthase

GSK3β glycogen synthase kinase-3 beta

H2O2 hydrogen peroxide

HCL hydrochloric acid

HDAC9 histone deacetylase 9

HIF-1α hypoxia-inducible factor 1-alpha

HMGN1 high mobility group nucleosome binding domain 1

HPRA Health Products Regulatory Authority

HS horse serum

IGF insulin-like growth factor

IGFBPs IGF-biding proteins

iKO inducible knockout

IL-10 interleukin-10

IL-6 interleukin-6

IL-β interleukin-beta

IMF intermyofibrillar mitochondria

IP3 inositol triphosphate

IR insulin receptor

IRE1 inositol requiring enzyme 1

kDa kilodalton

LC light chain domain

LC3 microtubule-associated protein 1A/1B-light chain 3

LMNB2 lamin B2

M1 pro-inflammatory macrophages

M2 anti-inflammatory macrophages

MAPK mitogen-activated protein kinases

mATP myofibrillar ATPase

M-CSF macrophage colony-stimulating factor

MDM2 mouse double minute 2 protein

mdx DMD mdx mutant mouse

MFF mitochondrial fission factor

MHC/MyHC myosin heavy chain

miPEPs microRNAs-encoded peptides

miRNAs/miRs microRNAs

MPCs muscle/myogenic progenitor cells

MQ-H2O milli-Q water

MRF myogenic regulatory factors

mRNA messenger RNA

MSC mesenchymal stromal cell

MTDH metadherin

mtDNA mitochondrial DNA

mTOR mammalian target of rapamycin

mTORC1 rapamycin complex 1

MuSK muscle associated receptor tyrosine kinase

MyHC myosin heavy chain

MyLC myosin light chain

MyoG myogenin

NAD nicotinamide adenine dinucleotide (oxidised form)

NADH nicotinamide adenine dinucleotide (reduced form)

NCAM neural cell adhesion molecule

ND1 NADH dehydrogenase 1

NFS1 cysteine desulfurase

NF-κB nuclear factor kappa-light-chain-enhancer of activated B cells

NOX NADPH oxidase

NRF2 Nuclear factor erythroid 2-related factor 2

NTM neurotrimin

$O2^{\bullet-}$ superoxide anions

OCT optimal cutting temperature

$OH^{\bullet}$ hydroxyl radicals

OPA1 optic atrophy type 1

OXPHOS oxidative phosphorylation

P/S penicillin-streptomycin

p53 tumour protein p53

P62 ubiquitin-binding protein p62

PAM peptidylglycine alpha-amidating monooxygenase

Pax3 paired box 3

Pax7 paired box 7

PBS phosphate-buffered saline

PDGFR platelet-derived growth factor

PDGFRα platelet-derived growth factor receptor A

PERK PKR-like ER kinase

PFK1 phosphofructokinase-1

PGC-1α peroxisome proliferator-activated receptor gamma coactivator 1-alpha

PPAR-γ peroxisome proliferator-activated receptor gamma

pre-miRNA precursor miRNA

pri-miRNA primary miRNA

QUAD quadriceps

REDOX reduction–oxidation

RIPA radioimmunoprecipitation assay buffer

RISC RNA-induced silencing complex

RNA-seq RNA-sequencing

ROS reactive oxygen species

RT-qPCR quantitative Real-Time polymerase chain reaction

RUNX1 runt-related transcription factor 1

SASP senescence-associate secretory phenotype

SAT senescence-autophagy transition

SCF Skp, Cullin, F-box containing complex

SEM standard error of means

SERCA sarco(endo)plasmic reticulum Ca2+-ATPase

SIRT sirtuin

SOD superoxide dismutase

SOL soleus

SR sarcoplasmic reticulum

SS subsarcolemmal mitochondria

TA tibialis anterior

TAE tris base, acetic acid and EDTA buffer

TBS tris-buffered saline

TBS-T tris-buffered saline tween

TCA tricarboxylic acid

TFAM mitochondrial transcription factor A

TGF-β1 transforming growth factor β1

TNFα tumour necrosis factor-α

TOM20 translocase of the outer mitochondrial membrane 20

TP53I11 tumour protein p53 inducible protein 11

UCPs uncoupling proteins

UPR unfolded protein response

VEGF vascular endothelial growth factor

WGA wheat germ agglutinin

Wnt wingless-type MMTV integration site

Acknowledgements

I, first and foremost, would like to thank my supervisors, Kasia Goljanek-Whysall, and Brian McDonagh for their guidance, support, and patience throughout this work; it simply would not have been possible without your collective efforts. I am exceptionally grateful to Kasia for allowing me this opportunity. Thank you for being someone that I could consistently depend upon with complete trust throughout this programme even with the challenges of global shutdowns and other nonsense that was dealt with all the time. Your tremendous worth ethic is unmatched. I also want to thank Brian for always going above what was required to ensure that I had the necessary skills needed to complete this work and for always being available to discuss anything.

I want to thank Barbara Coen for all the help in the Physiology department throughout this work; Donna Kennedy for being extremely supportive and for always being available to discuss problems, and ideas and for sharing precious reagents when needed. I also want to thank Rachel Humphrey for being extremely helpful with all my questions and always being supportive.

I would also like to thank Cindy Coleman for showing me many of the skills I needed to begin this work and for always looking out for me; I would not have been fortunate enough to get this PhD without your help and support during my MSc. I wish to acknowledge the Timothy O'Brien lab as well, for providing Kasia and myself with support and lab space during the beginning phases of this work.

I also wish to express my sincerest gratitude to my lab members for their contributions:

- María Borja González- for assistance with the Seahorse assay, as well as the storage of all the samples that were generated throughout animal work, and for putting in long lab days when needed. Thanks for also always helping me with printing and other annoying things that I would ask.
- Karen Guerrero Vazquez- for assistance in the bioinformatics searches and pathway analysis, and taking your time help me understand this process.

- Raul González Ojeda- for assistance with animal work, troubleshooting Western blots and antibodies, and support in ongoing cell experiments when I was unavailable. Thank you for flexibility as well and accommodating my experiments when needed.
- Jose C. Casas-Martinez- for assistance in Western blot troubleshooting and advice, ER stress information, assistance with reagents, antibodies and primers, and independent analysis of images.
- John Gostage- for support in cell culture when I was away, helping me with RT-qPCR and Western blot analysis and troubleshooting, independent analysis of data, as well as support moving between reality and the Matrix.
- Qin Xia- for the support during Western blots, troubleshooting and being flexible with your experiments to accommodate me when needed.
- Turki Aljuaid- for assistance with miR qPCR protocol and optimisation.
- Gibran Pedraza Vazquez- thank you for assistance in bioinformatics.
- Alan Keane- thanks for always having some useful piece of information that the lab needs, and for offering support wherever possible with animal experiments or any other procedure that needed extra assistance.

I also want to thank the lab, current and past: Chao Su, Penglin Li, Daniel McGonigle, Sarah Coyne, Sarah Fagan, and all KW lab members that have come through that have supported me throughout this experience with help in my experiments, offering advice, or just taking the time to see how things were going. I sincerely appreciate every member of the KW and BMD lab for their generosity.

Finally, I also want to thank my family at home for their support. Most importantly, I want to thank my biggest supporter, my wife, my sunshine, Nora, for everything she does and has done to make the completion of this work possible; Ég elska þig.

Declaration

I, Anthony J Sannicandro, declare that this thesis which I submit to the University of Galway for consideration of the award of Doctor of Philosophy has been composed by myself unless otherwise stated by reference or acknowledgement. I declare this material contained herein has not been submitted, in whole or in part, in any previous application for any degree.

Part of the writing in Chapter 1 has been previously published in: Journal of Applied Physiology, 2019 127(2). https://doi.org/10.1152/japplphysiol.00961 (2018), as "micro(RNA)-managing muscle wasting." By Anthony J Sannicandro, Ana Soriano-Arroquia, and Katarzyna Goljanek-Whysall-these authors contributed equally. The full manuscript can be found in (Appendix 1).

Abstract

Sarcopenia is age-related muscle loss and management is complex. The mechanisms underpinning age-related decline in muscle health include defective muscle regeneration and deterioration of neuromuscular junctions. microRNAs are small, non-coding RNAs that regulate expression of genes and are implicated in the regulation of muscle. Using bioinformatics and small RNA-seq from human myoblasts, we detected miR-199a-5p to be upregulated in age and was predicted to regulate genes associated with sarcopenia. Therefore, we used C2C12 cells as myogenic model and NSC-34 cells as a neuron-like model *in vitro*, and adult and old C57BL/6 mice (adult 5-6 months, old 23-24 months) *in vivo* to determine the effect of miR-199a-5p overexpression and inhibition on muscle. Our data, *in vitro*, indicated the negative role of miR-199a-5p on myogenic differentiation and myotube size of C2C12 cells. Inhibition of miR-199a-5p in C2C12 also partially restored myotube atrophy resulting from tunicamycin-induced stress of myotubes and increased mitochondrial activity. We found ER stress protein GRP78 upregulated with miR-199a-5p overexpression *in vitro*. We also observed neuronal growth protein GAP43 to be differentially expressed *in vitro* with miR-199a-5p overexpression. Luciferase assay identified these as likely targets of miR-199a-5p. We found, *in vivo*, that miR-199a-5p inhibition did not significantly affect muscle size but did improve muscle force. We examined the neuromuscular junction and found miR-199a-5p overexpression contributed towards increased instance of abnormal morphology and fragmentation, and with miR-199a-5p inhibition this was somewhat reversed. Adult mice treated with miR-199a-5p exhibited reduced expression of GAP43 neuronal growth protein. In old mice, we also found significantly differentially expressed autophagy markers with miR-199a-5p overexpression. Using a model of muscle regeneration in adult and old mice, we found no significant changes to muscle size or function. We can conclude that upregulated miR-199a-5p may lead to muscle loss *via* a compromised neuromuscular junction, potentially driven by dysregulated miR-199a-5p targets, although more work is needed to precisely understand the nature of this relationship.

1 Introduction

1.1 Skeletal muscle overview

Skeletal muscle is a vital component to the musculoskeletal system, and the largest organ in the body, and is responsible for wide variety of functions (1,2). Skeletal muscle serves to connect the skeletal system (i.e., bone to bone *via* tendon) and provide force to produce movement, stabilise body posture, assist in respiration, thermoregulation, and major metabolic functions such as storing glucose and amino acids (3). The human body contains more than 600 individual muscles that are part of the three main muscle types: skeletal, smooth, and cardiac (2), with skeletal muscle functioning through conscious, purposeful, contractions innervated by the somatic nervous system. Skeletal muscles are highly organised tissues enveloped in a connective tissue sheath called the epimysium. A skeletal muscle itself is comprised of bundles of muscle fascicles, that are themselves surrounded by a connective tissue called the perimysium. Each fascicle is made up of smaller bundles of myofibres (muscle fibres). The muscle fibres themselves are surrounded by a cell membrane called the sarcolemma (Figure 1.1.1).

Myofibres are composed of long filaments running in parallel to each other and are made up of myosin (thick) and actin (thin) filaments in a structured organisation of proteins called myofibrils. Myofibrils are surrounded by a network of tubes called the sarcoplasmic reticulum (SR), which is the specialised endoplasmic reticulum (ER) of the muscle, and is responsible for storage, reabsorption of calcium ions during muscle relaxation, and release of calcium ions during contraction (4). Flanking the SR are transverse tubules (T-tubules) which are tubes located throughout the sarcolemma and are responsible for propagating action potentials into the fibre. Myofibrils can further be broken down into repeating contractile subunits called sarcomeres. The sarcomere represents the fundamental contractile unit of the muscle. Many sarcomeres run along the length of the myofibre, and during contraction, these functional units shorten to allow for contraction of the muscle (Figure 1.1.2) (7).

Sarcomeres are small functional units, approximately 2μm in length and are bordered by the Z-discs, which serve as anchor points for the thin actin filaments and delineates one sarcomere from the next. The centre of the sarcomere is defined as the M line which divides the sarcomere in half, and contains the thicker myosin filaments, the

entirety of this area where only myofilaments exist is known as the H band (2). The striated appearance of muscle fibres that is visually observed is characterised by alternating light I bands, where there are only actin filaments, and dark A bands wherein actin and myosin filaments overlap (5). The myosin and actin filaments work in conjunction with accessory proteins: α-actinin which anchors acting in the Z-disc, myomesin which serves to assemble thick filaments into sarcomeres, desmin which contributes to sarcomere alignment, titin, which serves as a giant structural protein that runs in parallel with the thick and thin filaments connecting the Z-disc and M-line to form a continuous filament, and myosin binding proteins (MyBP-C, -H) that function to align and connect thick and titin filaments, and aid in the assembly of the filaments into precise lengths (5). Dystrophin, a cytoskeletal protein, serves to enhance structural stability of the muscle membrane (6). The thin actin filaments contain actin, tropomyosin, and troponins (C, I, and T), in addition they provide active sites for myosin heads to bind during the process of muscle contraction. The thick myosin filaments are composed of myosin with globular heads that serve to form cross-bridges with thin filaments, binding at the active sites on actin filaments (5).

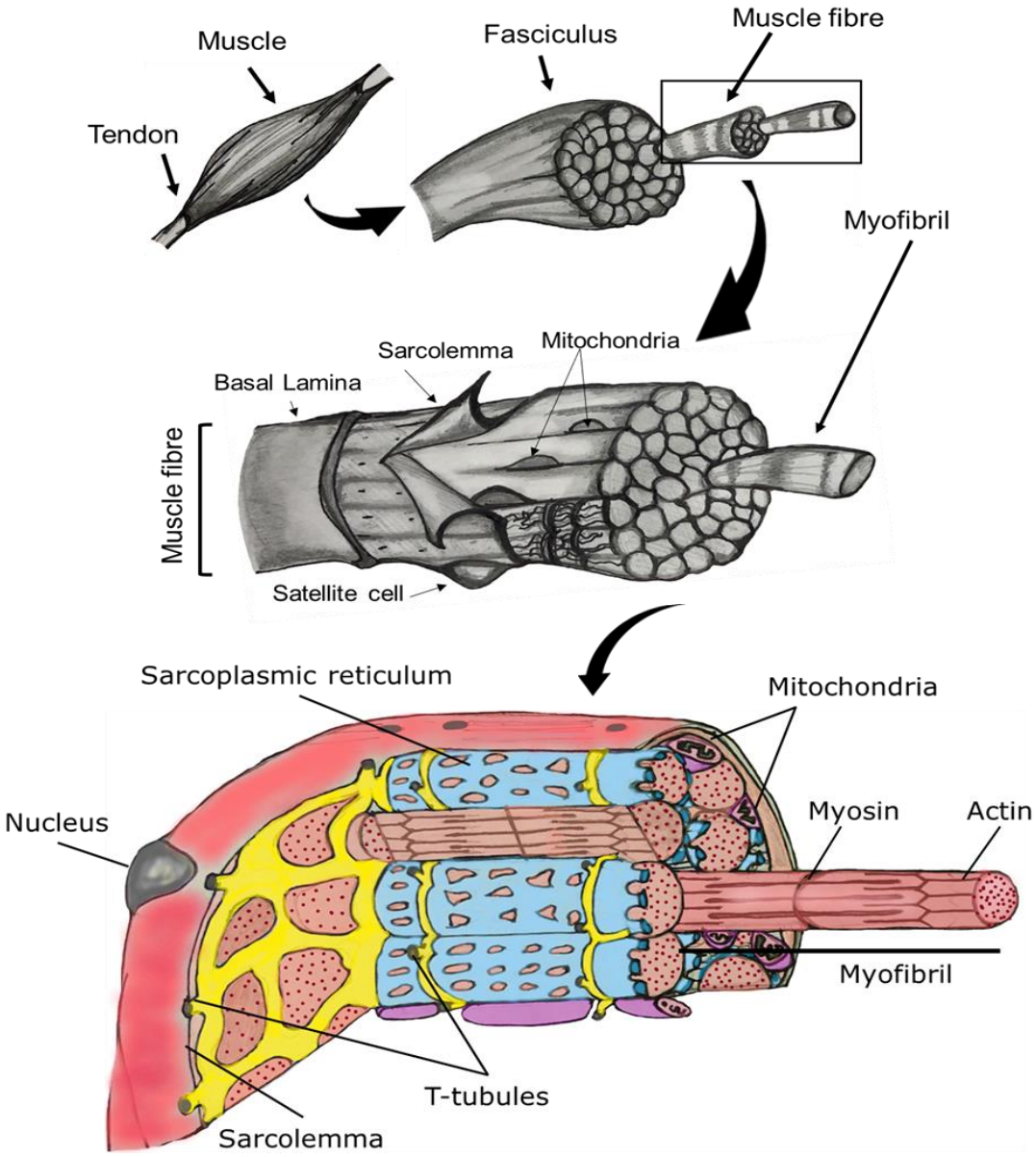

Figure 1.1.1 The structure of skeletal muscle is highly organised. Skeletal muscle connects the skeletal system at tendinous junctions. Thousands of skeletal muscle fibres are connected together by tissue sheaths, and bundles of fibres together form the fasciculus. Each muscle fibre is composed of myofibrils, which are long filaments of thread-like proteins that are critical for muscle contraction. Surrounding myofibrils are the sarcoplasmic reticulum which is the storage site for calcium and are located alongside the T-tubules, which are responsible for transmitting action potentials and initiating contraction. (Figure adapted and redrawn from (4)).

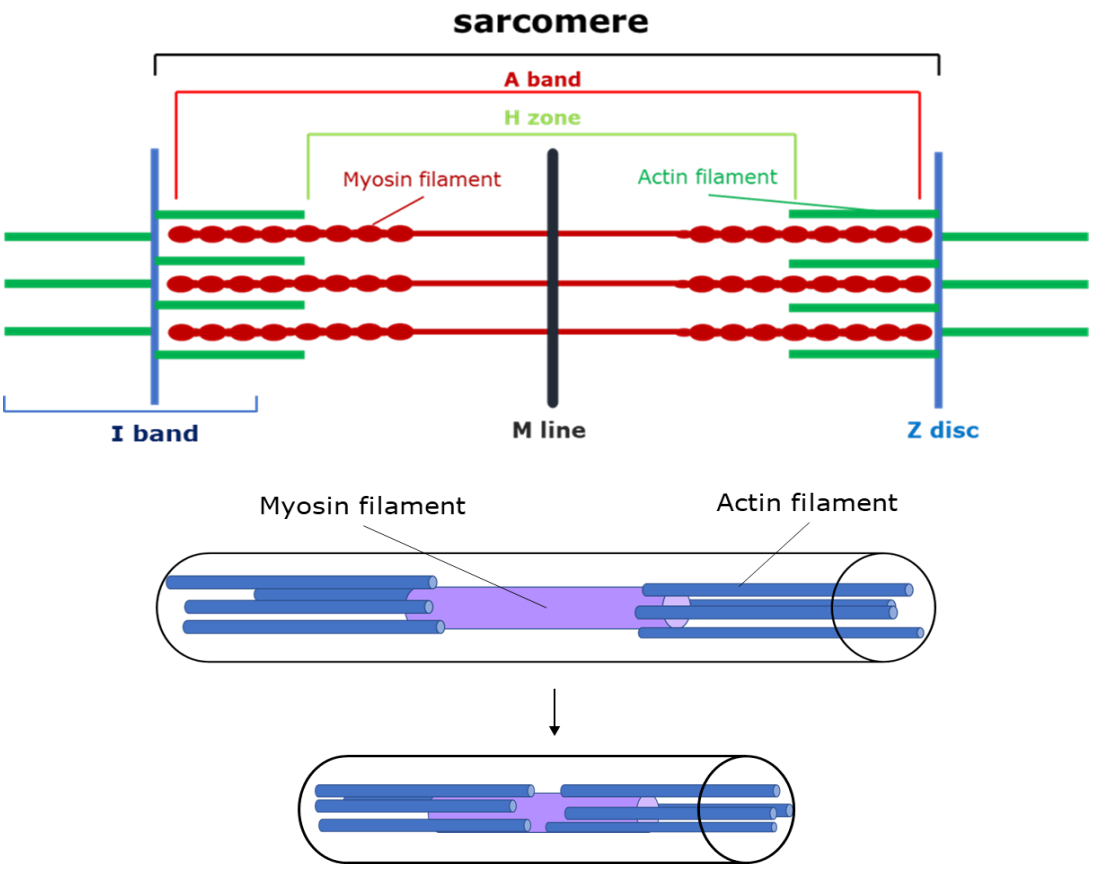

Figure 1.1.2 The sarcomere is the functional unit of contraction. The sarcomere represents the repeating contractile subunit of the muscle fibre. The sarcomere is bordered by the Z-discs where thin actin filaments bind, and the centre M line serves as the binding site for the thick myosin filaments. The area of overlapping actin and myosin filaments is referred to as the A band. The H zone is defined as the area containing myosin filaments only, and the I band is defined as the area where there are only actin filaments (Figure redrawn from (4)).

1.2 Mechanism of muscle contraction

Muscle contraction requires a highly co-ordinated sequence of events. The process of muscle contraction is referred to as the sliding filament mechanism of contraction, as the filamentous proteins slide past one another resulting in the shortening of the sarcomere. When a muscle contracts, the simultaneous contraction of all the sarcomeres along the muscle result in the shortening of the entire muscle (7). Muscle contraction occurs at the sarcomere following stimulation at the nerve end resulting in the propagation of action potentials along the T-tubules and subsequent release of intracellular Ca^{2+}. The Ca^{2+} interacts with troponins, physically moving the troponin-tropomyosin complex and allowing for the myosin heads to attach to the actin-binding

sites forming the myosin cross-bridge. This binding triggers the power stroke, which pulls the thin actin filaments centrally, shortening the fibre (Figure 1.2.1) (10).

Contraction first is initiated when action potentials travelling along the nerve reach the motor neuron and depolarisation of the presynaptic membrane occurs, opening voltage gated Ca^{2+} channels (8). The inward release of Ca^{2+} at the NMJ releases acetylcholine (ACh) which diffuses to the post-synaptic motor end plate and the gated ion channels in these receptors open and membrane depolarisation results (7,9). The action potential transmits along the sarcolemma in wave form throughout the T-tubules, coupled to the release of Ca^{2+} ions from the SR (10). This process wherein the action potentials are converted to contraction is referred to as excitation-contraction coupling (10). When the action potentials reach the sarcolemma, they travel through the T-tubules and are transmitted deep into the muscle. The T-tubules contain specialised receptors, called dihydropyridine receptors, located next to the SR (9). When depolarisation of the T-tubules occurs, dihydropyridine receptors undergo a conformational change that physically interacts with calcium channels on the SR called ryanodine receptors, which are responsible for releasing Ca^{2+} from the SR. The released Ca^{2+} binds to troponin C and the troponin-tropomyosin complex changes in confirmation, allowing myosin-binding sites to form cross-bridges with the newly exposed cross-bridge binding sites on actin (9).

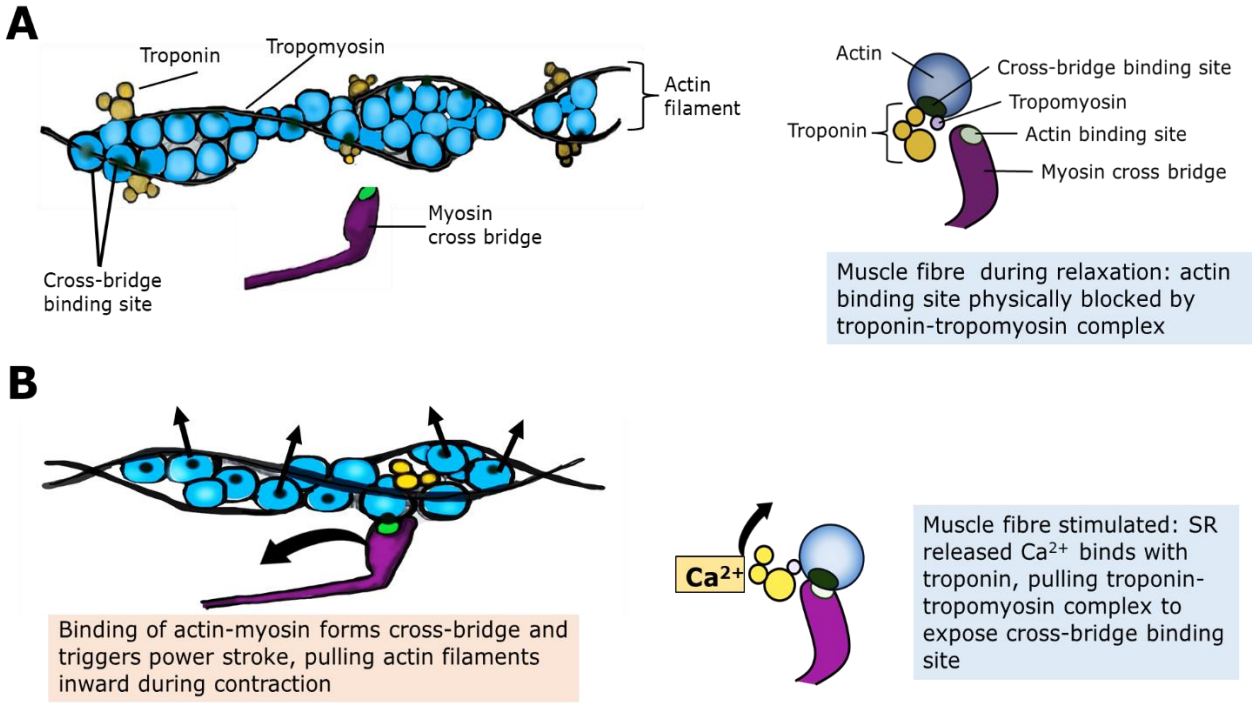

Figure 1.2.1 Sliding filament model of contraction. Muscle contraction occurs at the sarcomere following stimulation at the nerve end resulting in initiation of the sliding filament model of contraction. A) The relaxed muscle fibre is characterised by the blocking of the cross-bridge binding site to the myosin head by the troponin-tropomyosin complex. B) Propagation of action potentials along the T-tubules and subsequent release of intracellular Ca^{2+} binds to troponin C to pull on troponin-tropomyosin complex, exposing the actin binding sites allowing for binding of myosin heads and cross-bridge formation, and initiation of power stroke and contraction. (Figure adapted and redrawn from (4)).

One step of the contraction cycle requires one cycle of adenosine triphosphate (ATP) hydrolysis (4). Between each cycle of contraction in the sliding-filament model, the process begins with myosin attached to actin without the presence of ATP, this short stationary phase is known as rigor confirmation. Next, a single ATP binds to the myosin head, creating a confirmational change at the actin binding site, thus releasing the myosin head from actin filament. Additionally, the myosin lever arm is repositioned further along the actin filament, ATP is then hydrolysed yielding adenosine diphosphate (ADP), and one inorganic phosphate molecule bound to the myosin head. This creates a weak confirmational change that contacts the actin filament and releases the inorganic phosphate, which initiates the power stroke and generates the force of contraction on actin as myosin is returned to its original

position and the ADP molecule is released. This brings the myosin-actin confirmation back to the beginning of the cycle and return to rigor confirmation (4,9).

1.2.1 Control of the skeletal muscle contraction system

Skeletal muscle contraction is controlled by the nervous system and involves sensory and motor nerve fibres (2). Nerves contain both myelinated and non-myelinated sections, and skeletal muscle innervation results from large axons that travel out to innervate myofibres (2). Muscles are innervated by the outbranches of nerves at the muscle where many points of contact on the muscle surface are made. A single motor neuron and the associated muscle fibres being innervated are referred to as a single motor unit (7). Different motor neurons have different numbers of associated muscle fibres that they innervate, and there exists differences in patterns of NMJ innervation in vertebrates (11). Human NMJs differ from other species in that they are significantly smaller and contain extensive junctional folding compared to mouse NMJs which are larger in size and contain fewer junctional folds (11). Regardless of the differences between species, all NMJs have a nerve end, a synapse between the muscle and motor neuron, and the motor endplate on the muscle. The entirety of this complex is referred to as the NMJ. This is the key site for skeletal muscle contraction as it is where the muscle interfaces with nerves and where the stimulus for contraction originates after receiving nerve signals from the brain (Figure 1.2.2) (8,9).

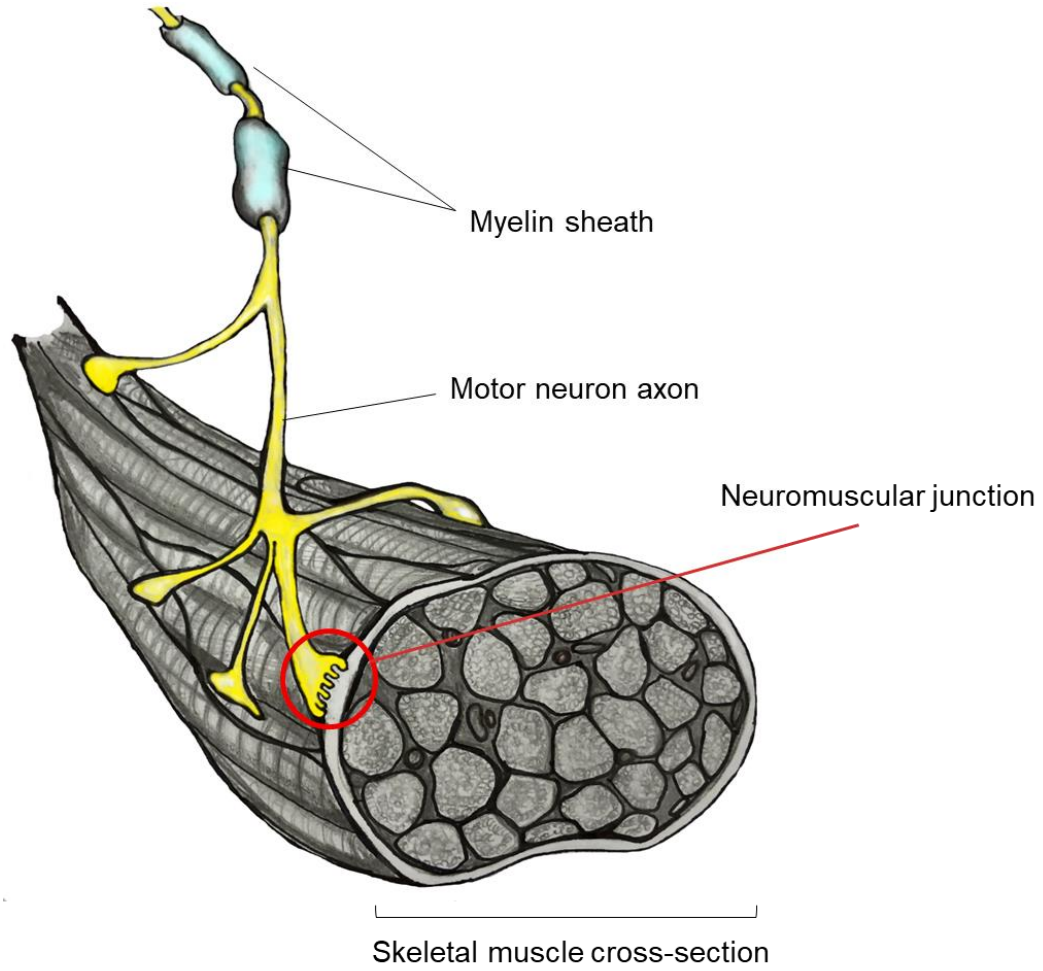

Figure 1.2.2 Gross skeletal muscle cross-section highlighting the NMJ. Motor neurons contain myelinated and unmyelinated segments that terminate in the NMJ. The terminal end of the motor neuron interfaces with the muscle at the motor end plate. The NMJ serves to begin the sequences of events leading to muscle contraction when an action potential reaches the nerve terminal of the NMJ. (Figure redrawn from (12)).

The NMJ is composed of three main sections: the pre-synaptic nerve terminal, the post-synaptic motor end plate, and the synaptic cleft between the nerve terminal and motor end plate (13). The pre-synaptic terminal is defined as the unmyelinated area of nerve branches that terminate in active zones which contain calcium channels, potassium channels, endoplasmic reticulum, mitochondria, and synaptic vesicles. The synaptic vesicles store approximately 10,000 molecules of the neurotransmitter acetylcholine (ACh), which is synthesised in the pre-synaptic terminal from acetyl coenzyme A (acetyl CoA) and choline and is the key neurotransmitter at the NMJ (14).

When an action potential reaches the terminal end of the neuron, calcium channels open and an influx of Ca^{2+} in the nerve terminal leads to ACh being released from the synaptic vesicles by exocytosis into the synaptic cleft space. Diffusing across the synaptic cleft, ACh binds to nicotinic receptors concentrated at the junctional folds of the sarcolemma of the target muscle. The ACh receptors are themselves gated ion channels, that open upon binding to ACh, allowing for the influx of Na+ into the muscle. The subsequent decrease in membrane potential is strong enough to allow for propagation of the action potential over the muscle membrane throughout the T-tubules, resulting in contraction *via* the sliding filament model (1.2) (13). The membrane is repolarised as ACh is metabolised into choline for future ACh synthesis, and acetate by acetylcholinesterase (13).

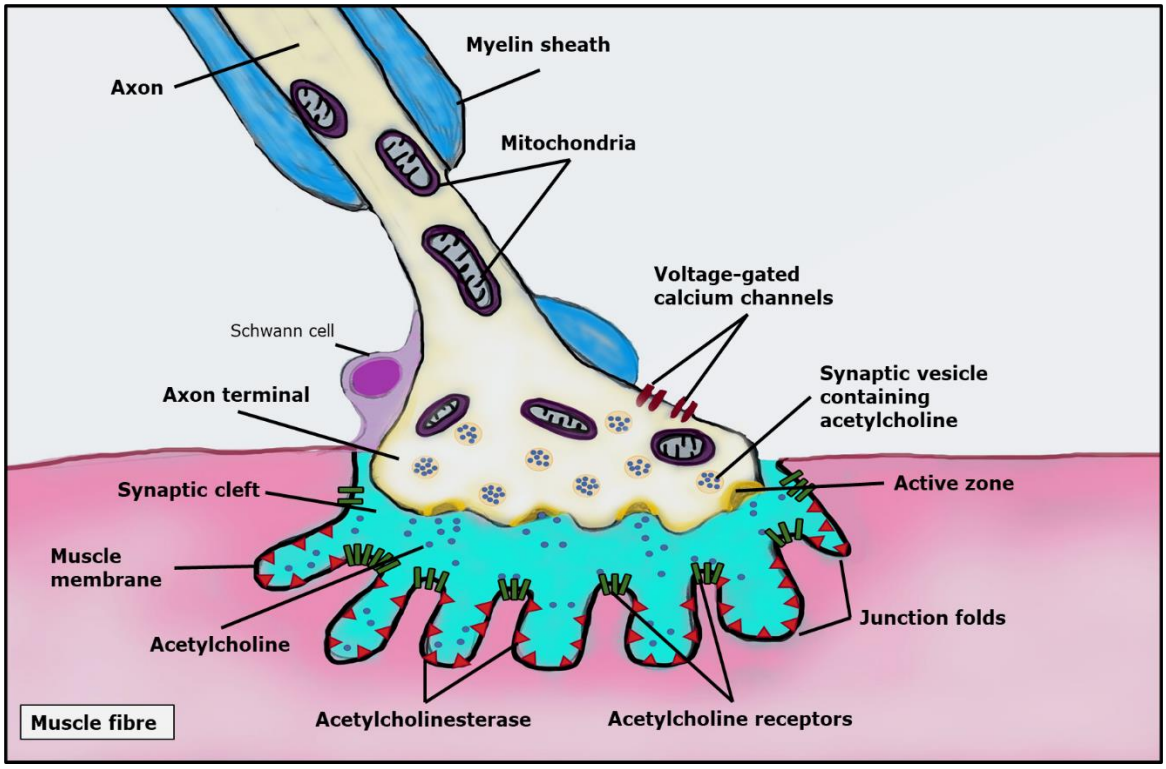

Figure 1.2.3. Cross section of the NMJ. The NMJ is the site where skeletal muscles interact with the nervous system. Transmission of an action potential from nerve to muscle initiates a sequence of events that results in muscle contraction. The NMJ is composed of a pre-synaptic axon terminal, a synaptic cleft and a post-synaptic motor endplate on the muscle that contains junctional folds. The terminal end of the nerve contains ACh in synaptic vesicles. (Figure redrawn from (15)).

1.3 Skeletal muscle fibre types

The structure and function of skeletal muscle largely depends on fibre type. The differences between types of fibres results from characteristic differences in metabolic type, neural input, and contraction rates (16). The contractility of skeletal muscle is determined by expression of myosin heavy chain (MyHC) isoforms (17). Myosin is composed of two MyHC that form the myosin filament, each MyHC has a head (N-terminal) and tail (C-terminal), and at the head-tail junction each MyHC interacts with two myosin light chains: a regulatory and essential (MyLC) (18). Both MyHC and MyLC have multiple isoforms (19). Rodent skeletal muscle contains seven MyHC isoforms, and are classified typically by type, there are two developmental isoforms (MyHC-embryonic, MyHC-perinatal) expressed in developing muscle, three 'type II' adult isoforms in 'fast-twitch' muscles (MyHC-IIa, MyHC-IIb, MyHC-IIx/d), and MyHC-β/slow in 'type I' slow twitch muscles (19). Human skeletal muscle contains the same isoforms except for MyHC-IIb, which appears in rodents (19–21).

Regulation of MyHC isoforms occurs through varying stimuli such as physiological, mechanical neurological and hormonal, among others (17). The speed of contraction is corelated with the ATPase activity associated with the MyHC in the muscle (17). Although a muscle might predominately contain one fibre type, two or more MyHC isoforms can be present in the same fibre, forming hybrid fibres (19). Further, while there exist similarities across species, MyHC-IIb has been detected in humans only at the mRNA level in a small subset despite humans possessing the encoding gene and has only been otherwise observed in rodents (20).

Table 1.3.1 MyHC isoforms in skeletal muscle

Gene	MyHC	Fibre type	Species	Chromosome	Ref
Myh7 MYH7	MyHC-β/slow	Type I, slow, and cardiac	Rodent, Human	14	(19,22)
Myh2, MYH2	MyHC-IIa	Type II, fast intermediate	Human, Rodent	17	(19,21)
Myh1, MYH1	MyHC-IIx	Type II, fast glycolytic	Human, Rodent	17	(19,21)
Myh4,	MyHC-IIb	Type II, fastest glycolytic	Rodent	17	(19–21)
Myh3, MYH3	MyHC-embryonic	Developing muscles	Human, Rodent	17	(19,21)
Myh8, MYH8	MyHC-perinatal	Developing muscles	Human, Rodent	17	(19,21)

The metabolic needs of the muscle are unique to each fibre type. The type I fibres require a network of vasculature, and myoglobin to store oxygen. In contrast, type II fibres function by primarily utilising anaerobic lactic acid fermentation to generate ATP (23,24). Muscle types are closely correlated to metabolism as each type is associated with ATPase activity and thus ATP production speed is closely related to fibre type. ATP production is regulated by cellular respiration and is the critical source of energy for the cells. The process of ATP production begins first through glycolysis producing two molecules of pyruvate for each molecule of glucose. This process yields two molecules of ATP by enzymes phosphofructokinase-1 (PFK1) and pyruvate kinase and two reduced NADH electron carrier molecules (25). The fate of pyruvate depends upon the presence of oxygen; if oxygen is present pyruvate will enter the mitochondria and begin the process of aerobic respiration (23). In the presence of oxygen, pyruvate molecules are oxidized by the pyruvate dehydrogenase complex, forming one acetyl-CoA molecule which is then fully oxidized to yield carbon dioxide and reduced electron carriers in the tricarboxylic acid (TCA) cycle (25). Upon completing the TCA cycle, the total yield is two molecules of carbon dioxide, one equivalent of ATP, three carrier molecules of NADH, and one carrier molecule of FADH2. These carrier molecules transfer electrons to the electron transport system (ETS), generating a proton motor force in the mitochondria producing 32 molecules of ATP per glucose molecule. This process is referred to as oxidative phosphorylation and is the primary source of ATP for type I muscle fibres

(23,24). If oxygen is not sufficiently present, pyruvate remains in the cytoplasm and is converted to into lactate by the enzyme lactate dehydrogenase, the reaction of which also involves the oxidation of NADH to NAD+. NAD+ is an essential cofactor for glycolysis and thus allows glycolysis to begin again to further produce ATP (23). As this process takes place in the absence of oxygen is it referred to as anaerobic respiration and is the primary source of ATP for faster fibres such as type IIx, as the process of anaerobic respiration is much faster than oxidative phosphorylation, however, anaerobic metabolism of glucose yields a net gain of 2 ATP, so while it is much faster it is far less efficient (23).

Type I fibres, found in both humans and rodents, are notably smaller than type II fibres and are able to maintain sustained contractions for longer periods of time than other fibre types. Type I fibres are highly enriched with capillaries, myoglobin, and mitochondria, allowing them an increased supply of oxygen for subsequent ATP production by aerobic metabolism (22). Type II fibres are also found in humans and rodents, and can be subdivided into type IIa, type IIb, and type IIx. Type IIa, which are also called intermediate fibres, utilise oxidative metabolism like in type I, but contain less myoglobin; these fibres are characterised by a hybrid phenotype that allows for faster force production than type I fibres and increased resistance to fatigue compared to other type II fibres (24). Type IIb is only seen in rodents and is the fastest MyHC isoform (19). Both humans and rodents contain type IIx fibres which are characterised by being much larger than type I, and much quicker at producing contractions due to their use of anaerobic glycolysis for ATP production (24). While these fibres are capable of much higher force and are capable of firing quickly, they fatigue at a faster rate due to build-up of cytosolic acidification and by-products (lactate, inorganic phosphate) which accumulate within the muscle and inhibit contraction (26). Human skeletal muscle contains all three fibre types, (MyHC-β/slow, MyHC-IIa, MyHC-IIx), however some muscle groups appear composed of predominately one type over another. For example, the human diaphragm is made up of approximately 55% type I, 21% type IIA, and 24% type IIX (22), whereas the human soleus (SOL) muscle of the lower limb is composed of an average of 80% type I fibres (23).

Motor control of muscle fibres is also key to their function. Muscles are innervated by α-motor neurons and are clustered in motor neuron pools in the spinal column, and all

of the motor neurons in the same pool innervate a particular muscle forming a one muscle to one motor pool confirmation (27). Each muscle fibre in a muscle is innervated by a single motor neuron, however a single motor neuron can innervate many muscle fibres. This combination of motor neuron and the corresponding muscle fibres that are innervated form the motor unit, and the number of fibres innervated by a motor unit is the innervation ratio. Smaller muscle groups involved in fine motor movements will have smaller ratios (a single motor neuron will innervate 10-100 fibres), thus enabling greater control, whereas muscles controlling gross motor movements will have higher innervation ratios (single motor neuron innervating 1000 or more fibres) (27). When a nerve signal is sent to motor neurons to execute a function, the order of neuron recruitment proceeds in and orderly fashion from smaller motor neurons to larger, due to the smaller membrane area and corresponding fewer numbers of ion channels and a larger input resistance. Smaller synaptic currents can therefore be sufficient to reach firing thresholds in smaller motor neurons first before larger motor neurons will reach firing threshold (27). With respect to muscle fibre types, small motor neurons innervate slow-type I fibres, intermediate size motor neurons innervate type IIa fast-intermediate fibres, and larger motor neurons innervate the fastest fibres type IIx/b (27).

Table 1.3.2. Summary of skeletal muscle fibre types

Fibre type	Species	Energy metabolism	Force production	Fatigue resistance	Ref
Type I	Human, Rodent,	Aerobic Oxidative	Low	High	(23,25,28)
Type IIa	Human, Rodent	Oxidative Glycolytic	Intermediate	Intermediate	(19,28)
Type IIb	Rodent	Anaerobic Glycolytic	Highest	Lowest	(19,23–25)
Type IIx	Human, Rodent	Anaerobic Glycolytic	High	Low	(19,23–25)

1.4 Development of skeletal muscle

Skeletal muscle development begins during embryogenesis in which the paraxial mesoderm begins to segment and give rise to compartments that ultimately form muscle, the dermomyotome and sclerotome. These compartments give rise to components of the musculoskeletal system, including skin, muscle, and bone (29).

The formation of muscle in the developing embryo progresses in waves that are in turn correlated with expression of genes throughout that are critical for skeletal muscle function in adulthood (30). As muscle is made up of multinucleated myofibres, each myofibre is itself formed by the fusion of mononuclear myoblasts forming multinucleated myotubes. This step is critical for not only developing muscle, but also during muscle repair in adulthood (31). The process begins by the activation of myogenic progenitor cells into myoblasts capable of fusion and proliferation. Skeletal muscle progenitor cells are known as satellite cells and are resident along the basal lamina of the muscle fibre. The differentiation and specificity of differentiation is regulated my myogenic regulatory factors (MRF), the drive cell fate towards myogenic lineage. (32).

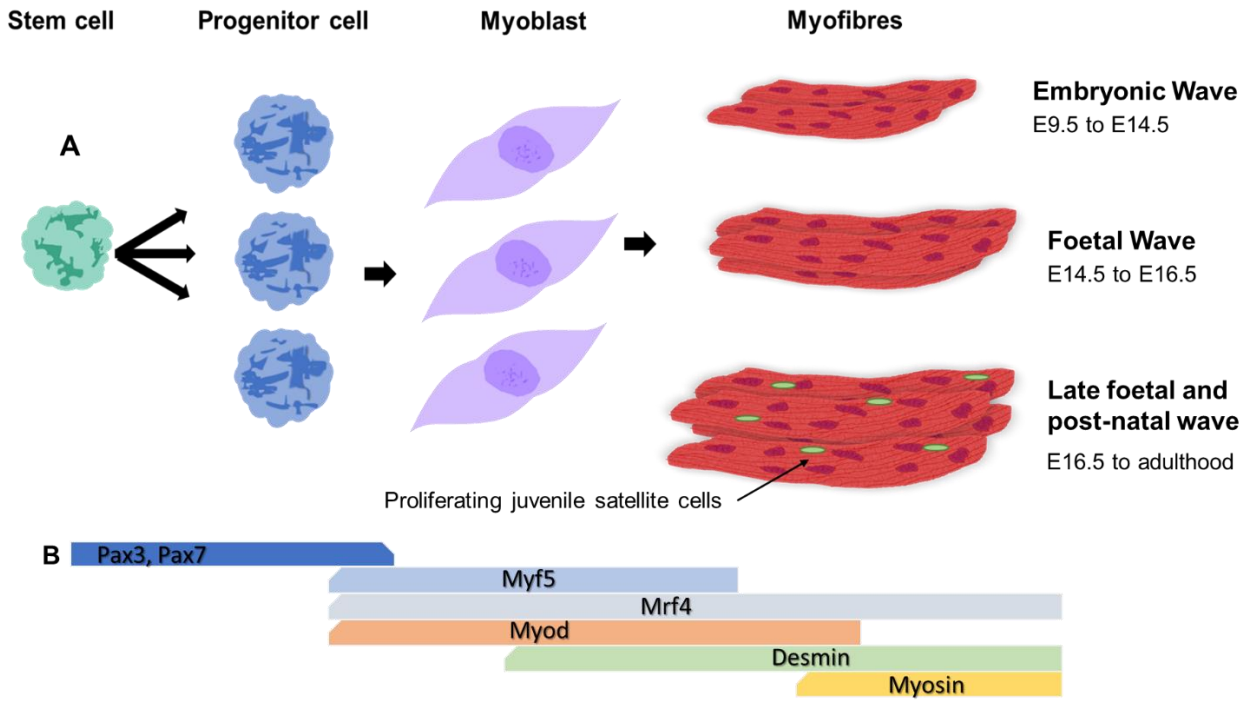

Figure 1.4.1 Progression of myogenesis. Myogenesis involves primary myogenesis to establish the basic muscle pattern (embryonic and foetal waves) and secondary myogenesis that allows for growth and maturation of muscle (A). Adult myogenesis involves for repair of damaged muscle by muscle progenitor cells (satellite cells). Embryonic myogenesis is linked to expression of muscle specific genes that are necessary for development (B). (Figure adapted/redrawn from (30)).

Primary fusion refers to mammalian myogenesis that occurs during embryonic development, as well as muscle regeneration the involves myoblast-myoblast fusion to form multinucleated cells and mature myotubes. In secondary fusion, mononuclear myoblasts fuse with previously formed multinucleated myotubes to increase the number of myonuclei along the muscle which increases cytoplasmic and protein synthesis yielding increased muscle size (32). Secondary fusion is predominant as it occurs in development as well as adulthood in the growth and maintenance of myofibres (31,32).

1.5 Molecular mechanisms of muscle maintenance

Maintaining muscle homeostasis is a key component to the overall health of the organism. Homeostasis of skeletal muscle requires a complex and dynamic equilibrium. The plasticity of muscle allows it respond dynamically and change in response to outside factors such as ageing and in disease. Muscle plasticity also allows for hypertrophy with use or changes in metabolic architecture, and the molecular mechanisms that control these abilities is complex. Skeletal muscle homeostasis depends on a fine balance between muscle hypertrophy, atrophy, and regeneration. Muscle hypertrophy and atrophy are both independent, but overlapping, processes controlled by specific signature pathways and transcriptional programmes (33). During ageing and disease states, the balance between anabolic and catabolic processes in muscle is altered resulting in a loss of muscle mass and function (33,34).

The primary anabolic pathway in muscle protein synthesis is the activation of serine/threonine kinase AKT by phosphoinositide 3-kinase (PI3-k/Akt), which upregulates mechanistic target of rapamycin (mTOR) and is itself regulated by factors such as growth factors like IGF-1, but also exercise, hormones and amino acid intake (35,36). The Akt pathway also controls the Forkhead Box O (FoxO) members 1, and 3, (FoxO1, FoxO3), by inhibiting transcriptional activity. Akt phosphorylation of FoxO represses transcriptional activity *via* promoting nuclear export and cytosolic localisation (37). FoxOs have been linked to protein degradation and are highly expressed in skeletal muscle (38).

The mTOR signalling pathway is a primary transducer of anabolic signalling in muscle and is required for cell growth, proliferation, and suppression of autophagy (39). IGF-1 plays a central role in this process and can function both *in vitro* and *in*

vivo to manage processes such as proliferation, differentiation, and hypertrophy. IGF-1 binds to receptor IGF-1R which activates the PI3-k/Akt kinase pathway and subsequently phosphorylates and activates the mTOR pathway, promoting protein synthesis and preventing protein degradation (Figure 1.6.1) (40,41).

Skeletal muscle catabolism is activated by ubiquitin proteasome system pathway (UPS) under the control of FoxO and nuclear factor-kappa B (NF-κB) (42,43) (Figure 1.6.1). Interestingly, these pathways are a part of physiological responses to stimuli such as exercise, however their dysregulation can result in muscle wasting. For example, NF-κB activation is a part of adaptation of muscle to different stressors, such as mechanical stress, however its persistent activation has been associated with muscle wasting through the UPS pathway (44). Other important catabolic pathways include the myostatin pathway (45,46), and autophagic-lysosomal proteolysis (47).

Autophagy and the autophagic pathways associated with muscle breakdown is an important component of skeletal muscle health in addition to other proteolytic pathways mentioned. Autophagy plays an important role in many cell processes; myofibrillar proteins are mainly degraded by the UPS, whereas dysfunctional organelles, and protein aggregates are degraded *via* autophagy. Autophagy involves the creation of autophagosomes, which serve to sequester cytoplasmic debris, and the fusion with lysosomes to allow for lysosomal degradation by hydrolases (40). Both uncontrolled and reduced autophagy are associated with detriments to skeletal muscle, therefore autophagy can contribute to atrophy during catabolic conditions, but homeostatic autophagic flux is needed for myofibre survival (48). In mammalian cells, the mTOR and Raptor complex, mTORC1, negatively regulates autophagy whereas AMPK is a positive regulator (49). Atrophy related protein breakdown is mediated by atrogenes under control of FoxO (Figure 1.6.1). Several autophagy genes under the control of FoxO3 have been demonstrated to code for autophagic processes, such as *LC3*, *ATG12*, and *BNIP3* (48). Ageing has been demonstrated to impact autophagy proteins such as ATG5, ATG7, and BECLIN1 which are downregulated in ageing, and ULK1, BECLIN1 and LC3 are downregulated in osteoarthritis, an age-related joint disease (48). Dysregulation of autophagic proteins in ageing is believed to contribute to deficits in the autophagy machinery. This has been observed in both mice and humans (49).

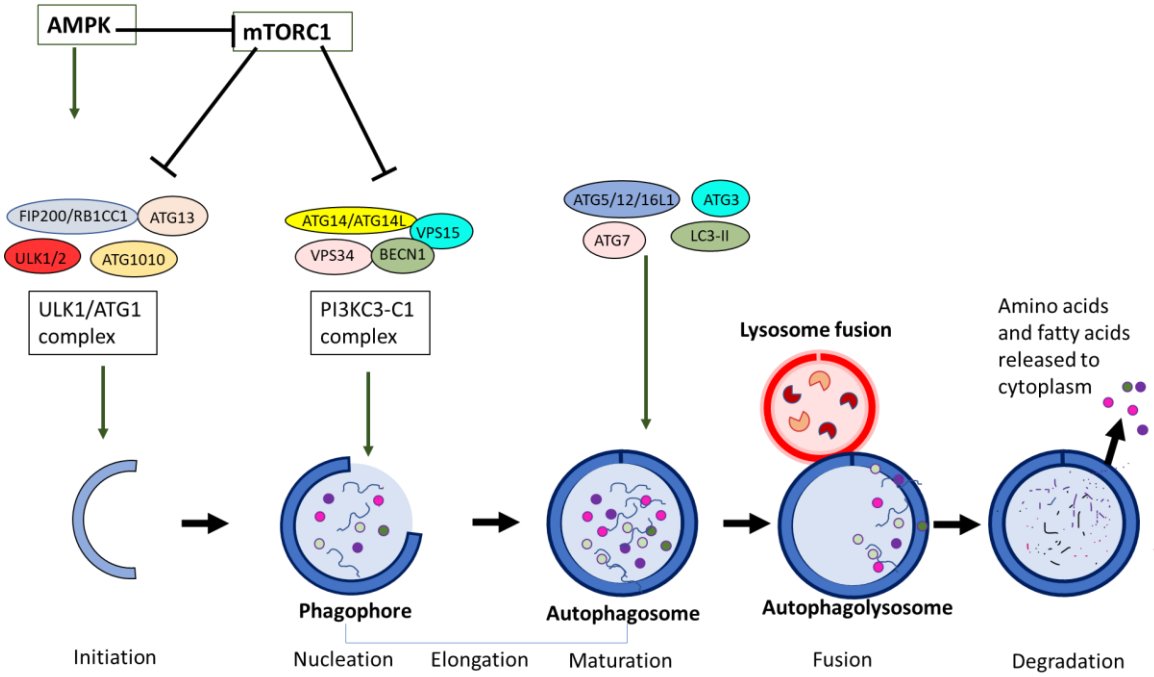

Figure 1.5.1. Autophagy involves a step-by-step sequence of events to degrade cellular debris. The ULK/ATG1 complex initiates autophagosome formation and is the mediator of autophagy upon activation. The ULK/ATG1 complex receives signals from mTOR to drive downstream autophagy proteins. The P13KC3-C1 complex assists in forming the nucleated phagophore, which elongates and matures. The autophagosome fuses with lysosomes to form the autophagolysosome, and the contents and inner membrane are degraded. The resulting contents of amino acids and fatty acids are sent back to the cytoplasm for reuse in cellular metabolism. (Figure adapted/redrawn from (50)).

Selective autophagy, such as autophagy leading to breakdown of mitochondria (i.e., mitophagy), has been suggested to lead to increase in reactive oxygen species (ROS) production (51), which in turn has been proposed to contribute to muscle loss in both ageing (sarcopenia) and disease. Moreover, oxidation-dependent protein alterations have been observed in people with muscle loss (49). It is suggested ROS may lead to dysregulation of autophagy. Autophagy is also important for satellite cell stemness, and ageing is associated with reduced satellite cell stemness and increased satellite cell senescence (49).

1.6 Hypertrophy, atrophy, and regeneration of muscle

1.6.1 Muscle fibre hypertrophy

Muscle hypertrophy is defined as increased myofibre size. In adults, the maintenance of muscle mass requires a balance between muscle protein synthesis, and muscle protein breakdown, the direction of which depends largely on growth factors, hormones, cytokines, and nutrients that serve to push the balance in either an anabolic (growth) or catabolic (atrophy) direction (52). The major pathway regulating protein synthesis and anabolism is mTOR: TORC1 complex (mTOR/TORC1), which is activated by upstream regulators like IGF-1. IGF-1 acts by binding to its receptor, tyrosine kinase receptor (IGF-1R), which in turn increases activation of downstream PI3k/Akt pathway. Downstream target of Akt is mTOR, which regulates cell growth and promotes muscle hypertrophy and an increase in protein synthesis by activating S6, a ribosomal protein (53). Akt also interacts with phosphorylation of glycogen synthase kinase-3β (GSK3β), and during hypertrophic conditions, GSK3β is phosphorylated, and its activity is inhibited, leading to activation of eIF2B and transcriptional activator β-catenin (41). Additionally downstream are FoxO1, and FoxO3, which are implicated in skeletal muscle differentiation and fibre type specification (54).

Activation can also occur through crosstalk with other pathways such as transforming growth factor beta (TGF-β) (52), and also interacts with the atrophy signalling pathways such as myostatin, which decreases phosphorylation of Akt and upregulates atrophy mediators, atrogin-1, and MuRF-1, components of the UPS (55). Hypertrophy is marked by an increase in muscle cross sectional area and increase in volume and mass. Exercise has been shown to be critical to the maintenance of muscle mass, especially during ageing (56). Exercise has been shown to positively impact protein synthesis, mitochondrial quality (57), as well as insulin sensitivity (58), which are all impacted by ageing (59).

1.6.2 Muscle fibre atrophy

Atrophy, or loss of muscle, occurs when muscle protein breakdown exceeds the rates of muscle protein synthesis, yielding a net loss of muscle mass. This can occur as a result of many diseases as well as inactivity, denervation, immobilisation, and nutrient deficiencies and contributes to overall poor health, loss of strength, and increased

frailty (53). The loss of muscle mass through any means is also correlated with metabolic disease such as diabetes, and poor recover from illness or injury (e.g., cachexia), and further contributes to general musculoskeletal decline by increasing fracture risk and bone strength (53). Atrophy is characterised by decreased protein content, fibre size, force production and fatigue resistance. As seen with hypertrophy, muscle atrophy can result from several different molecular triggers. The main pathways believed to activate the muscle degradation system include the UPS pathway, and the autophagy-lysosome pathway (60). The UPS is responsible for degrading damaged proteins and is important in muscle atrophy. The majority of proteins are degraded by the 26S proteasome through covalent attachment of a multi-ubiquitin chain (61). Proteins undergo enzymatic change and are ubiquinated through the effect of E1 ubiquitin-activating enzyme, E2 ubiquitin-conjugating enzyme, and E3 ubiquitin-protein ligases (61). Key to the regulation of protein degradation include atrogenes, muscle specific E3 ligases, muscle atrophy F-box (MAFbx)/Atrogin-1, and MuRF1, which are increased during muscle atrophy (41). There are other E3 ligases involved in muscle atrophy and denervation induced atrophy including, muscle ubiquitin ligase of the Skp, Cullin, F-box containing (SCF) complex in atrophy-1 (MUSA1), specific for muscle atrophy and regulated by transcription (SMART). Transcription factor, FoxO, regulates ubiquitin ligase expression and the phosphorylation by Akt results in exportation from the nucleus to the cytoplasm, when Akt is downregulated, FoxO is transported to the nucleus where it increases expression of ubiquitin ligases (61).

Autophagy is also another important proteolytic pathway that plays a key role in the removal of damaged organelles and misfolded and damaged proteins. Autophagy regulation overlaps with IGF-1 signalling pathways mTOR-mediated inhibitory phosphorylation of unc51-like kinase-1 (ULK1), and FoxO3-mediated induction of autophagy-related genes (41). The balance of proteolytic systems is required to ensure muscle homeostasis. It is believed changes in expression of genes driving these systems has been shown to disrupt normal regulation of downstream protein breakdown resulting in increased breakdown and atrophy (60).

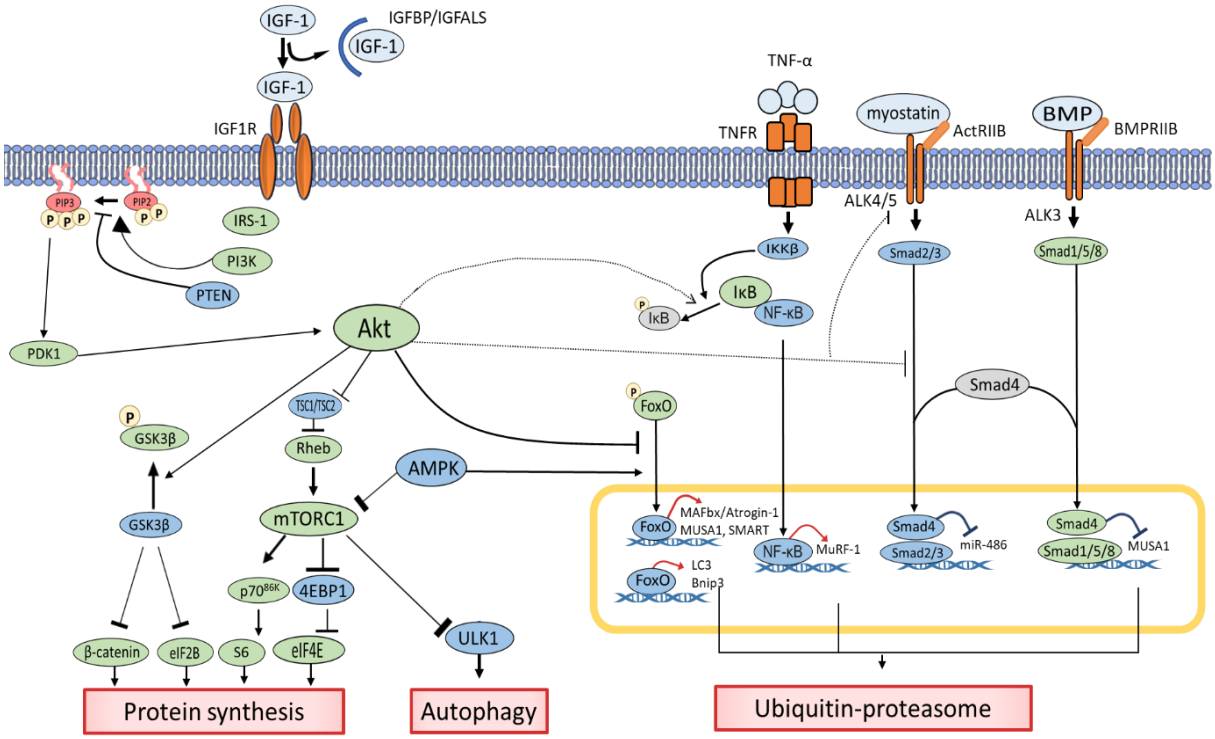

Figure 1.6.1 Hypertrophy and atrophy signalling pathways. IGF-1 binds to its receptor, IGF-1R, which then activates PI3K and converts PIP2 to PIP3 at the inner plasma membrane, promoting the activation of the Akt pathway. Akt activates protein synthesis by downstream targets of mTORC1, S6, and eIF4E as well as activating downstream targets of GSK3β, β-catenin, and eIF2B. Akt pathways can also supress the UPS by inhibiting FoxO mediation of E3 ligases. Cytokines such as TNF-α induce the NF-κB pathway leading to activation of the UPS. Myostatin, and BMP compete for Smad4, a mediator of the TGF-β signalling pathway which has crosstalk with Akt through myostatin signalling. Molecules that promote muscle hypertrophy are shown in green, molecules inhibiting protein synthesis are shown in blue. Dotted lines denote potential pathways in skeletal muscle. (Figure redrawn from (41)).

1.6.3 Muscle fibre regeneration

Skeletal muscle has the unique ability to regenerate new muscle fibres after injury or damage. Muscle can be susceptible to mechanical trauma as well as disease (62). The repair process is mediated largely by satellite cells, the resident muscle stem cell, which are quiescent in adult muscle until they are activated following insult (Figure 1.6.2) (63). The quiescent satellite cell resides in a niche between the sarcolemma and basal lamina and have differing gene expression profiles to active satellite cells, predominantly *PAX7*, *PAX3*, *CDH15*, *SDC4*, *CD34*, *ITGA7*, and *CXCR4*, and absent expression of *MYOD* (64). Satellite cells are activated in response to specific signals such as muscle damage, exercise, or disease. In the case of mechanical trauma,

necrosis of the damaged fibres begins shortly after the injury (Figure 1.6.3). Traumatic injury causes an influx of calcium into the muscle following disruption to the sarcolemma and basal lamina (65). Excess cytoplasmic calcium activates proteases and hydrolases and further releases hepatocyte growth factor (HGF) from the extracellular matrix which activates satellite cells by inducing mTORC1 activation G_0 to G_{alert} (64) (Figure 1.6.2). Shortly after the initial injury, neutrophils appear to remove damaged muscle cells while also secreting pro-inflammatory chemicals such as IL-6, TNF-α, chemokines such as CCL17, CCL2, and growth factors such as IGF-1, VEGF, FGF (65). This drives monocytes and macrophages to the site which are further important for muscle regeneration. Muscle regeneration involves two types of macrophages: M1 pro-inflammatory macrophages appear first and promote cell lysis, removal of cellular debris and stimulate increased myoblast proliferation; M2 macrophages act after M1 and are anti-inflammatory cells that promote myotube formation and attenuates the inflammatory process (65). Macrophage infiltration is critical in early phases of muscle regeneration to remove damaged myofibres. The polarisation of M1 to M2 macrophage is induced by cytokines and growth factors, such as IL-4, IL-10, and TGF-β, additionally, CCAT/enhancer binding proteins (C/EBP) of which CHOP is a member, has been shown to be important for the induction of M2 polarisation in the context of muscle regeneration (66).

After activation, satellite cells generate a subpopulation of myoblasts that can either differentiate or self-renew to keep a consistent pool of satellite cells. Activated satellite cells express *MYOD* and increased expression of cell cycle genes, as well they decrease *CD34* production, allowing the cells to migrate easier to the site of injury (67,68). The satellite cells dividing become myogenic precursor cells, and produce myogenic regulatory factors (MRF), the most important of which for muscle are *MYOD* and *MYF5*, the expression of both MRFs is critical to myogenic precursor differentiation (68).

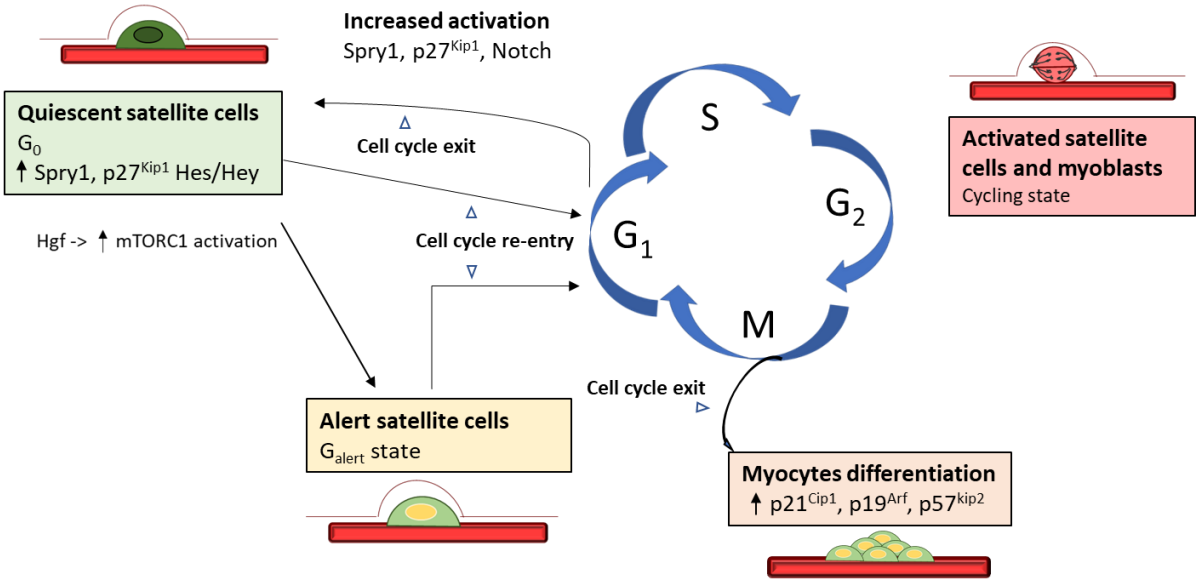

Figure 1.6.2 Satellite cell activation and differentiation. Satellite cells are quiescent in adult muscle but become activated in response to extrinsic signalling, after which they re-enter the cell cycle and begin proliferating. Activated satellite cells show different expression profiles of MRFs. (Figure adapted from (63)).

The final step to muscle fibre regeneration after injury is the fusion of satellite cells. The cells can fuse with existing fibres or form new myotubes by forming small new filaments that can recruit more cells to increase the size of the tube and further increase contractile protein expression (68). Revascularisation also must occur for the success of regeneration and the formation of new vasculature indicates early signs of normal regeneration, secretion of VEGF at the injury site. The final mark of successful regeneration is reinnervation of the fibres and is characterised by newly formed NMJs at the remaining axons and AChR clusters on the regenerated muscle fibres (69). The regeneration process is also possible in the case of denervation of the muscle, however the success of this process relies heavily on the age and status of the organism, as older animals have been shown to demonstrate defective reinnervation, as well as the speed in which the reinnervation occurs (70).

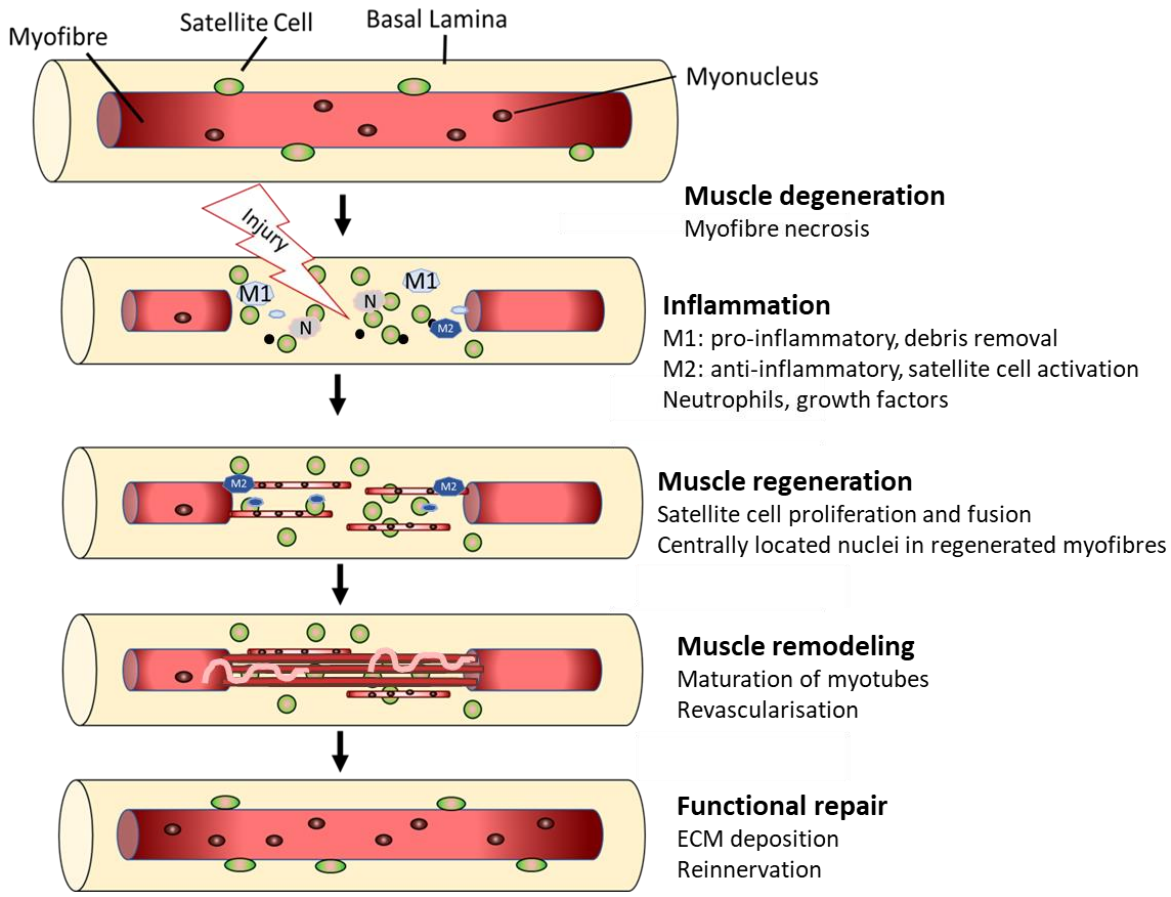

Figure 1.6.3. The main phases of muscle regeneration following injury. Skeletal muscle can repair itself following injury, largely due to satellite cell activation and inflammatory action. The main phases of muscle regeneration following injury are degeneration of the damaged fibres and necrosis followed by increased inflammation resulting in attraction of neutrophils and macrophages, (M1 pro-inflammatory and M2 anti-inflammatory) and satellite cell activation. Satellite cells fuse to form myofibres, and the myotubes are revascularized and reinnervated upon regeneration of the muscle. (Figure adapted from (65)).

1.7 Mitochondrial homeostasis in skeletal muscle

Mitochondria are adaptive organelles that are critical to the regulation of skeletal muscle metabolism and adapt in response to exercise, ageing and disease. Mitochondria contain an outer membrane, an intermembrane space, an inner membrane, and the inner mitochondrial matrix. The inner membrane is the site of ATP production and the location of mitochondrial DNA, and contains folds called cristae which serve to increase surface area (71). In addition to energy production, mitochondria also serve as a storage site for calcium, with calcium populating the inter membrane space and the mitochondrial matrix (72). Within skeletal muscle,

there are two main types of mitochondria; adjacent to the sarcolemma are the subsarcolemmal mitochondria which are key in providing ATP for membrane active transport, as well as gene transcription (73). The second type of mitochondria are located between myofibrils near the Z-lines of the sarcomere called intermyofibrillar mitochondria and are active in providing ATP to contractile proteins to facilitate contraction. Further, they play a role in calcium signalling in the muscle due to their proximity to the T-tubules and sarcoplasmic reticulum (73).

Mitochondria will adapt in response to stimuli like exercise by increasing biogenesis through activation of PGC-1α and activation of mitophagy, to increase organelle turnover and maintain a healthy pool of mitochondria; key to driving ATP synthesis through the ETS (73). Dysfunctional mitochondria are believed to be highly involved in the functional decline of muscle seen with ageing. Age-related mitochondrial dysfunction includes increased oxidative damage, decreased mitochondrial volume, and decreased mitochondrial biogenesis (74). Under normal conditions, mitochondria generate ATP through the TCA cycle and the ETS (section 1.3). The ETS is composed of multipolypeptide complexes (I-V) in the inner membrane of the mitochondria and electrons are received from carriers, NADH and FADH2 which are generated during the TCA cycle (74). During ageing, mitochondria undergo changes including reduced enzyme activity, altered respiration and decay in mitochondrial DNA (74). Additionally, the mitochondria experience phenotypic changes such as an abnormally rounded, large shape, which makes them more resistant to autophagy (75). The ageing process also alters the inner membrane, shortening cristae and homogenising the inner mitochondrial compartments. These structural changes occur in addition to reduced mitochondrial content within skeletal muscle (74).

1.8 The role of ER stress signalling in skeletal muscle

The ER is another key membrane-bound organelle responsible for the folding, processing, and post-translational modification of proteins, and is critical for protein quality control, calcium homeostasis, as well as lipid and cholesterol biosynthesis (73,76). In skeletal muscle, the ER is distinguished as specific to muscle as the SR. The SR is a membranous network throughout the cytoplasm running to the nuclear membrane and detects and transmits cellular signals. The proper folding and trafficking of proteins is crucial for cell function, and disruptions to the SR results in

accumulation of misfolded proteins and protein aggregates in the lumen of the SR. In normal conditions, foldases, and chaperones maintain proper protein folding, with incorrectly folded proteins getting degraded through autophagy or ER associated protein degradation (ERAD) (77). If misfolded proteins continue to accumulate, the unfolded protein response (UPR) will be triggered in attempts to restore ER folding capabilities. There are three main arms of the UPR: protein kinase R-like endoplasmic reticulum kinase (PERK), activating transcription factor 6 (ATF6), and inositol-requiring enzyme 1 alpha (IRE1α) (78). At baseline, chaperone protein, glucose-regulated protein 78 (GRP78) is bound to each of the three main sensors, maintaining an inactive state, but upon accumulation of misfolded proteins, GRP78 is released from all three main stress pathways, and each become activated with ATF6, and PERK being activated before IRE1α. IRE1α activation also initiates splicing of *XBP1* mRNA to *XBP1s*, which has many target genes that all act to restore ER function. Both ATF6 and PERK promote ER adaptations to folding errors, and IRE1α has a dual role in transmitting survival and pro-apoptotic signalling (77). Chronic ER stress results in a persistent UPR and induction of inflammation largely mediated by Jun NH2-terminal kinase (JNK), and nuclear factor-kappa β (NF-κβ) which are downstream of IRE1α. This ultimately leads to apoptosis through several pathways, such as IRE1-dependent decay of mRNAs (RIDD), C/EBP homologous protein (CHOP), pro-apoptotic B-cell lymphoma 2 (BCL-2) family members (Bim/Bak), caspase-12, and JNK (79). CHOP has been demonstrated to induce apoptosis through mitochondria-dependent pathway as downstream of CHOP are a category of BCL-2 proteins that are localised to the outer membrane of the mitochondria called BH3-only proteins regulate cell apoptosis (80).

Ageing impacts the ER stress signalling pathways in several ways including decreased chaperone protein (GRP78) concentration seen in aged mice, and lectins such as calnexin and calreticulin; the downregulation of calnexin has been suggested to sensitise cells to apoptosis and downregulated calnexin has been observed in aged rats (77). Other proteins such as CHOP have been shown to be upregulated with age in rodents, and elevated CHOP could be associated with increased sensitivity to oxidative damage (77). These age-related changes to ER stress response, notably the UPR have consequences for skeletal muscle, although the mechanisms are not yet clear, however in mice, ER stress has been associated with increased anabolic

resistance, or a reduced response to hypertrophic stimuli, and ER stress has been associated with impaired mTOR activity in C2C12 cells (77). As ageing demonstrates both a reduced capacity to manage ER stress and a blunted anabolic response to hypertrophy, it is likely uncontrolled ER stress has a role in sarcopenia, although this relationship still remains unclear (77). The ageing process is correlated with increased instances of misfolded proteins and accumulation of protein aggregates, as well as increased oxidative stress (81). As mitochondria are sources of ROS that can stimulate cell-signalling pathways and apoptosis. Evidence suggests dysfunctional mitochondria increase oxidative stress that inhibits function of the UPR, negatively affecting cell survival and may play a role in the pathogenesis of some neurodegenerative diseases (81). The ER stress signalling pathway is thus tightly correlated with ageing skeletal muscle as it is involved in critical pathways controlling skeletal muscle homeostasis (78,81).

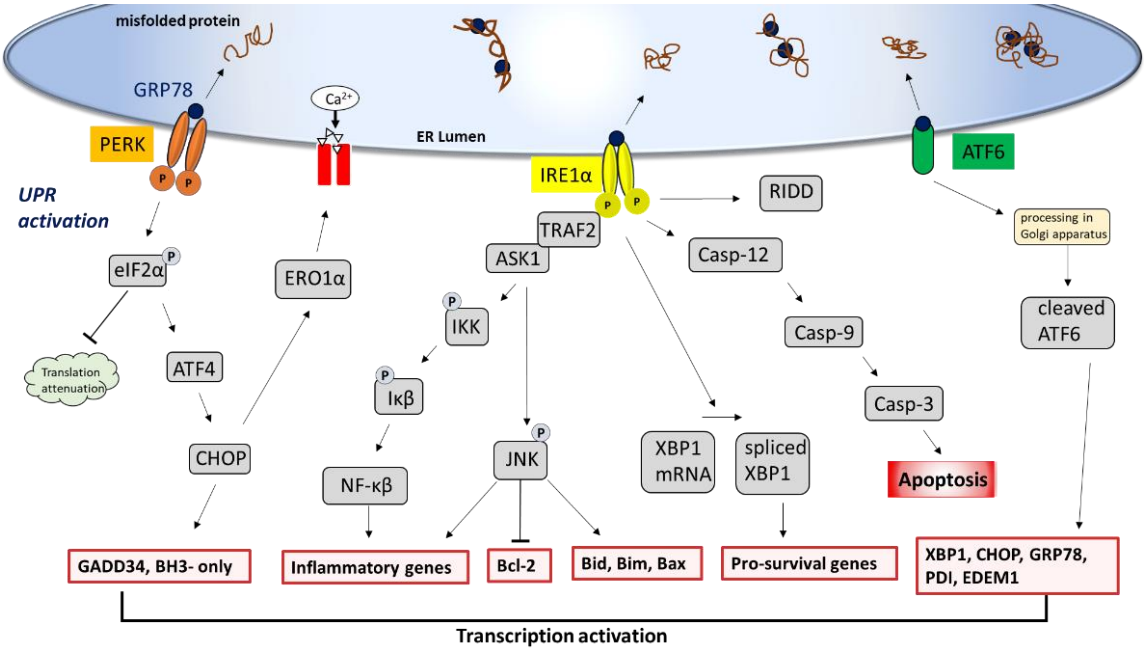

Figure 1.8.1. The ER stress response initiates the UPR *via* three transmembrane proteins. The UPR is mediated by disassociation of GRP78 from PERK, IRE1α, and ATF6. Activated PERK phosphorylates eIF2α and downstream activates CHOP. IRE1α activation similarly gets activated and induces splicing of XBP1 to XBP1s and also activates other downstream targets NF-κβ, and JNK which leads to degradation of pro-survival mRNA. Following release of GRP78, ATF6 is transported to the Golgi apparatus where it is cleaved into active ATF6, which regulates expression of key downstream genes involved in the UPR. (Figure adapted from (77)).

1.9 Skeletal muscle in disease

1.9.1 Sarcopenia

The consequences of ageing are inevitable and are characterised by large declines in musculoskeletal health including decreases to muscle mass and muscle strength. This age-related loss of muscle and strength referred to as sarcopenia, is a significant cause of frailty and a contributor to mortality in the aged population worldwide elderly (82). Diagnosis of sarcopenia is currently based on a reduction in lean body mass (83). Declining muscle mass, estimated at up to a 40% decrease in the cross-sectional area of the lower limb muscle between 20 and 80 years of age, is a significant contributor to impairments in mobility (59). The rate of muscle loss during ageing has been reported at 1-2% loss per year after age 50, with women reported to lose muscle mass at slower rates than men (59).

Sarcopenia is underpinned by progressive pathophysiological changes, which ultimately disturb muscle homeostasis. Among proposed mechanisms of sarcopenia, progressive myofiber atrophy (with type II muscle fibres potentially more susceptible to atrophy than type I fibres), alterations in satellite cell biology and therefore defective regeneration, adipose tissue infiltration, and chronic inflammation have been proposed (82,84,85).

Degeneration of neuronal cells and changes to neuromuscular junction morphology, similarly as in neuromuscular disorders such as amyotrophic lateral sclerosis (ALS), also plays a role in mediating the loss of muscle during ageing (85–89). At a cellular level, satellite cell senescence and defective autophagy have been suggested to be important players in muscle wasting (73,76) and sarcopenia and have been discussed comprehensively in a review by Larsson *et al.* (87).

1.10 Mechanisms of muscle atrophy

1.10.1 Muscle protein homeostasis

Muscle hypertrophy and atrophy are both independent, but overlapping, active processes controlled by specific signature pathways and transcriptional programs (90). During ageing and in disease, the balance between anabolic and catabolic processes in muscle is altered, resulting in a loss of muscle mass and function (82,85,90). The mTOR signalling pathway is a primary transducer of anabolic signalling in muscle

and is required for cell growth, proliferation, and autophagy suppression (section 1.6) (39), and it has been suggested that the reduced mTOR signalling in sarcopenia contributes to insulin and anabolic resistance following stimuli such as mechanical stress, insulin, and increased nutrient availability (39,91). Imbalanced protein synthesis and degradation result in either muscle hypertrophy, such as during resistance exercise, or atrophy, such as in sarcopenia, respectively. While the net loss of muscle may result in similar clinical presentation, differences exist in the underlying mechanisms contributing to muscle loss.

1.10.2 Senescence

As mentioned, autophagy is a key component to maintaining homeostasis for skeletal muscle, and dysregulation is associated with increased ROS, the elevation of which is thought to be associated with cellular senescence (92). Senescent cells have been suggested to contribute to muscle wasting through a senescence-associated secretory phenotype (SASP) (93). It has been demonstrated that removal of senescent cells can restore tissue homeostasis during ageing, therefore suggesting that targeted removal of senescent cells may provide new therapeutic opportunities for sarcopenia (94). While senescence is mainly associated with mitotic cells, replicative senescence in skeletal muscle, a postmitotic tissue, is debatable. Some reports demonstrated elevated levels of senescence-associated proteins in skeletal muscle from old mice (95). Interestingly, it has been shown that satellite cells undergo senescence resulting in their decreased regenerative potential, which may also contribute to sarcopenia development (76). Other forms of senescence-inducing stimuli also exist both intracellular, and extracellular, and likely have an impact on skeletal muscle in ageing. For example, oxidative stress, oncogene activation, and tumour suppressor loss are responsible for stress-induced senescence (96). Further, it is likely miR-mediated changes associated with ageing such as changes to miR biogenesis proteins could contribute to senescence (96).

1.10.3 Muscle regeneration

Adult skeletal muscle regeneration is largely dependent on satellite cells, the muscle stem cell population (97). Satellite cell availability and functionality determines regeneration and changes in satellite cell number have been demonstrated with ageing in both human and rodent studies (98–102). Moreover, satellite cells from older

individuals show a transcriptional profile switch, dysregulated autophagy, in addition to reduced regenerative potential (103–106). It has been recently demonstrated that satellite cells undergo irreversible senescence during ageing, thus contributing to the reduced regenerative potential of muscle in older individuals, thus satellite cells may be key to sarcopenia development (102). It has to be noted that satellite cells have been shown to be dispensable in muscle hypertrophy (107), but satellite cells in sarcopenia have been suggested to be negligible fore regeneration by others (108), thus, the degree to which satellite cells contribute to the development of sarcopenia remains to be established.

1.10.4 Fibro-adipogenic progenitor cells

A population of mesenchymal progenitor cells capable of differentiation into both adipocytes and fibroblasts, and resident in the interstitial space of the skeletal muscle fibres has been recently described. These cells called fibro-adipogenic progenitors (FAPs), are characterised by expression of markers such as platelet-derived growth factor receptor A (PDGFR-α), Sca1 (in mice) and CD34. FAPs are thought to be key for successful muscle regeneration and repair in healthy and young individuals (109). During muscle regeneration, FAPs proliferate and release signals, such as IL-6, to stimulate satellite cell differentiation (109,110). This regenerative potential might be also enforced by the differentiation of FAPs into fibroblasts, as fibroblasts are necessary for connective tissue repair of the extracellular matrix (65). However, a fibrotic scar may be formed during defective regeneration, and subsequent adipose tissue infiltration. This fatty degeneration, or myosteastosis, of the muscle is a characteristic of sarcopenic muscles (82,109).

Myosteastosis and fibrosis are mediated *via* TGF-β and PDGFR-α signalling pathways and by the activation of senescence markers such as p21 and $p16^{INK4a}$ in myofibroblasts (111,112). Uncontrolled activation and differentiation of FAPs into fibroblasts and adipocytes during muscle wasting has also been shown, resulting in infiltration of fatty tissue and fibrotic scars, limiting the proper regeneration and repair of the muscle (109,113). Age-related changes in the function of FAPs may be a yet undescribed mechanism contributing to sarcopenia development.

1.11 microRNA as regulators of molecular mechanisms of muscle

The control of signalling pathways regulating muscle hypertrophy, atrophy and regeneration occurs on the gene expression level. Among gene expression regulators are non-coding RNAs, and one class of small (≈22 nucleotides), non-coding RNAs are microRNAs (miRNAs/miRs). Found in animals, plants and some viruses, miRs negatively regulate gene expression post-transcriptionally (114). miRs regulate gene expression through degradation of mRNA transcripts or inhibiting translation and are involved in critical cell processes. The human genome is reported to have 2600 mature miRs (115) and it is believed miRs are predicted to regulate 60% of the human genome at the translational level, suggesting a role for miRs in modulating many physiological processes such as apoptosis, proliferation, and differentiation (116,117).

1.11.1 miR biogenesis: canonical pathway

As mentioned, miRs are short endogenous sequences of single-strand RNA molecules, and they are located throughout the genome and they are encoded by their own set of genes and are an integral component of the cell genetic programme, many are also evolutionarily conserved (118). Many miR genes are noncoding genes and the only transcriptional product is the miR, and others, the miR is located in the untranslated region (UTR), or within an intron of a protein coding gene (116). Roughly half of identified miRs are intragenic and processed from introns and few exons, and the other half are intergenic transcribed independent from the host gene and regulated by their own promoter. In some cases, miRs are transcribed in clusters to form a miR family (116). The biogenesis of a miR can be through canonical and non-canonical pathways (Figure 1.11.1).

The canonical miR maturation process begins with miR genes being transcribed in the nucleus by enzymes, RNA polymerase II or RNA polymerase III to produce primary miRNA (pri-miR) (119). Most miRs are polyadenylated and capped, which is characteristic of RNA polymerase II transcription. The next steps include the cleaving of the pri-miR by the endonuclease enzyme Drosha in conjunction with its RNA-binding protein, DiGeorge Syndrome Chromosomal Region 8 (DGCR8), which contains two double-stranded RNA-binding domains (119). On average, the human pri-miR contains a 33-base pair hairpin stem, two single-stranded flanking regions up and downstream of the hairpin, and a terminal loop (120). The double-stranded stem

and flanking regions are vital for DGCR8 binding and Drosha cleavage (121). This resulting precursor miR is called the pre-miR, that is next actively exported with the use of ATP to the cytoplasm *via* Exportin5 and Ras-related nuclear protein/GTP-binding nuclear protein RAN (Ran-GTP) (116). In the cytoplasm, the second processing step occurs whereby the endonuclease, Dicer along with its associated binding RNA protein trans-activation response RNA-binding protein (TRBP), cleaves off the loop sequence releasing the mature miR (Figure 1.11.1).

The product of this cleavage is an RNA duplex, named by the direction of the miR strand, thus the 5p strand comes from the 5' end of the pre-miR hairpin, whereas the 3p strand arises from the 3' end of the sequence. Both strands can be incorporated into a complex with Argonaute proteins 1-4 (AGO1-4) in humans in an ATP-dependent manner (122). Whether the 5p or 3p strand is incorporated into the RNA-induced silencing complex (RISC) as a mature miR varies. TRBP serves to identify the thermodynamic stability of the 5' end, or a 5' uracil nucleotide which is then loaded into the AGO/RISC complex as the guide strand (122). The second strand (passenger strand) is typically degraded, although might be incorporated into RISC in some circumstances (116). One example is miR-34 in humans, where both miR-34b-5p and miR-34b-3p are found in relatively equal proportions and target specific mRNAs (123). Both 5p and 3p strands can be selected as the guide strand depending on tissue type, cell type or biological state, and both 5p and 3p strands may have different biological functions (122,124). As the two strands have complementary base pairs, the individual miR strands contain different seed sequences; the seed region spans from nucleotides 2-8 canonically and is a key site of DNA target recognition (124,125).

After the miR duplex is loaded into the RISC complex, AGO protein is believed to remove the passenger strand by endonucleolytic enzyme activity (120). Passenger strand are generally unwound passively in an ATP-independent manner (126). Ultimately, the mature guide miR in the RISC complex then acts by binding to complementary mRNA sequences. This occurs usually by target recognition within the seed region of the miR, although complementary binding to the mRNA can occur along any region of the sequence (116).

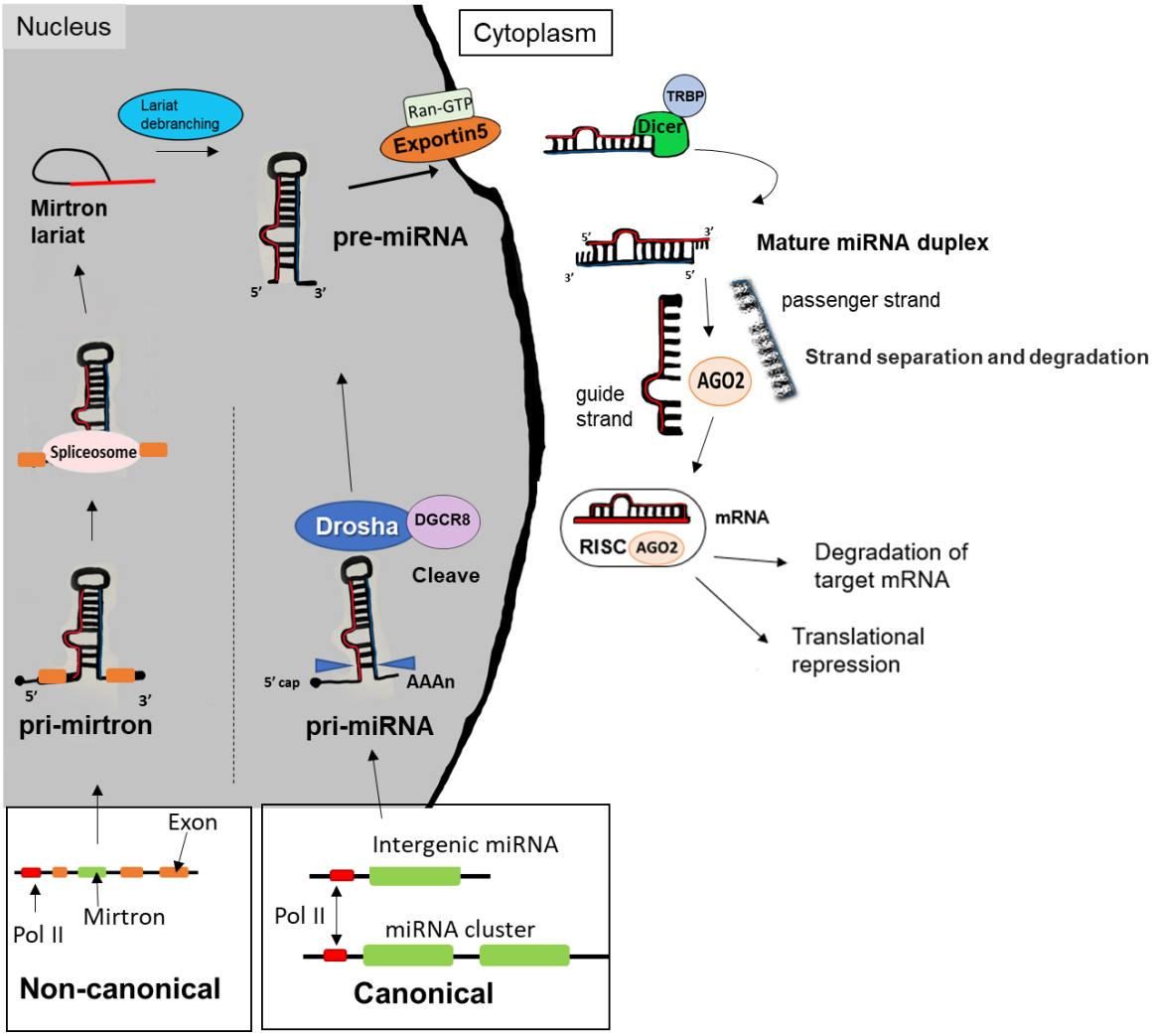

Figure 1.11.1. miR biogenesis The canonical generation of a mature miR begins in the nucleus by transcribing miR genes to generate a pri-miRNA. The pri-miRNA is processed by Drosha and DGCR8 to generate a pre-miR that is actively exported to the cytoplasm *via* Exportin5 and Ran-GTP. In the cytoplasm, Dicer and TRBP cleaves the hairpin loop to yield the miR duplex that is loaded into an AGO protein, the guide strand is selected, and passenger strand is degraded. The AGO and guide strand form the RISC complex that then can bind to its complementary target mRNA(s). The result of this binding is translational repression or otherwise target degradation. Non-canonical pathways exist such as mirtrons which are produced from introns at exon junction sites of mRNA. Mirtrons bypass Drosha and are instead the precursor miR is formed by splicing machinery and lariat debranching enzyme. (Figure adapted from (122)).

1.11.2 miR biogenesis: non-canonical pathways

In addition to the canonical miR biogenesis pathway, there exists non-canonical miR biogenesis pathways. The first major non-canonical pathway characterised and most common is known as the mirtron class of miRs, which are miRs that are located in

introns (116,127). The mirtron pathway generates pre-miR through the splicing of short introns with hairpin potential by ribonucleic protein spliceosome (128), and this splicing generates a non-linear product forming a lariat wherein the 5’ end of the intron is joined at the 3’ branchpoint. Hydrolysis of this linkage by lariat debranching enzyme yields a pre-miR that can then be transported to the cytoplasm for Dicer processing as with the canonical pathway (127).

While the canonical pathway and the mirtron pathway ultimately converge at the Dicer enzyme, Dicer-independent biogenesis of miRs has been demonstrated (129). The most well-known and unusual of these occurs with miR-451, a unique miR that has its dominant nucleotides extend across the terminal loop, a feature unique to miR-451. The stem sequence of the pre-miR is shorter (17 base-pairs) than what is required for Dicer, which, at minimum, needs >19 base-pairs and a sufficient 2-3 nucleotide overhang at the 3’ end to be a suitable substrate for hairpin cleavage; the majority of pre-miRs have a longer stem than is required by Dicer. An additional consideration that separates miR-451is the perfect base-pairing, where typically there will be several unpaired nucleotides that are thought to aid in the unwinding and degradation of the passenger strand of the miR duplex (129). Ultimately, while the majority of miRs follow the canonical biogenesis pathway, other biogenesis pathways exist that can generate fully functional miRs.

1.11.3 miR-mediated gene regulation

As stated in 1.11.1, the miR/AGO/RISC complex usually binds to its target mRNA to suppress gene expression. Most studies show miRs bind to the complementary sequence at the 3' UTR to induce mRNA deadenylation and decapping, although binding sites have also been demonstrated to exist at promoter regions as well as the 5’UTR and coding regions (116). In addition, miR binding sites determine the effect of the miR on gene expression. It is believed binding at the 3’ UTR, 5’ UTR and coding regions serve to reduce gene expression, while binding at the promoter region has been shown to induce transcription, although more research is needed to fully understand these mechanisms (Figure 1.11.2) (122). In addition to the canonical repression and degradation of target mRNA by small non-coding RNA such as miRs, gene activation can also be induced, namely by small activating RNAs (saRNA). The mode of action proposed for saRNA depends on the complementarity at the 5’ end to

the intended target. The seed sequence is similar in canonical miR tranlsational repsression in that the 2-8nt position defines the seed sequence. Similar to canonical miR mechanism of action, the saRNA is loaded into the AGO2 protein, that is then able to unwind the double strand RNA and subsequently enter the nucleus where it fomrs the assembly of the RNA-induced transcriptional activiation, similar to the RISC complex that is involved in supressing mRNA target translation (129). There is increasing evidence miRs may also activate gene expression, through targeting the promoter region, or AU-rich elements in the UTR of the target gene (130).

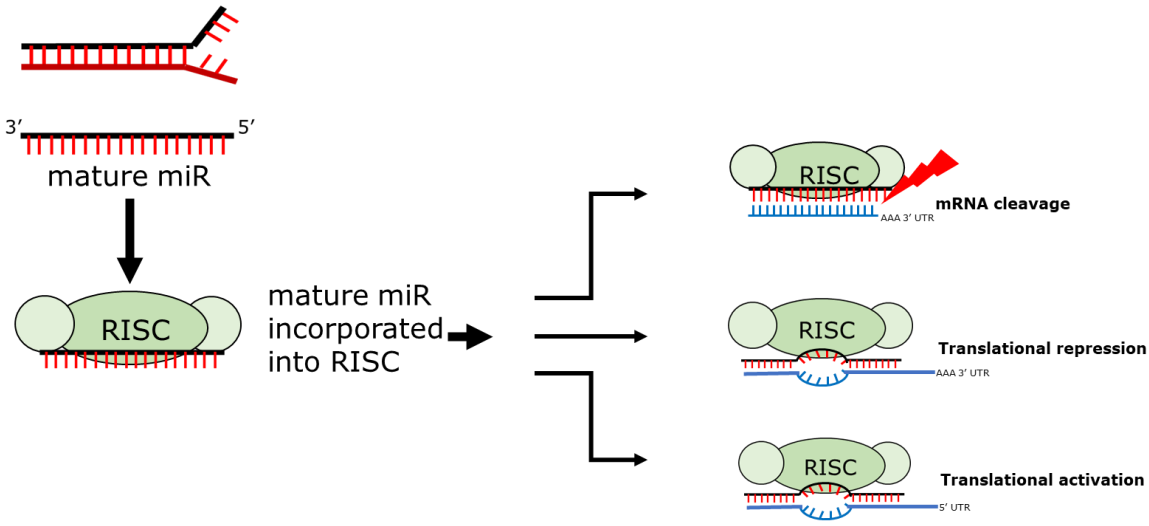

Figure 1.11.2. miR mechanisms of mRNA target interactions. The mature miR sequence is first incorporated into the AGO-RISC complex. Perfect complementarity with miR target induces mRNA degradation via enzymatic cleavage and degradation, or translational repression of the mRNA target. miR-mediated activation of mRNA targets can also be induced. (Figure adapted from (131)).

As stated, there are different methods in which miRs regulate gene expression. One of the main is through gene silencing by the miR/RISC complex binding to complementary sequences on the mRNA called miR response elements (MRE). A fully complementary miR:MRE binding activates AGO2 endonuclease activity and subsequent mRNA cleaving (122). In the majority of animal cells, the miR:MRE interactions are not completely complementary, and most MREs contain central mismatches with their miR complement which prevents the cleavage by AGO2 activity; usually, functional MRE interaction occurs via the 5' seed region of the mRNA (125). The RISC formation also involves the recruitment of the GW repeat-containing protein GW182 (TNRC6A-C in humans), which recruits effector proteins,

poly(A)-deadenylase complexes PAN2-PAN3 and CCR4-NOT which initiate poly(A)-deadenylation. Interaction between GW182 and poly(A)-binding protein C (PABPC) also promotes deadenylation (132). After this, decapping proteins, such as DCP1/DCP2 (122), and DDX6 (133), following this, exoribonuclease 1 (*XRN1*) facilitates 5′−3′ degradation (132). The mechanisms of translational repression and mRNA degradation and whether these pathways act sequentially or simultaneously is still unclear.

While most evidence has shown miRs negatively regulate gene expression, some studies have demonstrated upregulation of gene expression by miRs. This has been seen in quiescent cells like oocytes (134). Other examples include miRs binding to the 5'UTR of mRNAs encoding ribosomal protein translation and biogenesis (135). Other proposed mechanisms include RNA activation (RNAa) a process of transcriptional activation where the interaction of the miR on the promoter region triggers the recruitment of transcription factors and RNA polymerase II to activate gene transcription (134). Many miRs have been reported to promote or maintain gene expression in both human and mouse cell lines (136). This mechanism has only recently been discovered; however, but it has been shown to require the basic components of miR-mediated gene regulation: AGO, Dicer and Drosha enzymes, enriched RNA polymerase II at target sites (136). Groups of genes can also be regulated by miRs, as the 2-8 nucleotide seed sequence required for target recognition can be shared by different miRs, however, other locations within the sequence at 3' or 5' UTRs, as well as the promoter region may be binding locations for miRs, therefore it is likely many miRs can regulate groups of genes, either alone or in cooperation with other miRs (131).

1.12 Skeletal muscle and the role of miRs

The role of miRs has been implicated in the development and regulation of muscle homeostasis (137). By influencing expression of multiple target genes, miRs provide a responsive mechanism that enables cells to react to changes within their immediate or surrounding environment. Given their role as novel regulators of gene expression and their vast deregulation in a variety of pathophysiological conditions, miRs are emerging as molecular regulatory mechanisms of ageing and sarcopenia.

1.12.1 miRs in muscle development and regeneration

Myogenesis occurs during development as well as in adulthood during muscle regeneration. The cells involved in myogenesis include muscle progenitor cells from within the myotome, satellite cells, and adult skeletal muscle stem cells (138). Muscle-specific miRs have been described, such as miR-1, miR-133, miR-206, also called "myomiRs," and miR-208, miR-486, and miR-499 (139–142). The role of miRs in myogenesis has been demonstrated in Dicer, a key enzyme in miR maturation, knockout mice, which show delayed myogenesis and satellite cells unable to reach terminal differentiation (143,144). Several miRs have been associated with both muscle development and disease; for example, the expression of *PAX3* and *PAX7*, key transcription factors in early myogenesis, is regulated by miR-206 in myogenesis during development and adult skeletal muscle regeneration (143,145). Both miR-1 and miR-133 have been shown to control the SWI/SNF subunit composition (chromatin remodelling complex) during development and disease (146–148), and miR-208b and miR-499 have been demonstrated to regulate myofiber type composition (149). Satellite cell depletion, senescence, and functional decline have been proposed to be associated with the development of sarcopenia (76). Cheung *et al*. (144) have demonstrated that mice with satellite cells depleted of Dicer show reduced muscle regenerative capacity and premature muscle wasting. In a different study, the Let-7 family of miRs, a regulator of cellular proliferation and expression of Pax-7, a key myogenesis transcription factor, was upregulated in muscle of older people and has been suggested to play an important role in satellite cell functional decline during ageing (34). Finally, exogenous administration of miR-1, -133, and -206 by local injection has been shown to accelerate muscle regeneration after injury in rats, suggesting that miRNAs might be used as a therapeutic strategy against muscle damage (150).

1.12.2 miRs regulating muscle hypertrophy and atrophy

miRs have been shown to maintain muscle homeostasis in adulthood, including control of muscle hypertrophy and atrophy as well as muscle adaptation to exercise, which are all disrupted during ageing (151,152). Changes in miRs levels in muscle, for example, miR-133 or miR-206, are associated with a myriad of age-related degenerative pathologies, including muscle atrophy and ageing (34,82,153–156). Several miRs have been shown to be differently expressed in the muscle of older

humans and rodents, and several miRs have been reported to have roles in myogenesis. These miRs have been observed in both humans and mice, and include Let-7, miR-1, miR-18a, miR-16, miR-19b, miR-20a, miR-21, miR-23a, miR-27a-3p, miR-29, miR-106a, miR-133a, miR-133b, miR-143, miR-146a, miR-181a, miR-206, miR-208b, miR-378, miR-486, miR-499, miR-969, and miR-199a-5p (Appendix 1).

Some of the miRs downregulated in muscle of aged mice, such as miR-133 and miR-181, have been shown to regulate muscle hypertrophy or atrophy through regulation of anabolic pathways and Sirt-1, respectively (157–161). Sirt-1 plays an important role in regulating autophagy. Autophagy has been demonstrated to play a key role in maintaining muscle mass, neuromuscular communication, as well as stem cell stemness (162–164). Anabolic resistance, a process well-characterised during sarcopenia and immobilisation, is the inability to effectively initiate protein synthesis following the ingestion of protein or exercise (165,166). Several miRs have been shown to be upregulated following exercise and following protein ingestion (167–170). Drummond *et al.* (168) have shown decreased expression of miR-1 expression in the muscle of younger, but not older, individuals following exercise, whereas the primary but not mature miR-133a and miR-206 transcripts were differentially regulated in the muscle of young and older people. These data suggest that the lack of change in miR-1 expression in the muscle of older people following exercise and protein ingestion may contribute to anabolic resistance during ageing. With more data emerging on the capability of miRs to regulate muscle mass, it is possible that miR-based approaches could be developed into therapeutic approaches in the future (171)

1.12.3 miRs and neuromuscular communication

Deterioration of neuromuscular communication is an important aspect of muscle wasting in both ageing and disease. The expression of miRNAs miR-23a and miR-29b has been shown to be increased in skeletal muscle during ageing, and in disease, these miRs have been associated with the disruption of the mitochondrial-related gene expression in the muscle (82,187,198), and further, miR-206 has also been shown to be upregulated in a mouse model of ALS (208). ALS is the most common neurodegenerative disease in adults, characterized by muscle atrophy, denervation, and paralysis. miR-206 deficiency in these mice accelerates the progression of the

disease (208). Interestingly, the authors suggest that changes in miR-206 expression are a part of compensatory mechanism aiming at improving neuromuscular degeneration rather than a part of a mechanisms driving this degeneration (174). This proposed mechanism is associated with retrograde transport from muscle to nerve. Another study investigating communication from muscle to nerve demonstrated that myofibers can release exosomes, membranous vesicles of ~50–150 nm in diameter with roles in cell-to-cell communication, which contain miRs (174). The miR content of these vesicles was reported to change after denervation. More importantly, miRs contained within exosomes released from myofibers were taken up by other cell types and this was associated with changes in miR and its target levels in the recipient cells(174). It remains to be established whether miR-based interventions can restore neuromuscular interactions during ageing.

1.12.4 miRs and cellular senescence

While muscle is a postmitotic tissue, and therefore cells are unlikely to undergo replicative senescence, old and senescent satellite cells have been demonstrated in mice (76). Our group has demonstrated an important role of miR-143 in regulating satellite cell senescence during ageing (205). Downregulation of miR-143 in satellite cells from old mice was associated with increased cell viability; however, this was at the cost of cellular senescence, suggesting miR-143 downregulation in satellite cells during ageing may be a part of a compensatory, rather than causative, mechanism (205).

Another miR, miR-29, has been characterised as a senescence-related miR. miR-29 is increased in the skeletal muscle during ageing and enhances cellular senescence by targeting distinct pathways involved in muscle growth and satellite cell proliferation, including IGF-1, p85, and B-myb (198). However, miR-29 seems to have an antifibrotic activity in multiple tissues (197) and the loss of miR-29 in myoblasts contributes to the pathogenesis of Duchenne muscular dystrophy by promoting myoblast transdifferentiation into myofibroblasts (199). As the importance of senescence in skeletal muscle functional deterioration remains to be established, the potential of miRs targeting senescence-associated genes as therapeutics for sarcopenia remains elusive.

1.12.5 miR involvement in regulation of mitochondrial dynamics

The function of skeletal muscle, an energy-demanding tissue, is highly associated with mitochondria. Changes in mitochondrial dynamics have been previously reported, and it has been suggested that dysfunctional mitophagy and mitochondrial generation may be key to muscle atrophy (57). Several miRs have been shown to regulate the mitochondrial homeostasis and cellular metabolism (210,221,222).

For example, miR-696 has been shown to target peroxisome proliferator-activated receptor γ-coactivator-1α (PGC-1α), a transcription factor key to mitochondrial biogenesis, and its downstream effectors; pyruvate dehydrogenase kinase-4 and cytochrome c oxidase subunit II (COXIV) (219). Overexpression of miR-696 led to decreased fatty acid oxidation (219). Another study has shown miR-133a-deficient mice have decreased mitochondrial mass and exercise tolerance and lower levels of PGC-1α and NRF-1 (170). Phenotypically this is similar to sarcopenia, suggesting a role for miR-133a in maintaining mitochondrial dynamics in skeletal muscle. Furthermore, Russell *et al*. (187) demonstrated disrupted mitochondrial homeostasis with a decrease in the levels and activity of PGC-1α, NRF-1, COXIV, and ERRα in the mouse model of ALS. Another miR, miR-23, has been shown to be upregulated in mouse models of ALS (187,208), and the overexpression of miR-23 in wild-type mice has been associated with mitochondrial dysfunction similar to the animal models of ALS, suggesting a regulatory effect of miR-23 in muscle wasting during ALS (187). However, a different study found miR-23a to decrease the expression of Atrogin-1 and Murf1, ubiquitin ligases upregulated in models of muscle atrophy, with miR-23 overexpression protecting against glucocorticoid-induced atrophy (186). In addition, miR-23 expression is decreased in other models of atrophy in rat and C2C12 myotubes (188). This suggests that the mechanisms responsible for the different models of atrophy may differ, which is in line with data by Soares *et al*. (33) demonstrating that miR function is context dependent in different models of muscle atrophy.

1.12.6 miRs and Fibro-Adipogenic progenitors

Interestingly, miRs have also been shown to regulate the functionality of FAPs. For example, fibroblasts growth factor-2 has been shown to induce miR-29a expression in FAPs and in myogenic progenitors, which in turn stimulated myoblasts proliferation

(200). It has also been reported that activation of the expression of myomiRs can block adipogenesis of FAPs and enhance muscle regeneration (146) . Moreover, miR-23a overexpression has been shown to reduce lipid accumulation within the skeletal muscle by inhibiting the differentiation of PDGFR-α+ progenitor cells into adipocytes (189,223). MyomiRs have also been shown to regulate FAP functional phenotype in dystrophic mice through regulation of BAF subunits, part of the SWI/SNF chromatin remodelling complex (146). Interestingly, regulation of BAF subunits has also been demonstrated during embryonic myogenesis (148). These data suggest that miRNAs may serve potent therapeutic tools against fibrosis and fatty degeneration during sarcopenia and disease by regulating FAPs. Clearly, miRs are one of the important mechanisms underlying muscle atrophy, and investigation of miR-associated mechanisms of muscle wasting will be important to understanding their full role in the progression of sarcopenia and potential in the design of future therapeutics.

1.13 miRs as potential therapeutics

Current interventions for sarcopenia and other muscle-wasting disorders, such as cachexia, focus on progressive resistance training, orexigenic drugs, and anabolic agents (224). Recently, a dual activin-type II receptor (ActRIIA/ActRIIB) antibody inhibitor to myostatin has been shown to enhance muscle hypertrophy in mice (225), although challenges remain with respect to human clinical trials (225). Other interventions focus on either: anabolic pathways, as in androgen hormone replacement and growth hormone secretagogues such as ghrelin (224), or on inhibitory pathways such as in myostatin-blocking therapies, angiotensin receptor blockers, and β-adrenoreceptor blocking (224,226). These options are being evaluated as potential treatments for ameliorating muscle loss, however, few clinically validated options exist, demanding a need for further investigation. Moreover, the development of novel therapies for muscle wasting is somewhat slowed down by the lack of robust and reliable non-invasive biomarkers of muscle wasting, with creatine kinase being the most commonly used assay (227).

Due to their relative stability in biofluids; miRs have been shown to be stable in serum and plasma for up to 48 hours at room temperature (228) and reported changes in circulating miR levels in various muscle disorders, miRs have been proposed novel

biomarker of muscle wasting (reviewed in (227,229)). Furthermore, as miRs are small molecules with limited immune concerns, they are promising therapeutic candidates.

Investigation into miR therapies to treat challenging diseases remains an area of ongoing exploration. Two approaches are currently being used to modulate miR activity: synthetic double-stranded miRs or viral-based miR delivery to overexpress miRs and chemically modified antagomir (AM) oligonucleotides to inhibit miR function (230). Several companies have developed or are working toward miR pharmaceuticals in different fields of medical research, including cancers, metabolic diseases, neurological diseases, cardiovascular disease, inflammatory diseases, and others (209), but few miR therapies have gained clinical traction (168).

There have been thousands of miR-associated patents filed in the US and Europe, and Asia, and patents have been filed for several different diseases and targets (231). Several miR-based therapies have entered clinical and pre-clinical phases, and one miR-based therapeutic, the compound SPC3649 (Miravirsen), an inhibitor of miR-122 against hepatitis C virus (Santaris Pharma), has entered a phase II of clinical trial (232,233). Miravirsen was reported to be well tolerated with no dose-limiting toxic effects or treatment discontinuations due to adverse effects (234). The miR-34 mimic-based drug (MRX34) for treatment of liver cancer is currently in clinical phase I, and other miR-based therapeutics are in the preclinical stage (230,235). Some current pre-clinical studies include miR-15, and miR-195 for the treatment of post-myocardial infarction and miR-155 for the treatment of amyotrophic sclerosis, and miR-378 for cardiometabolic disease (231).

These studies provide encouraging evidence that pharmacological modulation of miR activity is feasible in human patients. However, issues remain with the use of miR-based therapies, particularly stability of RNA drugs (231) as well as effective delivery to certain sites such as tumour sites in the case of cancer-based miR therapeutics (236).

Identifying miR targets of interest remains an area of critical investigation, and the heterogeneity of miRNA expression continues to remain a challenge to the progression of miRNA pharmaceuticals (237). Ensuring the specificity of targets will also continue to be a challenge in limiting the potential of unwanted off-target effects and toxicity (238). New methods for improved miR target validation and

characterization of off-target effects are needed to progress the development of miR-based therapeutics. Suitable delivery systems, including tissue-specific delivery, that allow for stability and safety are also concerns facing current research in miR therapeutics. Other issues remain to be resolved, such as understanding the long-term effects of modulating miR activity in vivo, establishing efficacy and safety of miR-based therapeutics in human patients, and modelling of pharmacokinetics and pharmacodynamics of these molecules.

Dysregulated miRs in muscle ageing and multiple disorders associated with muscle wasting indicate they could be viable therapeutic targets for muscle loss. Several issues may impede this development. It appears that changes in miR expression in muscle, as well as miR function, can vary depending on the disease underlying muscle wasting. Moreover, few studies have investigated miR targets and potential off-targets in muscle and other tissues following systemic miR mimic/antagomir delivery. Indeed, functional studies of miRs in skeletal muscle during ageing or disease are still in their infancy as compared with miR research in diseases such as cancer. With local delivery not feasible due to the size of muscle tissue, tissue-specific delivery will be very important for muscle therapies to avoid delivery of miR mimics/antagomiRs into other tissues, such as liver or lungs when using systemic delivery. Therapies for muscle wasting will also require careful optimization of sufficient but safe doses of miR mimics/antagomiRs.

In summary, the rapidly expanding number of functional miR studies in muscle provides a basis for development of miR-based approaches for improvement of muscle mass and function. Despite large numbers of patents filed for therapeutic use of miRs in different disorders, very few patents have been filed to use miR-based approaches for treatment of muscle wasting, and none have been filed for sarcopenia. Much remains to be learned about the function of miRs in muscle wasting due to ageing or disease, and the optimal delivery systems for efficient and safe manipulation of miRNA activity will be key in development of miR-based therapies for muscle loss.

1.14 Hypothesis

The levels of miRs are dysregulated in skeletal muscle during ageing and disease. miRs regulate multiple signalling pathways simultaneously. We hypothesise that

modulating altered miR levels to physiological levels of miRs in skeletal muscle during ageing and disease will improve muscle mass and strength through re-balancing the activity of the molecular networks regulating muscle homeostasis, therefore maintaining muscle mass and strength in ageing and disease.

1.14.1 Objectives

The objectives of this study where:

I. Characterise changes in miR: target interactions in sarcopenia using omics and bioinformatic approaches.
II. Validate novel miR: target interactions disrupted during ageing and disease *in vitro* using immunoassays, as well as RT-qPCR to analyse relative gene expression changes and western blotting to determine protein expression changes.
III. Provide *in vivo* proof-of-principle for therapeutic potential of novel miR-199a-5p inhibitor (antagomiR) for loss of muscle mass and function.

Chapter 2. Materials and methods

2 Materials and methods

2.1 List of materials, equipment, and reagents used in this project

Name	Company	Cat Number
100 bp DNA ladder	NE Biolabs	N3231
25X dNTP Mix (100 mM)	Thermo Fisher	4368814
2-Propanol	Merck	I9516
3PRIMEG/02 48 x 0.2ml, 3 PrimeG Gradient Thermal Cycler	Techne	93945-09
4′,6-diamidino-2-phenylindole (DAPI)	Merck	268298
Acrylamide/Bis-acrylamide, 30% solution	Merck	A3699
Agarose Ultrapure	Thermo Fisher	16500
Amersham™ Protran® Western blotting membranes, nitrocellulose	Cytiva	GE10600002
Ammonium persulfate	Merck	A3678
Ammonium Persulfate	Merck	A3678
Barium chloride	Merck	342920
Bovine Serum Albumin BSA	Merck	A2153
Cell Counting Kit-8	Merck	96992
Cell culture flask, T-175	Sarstedt	83.3912
Cell culture flask, T-25	Sarstedt	83.3910
Cell culture flask, T-75	Sarstedt	83.3911
Cell culture plate, 12 well	Sarstedt	83.3921
Cell culture plate, 24 well	Sarstedt	83.3922
Cell culture plate, 6 well	Sarstedt	83.3920
Cell culture plate, 96 well	Sarstedt	83.3924
Cell scraper, 2-position blade, size: S, handle length: 24 cm, blade length: 1.35 cm, sterile	Sarstedt	83.3950
Chloroform isoamyl alcohol mixture	Supelco	25666
DMEM-high glucose	Merck	D5671

Dimethyl Sulfoxide	Merck	41639
Dulbecco's Modified Eagle's Medium/Nutrient Mixture F-12 Ham	Merck	D6421
Dulbecco's Phosphate Buffered Saline	Merck	D8537
Electric Pestle	VWR	SCERSP749540-0000
Epredia 125 ML OCT embedding cryo-embedding Matrix	Epredia	12678646
Ethanol	Merck	51976
EVOS M5000 Imaging System	Thermo Fisher	AMF5000
EVOS M7000 Imaging System	Thermo Fisher	AMF7000
F-12 media	Gibco	21765029
Fast SYBR™ Green Master Mix	Applied Biosystems	4385617
Foetal Bovine Serum	Merck	F7524
Film, free of DNase/RNase, material: PO, transparent, optimised **for qPCR**	Sarstedt	95.1994
Fisher BioReagents™ EZ-Run™ Pre-stained Rec Protein Ladder	Fisher Bioreagents	BP36031
Glycerol	Merck	G5516
Glycine	Merck	G8898
GSM Grip-Strength Meter for mice and rats	Ugo Basile	47200UB
Horse Serum	Merck	H1270
Hydromount	National Diagnostics	HS-106
Laminin	Merck	L2020
Leica CM3050 S Cryostat	Leica Biosystems	CM3050 S
Methanol ≥99.9%	Merck	34860
Mini Gel Tank and Blot Module Set	Thermo Fisher	NW2000
Minimum Essential Medium Eagle	Merck	M7278
miRcury LNA RT Kit	Qiagen	339340

miRcury LNA SYBR Green PCR Kit (4000)	Qiagen	339347
miRvana™ miRNA Isolation Kit, without phenol	Thermo Fisher	AM1561
miScript II RT Kit	Qiagen	218160
N,N,N′,N′-Tetramethylethylenediamine	Merck	T9281
Nanodrop 2000	Thermo Fisher	N/A
Odyssey® Fc Imaging System	LI-COR Biosciences	OFC-1025
omniPAGE Mini Vertical Protein Electrophoresis System	Cleaver Scientific	VS10
Owl™ EasyCast™ B2 Mini Gel Electrophoresis Systems	Thermo Fisher	B2
PCR plate half skirt, 96 well, transparent, Low-Profile	Sarstedt	72.1981.232
PCR single tube, 0.5 ml, Biosphere® plus	Sarstedt	72.735.100
Penicillin-Streptomycin	Merck	P4333
Phosphatase Inhibitor	Merck	P0044
Ponceau S	Merck	P3504-10G
PowerEase™ 90W Power Supply (115 VAC)	Fisher Scientific	PS0090
Protease Inhibitor	Merck	P8340
Protein Assay Dye Reagent Concentrate	Bio Rad	5000006
Random Hexamers (50 µM)	Thermo Fisher	N8080127
REDTaq® ReadyMix™ PCR Reaction Mix	Merck	R2523
Retinoic Acid	Thermo Fisher	10552611
RiboLock RNase Inhibitor (40 U/µL)	Thermo Fisher	EO0384
RiboLock RNase Inhibitor (40U/µL)	Thermo Fisher	EO0381
RIPA Lysis Buffer, 10X	Merck	20-188

RNAse-free water	Merck	3098
Seesaw-Rocker Large 230V	Stuart	51900-32
Sense Beta Plus Microplate Reader	Hidex	425-311
Serological pipette, 10 ml	Sarstedt	86.1254
Skeletal muscle cell GM supplemental pack	Merck	C-39360
Skeletal Muscle Cell Growth Medium	Merck	C-23060
Sodium Dodecyl Sulfate	Merck	L3771
StepOnePlus™ Real-Time PCR System	Applied Biosystems	4376600
SuperScript™ II Reverse Transcriptase kit (includes 5X First-Strand Buffer and 0.1 M DTT)	Thermo Fisher	18064014
SYBR™ Safe DNA Gel Stain	Thermo Fisher	S33102
Transfer Pipette	Sarstedt	86.1171
Triton X-100	Merck	T8787
Trizma® base	Merck	T1503
Trizma® hydrochloride	Merck	T3253
TRIzol™ Reagent	Thermo Fisher	15596018
TrypLE™ Express Enzyme (1X) no phenol red	Thermo Fisher	12604013
Tween 20	Merck	P9416

2.2 C2C12 and NSC-34 immortalised mouse myoblasts

C2C12 are an immortalised myoblast line established from an adult C3H mouse leg limb muscle (239,240). C2C12 cells were used to investigate the early stages of myogenesis and the effects of miRs on these cells.

2.2.1 C2C12

Myogenic *in vitro* assays were performed using C2C12 mouse myoblasts (Figure 2.2.1) gifted by Dr Howard Fearnhead (University of Galway) were used to assess miR influence on muscle hypertrophy and atrophy.

2.2.2 NSC-34

NSC-34 (motor neuron enriched, embryonic mouse spinal cord cells with mouse neuroblastoma) cells (Figure 2.2.1) gifted by Dr Brian McDonagh (University of Galway), to assess miR effect on nerve and neuron-like cells. All cells were cultured in T-75 flasks for a period of 2-3 days or until cells reached 70-80% confluency.

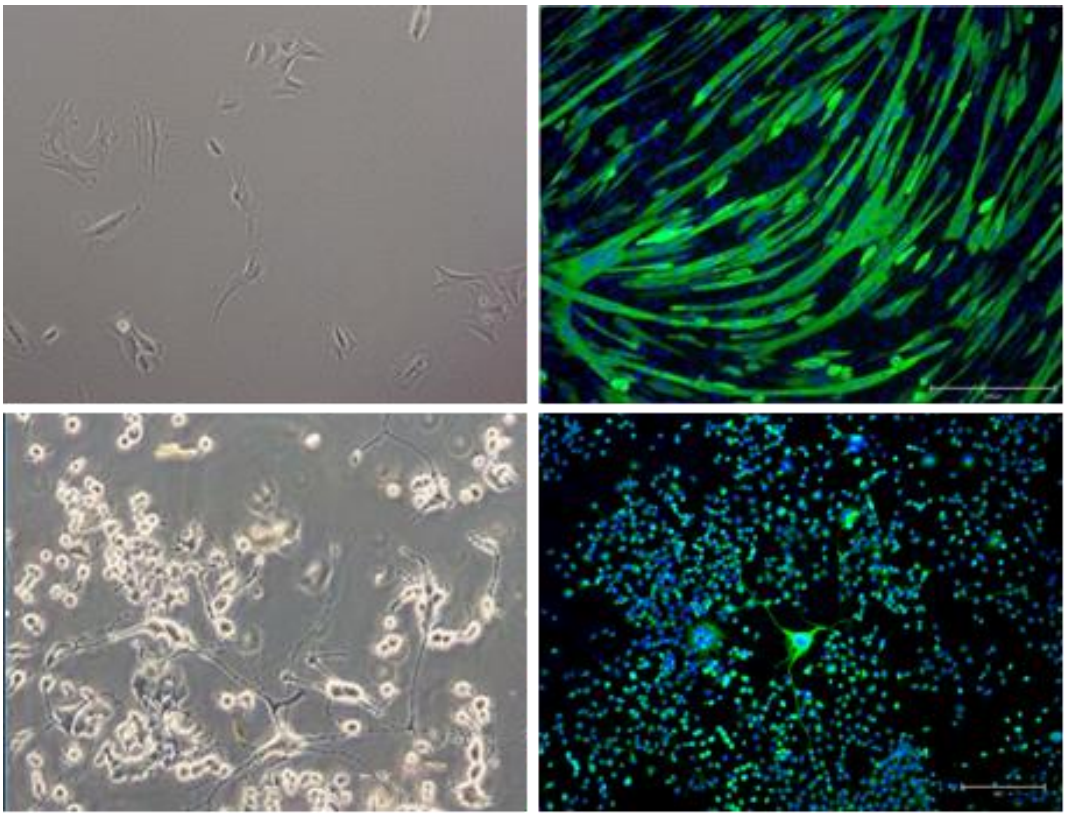

Figure 2.2.1. C2C12 and NSC-34 are capable of differentiation. C2C12 and NSC-34 cells were used in experiments as models of muscle cells, and nerve/neuron cells. Top L-R undifferentiated C2C12 cells and differentiated C2C12 cells stained with MF20 antibody. Bottom L-R undifferentiated NSC-34 cells and BIII Tubulin stained differentiated NSC-34 cells. Scale 300 µm.

2.3 Human primary myoblasts

Primary human myoblasts were isolated from biopsies obtained from adult (n=6, 30 ±2.8 years of age), and old (n=6, 69 ±5 years of age) human female donors. All donors had BMI values <25. Full information on donors is presented in 3.2.1

2.4 Cell culture media

2.4.1 C2C12 proliferation and differentiation

C2C12 cells were cultured in standard growth medium comprised of Dulbecco's Modified Eagles Medium (DMEM) High glucose: 4.5g/L (Merck D6429) supplemented with 10% foetal bovine serum (FBS) (Merck F7524) and 1% penicillin/streptomycin (P/S) (Merck P4333; as described in Goljanek-Whysall *et al*., 2012 (137)). The cells were passaged every 2-3 days, maintained at 60%-70% confluence.

C2C12 myoblast differentiation was done by culturing the cells in DMEM High glucose supplemented with 2% horse serum (HS; Merck H1270) and 1% P/S. once reached 80% confluency

2.4.2 NSC-34 growth and differentiation

NSC-34 proliferation was achieved by culturing NSC-34 cells in 10% DMEM High glucose, 1% P/S as described for C2C12 growth (2.4.1). Differentiation assays were performed with DMEM and Nutrient F-12 Ham mix in a 1:1 ratio, with additional media components being added: 1% serum (HS or FBS), 1% minimum essential medium, 1% P/S, and 1 µM all-trans retinoic acid. Differentiation was performed when the cells were allowed to reach 60%-70% confluence. Upon reaching confluency, the media was changed to the appropriate volume of DM, and the cells were allowed to culture for 7 days to differentiate.

2.4.3 Human primary myoblast culture medium

Human myoblasts were cultured in a skeletal muscle growth medium (Merck C-23060) supplemented with the skeletal muscle cell GM supplemental pack (Merck C-39360). This medium contains supplements and culture additives for skeletal muscle cells to support growth and culture conditions:

- Foetal Calf Serum 0.05 ml / ml

- Fetuin (Bovine) 50 µg / ml
- Epidermal Growth Factor (recombinant human) 10 ng / ml
- Basic Fibroblast Growth Factor (recombinant human) 1 ng / ml
- Insulin (recombinant human) 10 µg / ml
- Dexamethasone 0.4µg / ml

The media for human cells above was created by mixing the ingredients in a sterile tissue culture biosafety II cabinet and storing at 4°C.

2.5 Cell culture

For cell culture, all work was performed in a class II biological safety cabinet and all items (e.g., flasks, pipettors etc) were cleaned with 70% ethanol (ETOH) prior to being brought into cabinet workspace. Cells were seeded at a density of approximately 4000 cells cm^2 into T-75 culture flasks. For all experiments using C2C12 cells, standard 6-well plates (0.3×10^6 $well^{-1}$) and 12-well plates (0.1×10^6 cells $well^{-1}$) were used: 6-well plate = 9.6 cm^2 $well^{-1}$ 12-well plate = 3.5 cm^2 $well^{-1}$. Cells were cultured in GM and incubated in a 5% O2, 5% CO2 atmosphere at 37°C. Replacement medium or passaging of cells was performed every 2-3 days, with dissociation of cells for re-seeding or freezing performed when cell growth had reached approximately 70%-80% confluence.

For passaging of cells, dissociation was achieved using TrypLE Express (Life Technologies 12604-013), a recombinant microbial produced trypsin replacement enzyme, according to the following protocol: first the reagents were warmed to 37°C: Cell culture medium, Dulbecco's phosphate buffered saline (PBS), TrypLE Express Enzyme (1X). The media was removed from flask using sterile strippette and discarded. Next, cells were washed with PBS, 3 ml for T-75 flask. Next, the PBS was aspirated, and disposed, and 1 ml of TrypLE Express (T-75) was added and rotated throughout the flask. The TrypLE was swirled around the bottom of the dish to wash the cells, then removed immediately. The flask was incubated in sterile culture incubator (37°C with 5% CO_2) for approximately 5 minutes. Next, the flask was sharply tapped on bottom to dissociate cells. Once the cells were lifted and mobile, 10 ml of growth medium (FBS containing) was added to the flask, and cells were then seeded in new T-75 flask, or well-plates for assays. Cell seeding concentration dependent on assay to be performed (Table 2.5.1).

Table 2.5.1. Experiment layout for miR transfections

Experiment	Nr cells	Transfection	Sample collection/staining
Differentiation	10,000/well (6-well plate) or 75000/well 12-well plate	Day 1 (Day 0 – plating); Treatment + DM	Day 5 MF20 staining
Proliferation Ki67	50,000/well 12-well plate	Day 1 (Day 0 – plating); Treatment + DM	Day 2 ki67 staining
Proliferation MTT	10,000/well 96-well plate	Day 1 (Day 0 – plating); Treatment + DM	Day 2/3 MTT assay, spectrophotometer
Viability	50,000/well 12-well plate	Day 1 (Day 0 – plating); Treatment + DM; also can use 5nM TNF, IL6, IL1 or H2O2 – 50uM to induce cell death	Day 3/5 Ethidium bromide/acridine Orange staining, photographs on fluorescent microscope
Myotube atrophy/hypertrophy	100,000/well (6-well plate) or 75000/well 12-well plate	Day 5 (Day 0 – plating, Day 1 – DM)	Day 8
RNA	As above for undifferentiated or differentiated cells	Day 1 (undiff), Day 5 (diff)	48-72h after Day 1
Protein	As above for undifferentiated or differentiated cells	Day 1 (undiff), Day 5 (diff)	48-72h after Day 1

2.5.1 Cell expansion

Culture media was replaced every 2-3 days. C2C12 cells were split and passaged at 70-80% confluency to prevent unplanned differentiation of cells into terminally differentiated myotubes. NSC-34 cells were cultured as C2C12 cells, with medium changed every 2-3 days and splitting and passaging performed at 80% confluence.

2.5.2 Laminin coating for human myoblast cultures

Coating of plastic cell culture surfaces with laminin was performed in culture vessels for the purpose of culturing human myoblasts. Cells were cultured in either T-25, or T-75 flasks. Additionally, laminin coated culture plates used subsequently in immunostaining for the purpose of high-resolution visualisation of specific processes/proteins. Cells were seeded in either 12-well or 6-well plates. Prior to cell seeding, glass cover slips of the appropriate size for the wells (Table 2.5.2) were placed in the plate, and all cover slips were coated with a final concentration of 10

µg/ml of laminin (Merck Aldrich L2020) in 1X PBS and incubated at least for 10 minutes before plating the cells. The laminin was then removed completely prior to seeding the cells.

Table 2.5.2 Culture dish sizes and volume of laminin

Culture vessel	Area (per well)	Volume of 10 µg/ml laminin
35 mm dish	10 cm^2	1 ml
60 mm dish	20 cm^2	2 ml
100 mm dish	60 cm^2	4 ml
24-well plate	2 cm^2	200 µl/well
12-well plate	4 cm^2	500 µl/well
6-well plate	10 cm^2	1 ml/well
T-25	25 cm^2	3 ml/well
T-75	75 cm^2	5 ml/well

2.5.3 Cell differentiation

Cells used in all experiments were capable of differentiation into mature myotubes (terminally differentiated, multinucleated muscle cells; C2C12 cells) or neuron-like cells (NSC-34 cells). For differentiation assays, cells differentiation was initiated upon 70-80% confluency. Culture medium was changed to differentiation medium (DM) optimal for each of the different cell types used (2.2). The cells were differentiated within 5-7 days depending on the quality of the cells and differentiation speed of the cells. Flasks/wells containing cells for differentiation were first cultured in growth conditions until the required confluency and the media was then removed and cultures were supplied with the required volume of DM and cultured as described previously (2.5).

2.5.4 Cryopreservation and thawing of cells

To cryopreserve cells for later use and to generate a stock line of cells for experiments, cells were detached from the culture media using TrypLE, the collected cell pellet was next resuspended in a 90% FBS/10% DMSO freezing solution at a ratio of 0.5 ml of freezing medium per $1x10^6$ cells. From this suspension, cells were aliquoted into cryotubes at a density of $1x10^6$ cells per cryotube and placed in a

defrosted Cryo-°C freezing container (Nalgene 5100-0001). This container was quickly transferred to a -80°C freezer to achieve a -1°C/minute rate of cooling. After 24 hours, the cryotubes were then transferred to liquid nitrogen for long-term storage.

Thawing and plating of previously cryopreserved cells was performed by first adding appropriate volume of growth medium to a flask. The cells were next quickly removed from cryostorage and brought to the biosafety cabinet to thaw before being added to the culture flask. The flask was then gently rotated to evenly disburse cells and immediately incubated in sterile culture incubator (37°C with 5% CO_2) for approximately 4 hours to allow cells to adhere to flask. After cells have adhered, the media containing DMSO was removed and 10 ml of fresh growth medium (FBS containing) was added to the flask, and flask was then cultured as normal.

2.6 Treatment of cells with miR mimics or antagomiRs

To examine the function of miR in muscle or nerve *in vitro*, cells were transfected at undifferentiated or differentiated states with miR mimics or antagomiRs. miR mimics are chemically synthesised RNA molecules that function to imitate endogenous miRs. Chemical modifications and sequence changes can be included to increase the stability of the mimic. AntagomiRs (AM) are similarly chemically modified oligonucleotides that serve to block endogenous miRs by specific complementary binding. For these experiments, all miR mimics used for both *in vitro* and *in vivo* were modified with cholesterol-conjugated chemistries by their manufacturer with cholesterol passive strands and phosphothioate modified nucleotides, and 2'-O-methylation modified nucleotides to increase stability. The sequences were custom designed. A scrambled non-specific control AM sequence (Scr) was used as control for transfections.

2.6.1 Sequences of miR and antagomiR mimics

Description	**miR sequences**
Scrambled (Scr) control	5'-CUCGUUCCUGGUCGUCACCAGU-3'
miR-199a-5p miRIDIAN mimic based on mmu-	5'-CCCAGUGUUCAGACUACCUGUUC-

miR-199a-5p MIMAT0000229	3’
antagomiR-199a-5p	5’-GAACAGGUAGUCUGAACACUGGG-3’

All miR/AM mimics were diluted with RNase-free water according to manufacturer’s guide to produce a stock solution of 100 µM. To produce working concentrations, aliquots of miR, antagomiR and Scr control mimics were diluted to 200 nM ml^{-1} of medium, and 100 nM ml^{-1} of medium for miR mimics. Concentrations of miR and antagomiR mimics for both *in vitro* and *in vivo* experiments were decided based on previous lab optimisation by the Whysall lab (241), and miR incubation times were also decided based upon previous lab data from the Whysall lab (241). For *in vitro* experiments, phenotype measurements were performed as described in Table 2.5.1. For i*n vivo* experiments involving sarcopenia, IV miR delivery was delivered in 2 injections over 3 weeks (days 1, 10), and for muscle regeneration experiments, IV miR delivery was delivered in 3 injections over 4 weeks (days 1, 8, 15) to account for the increased turnover observed in muscle regeneration and to allow for consistent dosing of miR mimics.

2.7 Immunostaining of cells *in vitro* following miR transfection

Immunostaining was used to as a means of detecting specific targets of interest in samples. These targets have relevance to muscular and neuromuscular ageing and disease.

2.7.1 Antibodies and stains used for all immunostaining

Antibody	**Manufacturer**	**Cat Number**
2H3 (neurofilament marker)	Developmental Studies Hybridoma Bank	AB2314897
Alexa Fluor 488nM (highly sensitive green-fluorescent dye)	Thermo Fisher	A21042
Alexa Fluor 647nM conjugate (highly sensitive red-fluorescent dye)	Thermo Fisher	B35450

Anti-beta III Tubulin antibody	Abcam	ab7751
Anti-CHOP	Cell Signalling	L63F7
Goat anti-Mouse IgM (Heavy chain) Cross-Adsorbed Secondary Antibody, Alexa Fluor™ 488	Thermo Fisher	A21042
IRDye® 680LT Goat anti-Mouse IgG Secondary Antibody	Li-COR	92668020
IRDye® 800CW Goat anti-Rabbit IgG Secondary Antibody	Li-COR	92632211
MitoTracker™ Green FM	Merck	M7514
Myosin Heavy Chain MF20 antibody	Developmental Studies Hybridoma Bank,	MF20-C
Anti-SV2 (synaptic vesicle marker)	Developmental Studies Hybridoma Bank	AB2315387
Anti-VDAC (voltage-dependent anion channel)	Cell Signalling	D73D12
Wheat Germ Agglutinin (WGA), Fluorescein	Vector Labs	FL-1021
Hoechst 33342 Dye	Merck	
4′,6-diamidino-2-phenylindole (DAPI)	Merck	268298

2.7.2 Immunostaining general protocol

The basic procedure for immunostaining cells was performed as a method of detecting specific protein targets of interest in samples. Immunostaining was performed on cells and tissues. Antibodies used in the immunostaining protocols in these experiments were tagged with fluorophores to visualise where the antibody binds (242). The basic procedure for immunostaining was performed by first removing all media from the wells. The cells were next washed with PBS for 5 minutes. The samples were next fixed by incubating cells with ice-cold methanol for 5 minutes. The cells were next washed 3 times for 5 minutes in PBS. Following this, the samples were blocked using an appropriate blocking solution to limit non-specific antibody binding; generally: 1%

BSA, 10%HS, 0.3M glycine in PBST (PBS+ 0.1% Tween 20). Blocked for 30 minutes to 1 hour. After blocking, primary antibody: (1:500 in diluted 2% block) was added and incubated 2-24 hours (4°C). Cells were next washed 3 times for 5 minutes. The secondary antibody: (1:2000 in diluted block) was next added and incubated, covered, at room temperature for 45 minutes to 1 hour. Cells were next again washed 3 times for 5 minutes before incubation with DAPI: 1:10,000 in PBS). Cells were finally washed for 5 minutes. If coverslips were used, they were next mounted on glass slides with hydromount and allow to dry overnight at room temperature before storage at 4°C and Imaging.

2.7.3 MF20 immunostaining

The MF20 antibody can be used to detect myosin II heavy chains, which are a marker of myogenic differentiation in skeletal muscle (243). MF20 immunostaining was performed on C2C12 cells to visualise the differentiation capabilities of the cells when transfected with miR mimics. MF20 positive stained cells were assessed by myotube diameter, overall area, and fusion capabilities to determine the effect of miR treatment on size and myogenic potential.

To perform MF20 staining, all media was removed from wells, and briefly washed by gently pipetting a small volume of cold PBS against the wall of the well to rinse all excess media. The PBS was removed and fixed in ice cold, 100% methanol for 5 minutes. The methanol was then removed, and the samples blocked in 10% horse serum in PBS for 1 hour on a rocker at room temperature. The block was then taken off and the samples were incubated for 2 hours with primary antibody MF20 (1:500 in (2% horse serum in PBS)). The primary antibody was recovered, and the cells were washed 3 times for 5 minutes in PBS before the secondary (anti-mouse 488, (1:2000 in (2%)) was added and allowed to incubate covered at room temperature for 45 minutes. The secondary antibody was removed, and the wells were washed 3 times for 5 minutes in PBS once more before a final incubation for 10 minutes covered at room temperature with DAPI (1:10,000 in PBS). The wells were washed once more for 5 minutes in PBS, covered before adding fresh PBS to cover each well sufficiently and stored in 4°C until Imaging. All Imaging was performed within three weeks to ensure the best images possible.

2.7.4 MitoTracker Green staining to assess mitochondria

The MitoTracker Green stain is one of several mitochondria specific dyes to label mitochondrial proteins. MitoTracker Green is a fluorescent dye used to bind free thiol groups of cysteine residues belonging to mitochondrial proteins on live, non-fixed cells(244). The main output for analysis is fluorescence is mean or median fluorescence intensity, which allows for image analysis to be performed and comparisons made between control and miR-treated groups.

The MitoTracker Green protocol was performed by first making Hanks' Balanced Salt Solution (HBSS; 1 litre):

Component	**Amount**	**Concentration**
Sodium Chloride (mw: 58.44 g/mol)	8 g	0.14 M
Potassium Chloride (mw: 74.55 g/mol)	0.4 g	0.005 M
Calcium Chloride (mw: 110.98 g/mol)	0.14 g	0.001 M
Magnesium Sulphate Heptahydrate (mw: 246.47 g/mol)	0.1 g	0.0004 M
Magnesium Chloride Hexahydrate (mw: 203.30 g/mol)	0.1 g	0.0005 M
Sodium Phosphate Dibasic Dihydrate (mw: 177.99 g/mol)	0.06 g	0.0003 M
Potassium Phosphate Monobasic (mw: 136.09 g/mol)	0.06 g	0.0004 M
D-Glucose (Dextrose) (mw: 180.16 g/mol)	1 g	0.006 M
Sodium Bicarbonate (mw: 84.01 g/mol)	0.35 g	0.004 M

Working in biosafety II cabinet at all times until Imaging, the media was first removed from cells and washed in sterile HBSS for 3 minutes. Next,Hoechst dye (1:10,000 in HBSS) was added, incubated in tissue culture incubator for 5 minutes. The Hoechst stain was then removed and cells were washed in HBSS quickly.Next the MitoTracker Green (1:10,000 in HBSS) dye was added and the plate incubated in tissue culture incubator for 30 minutes. Finally, the dye was removed and wells washed in HBSS for 1 minute. Fresh HBSS was added and live cells were imaged using the EVOS microscope.

2.7.5 Tubulin staining of NSC-34 differentiated cells

Tubulin staining was performed on differentiated NSC-34 cells to assess the effect of miR treatment on neuron growth, as βIII Tubulin may be used as a biomarker for neural cell differentiation (245), and anti-β III Tubulin antibody staining can be used as a neuronal marker in cells.

For NSC-34 cells, the protocol for βIII Tubulin staining was performed by first removing all media from wells and then rinsing gently in PBS. Samples were next fixed in methanol for 5 minutes. Before being washed in PBS again for 3 minutes. After this, samples were blocked in 10% HS in PBS for 30-60 minutes on rocker at lowest speed. Next, the block was removed and primary antibody – βIII Tubulin (1:750 in 2% block) was added and allowed to incubate for 2 hours. The primary antibody was recovered, and the cells washed 3 times for 5 minutes in PBS. Next, the secondary antibody, anti-Rat (1:2000 in 2% block) was added and incubated for 60 minutes covered at room temperature. The secondary was then removed, and the samples were wash 3 times for 5 minutes in PBS, covered before being stained with DAPI (1:10,000 in PBS) 5 minutes, covered. Finally, samples were washed 2 times for 5 minutes in PBS, covered before being imaged with the EVOS microscope Imaging system.

2.8 Immunostaining of muscle tissues

Muscle tissues which were cryopreserved and cryosectioned were stained to determine effect of miR or antagomiR on tissues at the muscle level. Morphological changes to fibre size, as well as changes related to muscle regeneration and damage can be visualised and assessed to determine hypertrophy or atrophy of the muscle. Staining was also performed to assess NMJ characteristics and the effect of miR treatment on NMJ morphology.

2.8.1 Wheat Germ Agglutinin (WGA) fibre staining

The size of muscle fibres of mice was assessed using WGA to investigate the effects of miR treatment on muscle fibre size. WGA sections were cut cross-sectionally to provide a view at the fibres from this orientation. WGA staining allows for visualisation of membranes and nuclei within the muscle. The procedure for WGA staining was performed by first taking samples to -20, after which they must not be allowed to go back into lower temperatures. Samples were allowed to air-dry for 5-10

minutes, and each section was marked with a hydrophobic pen to create a barrier around the section. A quick wash in PBS was performed before fixing the samples in ice-cold methanol for 5 minutes. Slides were then blocked in PBS containing 10% FBS for 10 minutes. Next, slides were incubated with WGA (1:2000 in PBS), and DAPI (1:10,000 in PBS) for 30 minutes covered. Finally, 3 washes for 5 minutes each were performed with PBS before mounting cover slip with hydromount. From here all samples kept covered and at 4°C.

2.8.2 Neuromuscular junction (NMJ) staining of longitudinal muscle sections

Longitudinal sections were taken and then stained for specific neuromuscular components of interest to examine the effect of miR treatment on the neuromuscular junction and related structures. As the NMJ runs along the muscle longitudinally, cross sections are insufficient for Imaging of the NMJ, and longitudinal sections must be made to visualise the nerve and the NMJ in the correct anatomical position. Sections were made with a cryostat (Leica) as described in 2.15.6.

The procedure for NMJ staining of longitudinal sections was performed by first allowing sections to air-dry for 5 mins, and then marking the contours of sections with a hydrophobic barrier pen. Slides were then washed with PBS 3 times for 5 minutes at room temperature, and next permeabilised and blocked with PBS containing 1% Triton-X, 4% BSA, 1% goat/donkey serum (depending on secondary needed) for 2 hours at room temperature. Following blocking, slides were incubated with primary antibodies (made up in 10% block solution) overnight at 4°C (pan-axonal neurofilament marker 2H3 – 1:50; SV2 synaptic marker – 1:50). Slides were kept covered. The next day, the slides were washed 3 times for 10 minutes with PBS and then incubated with secondary antibodies ((488nm) -1:1000 in same block as primary) and incubated covered for 2 hours at room temperature. Samples were again washed 3 times for 10 minutes in PBS. Next, the samples were incubated with α-bungarotoxin conjugate 647 (1:500 in same block as primary/secondary) for 1 hour at room temperature. Finally, slides were washed 3 times for 10 minutes with PBS and glass cover slips were mounted with hydromount.

2.9 RNA isolation

RNA was isolated from cells and tissues (skeletal muscle, sciatic nerve). RNA isolations were performed with either a TRIzol/chloroform method on cells or

utilising a manufacturer kit (miRvana) for the isolation of total RNA from mouse tissue. The miRvana kit was used to isolate RNA from skeletal muscle and to yield the most amount of RNA possible.

2.9.1 RNA isolation from cells using TRIzol/chloroform method:

All work with TRIZol and chloroform was performed in a biosafety fume cabinet, and all equipment was cleaned with ETOH 70% prior to use to avoid potential RNAses and contaminants. Plates containing cells from culture room were brought to fume hood along with TRIzol and chloroform. The medium was removed and TRIzol was added directly to the cells in the plates: 1ml T75 flask,0.5 ml/well T25 flask or 6-well plate,0.3 ml/well 12-well plate. Using a cell scraper, all the cells from the plate were scraped into the TRIzol and transferred to a new labelled 1.5 ml Eppendorf one well for each sample tube. Chloroform was added to each of the tubes (200 µl for a 6-well plate, and 100 µl for a 12-well plate) and the tube was shaken vigorously by hand for 15 seconds before being incubated for 5 minutes at room temperature. The samples were then centrifuged at maximum speed (15,000RCF) for 15-30 minutes in a 4°C centrifuge. The aqueous phase with RNA was transferred into a new Eppendorf. The RNA was precipitated by adding 100% isopropanol to the aqueous phase (500 µl for 6-well plate or flask and 250 µl for a 12-well plate), and incubating at room temperature for 15-30 minutes before another 15 minutes in 4°C centrifuge at max speed. The supernatant was removed and discarded. The RNA was then washed by adding 100 µl of 80% ethanol and centrifuged at 15,000g at 4°C for 2 minutes. The supernatant was next removed as above, and centrifuged briefly – 15,000g 4°C for 30 seconds. The tubes were then allowed to air dry for 5-10 minutes at room temperature. The RNA was then suspended in 10 µl of RNase-free water. Samples were finally assessed with the NanoDrop2000 spectrophotometer.

2.9.2 RNA isolation protocol using miRvana kit

RNA isolation protocol with miRvana kit utilising kit components was performed to provide increased purity and yield of total RNA from tissue samples such as skeletal muscle and nerve. Prior to beginning, all surfaces and pipettors were cleaned with ETOH 70% or RNAse AWAY to disinfect surfaces from potential RNAses and other contaminants.

The protocol for miRvana RNA isolation is the same for both cells and tissues. First, Acid-Phenol: Chloroform was added in a volume that is equal to the lysate volume before the addition of the miRNA homogenate additive. Volumes used were 100 µl volume for 12 or 6-well plate, 300 µl volume for muscle tissue. The sample was next vortexed for 30-60 seconds and centrifuged at room temperature for 5 minutes at 10,000g. Next, the aqueous top phase was transferred to a sterile Eppendorf noting volume recovered, and add chloroform to aqueous phase, 100 µl per 500 µl of aqueous phase. The sample was then incubated 5-10 minutes on ice and then centrifuged at max speed for 15 minutes at 4°C. The top phase was saved and removed for next steps.A heating block was used to pre-heat Eppendorf of RNase-free water to 95°C. The isolation was then followed by adding ethanol in the amount of 1.25x the volume of the aqueous phase. For each sample, a filter cartridge was placed in a kit collection tube for each tube. The lysate/ethanol mix was pipetted up and down and added into the filter cartridge, centrifuged for 15 seconds at 10,000 RCF. The flow-through was discarded, and repeated until all the mixture passed through the filter. The collection tube was reused for washing steps. Next, 600 µl of Wash Solution 1 was added to filter cartridge and centrifuged for 10 seconds, and an additional 500 µl of Wash Solution 2/3 was repeated with another 15 second centrifuge. After discarding the last flow-through from the last wash, the column was spun once more to ensure all material was taken through the column. The filter cartridge was added to a new collection tube and 100 µl of pre-heated (95°) water was added. The tube was then centrifuged quickly through to collect the elution in the collection tube and stored at -20°C. The RNA concentrations were then checked on the NanoDrop2000 spectrophotometer.

2.9.3 NanoDrop2000 assessment of RNA quality

All RNA samples used in experiments were tested using a NanoDrop2000 spectrophotometer for quality. Purification was confirmed using absorbance ratios. Both 260/280 and 260/230 demonstrate the purity of the RNA in the sample. The absorbance ratio 260/280 was used as a means of detecting protein contamination: when ≥ 2.0, it indicates purer RNA, similarly the absorbance ratio 260/230, when

smaller than 2.0, indicates contamination potentially caused by organic compounds absorbing at 230nm (246).

2.10 cDNA synthesis from isolated RNA

RNA was then used to create cDNA for qPCR applications; cDNA synthesis (mRNA) was performed using 500 ng RNA and SuperScript II (Thermo Fisher Scientific), and cDNA synthesis(microRNA) was performed using 100 ng RNA and miRCURY LNA RT kit. Both applications were subsequently used for qPCR.

2.10.1 cDNA synthesis for mRNA cDNA:

All work was done on ice, and all materials and reagents were kept on ice throughout the experiment.In PCR-grade tubes cDNA reaction tubes, each sample was generated with 500 ng of RNA in 10 µl of total volume in nuclease-free H2O. To this, 1 µl of random hexamers was added. The master mix was prepared, with 10% overage for pipetting. For each reaction the following was prepared:

Reagent	**Volume (per reaction)**
RT Buffer	4 µl
DTT	2 µl
dNTP	1 µl
Superscript II	1 µl
Ribolock	1 µl

Samples were next run in thermocycler at 65° for 10 minutes, then paused and immediately placed on ice for the addition of the master mix at a volume of 9 µl per reaction. The programme was resumed and run at 42° for 60 minutes. Upon completion, the samples were diluted 10X (180 µl H2O) and stored at -20 until use.

2.10.2 cDNA synthesis for miRCURY miR cDNA

RNA yields were used for cDNA synthesis of miRs. Due to miRs small size, special considerations need to be taken before further techniques such as qPCR are

performed. To ensure good quality cDNA synthesis of miRs, the miRCURY LNA RT Kit was used to provide a single-step solution to generating miR cDNA.

The UniSp6 RNA spike-in was resuspended on initial use by adding 80 µl nuclease-free water to the tube, which was then mixed by vortexing and spun down. The aliquot was incubated 20–30 min on ice to completely dissolve the RNA spike-in. The template RNA and 5× miRCURY RT Reaction Buffer were next thawed on ice. RNase-free water was thawed at room temperature (15–25°C).Immediately before use (not earlier as the enzyme s temperature sensitive), the 10x miRCURY RT Enzyme was removed from the freezer. Each sample template was adjusted to provide RNA at a concentration of 5 ng/µl and a PCR tube was used for each reaction. The reverse transcription master mix was then prepared on ice as follows:

Reagent	**Volume (per reaction)**
5x miRCURY RT buffer	2 µl
RNAse free water	4.5 µl
miRCURY RT Enzyme mix	1 µl
synthetic RNA spike in	0.5 µl
10ng RNA	2 µl

After the master mix was thoroughly mixed, 10 µl of master mix was added to each reaction tube. Using a thermocycler (3Prime), the samples were run as follows: 60 minutes at 42°, followed by 5 minutes at 95° (to inactivate reverse transcriptase). Immediately cool to 4° and add 590 µl of H2O prior to use. Samples were stored at -20°.

2.11 Real-time quantitative PCR (RT-qPCR)

Real-time quantitative polymerase chain reaction (qPCR) was used to detect and quantify gene expression of miR targets with relevance to skeletal muscle and nerves. Changes in gene expression, (increase or decrease) in response to different miR treatments can measured by measuring cellular changes at the mRNA level.

Table 2.11.1. List of primer sequences used for qPCR

Gene	Sequence
18s F	5’ –CGG CTA CCA CAT CCA AGG AA GG – 3’
18s R	5’ –CCC GCT CCC AAG ATC CAA CTA – 3’
Acvr2a F	5’ –AAG ATG GCC TAC CCT CCT GT- 3’
Acvr2a R	5’ –GGT GGT CCT GGG TCT TGA GT- 3’
Acvr2b F	5’ –CCC ACT TCA GGA CAA GCA GT- 3’
Acvr2b R	5’ –GGC AGC AAT GAA CTG CAA CA- 3’
Atg5 F	5’ –TCA GCT CTT CCT TGG AAC ATC AC – 3’
Atg5 R	5’ –TCT GCA GTC CCA TCC AGA GC – 3’
B2M F	5’ – GGA GAA TGG GAA GCC GAA CA – 3’
B2M R	5’ – TCT CGA TCC CAG TAG ACG GT – 3’
Cav2 F	5’ –GAT CCC CAC CGG CTC AAC- 3’
Cav2 R	5’ –CAC CGG CTC TGC GAT CA- 3’
Chop F	5’ –CTG CCT TTC ACC TTG GAG AC- 3’
Chop R	5’ –CGT TTC CTG GGG ATG AGA TA- 3’
Cox IV F	5’ –TTC TTC CGG TCG CGA GCAC- 3’
Cox IV R	5’ –GCT CTG GAA GCC AAC ATT CT GC- 3’
Cox1 F	5’ – CAC TAA TAA TCG GAG CCC CA – 3’
Cox1 R	5’ – TTC ATC CTG TTC CTG CTC CT – 3’
Gap43 F	5’ – AGG CTC ATA AGG CTG CGA CC – 3’
Gap43 R	5’ – CTG GGG CTG CAT CGG TAG TA – 3’
Grp78 F	5’ –CGA GTC TGC TTC GTG TCT CC – 3’
Grp78 R	5’ –CAC ACC GAC GCA GGA ATA GG – 3’
Hdac9 F	5’ –AGC AAT AAG GAA AAG GCT GG GA – 3’
Hdac9 R	5’ –ATC AGA AGG GCT GAC GGT T– 3’
LC3B F	5’ – CAT GCC GTC CGA GAA GAC CT – 3’
LC3B R	5’ – CGC TCT ATA ATC ACT GGG ATC TT GG – 3’
Nd1 F	5’ – CCT ATC ACC CTT GCC ATC AT – 3’
Nd1 R	5’ – GAG GCT GTT GCT TGT GTG AC – 3’
Nrf1 F	5’ – GCA CCT TTG GAG AAT GTG GT – 3’
Nrf1 R	5’ – CTG ACG CTG GGT CAT TTT GT – 3’
Nrf2 F	5’ – TGG GCC CTG ATG AGG GGC AGT G –

	3’
Nrf2 R	5’ – TCC GCC AGC TAC TCC AGG TTG G – 3’
p62 F	5’ – GAG GCA CCC CGA AAC ATGG – 3’
p62 R	5’ –ACT TAT AGC GAG TTC CCA CCA- 3’
Pgc1-α F	5’ –TTC CAC CAA GAG CAA GTAT – 3’
Pgc1-α R	5’ –CGC TGT CCC ATG AGG TATT – 3’
S29 F	5’ – ATG GGT CAC CAG CAG CTC TA – 3’
S29 R	5’ – GTA TTT GCG GAT CAG ACC GT – 3’
Sirt-1 F	5’ –GAT GAC AGA ACG TCA CAC GC- 3’
Sirt-1 R	5’ –ACA AAA GTA TAT GGA CCT ATC CGC- 3’
Smarcd1 F	5’ –TGC AGG GAC CTC AAG ACGA- 3’
Smarcd1 R	5’ –CCC AGG GCT TGC TCT AAC TC- 3’
Tom20 F	5’ – AGT CGA GCG AAG ATG GTGG – 3’
Tom20 R	5’ – GCC TTT TGC GGT CGA AGT AG – 3’
Xbp1 F	5’ –GAA CCA GGA GTT AAG AAC ACG- 3’
Xbp1 R	5’ –AGG CAA CAG TGT CAG AGT CC- 3’
miRCURY primers	
Snord68	YP00203911
UniSp6	YP00203954
miR-199a-5p	YP00204494
miR-199a-3p	YP00204536
miR-199b-5p	YP00204152

2.11.1 Standard RT-qPCR procedure

All reagents and procedures were kept on ice at all times. The primers were diluted in H2O from stock primers 1:10 to achieve working concentrations. A master mix was created to include 10% volume overage:

Reagent	**Volume**
10uM Primer F	0.3-0.5 µl

10uM Primer R	0.3-0.5 µl
2x FAST SYBR Green	5 µl

The PCR plate (on ice) was loaded with the required volume of master mix (5.6-6 µl) for each well in which a reaction was to take place. Samples were loaded in triplicate or duplicate. Next,5 µl of diluted cDNA was added to each reaction well. Each new group of cDNA should have 2 housekeeping genes ran prior to running first target gene of interest to ensure cDNA quality (S29, B2M, S18, U6 etc). The plate was covered with PCR optical filmand then spun for ≈30 seconds in PCR plate spinner. The run method for standard qPCR was as follows:

Set run in StepOne Plus PCR machine:94° 10 mins,40 cycle annealing:95° 10 sec,58-64° (default 60°) 15 sec ,72° 20 sec. Melt curve 55° to 95° in 0.5° increments and then plate read.

Melt curve data was recorded and assessed to ensure primer specificity for each plate. Analysis of RT-qPCR was performed utilising comparative Ct method and relative quantification. Housekeeping genes, *β2M*, and *S29* were used and assessed graphically to ensure a stable baseline reference gene, with ±2 cycles being used as the cut-off range for housekeeping Ct values. For analysis, the difference in the ΔCt values between the experimental and control samples (ΔΔCt) was calculated. The fold-change in expression of the gene of interest between the two samples was equal to $2^{(-\Delta\Delta Ct)}$. This method was used for all RT-qPCR experiments.

2.11.2 qPCR protocol for miRs using miRCURY kit

For some applications, miRCURY qPCR was used to detect miR levels in samples. This kit utilises specific sequences that are designed for the miR target of interest, which was used to get increased specificity.

As with other qPCR applications, all reagents and samples were kept on ice. Primers were initially diluted on first use by spinning down and suspending in 200 µl of nuclease-free water. A master mix was prepared using manufacturer's protocol:

Reagent	**Volume**

2X miRCURY SYBR Green	5 µl
PCR Primer Assay	1 µl
ROX Dye	0.5 µl
RNase-free H20	0.5 µl

The master mix (7 µl per reaction; noted volumes are for StepOne PCR machines only as per manufacturer specs) was added to all reaction wells, and 3 µl of diluted cDNA was added to wells, loading samples in duplicate or triplicate. The plate was covered inoptical PCR adhesive film and spun in plate spinner for 30 seconds. After this, the plate was run using a special run method as follows:

Step	**Time**	**Temperature**
Initial activation	2 min	95°
2-step cycling		
Denaturation	10 sec	95°
Annealing & Extension	60 sec	56°
Number of cycles	40X	
Melt curve		60°-95° (0.5° increments)

Analysis was performed using standard gene qPCR analysis techniques previously mentioned.

2.11.3 Visualisation of PCR products using gel electrophoresis

Agarose gel preparation for electrophoresis was performed by mixing 3g Agarose powder and150 ml Tris-Borate-EDTA (TBE).The solution was microwaved for 1.5-2 minutes to dissolve the agarose powder in the buffer, before being stirred and allowed to cool slightly. Next, SYBR safe (1:10,000, (15 µl)) was added, and the solution was stirred rapidly to distribute. The mixture was then poured into the agarose cuvette and the required comb was inserted and allowed to set for 1 hour. The combs were next removed, and the tank was filled with running 1X TBE buffer. The wells were then loaded by adding 1.5 µl of 50-100 bp ladder into first well, and then sample wells with sample PCR product in 11 µl volume. The gel was allowed to run at 120V for 1 hour 20 minutes before being imaged on theLI-COR Odyssey Fc 600nm (Blue) channel.

2.12 Muscle tissue processing *in vivo*.

2.12.1 Processing of frozen muscle

From previously dissected, frozen muscle tissue (TA, or GAS), whole muscle samples can be broken down and used for protein and RNA analysis to investigate the effects of miRs at protein and gene levels respectively.

The basic protocol for processing frozen muscle tissue was performed by first assembling the required tools: sterile scalpel, spatula, forceps, ceramic mortar, ceramic pestle, and samples on dry ice in foam cooler box. Using forceps, the muscle was held in place and a scalpel was used to shave the tissue down as much as possible, working inside mortar, within cooler of dry ice. Next, a pre-chilled pestle was used to pound slices of muscle tissue into a fine powder, as small as possible. Muscle powder was divided in half; half was scraped with spatula into a sterile Eppendorf to later use for protein applications (Figure 2.12.1).

Figure 2.12.1. Processing of frozen muscle tissue using handheld method. Frozen muscle samples were pulverised using a chilled mortar and pestle, and the powdered muscle was then split in half for protein and RNA applications.

The remaining half of muscle was scraped into sterile Eppendorf and processed as follows:

- For TRIzol method, added 1 ml of TRIzol. This volume is sufficient for typical amounts of muscle.
- For miRvana kit, place in Eppendorf with 500 µl- 1 ml of kit-provided *Cell Disruption Buffer*. Homogenise using motorised disruptor.

Samples were then frozen at -80°C until later use or proceeded to RNA isolation method required and continue as protocol.

2.12.2 RNA isolation from muscle using TRIzol

The TRIzol RNA isolation process was performed on muscle by first cleaning all work surfaces and pipettors with 70% ETOH or RNase AWAY prior to beginning. If muscle stored was in RNAlater, muscle was rinsed with water, and then quickly frozen in dry ice or isopentane/LN2. Previously frozen muscle was processed as described in 2.12.1. Volumes of for muscle tissue were as follows:

- 1 ml TRIzol/ sample
- 200 µl chloroform for 1 ml of TRIzol

First, chloroform was added to each of the TRIzol-containing tubes; 200 µl chloroform for 1 ml of TRIzol, the tube was then shaken vigorously by hand for 15 seconds, and then incubated for 5 minutes at room temperature. Samples were then centrifuged at 15,000RCF (maximum speed) for 15-30 minutes at 4˚C.The aqueous phase with the RNA was transferred into a new clean Eppendorf being careful not to take the medium while phase as it contains proteins such as RNases that degrade RNA. The RNA was then precipitated by adding 100% isopropanol to the aqueous phase (500 µl for 1 ml TRIzol) and then being incubated at room temperature for 15-30 minutes. Samples were next centrifuge at 15,000RCF at 4°C for 15 minutes and the supernatant was removed and discarded. The RNA was then washed by adding 100 µl of 80% ethanol and centrifuge at 15,000RCF at 4°C for 2 minutes. The supernatant was removed once again, and the sample centrifuged for 30 seconds to remove excess ETOH. The sample were allowed to air dry for 5-10 minutes at room temperature, before being resuspended in 10 µl of RNase-free water. NanoDrop2000 was used to assess RNA quality and all samples were kept at -80°C.

2.13 (246)Protein Isolation

2.13.1 Basic procedure for protein isolation of cells and tissues

Protein isolation is a critical step in analysing miR influence on protein levels in cells and tissues. All the steps for protein extraction were carried out on ice, to prevent proteases' activity and preserve protein content of the sample.

Reagents:

- RIPA Lysis Buffer 1X (*0.5M Tris-HCl, pH 7.4, 1.5M NaCl, 2.5% deoxycholic acid, 10% NP-40, 10mM EDTA*)
- Protease Inhibitor Cocktail [1 µl per 1000 µl of Buffer]
- Phosphatase Inhibitor [1 µl per 1000 µl of Buffer]
- Electric Pestle
- ETOH 70%
- Cell Scraper

Procedure for isolation of protein from cells was performed by first removing all media from wells,and then washing cells briefly with cold PBS to remove all remaining media. The PBS was then removed, and ice-cold RIPA 1X buffer supplemented with protease inhibitor (1:1000) and phosphatase inhibitor (1:1000) was added. For cells, 80-100 µl of RIPA buffer to be used for 6-well plates based on confluency. For tissues, 500 µl to 1ml of RIPA was used based off amount of muscle used. For cells in plates, using a new cell scraper for each condition (e.g., Scr, miR), the cells were scraped and collected into a sterile Eppendorf for each replicate. Thecell suspension was then homogenised for 30 seconds on ice using handheld electric pestle. Tissues samples were homogenised similarly within the Eppendorf and on ice until well homogenised. The Eppendorfs were then centrifuged at 4ºC for 5 mins at 12000g/RCF. Thesupernatant containing isolated protein was transferred to a new sterile Eppendorf and stored at -20°.

2.13.2 Protein quantification assay (Bradford)

The Bradford protein assay is used to measure the concentration of total protein within a sample and was used to provide consistency across samples.

Materials and methods

Reagents:

- Bradford Reagent (Diluted 1:4 in H2O)
- Protein Standards (Stock BSA 10 mg/ml, diluted 1:1000 in H2O before making standard dilutions)
- Protein Samples (Diluted 1:500-1:1000 in H2O)

The protein quantification assay was performed by preparing the protein samples 1:500-1:1000 in new Eppendorfs. The BSA standards were then prepared by diluting the stock BSA 1:1000 in H2O before creating the following list of standards:

Standard	H20(µl)	BSA(µl)
0	1000	0
1	900	100
2	800	200
3	700	300
4	600	400
5	500	500
6	400	600
7	300	700
8	200	800
9	100	900
10	0	1000

Next, following dilutions, 100 µl of previously diluted Bradford reagent was loaded into each well of a 96-well plate. The standards were next loaded in quadruplicate at a volume of 100 µl in the top rows: A, B, C, D, running from left to right. Next,100 µl of diluted sample was loaded to the bottom four rows of the plate E, F, G, H, in quadruplicate and running from left to right. Next, the plate was loaded into the Hidex plate reader and read at 595nm. The data was next put into excel where it can be analysed.

The absorbance of the BSA standard was plotted. The best fit of the data was determined using the equation "y=mx" where y = absorbance at 595 nm and x = protein concentration (Figure 2.13.1 Representative image of BSA standard. BSA standards were graphed, and protein content of Bradford assay was then compared against standards to quantify protein content in the sample..

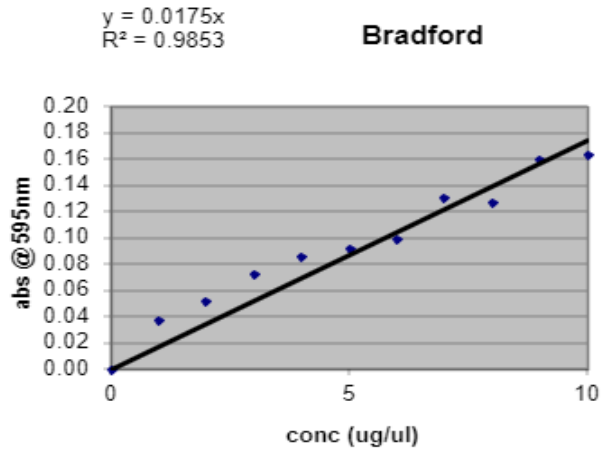

Figure 2.13.1 Representative image of BSA standard. BSA standards were graphed, and protein content of Bradford assay was then compared against standards to quantify protein content in the sample.

It was ensured the line passed through (0,0), and the data for the standard curve were correct for the calculations, higher R^2 value denotes tighter fit to line. The sample with lowest protein content was selected and the rest of the samples were diluted to the to the same level of concentration of protein as with the lowest value. The original samples were diluted with Laemmli buffer to get them all to the same concentration.

Laemmli Sample Buffer (4X)

1.25 ml 1M Tris pH 6.8

3.0 ml glycerol

1.0 ml 20% SDS

1.0 ml β-mercaptoethanol (BME)

5 mg bromophenol blue

Total volume was brought to 10 ml with MQ-H2O and stored at –20°C.

2.14 Western blot

Western blot was used to detect levels of specific proteins in a sample. Gel electrophoresis is used to separate proteins by molecular weight, and the gel can then be transferred to a membrane and incubated with various antibodies to detect protein changes as a result of miR treatment.

2.14.1 Western blot reagents:

10X (Running) Buffer (pH 8.3) was made by combining 30.3 g, Tris Base 144.0 g Glycine, 10.0 g SDS and dissolving materials in total volume up to 1,000 ml with

MilliQ-H2O (MQ). The buffer was next stored at 4°C, and diluted before use 1:10 (1X, 100 ml + 900 ml).

Resolving Buffer (1.5M Tris-HCl, pH 8.8) was made by dissolving Tris base in 80 ml of MQ-H2O. The pH was adjusted to 8.8 with HCl. Total volume was brought to 100 ml with MQ and stored at 4°C
Stacking Buffer (0.5 M Tris-HCl, pH 6.8) was made by adding Tris HCl dissolved in 60 ml MQ-H2O, next, the pH was adjusted to 6.8 with HCl. Total volume was brought to 100 ml with MQ and stored at 4°C.

Ammonium Persulfate (APS) was added to aid in gel polymerisation, a 10% APS working solution was made by dissolving100mg ammonium persulfate in 1 ml MQ-H2O; made just prior to casting gels.

Stacking gel (4%)

- 3.05ml H2O
- 0.65ml Acrylamide/Bis 30%
- 1.25ml Stacking Buffer
- 0.05ml 10% SDS
- 25 µl 10% APS
- 5-7 µl Tetramethylethylenediamine (TEMED)

Gel was made by mixing components just prior to casting in gel to prevent premature polymerisation.

The following (Table 2.14.1, Figure 2.14.1) were used to provide consistent gel percentages for repeated experiments requiring specific molecular weights.

Table 2.14.1. Volumes of gel reagents for two gels by gel percentage

Gel %	Water (ml)	30% Acrylamide/Bis (ml)	Resolving Buffer (ml)	10% SDS (ml)	10% APS (ml)	TEMED (ml)
4	8.5	1.82	3.5	0.140	0.090	0.020
5	7.9	2.38	3.5	0.140	0.090	0.020
6	7.47	2.8	3.5	0.140	0.090	0.020
7	7.05	3.22	3.5	0.140	0.090	0.020
8	6.5	3.78	3.5	0.140	0.090	0.020
9	6.07	4.20	3.5	0.140	0.090	0.020
10	5.65	4.62	3.5	0.140	0.090	0.020
11	5.09	5.18	3.5	0.140	0.090	0.020
12	4.67	5.60	3.5	0.140	0.090	0.020
14	3.69	6.58	3.5	0.140	0.090	0.020

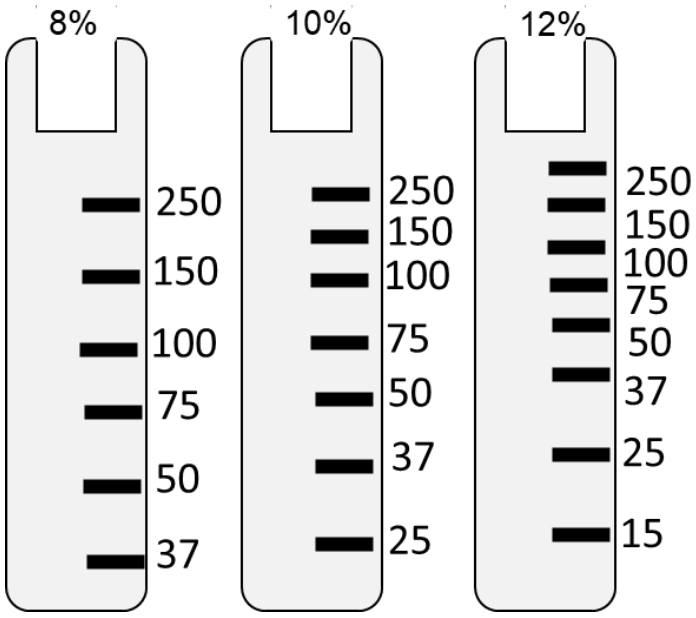

Figure 2.14.1. Gel percentages and molecular weight guide

Ponceau S Stain was made for staining membranes for total protein loading. The stain was made with 0.1 % Ponceau in 5% acetic acid. Membranes were incubated in a small volume (1-3 ml) until bands were visible. The membranes were then washed vigorously with methanol-containing transfer buffer to remove stain.

Transfer buffer (25 mM Tris pH 8.3, 192mM Glycine)
10X Transfer (500ml)was made by dissolving 72g Glycine and15g Tris Base in H2Ofor 1X concentration (500ml),100 ml Methanol was combined with50 ml 10X transfer buffer and topped up to 500 ml with MQ-H2O

Tris-Buffered Saline (TBS)
TBS was made by combining 20 mM Tris, with150 mM NaCl(pH 7.4).

10X TBS (1L)
A 10X TBS solution was made my dissolving 24g Tris Base, 88g NaCl,in 800-900ml of MQ-H2OpH to 7.4 and then topping up to 1 litre.

TBS-T 1X
TBS-T 1X was made by combining 900 ml MQ-H2O with 100 ml 10X TBS and0.5 ml Tween 20.

10% (w/v) SDS

Made my dissolving 10g SDS (Lauryl Sulphate) in 90ml water with gentle stirring. The total was brought to 100 ml with MQ-H2O and stored at room temp.

Block 3% Milk (100ml)

Blocking solution was made by adding 3.0g evaporated milk powder in 80ml TBS-T, and then topping up to 100 ml with TBS-T.

2.14.2 Gel preparation for western blot applications:

First, glass casting plates were assembled and watertight seal was ensured by adding water and examining for leaks. This was done as the resolving gel was being made. A gel percentage that would facilitate the size of the proteins of interest was used for each protein. Standard gel percentage was 12% with a 4% stacking gel. When casts were set and sealed, half the gel mix was added to each cast/plate. A small bit of butanol and water (200 µl) mix was added to the top of each gel to create an even line and prevent evaporation. The resolving gel was set for 1 hour. After the resolving gel set, the top of the gel was rinsed with H2O. The stacking gel (4%) was added to each cast. After loading stacking gel, the required combs were inserted and allowed to set an additional 30-60 minutes. After the stacking gel has set, the gel was loaded and run. The running tank was filled with 1X running buffer. The combs were carefully removed, and samples were loaded right to left starting with molecular weight ladder. Typical volume for molecular weight marker 3-5ul.Sample volume to load per well 20-30 µg. The gel was then run at 80v until into the resolving gel (approximately 30-45 mins) and then adjusted to 120v. Total gel time was an additional 2 hours after adjusting to 120v. Gels were run until samples reached bottom of the cast for complete gel run. After the run, the casts were opened, and the gel was removed under running deionised water prior to the transfer.

2.14.3 Gel transfer (semi-dry) and blotting procedure:

A total of 6 filter papers and one blotting membrane were used per gel. The amount required is dependent on type of transfer and equipment. Three above and three below

the gel and membrane (Figure 2.14.2) were used to ensure a good confirmation and transfer of proteins.

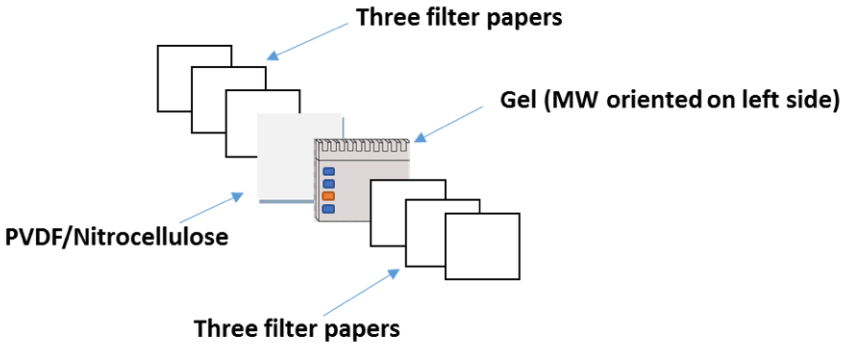

Figure 2.14.2 'Sandwich' layout for semi-dry gel transfer. A total of 6 different filter papers were used for each gel to ensure sufficient contact between surfaces.

The stack was assembled and placed in the transfer unit (Cleaver Scientific) and the entirety was sufficiently covered with a small amount of transfer buffer 1X .The stack was as: 3 filter papers, membrane, gel, 3 filter papers, and cover entirety with a small amount of transfer buffer. Ensuring it was completely saturated with buffer, the stacks were then rolled with a roller to remove bubbles. Each gel was run at 100 mA per gel for 60 to 75 minutes. After run completion, membranes were next incubated in ponceau stain for approx. 1-2 mins. After incubating in ponceau, membranes were then imaged to maintain as a representation of protein loading and to be used for image analysis. The membrane was then rinsed with deionised water and small amount of transfer buffer to remove residual ponceau. Membranes were then blocked for 1 hour at room temperature on a rocker with 3% milk in TBS-T.

Membranes were next incubated in primary antibody overnight in cold room on rocker. Primary antibody 1:1000 diluted in block. The following day, 3x10-minute washes in fresh TBS-T were performed, and the membranes were next incubated rocker for 1 hour at ambient temperature and covered with the appropriate (anti-mouse or anti-rabbit, etc.) secondary antibody diluted in TBS-T. Fluorescence AB (Li-Cor) 1:10,000-1:25,000 (kept covered from light.). Next the secondary was removed and3x 5-minute washes in fresh TBS-T were performed. Finally, the membrane was covered in an additional 2-3 ml of TBS-T and kept covered at 4°C until imaging.

2.14.4 Imaging blots using LI-COR and Image Studio Lite

All western blot images were obtained using a LI-COR Odyssey Fc Imaging system and Image Studio Lite software (v5.25). Exposure times were set at 10 minutes for all Imaging runs. Images were then exported as TIF files. All subsequent image analysis was performed with ImageJ, by performing densitometry as described by Stael *et al*. (247). All data were normalised to ponceau stain of total protein prior to statistical analysis.

2.15 Procedures and methods for *in vivo* experiments

2.15.1 Animals used for experiments

All experiments described here were approved by the University of Liverpool Animal Welfare and Ethical Review Body (AWERB) and performed in accordance with UK Home Office guidelines under the UK Animals (Scientific Procedures) Act 1986, and by the National University of Ireland, Galway Animal Welfare Body (AWB) and in accordance with the guidelines set by the Health Products Regulatory Authority (HPRA; project authorisation P091).

Mice used in all experiments were wild-type C57Bl/6 males obtained from Charles River (Margate), maintained under specific-pathogen free conditions. All animals were housed in polypropylene cages of 2–6 littermates. Animals were kept on standard 12-hour light/dark cycles at 21±2°C and fed standard RM1 maintenance diet *ad libitum* (No.1; Special Diet Services, Witham UK). Each treatment group had 8-10 mice; power analysis was performed as in Goljanek-Whysall *et al*. (160). For each experiment, n = 3-7 biological replicates per group, unless stated otherwise. Ages for mice were defined as adult: 5-9 months old. old: 18-24 months old, unless stated otherwise.

Ageing of mice was performed to provide a murine model of sarcopenia. Male C57BL6/J mice at approximately 24 months old were used as muscle loss is significant at this age. Old mice were used as the simplest and most representative model of ageing (248). Delivery of miRs was performed as described in section 2.15.4. Barium chloride injection was used to injure the muscle of the gastrocnemius muscle to provide a murine model of muscle regeneration.

2.15.2 Dissection and tissue collection

Mice were culled by anaesthetic overdose and cervical dislocation 4-weeks after the first treatment, and tissues were immediately collected. Each lower limb muscle, organs and sciatic nerves were removed and weighed. Samples were either frozen at -80°C for later sample processing (RNA and protein isolation) or placed in OCT and snap frozen in isopentane/LN2 for later histology

2.15.3 The role of miR-199a in NMJ homeostasis *in vivo*

Manipulation of miRs *in vivo* was used to assess the effect of miR treatment on skeletal muscle and the neuromuscular junction. To manipulate miR-199a-5p levels, mice were injected with either: Scr control, miR-199a-5p mimic, or antagomiR-199a-5p mimic, at a concentration of 2mg/kg bodyweight every other week during the experimental period. All mimics were delivered intravenously by tail vein injection under general anaesthesia as described (section 2.15.4).

2.15.4 Intravenous (IV) injections *in vivo*

Injections were performed in vivo to deliver miR mimic agents to the animal via intravenous injection of the tail vein. The following materials were readied prior to the procedure:

- Sterile PBS
- Isoflurane anaesthesia
- 30g insulin needle (1/2-5/8 inch)
- 1ml insulin syringe
- PPE: Fully gowned, goggles.

All miRs were injected each at 0.5mg/kg dose (total dose 2mg/kg BW), total volume 50ul, or sterile PBS saline solution as negative control. The animal to be injected was first placed within the induction box to induce general anaesthesia (oxygen flowmeter to 0.8 to 1.5 L/min. 3% to 5% Isoflurane for induction). After confirmation animal was asleep via pedal reflex, the animal was placed on maintenance anaesthesia 0.4 to 0.8 L/min. Isoflurane vaporiser to 2 to 2.5%). The animal was then moved to a nose cone mask and the tail was palpated to locate the lateral tail veins. The tail was then straightened with the non-injecting hand, and the needle was inserted bevel facing up at an approximate 30-degree angle into either the right or left tail vein. Once the

needle was inserted, the needle was briefly aspirated to ensure the location of the injection, and upon confirmation, the substance was slowing injected into the vein.

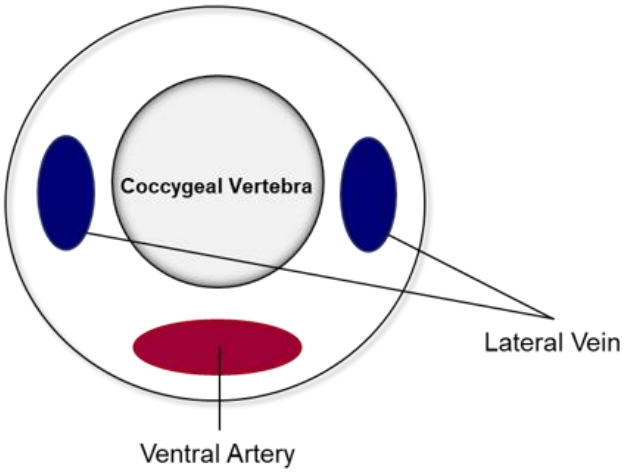

Figure 2.15.1. Cross section of mouse tail highlighting lateral tail veins for IV injection.

Once the injection was complete, the needle was removed and disposed of in sharps bin. The animal was then given oxygen to recover if required, and then placed in the warming incubator for recovery, or until the animal could be returned to the animal holding room.

2.15.5 Assessment of tissues following miR delivery *in vivo*.

Assessment of tissues following *in vivo* experiments was performed after 3 weeks for the sarcopenia model, and after 4 weeks for the regeneration model, to provide data on skeletal muscle and the responses of miR manipulation. Tissues were assessed by histology, using cryosections to visualise the muscle. Histology of skeletal muscles and joints was performed as follows to visualise and assess skeletal muscle morphology:

Skeletal muscles (gastrocnemius, tibialis anterior, and quadriceps) were first dissected. Muscles were cut in half laterally, covered in OCT compound and then immediately snap frozen in isopentane/LN2, if they were to be used for sectioning. For each animal the muscles from one hindlimb were processed for histology whilst the other was used for downstream applications. The samples were kept at -80° until sectioning. Muscles were cryosectioned (transverse) at 8-10 µm thickness using a

cryostat (Leica) (2.15.6). Serial sections were collected using glass slides and allowed to air dry. On completion of sectioning, slides were frozen in -20°C until further staining. Sections were nextfixed using ice cold methanol and stained with WGA and DAPI as described in 2.8.

2.15.6 Cryosectioning of muscle tissue

Sectioning of frozen muscle tissue was performed to visualise the muscle both cross sectionally and longitudinally (Figure 2.15.2). The fibres were then immunostained to assess the changes to the muscle with the introduction of miR mimic or antagomiR mimic. The protocol for the cryosectioning of muscle was performed by first obtaining the required safety equipment, lab coat, gloves, and optionally, cut-resistant gloves. Care was taken to ensure the sliding window was not open for long at any point to avoid accumulation of moisture and to ensure maintenance of proper chamber temperature (-21 to -23°C). The samples were first removed from the -80 freezer and left inside the cryostat for at least 30 minutes to allow the samples to come to the temperature in the cryostat (-22/-23°C). After this point samples can only be kept at -20 degrees. Using OCT compound, the samples were oriented on the cutting blocks and coated in OCT to hold them in place before being allowed to solidify in the cryostat. The tissue was then securely attached to the block before mounting the block onto the specimen head inside the cryostat. Next, thedesired section thickness was selected.Cross sections were taken using 8-10μm thickness for muscle section (WGA/NMJ).

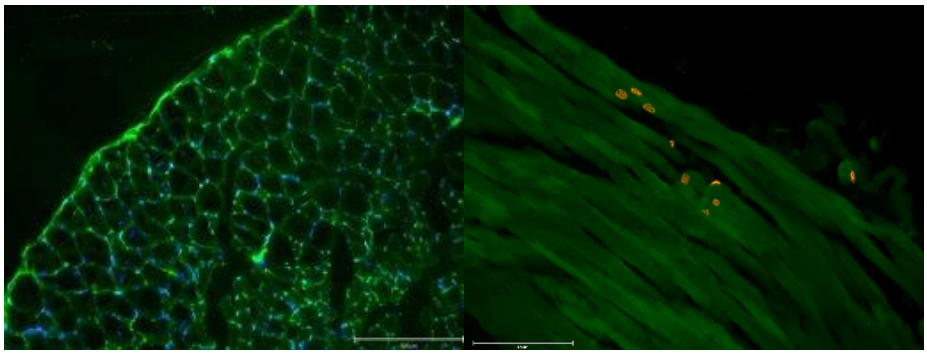

Figure 2.15.2 Section examples of muscle tissue. Skeletal muscle from mice was cryosectioned in different orientations. Cross sections (L) and longitudinal sections (R) were taken for histology.

Once accurately aligned, the tissue was trimmed (by choosing TRIM option) at higher thickness (e.g., 20 µm) until the area of interest was reached.The anti-roll plate was used for collecting good quality sections. Sectioning was then begun by slowly turning the handwheel to yield full slices of the tissue. The section was adhered to the glass slide by touching the surface to the section taking care not to move or tear the section. Sections were taken from entire muscle belly, including near origins/insertions, and main belly of muscle. A standard light microscope (located in the vicinity of the cryostat) was used to quickly assess the quality of sections prior to commencing full muscle sectioning. Samples were then kept at -20° until they were stained and imaged.

2.16 Target selection of miRs

All target searches were performed through the MIENTURNET tool. Targets for miRs were predicted using TargetScan v.8.0 (https://www.targetscan.org/vert_80/) and miRWalk (http://zmf.umm.uni-heidelberg.de/apps/zmf/mirwalk2/) using mouse and human searches and broadly conserved miR target site settings. MiRBase database (Release 22.1) was used to search and compare miR sequences, unless otherwise stated.

2.17 Statistical analysis

Statistical data are represented as mean ± SEM. For comparisons of means between two groups, (*i.e.*, adult and old) (249) in humans and mice (section 3.3), data normality was assessed using GraphPad prism, and for all normally distributed data, an unpaired (as there were no pairwise comparisons), two-tailed, Student's t-test was performed using Prism version 5.03 software package for Windows (GraphPad Software, www.graphpad.com), with p-value < 0.05 considered as statistically significant. The data that was found to not be normally distributed was analysed using non-parametric analysis in GraphPad as described in (249).

For comparisons between three or more groups, (sections 4.3, 5.3, 6.3), normality was assessed, and for all normally distributed data, a one-way analysis of variance (ANOVA) was performed. Non-parametric analyses were performed in instances of data that was not normally distributed. One-way ANOVA was used to compare means of three groups, with one treatment variable (249) (miR treatment), as we were only interested in the effect of miR-199 overexpression or inhibition. A Dunnett’s post-test

was performed to compare the treatment groups (miR-199, and AM-199) with the control group (Scr). Adult and old mice were analysed separately to ensure treatments were only compared within age groups. One-way ANOVA analyses for qPCR, protein and image analysis were performed using GraphPad Prism version 5.03, with p-values ≤ 0.05 considered statistically significant.

2.18 Microscopic Imaging

2.18.1 Immunostaining microscopy

Images of well plates, flasks, and slides were all created using the EVOS microscope Imaging system. The EVOS M5000, and EVOS M7000 systems (Thermo Fisher) were used for imaging. Fluorescence microscopy for immunostained sections was also performed using these systems, and utilised the EVOS GFP light cube (AMEP4951), EVOS DAPI light cube (AMEP4950), or EVOS Cy5 light cube (AMEP4956), to image green, blue, or red channels, respectively. Images were taken at 10X or 40X magnification. At least 5 images were taken per each image. Images were exported as TIF files. Semi-automated quantification followed by manual correction was performed using ImageJ for the purpose of muscle section analysis (WGA). MF20 immunostaining was quantified using ImageJ to manually count myotubes containing 2 or more nuclei, and the threshold tool and line tool were used to calculate area, and diameter, respectively. For NSC-34 immunostaining, ImageJ was used along with the free ImageJ 'NeuriteTracer' plugin to quantify neurite length. Statistics were calculated using one-way ANOVA with Dunnett's post-test to compare Scr controls to miR-199 and AM-199 treatment. All statistics were performed as described in 2.17.

2.18.2 Western blot

Western blots were imaged using the LI-COR Odyssey Fc imager, using 700/800nm channels depending on secondary antibody species. Exposure time was set at 10 minutes for each blot. Intensity of bands was determined against total protein as determined by quantification of ponceau stain, and normalised. Statistics were performed using one-way ANOVA and Dunnett's post-test (described in 2.17).

Chapter 3 Changes to miR-199a-5p expression levels in ageing

3 Changes to miR-199a-5p expression levels in ageing

3.1 Introduction

The consequences of ageing include progressive muscle atrophy, loss of functional capacity, and diminished regenerative capabilities *via* molecular changes; many of which might be driven by changing miR levels (250). As mentioned previously (1.11), miRs have been demonstrated to play key roles in maintaining homeostasis of all major body systems, and it is likely the ageing process is correlated to miR levels disruption seen in aged organisms. Upregulation or downregulation of miRs, especially specific miRs driving transcriptional regulation of key ageing genes control muscle, oxidative stress, neurodegeneration, and inflammation (250). Gene dysregulation and the associated musculoskeletal changes, such as muscle loss, ultimately leads to increased incidences of frailty and reduced functional capacity.

Gene transcript expression profiling show differentially expressed genes associated with ageing include metabolism, mitochondrial function, and cellular senescence (151). It has been proposed that one of the driving factors of ageing is modifications to mRNA processing. Gene enrichment data has also shown that the most robust pathways associated with ageing involve mRNA binding, mRNA processing and RNA splicing (298). It has therefore been reported that miRs may possibly explain the modification levels of genes that control splicing; miRs have been shown to regulate proteins encoding for mRNA stability, translation, and splicing (299). Previous studies from our group show miR and mRNA expression profiling performed on the tibialis anterior (TA) muscle of adult and old mice demonstrated miRs upregulated and downregulated in muscle during ageing (158).

Other miRs with roles in muscle such as miR-181a, miR-133a, miR-26a, miR-499 have demonstrated roles in muscle during ageing with consequences to age-related genes like *Sirt1* (158). The role of miR-199a-5p has been observed in cardiac muscle to regulate autophagy through targeting Atg5 in cardiac muscle and increased miR expression was related to myocardial hypertrophy (251). The role of miR-199a-5p has been studied little in skeletal muscle, however current literature suggests miR-199a-5p expression is induced in muscular dystrophy and has been identified as a regulator of the Wnt signalling pathway, a highly conserved pathway and one of the central mechanisms regulating tissue morphogenesis during embryogenesis and repair (252).

Further literature supports dysregulated miR-199a-5p gene in mice is associated with increased incidence of some neurodevelopmental abnormalities (253). Despite these data, there remains a lack of knowledge on miR-199a-5p in ageing muscle and neurons.

We hypothesised that miR-199a-5p would be upregulated during ageing, and upregulated miR-199a-5p would dysregulate targets that would be associated with mitochondria, myogenesis, and autophagy, all of which are critical to muscle in ageing. To assess this, in this chapter we aimed to determine the potential effects of miR-199a-5p changes in expression in ageing through bioinformatic analyses. We used human primary myoblasts obtained from female donors of young and old ages and performed small-RNA sequencing to obtain a list of differentially expressed miRs. We then performed an exploratory investigation into several of the differentially expressed miRs that were altered with ageing, of which miR-199a-5p was one of the selected. We selected this miR because it was shown in the literature to exhibit altered expression in dystrophic muscle (252), as well as in neurodegenerative diseases such as Alzheimer's disease (254), and ALS (255), and therefore we aimed to elucidate if this miR may be relevant in regulating neuromuscular biology, as the nerve and muscle are both potentially regulated by miR-199a-5p.

We then ran miR-199a-5p through bioinformatic search tools and databases to determine which pathways and targets would be the most impacted during age related muscle loss (sarcopenia) to better understand which targets would be the best candidates for further exploration.

These data were used to inform subsequent experiments and further identify potential gene targets of miR-199a-5p both *in vitro* (chapter 4, and chapter 5) and *in vivo* (chapter 6). Muscle biopsies from adult and old *vastus lateralis* muscles were used to assess the selection of miRs that are dysregulated in ageing of which miR-199a-5p is a candidate and to determine subsequent miR targets of interest.

The potential effect on skeletal muscle and neuromuscular homeostasis was assessed by investigating function of predicted target genes of miR-199a-5p in the context of skeletal muscle (TA) and sciatic nerves, in both humans and in mice.

3.2 Materials and methods

3.2.1 Human samples

Human samples and primary myoblasts were obtained by Dr Ana Soriano. All experimentation involving human tissue described herein was approved in advance by University of Liverpool, University Hospital Aintree Hospital and Southwest Wales Research Ethics Committee (Approval No: 13/WA/0374). Experiments were performed according to good practice guidance. The University of Liverpool acted as the ethics sponsor for this study. All donors gave informed consent for the enrolment of this study. The muscle biopsies were isolated from the quadriceps muscles of healthy females, with normal BMI, there were no underlying conditions and with no known confounding factors (BMI <25): adult: 30 ±2.8 years old and aged: 69 ±5 years old. Sample information is presented in (Table 3.2.1). From the isolated biopsies, primary myoblasts were isolated from each donor and cultured as described in 2.5. Cells where characterised by as described by Soriano *et al*. (256). Cells were cultured until passage number 5 (P5) to ensure sufficient cell numbers for small RNA-seq. To detect changes in microRNA expression, we used the balanced design of groups: healthy adult and older women with nu underlying health issues or medication. We deemed 1.5-fold differences in miRNA expression as biologically important based on our data ((85,158)). Based on our primary outcome: miRNA expression changes during ageing, n=6 in each group was deemed sufficient to detect these changes (power 90%, family-wise alpha=0.05).

Table 3.2.1. Muscle sample donor information

Donor ID	Age (years)	Gender	BMI
Young 1	36	Female	<25
Young 2	28	Female	<25
Young 3	32	Female	<25
Young 4	34	Female	<25
Young 5	32	Female	<25
Young 6	31	Female	<25
Old 1	68	Female	<25
Old 2	74	Female	<25
Old 3	68	Female	<25
Old 4	64	Female	<25
Old 5	66	Female	<25
Old 6	63	Female	<25

3.2.2 Muscle digestion

Tissue digestion of biopsy samples was performed as described by Soriano *et al.* (256). Briefly, a 250 mM CaCl2 working enzymatic solution was first made using: 277mg of stock CaCl2 in 10mL 1x DPBS, and then filtered with a 0.2 µm filter membrane, and working solution of 1.5/mL of collagenase D, 2.4 U/mL of Dispase II and 2.5 mM CaCl2 in serum-free DMEM (Dulbecco's Modified Eagle's Medium) was also made prior to sample digestion. The muscle biopsy samples were digested as follows: following sample collection, 2mL of collagenase-dispase-CaCl2 solution per 18 - 19 mg of muscle tissue was used. The muscle was washed in 70% ethanol, wash with fresh DPBS, and placed on a new dish with 1mL of enzymatic solution. The muscle was next cut into small pieces (approximately >0.5 mm^2) with sterile scissors or a surgical scalpel before transferring the sample into a falcon tube with the remaining 1 mL of the collagenase-dispase-CaCl2 solution. The tissue was then incubated at 37°C for 40 min with agitation. Growth medium was next added and pipetted up and down and then filtered through a 70µm cell strainer. The solution was centrifuged at 443 x g for 5 min at RT to pellet the cells, supernatant was discarded, and the cell pellet was dissolved in F-12 media (Ham's F-12 Nutrient Mix), 20% FBS, 10% HS, 1% p/s, 1% α-glutamine and 2.5 ng/mL of FGF-b (Recombinant human basic Fibroblast Growth Factor).

3.2.3 Primary cell culture

Before seeding of cells, culture surfaces were coated with 10µg/mL of laminin in 1x DPBS (Dulbecco's Phosphate Buffered Saline) as described in 2.5.2. A total of 5.50 x 10^4 cells in total were plated directly on the laminin coated vessel and incubated for 24h in a 37 °C, 5% CO_2 incubator. The cells were visualised under the bright-field microscope (100X total magnification) the following day, and the media changed to fresh F-12 media with 20% FBS, 10% HS, 1% P/S, 1% α-glutamine and 2.5 ng/mL of FGF-b. The media was changed every 2-3 days until appearance of groups of cells forming. At first passage, the media was changed to primary human culture medium as described in 2.4.3. and then cells were cultured as previously described in 2.5.

3.2.4 RNA isolation and small RNA-seq

RNA was isolated from primary human cells as described in section 2.9 from human primary cells at passages 3-5. In short, the medium was removed and TRIzol was

added directly to the cells in the plates: 1ml T75 flask, 0.5 ml/well T25 flask or 6-well plate, 0.3 ml/well 12-well plate. Using a cell scraper, all the cells from the plate were scraped into the TRIzol and transferred to a new labelled 1.5 ml Eppendorf, one well for each sample tube. Chloroform was added to each of the tubes (200 µl for a 6-well plate, and 100 µl for a 12-well plate) and the tube was shaken vigorously by hand for 15 seconds before being incubated for 5 minutes at room temperature. The samples were then centrifuged at maximum speed (15,000RCF) for 15-30 minutes in a 4°C centrifuge. The aqueous phase with RNA was transferred into a new Eppendorf. The RNA was precipitated by adding 100% isopropanol to the aqueous phase (500 µl for 6-well plate or flask and 250 µl for a 12-well plate) and incubated at room temperature for 15-30 minutes. The supernatant was then removed and discarded. The RNA was then washed in 80% ethanol and centrifuged, and the supernatant was next removed as above, and centrifuged briefly – 15,000g 4°C for 30 seconds. The tubes were then allowed to air dry for 5-10 minutes at room temperature. The RNA was then suspended in 10 µl of RNase-free water and assessed with the NanoDrop2000 spectrophotometer.

Small-RNA sequencing was performed using the Illumina HiSeq 4000 at 2 × 150-base pair (bp) paired-end sequencing, generating data from >280 M clusters per lane. An RNA-Seq library from submitted total RNA sample was performed using the NEBNext® small RNA library preparation kit. Sequencing was performed at the Centre for Genomic Research, at the University of Liverpool (https://www.liverpool.ac.uk/genomic-research/). Analysis of differentially expressed miRs was performed in collaboration with Dr Simon Moxon, University of East Anglia UK.

Mature miR sequences were downloaded from miRBase (v22.1 mirbase.org/ftp.shtml) in FASTA format. To align sRNA reads, the FASTA format miRBase sequence files were made non-redundant using java code and Uracil bases (U) were changed to thymine (T). Small RNA reads were converted from FASTQ to FASTA format and then processed to trim sequencing adaptors using the Perl script "Remove adaptors"(257). The first 8 bases were recognised as the adapter sequence. The processed reads were then aligned to the processed mature miR sequences allowing zero mismatches using PatMaN (258) (parameters: -s -e 0 -g 0 and -s -e 1 -g 0). Custom java code was used to parse the alignment files and generate an aligned

read count table across all samples. The DESeq2 (259) method within iDEP (260) (version 91) was used for normalisation of counts between samples and differentially expressed (DE) miRs using default settings.

Data were assessed using pairwise comparisons, and correlation heatmaps and principal component analysis (PCA) plots were visualised using the Clustvis web tool (261). DE miRs were extracted by applying the threshold of p-value < 0.05, generated using the Benjamini–Hochberg method (262), and an absolute value of log2 fold change of 1.0 (|log2FC| > 1, equating to a 2-fold change) (263), data were assessed for normality and statistics were performed as described in 2.17.

3.2.5 cDNA synthesis and RT-qPCR

Muscle tissue and sciatic nerves were processed for RNA as described in 2.12.1. RNA was isolated using TRIzol/chloroform standard RNA isolation protocol and RNA purity was assessed on a Nanodrop 2000 spectrophotometer as described in 2.9. Synthesis of cDNA was performed using SuperScript II (100-500ng RNA). RT-qPCR was performed using FAST SYBR Green Master Mix (Applied Biosystems 4385612). Relative expression was to β2-microblobulin or S29 and was calculated using delta-delta Ct method; and changes in relative expression were then analysed. Statistics were performed as described in 2.17. An in-depth RT-qPCR protocol is listed in 2.11. Primer sequences are listed in Table 2.11.1.

3.2.6 Identification of miR-199a-5p predicted targets and pathways

Target genes of miR-199a-5p were found using MIENTURNET (http://userver.bio.uniroma1.it/apps/mienturnet/), a web tool for miRNA-target enrichment and network analysis, using “hsa-miR-199a-5p” as the search term. Validated gene targets were selected using the miRTarBase tool in MIENTURNET, with threshold for the minimum number of miRNA-target interactions set to “1” to determine at least one interaction required, threshold for the adjusted p-value (FDR) set at “0.05”, and filter by evidence set to “strong”. Predicted targets of miR-199a-5p were found using TargetScan 8.0 (https://www.targetscan.org/vert_80/) to obtain a list of predicted targets. Predicted targets were then entered into the following databases: 'GO_Molecular_Function_2021', 'GO_Cellular_Component_2021', 'GO_Biological_Process_2021', 'Reactome_2022', ‘Panter_2016’, ‘WikiPathway_2021_Human’, 'KEGG_2021_Human', to determine relevant

pathways affected by miR-199a-5p. We used both predicted targets and validated targets approach dure to a bias of validated targets being validated most commonly within the context of cancer and this approach would risk missing biologically relevant targets in muscle ageing. Therefore, we looked at both predicted (high confidence) and validated targets to probe for targets that are relevant to neuromuscular biology.

3.3 Results

3.3.1 miR-199a-5p is upregulated during ageing in humans

Primary myoblasts from human quadriceps were processed for RNA and small RNA-seq was performed. The results demonstrated several miRs were differentially expressed during ageing; we determined a set of miRs downregulated (Table 3.3.1), and upregulated (Table 3.3.2) with age. Of the miRs upregulated with age, miR-199a-5p was found to be upregulated ($p<0.05$) in old primary human myoblasts. The heatmap of differentially expressed miRs in adult and old primary myoblasts shows clear delineation in miR expression in miR-199a-5p, and a significant upregulation was observed across all old muscle cells (Figure 3.3.1).

Table 3.3.1 Downregulated miRs in old human primary myoblasts.

miRNA	baseMean	log2FoldChange	lfcSE	stat	p-value	p-adj
hsa-miR-431-5p	93.86403712	-1.704323184	0.368834832	-4.620830346	3.82207E-06	0.000654848
hsa-miR-410-5p	24.22861923	-1.795392668	0.460438	-3.899314715	9.64653E-05	0.012395794
hsa-miR-503-5p	47.03010978	-1.451842707	0.394688852	-3.678448735	0.000234657	0.02010227
hsa-miR-132-5p	287.5697033	-1.488294941	0.456273558	-3.261847888	0.001106885	0.051900891
hsa-miR-493-3p	7280.729975	-1.350581131	0.416574399	-3.242112656	0.001186471	0.051900891
hsa-miR-487a-3p	30.34296835	-1.318549122	0.410354449	-3.213195631	0.001312668	0.051900891
hsa-miR-133b	63.10349027	-1.784606078	0.604652661	-2.951456584	0.00316279	0.085641714
hsa-miR-370-3p	29369.207	-1.251400738	0.417093741	-3.000286543	0.002697257	0.085641714
hsa-miR-27a-5p	3224.83283	-0.994205662	0.335847139	-2.960292185	0.003073474	0.085641714
hsa-miR-3911	3.39341761	-1.807877204	0.635024451	-2.846941093	0.004414153	0.098646723
hsa-miR-1228-5p	27.66321469	-1.421450392	0.496514632	-2.862857006	0.0041984	0.098646723
hsa-miR-139-3p	17.73754363	-1.534481649	0.561516335	-2.732746233	0.00628087	0.128861021
hsa-miR-188-5p	29.28232568	-1.464472067	0.540794334	-2.708001868	0.006768964	0.128861021
hsa-miR-4435	5.411242305	-1.46099215	0.567141352	-2.576063524	0.009993228	0.138210364
hsa-miR-675-5p	103.5950518	-1.244604089	0.483183819	-2.57583975	0.009999698	0.138210364
hsa-miR-345-5p	164.8757033	-1.22114247	0.461589338	-2.645517061	0.008156617	0.138210364
hsa-miR-143-3p	178062.9739	-1.181853312	0.460398041	-2.567025065	0.01025752	0.138210364
hsa-miR-432-5p	347.7006519	-0.963371677	0.370730058	-2.598579897	0.009361026	0.138210364
hsa-miR-500a-3p	272.3613067	-0.941212681	0.357141494	-2.635405568	0.008403681	0.138210364

Table 3.3.2 Upregulated miRs in old human primary myoblasts

miRNA	baseMean	log2FoldChange	lfcSE	stat	p-value	p-adj
hsa-miR-1246	93.28803616	3.878436425	0.51721394	7.498708223	6.44498E-14	3.31272E-11
hsa-miR-204-5p	609.2070917	2.567177395	0.520502148	4.93211681	8.13432E-07	0.000209052
hsa-miR-195-5p	152.8930537	1.315358159	0.346247253	3.798898463	0.000145341	0.014941015
hsa-miR-4773	4.631283674	2.131378364	0.594566481	3.584760379	0.000337388	0.021677168
hsa-miR-196b-5p	1672.589699	1.195487926	0.330511384	3.617085471	0.000297939	0.021677168
hsa-miR-26a-5p	344776.5212	1.27172803	0.363577162	3.49782154	0.000469075	0.026789389
hsa-miR-29c-3p	15.92770053	1.453673488	0.451291901	3.221137989	0.001276827	0.051900891
hsa-miR-1262	7.994847915	1.663948154	0.535894288	3.104993264	0.001902834	0.069861176
hsa-miR-3613-5p	1256.196998	1.186277621	0.389085155	3.048889445	0.00229689	0.078706761
hsa-miR-1255a	103.4673282	1.460113994	0.494757965	2.951168242	0.003165744	0.085641714
hsa-miR-26a-2-3p	126.8479317	1.213172746	0.425720567	2.849692592	0.00437615	0.098646723
hsa-miR-34a-5p	460.8103641	0.814286258	0.282841305	2.878951006	0.003990003	0.098646723
hsa-miR-505-5p	20.89779269	1.379214608	0.489290165	2.818807136	0.004820247	0.103233626
hsa-miR-34c-3p	17.6329105	1.463874187	0.540042732	2.71066362	0.006714871	0.128861021
hsa-miR-217	22.13980589	1.22017217	0.471669875	2.586919867	0.009683811	0.138210364
hsa-miR-664a-3p	216.2947115	1.144087063	0.440470577	2.597419947	0.009392701	0.138210364
hsa-miR-26b-5p	2428.405853	1.122610343	0.437456684	2.566220577	0.010281342	0.138210364
hsa-let-7a-5p	388168.0934	1.100124993	0.413019098	2.663617735	0.007730535	0.138210364
hsa-miR-539-5p	22.82356084	1.032802675	0.398098165	2.594341712	0.009477224	0.138210364
★ hsa-miR-199a-5p	100122.6382	0.712147809	0.278253275	2.559351046	0.010486779	0.138210364

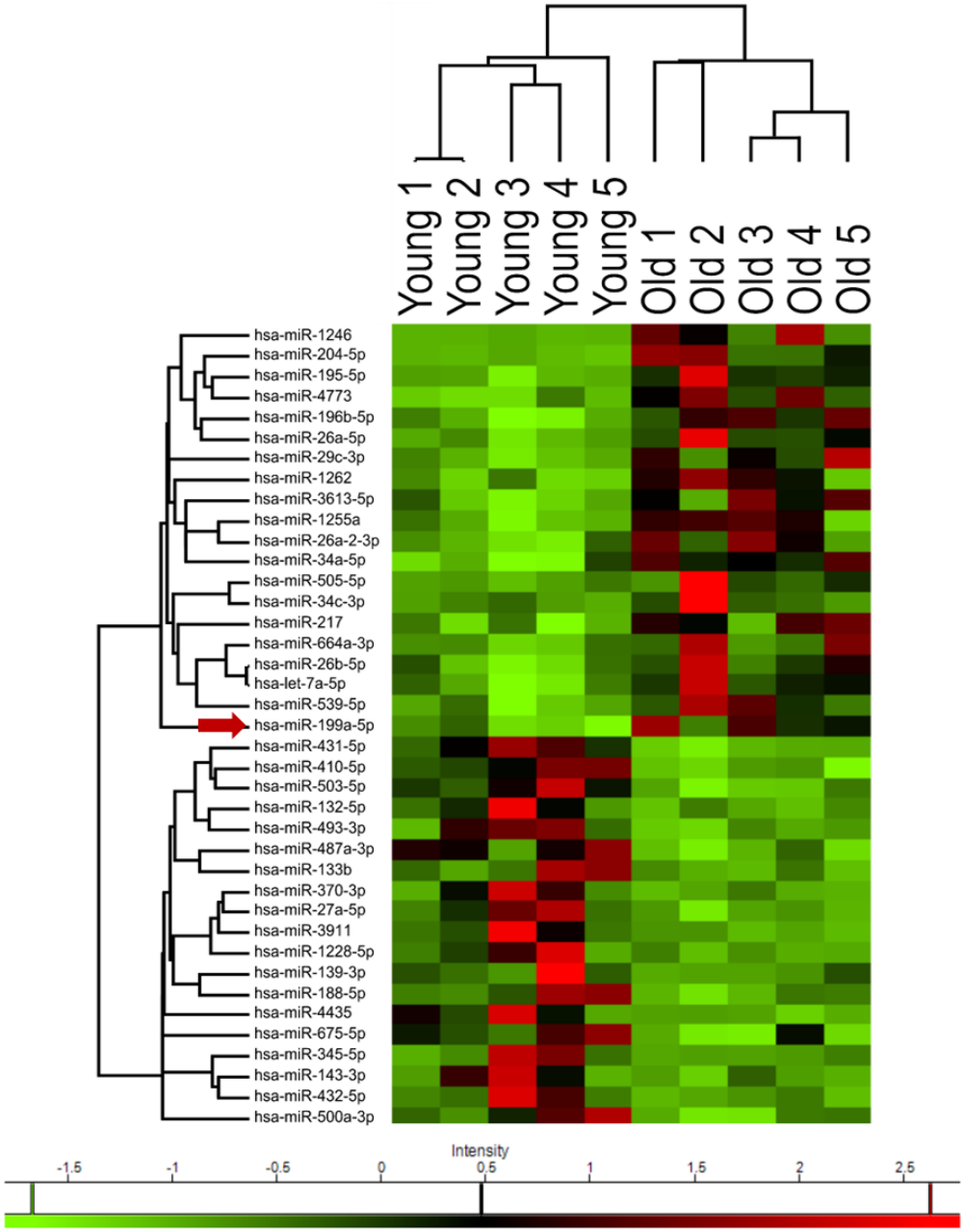

Figure 3.3.1. Heatmap of differentially expressed miRs in adult and old skeletal muscle. Muscle from older people shows differential expression (upregulation and downregulation) of several miRs. Expression of miR-199a-5p (red arrow) was shown to be upregulated in old skeletal muscle as determined by small RNA-seq. Red arrow—miR-199a-5p; p value <0.05.

3.3.2 miR-199a-5p targets genes associated with ER stress, mitochondria, and neuronal regulation.

The free webtool MIENTURNET (http://userver.bio.uniroma1.it/apps/mienturnet/) was used to search published databases for validated and predicted targets of miR-199a-5p. The miRtarbase search tool 9.0 (264) results showed miR-199a-5p has validated targets involved in: UPR regulation (Atf6, Grp78), activin receptor signalling (Acvr1b), neuron regulation (Tgf-β2), oxidative stress (Hif-1α), and mitophagy (Becn1) among others (Table 3.3.3). A Targetscan search was also performed with Targetscan version 8.0 (https://www.targetscan.org/vert_80/) to compile a list of predicted miR-199a-5p targets based off of conserved seed sequences to increase the amount of potential targets. The results of this search showed 634 predicted targets. Targets included mitochondrial biogenesis gene, Pgc-1α, activin receptors, Acvr1b, Acvr2a, Acvr2b, and ER stress marker Hspa5 (Grp78) (Table 3.3.4). Additional predicted targets included Smarcd1 involved in neuronal differentiation (265), and Wnt2, a Wnt family member with multiple roles including myogenesis (266). Wnt2, Acvr1b, and Grp78 were observed in both validated and predicted targets. Validated miR targets searched using miRtarbase through the MIENTURNET tool include Atf6, and Hspa5 (Grp78), associated with the UPR (Table 3.3.3). Other validated targets include mitochondria-associated targets Hif-1α associated with oxidative stress and Becn1 associated with mitophagy. Also present is Tgf-β2 associated with neuron function. Targetscan 8.0 was used to compile a list of all predicted gene targets of miR-199a-5p in humans (Table 3.3.4), based on seed sequence of miR-199a-5p and the gene. Results of this search showed predicted targets include ER stress marker Hspa5 (Grp78), Pgc-1α, as well as activin receptors, Acvr1b, Acvr2a, Acvr2b. Other relevant predicted targets include Wnt2, and Smarcd1.

Table 3.3.3. miRtarbase validated miR-199a-5p targets

miRTarBase	
has-miR-199a-5p	
microRNA Target Gene	
EZH2	DRAM1
IKBKB	BECN1
LIF	MAFB
JUNB	WNK1
DDR1	NFKB1
EDN1	ACVR1B
MAP3K11	CDH2
HIF1A	SNAI1
SMARCA2	GSK3B
CD44	FZD4
TMEM54	WNT2
SMAD4	JAG1
SULT1E1	HK2
GPR78	KRAS
ERBB2	SMAD3
UNG	ETS1
CAV1	CCR7
SIRT1	PDE4D
HSPA5	TGFB2
ATF6	PIK3CD
ERN1	SETD2
KL	CLTC
APOE	RAB21
DNAJA4	OSCP1
ERBB3	PIAS3
CDH1	PSMD9
PTGS2	CDKN1C
LIN7A	ITGA3
ARHGAP12	FZD6
CTSC	MAP4K3
RND1	TGFBR1
NECTIN1	SLC27A1

(264)

Table 3.3.4. Predicted target genes of miR-199a-5p

ZNF776	PREPL	GCNT2	UBE2Q1	UNG	PAOX	MARCH7	ATP1A2	PNP	MAPRE2	EXTL3	EMC10	RGP1	ATG4D
ZNF439	USP37	AKAP1	SORL1	NAA40	SLC35E4	OSR1	CDH2	KIAA1324L	UBALD2	ZNF738	SIRT1	SERPINE1	DENND2C
ZNF544	CLK2	FAM222B	SRRM4	RGMA	SH3PXD2A	RNF11	MANEAL	SRL	CHCHD4	CCDC176	MARK4	PCDH17	PRPF40A
ZNF791	ZNF300	ALS2	OSTM1	GRB10	WBP11	ZNF516	REEP2	HIP1R	CDKN1B	NUFIP2	KLHL29	ABTB2	TMEM245
ZNF788	SMARCD1	GPR89B	NOTUM	FAM188A	PLEKHH1	FPGS	PAK4	PTGIS	PPFIBP1	GPR124	SUCO	ADAMTSL3	CNN1
ZNF627	DEPDC1B	MAGT1	ETV6	ZNF528	MGAT3	SAT1	R3HDM1	PPL	EIF5B	KLHL6	FSTL4	TANC2	PPP4R1L
ZIK1	MINPP1	SLC24A3	PPP6C	CCNL1	RPS6KA5	LARGE	ST6GAL1	SLC36A4	RAB21	CEP85L	BEND3	HIF1AN	ARHGAP17
ZNF772	RBBP4	ZNF846	MYH9	GNG5	CRYBB3	NPAS2	RFFL	NOTO	PHACTR4	PPP1R12A	ZNF652	USP31	PLXNA2
ZNF709	RORB	B3GNT1	ZNF415	RALGAPA1	TMEM123	ZCCHC4	ARHGAP19	M6PR	WDR44	ACVR2B	MIER3	RSF1	SEC24C
ZNF584	HIF1A	TGFB2	MINOS1-NE	ZFYVE27	RGMB	PKN2	SMARCE1	ACVR2A	CREBRF	LASP1	ADD3	TENM4	FOXC2
ZNF625	DDX3Y	ZNF329	ITGA4	KCND3	MFHAS1	KPNA4	ZNF512B	DDX3X	ANK3	GRIK3	EMC7	MON1B	JPH3
ZNF256	THUMPD3	EPB41L1	HHIP	LYSMD3	JAG1	DRAM1	WNT7B	RAB10	ITGA3	MBD5	CELF2	CNOT6L	SNX6
ZNF547	ACER2	ZNF233	NBL1	SNAI1	STOX2	SLC9A8	ZEB1	ANKRD13C	TMEM215	PURA	NFIL3	DONSON	ZBTB18
MAP3K11	IKBKB	VPS26A	ZNF148	DPP8	SLC35A3	HSPA12A	ULK3	NCOA2	ZNF629	HEATR3	GOSR1	PACRGL	TET2
LIN7C	ZNF618	FLRT3	FAM76B	NTNG1	PDE7A	RBM23	MTMR3	DEPDC5	CHN2	MAPK4	ZNF667	PTPN9	APPBP2
PVRL2	ZNF641	CCDC43	SLAMF8	AP1G1	YAF2	CAPRIN1	CDH8	ETS2	MCFD2	PRDM16	PARP12	C17orf85	ACTG1
ZNF561	BTRC	GJA5	AUTS2	GPRC5A	MPP5	FAM178A	RANBP10	RGS10	EHD4	MAP2	DDI2	CA12	TAOK1
DDR1	SLC24A4	PODXL	ONECUT2	HSPA5	STON2	RLIM	WNK3	MAML3	MINK1	KIAA2018	MAP4K3	CABP7	ITFG3
RP11-1396(	TMEM135	FZD6	SLC25A37	CACNB2	FAM126B	EXOC8	KIT	PLXNB1	ZNF654	RBM24	SLC35B3	BTG1	USP27X
ZNF23	ZBTB37	ANGEL2	ZFP91	PPP1R9A	TERF2	NAB2	KIAA0355	DESI1	GPD2	DLC1	SULT4A1	ZBED4	TRMT1L
BCAM	SMARCAD1	ARF6	PPM1L	MYEF2	MAP3K5	LARP4	CRIM1	ATG14	ACVR1B	KLHL3	TM9SF3	ZNF480	ZNF784
SHOC2	CLIP1	PPP1R2	ZNF394	CCDC120	ZNF704	TSPAN3	CBL	AGO3	GSK3B	TIMM10	BCAP29	CBX5	MATN2
HAPLN1	TRPM4	FAM107B	ARHGEF5	FZD4	ZNF710	KIAA1109	SRSF1	LIMD2	E2F6	TMEM178B	CDKN1C	GRHPR	SET
ZFP2	FXR1	ACPT	FSD1	SRRM1	POU3F1	RANBP2	MEF2D	AMN	MFSD6	UBQLN4	KLHL23	NCKAP1	PRDM5
TST	LAMC1	ARHGAP12	ROCK1	PPARGC1A	BTBD9	NAALADL2	POGK	PARVA	TTC9	RANBP3	ZSCAN29	IST1	KIAA1958
MYRF	EPB41L3	TAF9B	KANK2	CLTC	LRP4	PNPLA6	SP2	SMARCA4	DERL2	PLXND1	CECR2	GINM1	GIT1
CELSR1	FAM169A	GPR89A	SOX4	CDKN2AIP	KPNB1	UHMK1	COL8A1	SNTB1	TAB3	HDLBP	FUT9	PTPMT1	ITCH
GPR63	SLC35E1	RASSF2	ARHGAP29	CSGALNAC1	PBRM1	RAB27B	CD276	DST	FBXO30	RIN2	NLRC3	INTS8	YIPF2
CDCA7L	FBXO33	TMEM66	RRAGC	EVX2	ABCA1	BTBD3	CSRNP2	FAM179A	CCBL2	FBXO9	KIAA0753	EIF2B2	SWAP70
NSG1	RGS17	METTL21A	SNN	WNT2	NFE2L1	TSPAN5	GANAB	GATAD2B	NLK	ARHGAP20	ATXN7	TSPYL1	C15orf61
RAD23B	ZMAT2	UBL3	RFESD	MICAL3	RIMS1	RHEB	ZNF226	STRN	BROX	CSNK1D	PMP22	YIPF6	AIP
ZBTB42	TIGD5	GPR89C	KLF9	BAAT	E2F3	CSDC2	ATP2B2	BLCAP	ATP13A2	SPRED3	ERLIN1	MAPK8	TRIP4
CRYBG3	XPOT	ABHD17C	AFTPH	IL23R	ATXN3	ITGA8	AL590483.1	LMAN2	FIGN	AKAP13	RNF38	FCHSD1	MRPL22
RBM47	SRGAP3	ASRGL1	SLC24A2	GRIP1	C18orf25	TBC1D8	ARID2	RAD54L2	KIAA0040	SLC46A1	WDTC1	TSR2	P2RX7
PDPN	RFX3	SLC25A23	NUPL1	IPO8	ARIH2	PVRL1	MAX	WDR76	OTX1	SPRYD7	XYLT1	AHSA2	DDX6
HMCN1	STAG1	CCNJ	ARHGEF12	ABCC1	HOXB6	RTN4RL2	HAS2	ZNF706	PAXBP1	USP19	RASSF3	ZBTB20	
MGAT4B	CLCN3	LEPREL1	AGO1	SACS	TENM2	ZNF286B	BCL7A	CNOT6	PLXNC1	ZBTB5	DNAJB5	ZNF703	
MAB21L1	ZCCHC2	SUN1	SYT14	JUNB	RB1	UBE2G1	NFYA	PRR14L	AQP11	RRP15	WIPI2	DDX5	
FP15737	MN1	SOS2	CAV1	ETS1	NAA15	VGLL2	KLF12	MKL2	HSPA4	NCOR1	DYRK1A	ZC2HC1C	
LCOR	HSPBAP1	C1GALT1	EXOSC3	MUC21	RAD51L3-R	FER	NIPAL3	ADRBK2	CCDC88C	SOX6	NCSTN	DUSP14	
RP11-122A3	STRADB	RAB9B	ZSWIM4	PAX3	USP46	PXN	TXNRD1	TLN1	PDE4D	ABCC5	ZNF24	SP1	
ARHGAP21	VEGFA	MARCH8	ERBB4	CYLC2	WAPAL	RBPMS	PPM1B	SAR1A	TOX3	ANKRD52	HLF	TMEM63B	
ZNF225	GMEB1	NINL	MYO5A	ACHE	MIOS	ATXN7L1	CTNNA2	TBL1XR1	APMAP	INO80D	STX4	GPR180	
TSPAN6	EPHA7	CACUL1	ZBTB8A	ZNF594	ADAMTS5	UBAP1	CEP72	FANCA	STK4	KIAA0226	RUNX1T1	COL5A3	
ECE1	CLOCK	ZNF579	GBP1	SORCS3	PHTF2	PAN3	UBN2	ZDHHC21	FKBP5	ZNF740	DENND6A	SEMA3F	
SULF1	PI4KA	BICC1	PCYOX1	HGF	RNMTL1	TBC1D14	CDC73	MRPS25	TMED8	ZNF614	HOXA7	TRAF3	

3.3.3 miR-199a-5p predicted target genes are associated with neuronal homeostasis and Wnt signalling.

We next analysed the list of predicted target genes and compared them across currently published databases to identify cellular, molecular, and biological functions of the predicted targets to elucidate the potential areas of miR-199a-5p regulation. The results of these searches showed miR-199a-5p predicted targets are associated with cellular components related to activin receptor complex, trans-Golgi apparatus. Molecular function analysis highlighted tau-protein kinase activity as well as protein serine/threonine kinase activity. Biological process analysis highlighted Wnt signalling, phosphorylation, neuron differentiation, and apoptosis (Figure 3.3.2).

Other pathway analyses (Panther, Reactome, WikiPathways, and KEGG) similarly showed that miR-199a-5p predicted target genes are associated with Wnt signalling and binding, mTOR signalling pathway, and calcium pathways. Further predicted target genes are associated with Alzheimer's disease and cancers (Figure 3.3.3). Next, these databases: 'GO_Molecular_Function_2021', 'GO_Cellular_Component_2021', 'GO_Biological_Process_2021', 'Reactome_2022', 'KEGG_2021_Human', were combined, and the validated miR-199a-5p targets that were obtained were searched to determine the most significant pathways that are related to the target list. Significantly affected pathways included tau-protein kinase activity, Wnt signalling and mTOR signalling. Other pathways affected by miR-199a-5p targets included regulation of phosphorylation, calcium transport, and nervous system development (Figure 3.3.4).

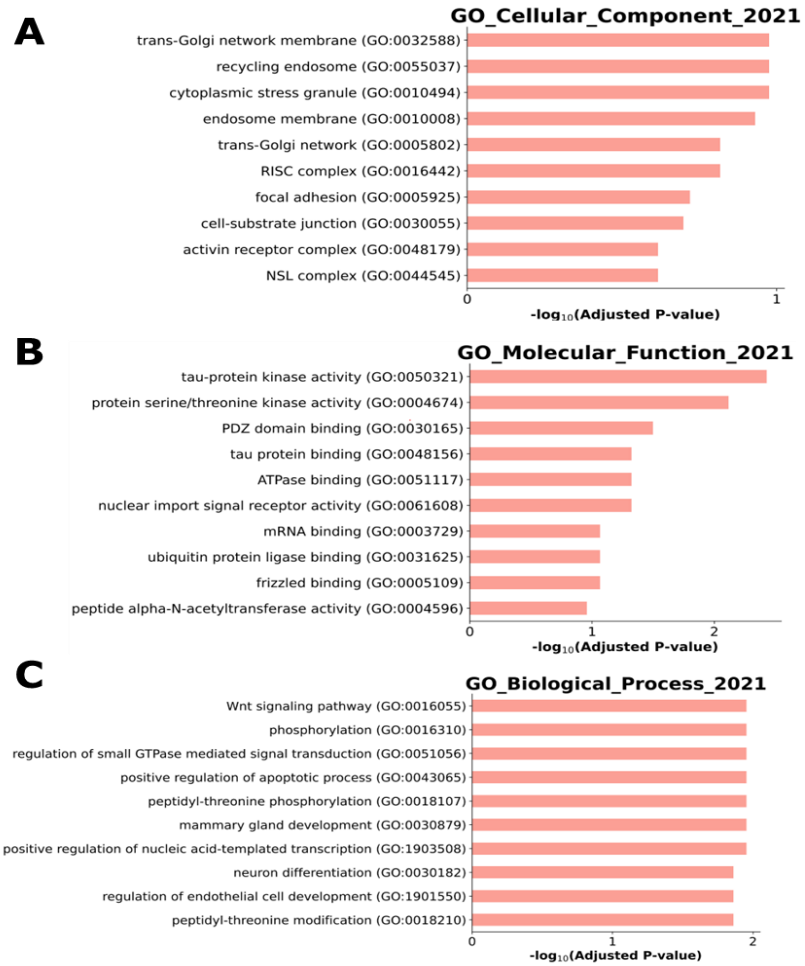

Figure 3.3.2. miR-199a-5p predicted targets are associated with activin receptor complex formation, kinase activity, and Wnt signalling. The predicted target genes of miR-199a-5p were searched in over 200 databases. GO cellular function, molecular function, and biological process analysis demonstrated miR-199a-5p is associated with Golgi apparatus and activin receptor (A). Further associated with miR-199a-5p was tau-protein kinase activity and protein serine-threonine kinase activity (B) as well as Wnt signalling, apoptosis, and neuron differentiation (C). Threshold for minimum target interactions '1', p-value '0.10', adjusted p-value '0.10', gene: pathway ratio '0.05'. FDR < 0.05.

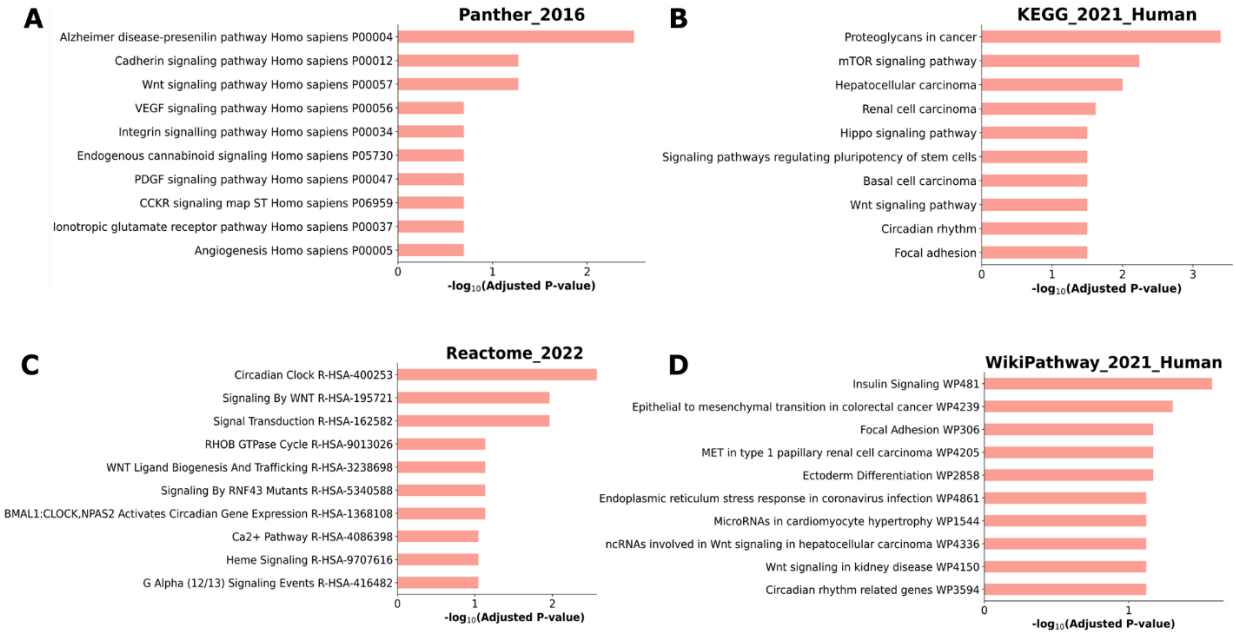

Figure 3.3.3. Pathway analysis of predicted miR-199a-5p target genes. Predicted target genes of miR-199a-5p were input into databases to determine significant pathways. Pathways related to Wnt signalling, calcium signalling, insulin signalling and mTOR signalling pathways (A,B,C,D) were found to be associated with miR-199a-5p predicted target genes. Also associated with miR-199a-5p predicated targets are cancer and Alzheimer disease (A,B,D). Threshold for minimum target interactions '1', p-value '0.10', adjusted p-value '0.10', gene: pathway ratio '0.05'. FDR < 0.05.

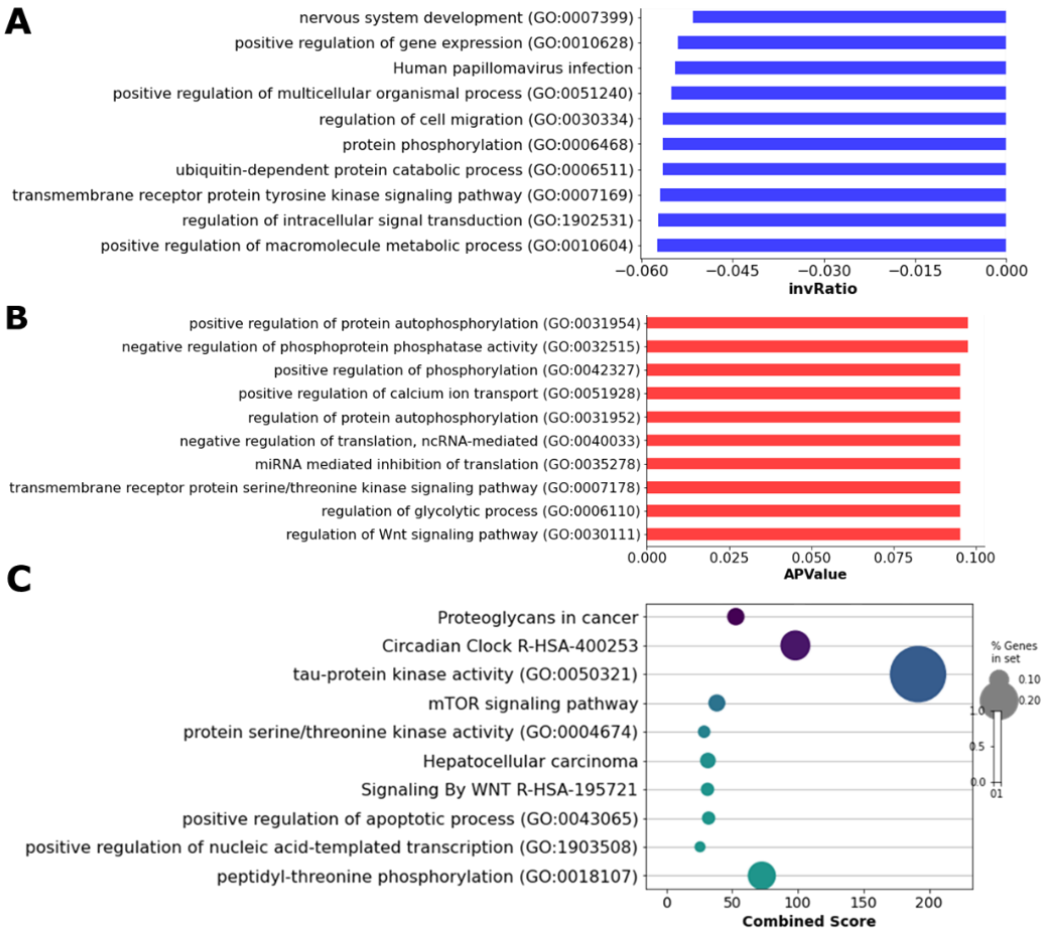

Figure 3.3.4. Combined database pathway analyses show miR-199a-5p is predicted to regulate genes involved in mTOR signalling, phosphorylation, and nervous system. A search of validated miR-199a-5p target genes across multiple gene pathway databases showed the most significant pathways affected by predicted target genes. The predicted target genes are involved in nervous system development (A,C), Wnt signalling (B), phosphorylation (B,C,), mTOR signalling (C), and calcium transport (B). Threshold for minimum target interactions ‘1’, p-value ‘0.10’, adjusted p-value ‘0.10’, gene: pathway ratio ‘0.05’. FDR < 0.05.

As we had observed these changes to miR expression in human muscle cells, we next wanted to determine the effect of miR expression in young and old mice to see if these changes would persist in mice during ageing.

3.3.4 miR-199a-5p is upregulated in skeletal muscle during ageing in mice, and its targets are differentially expressed in ageing.

We next aimed to determine the effect of ageing on miR-199a-5p in skeletal muscle of mice, to assess if mice also exhibited increased expression of miR-199a-5p with age. The TA muscle and sciatic nerves of adult and old mice were processed for RNA as described in 2.12.2, and RT-qPCR for miRs was performed as described in 2.11. The results of RT-qPCR for miR-199a-5p expression in adult and old mice showed that miR-199a-5p expression is significantly upregulated in skeletal muscle of old mice as compared to adult mice. The expression of miR-199a-5p in sciatic nerves showed no significant differences between adult and old mice, although a noticeable non-significant increase in miR-199a-5p expression was observed in adult mice sciatic nerves (Figure 3.3.5).

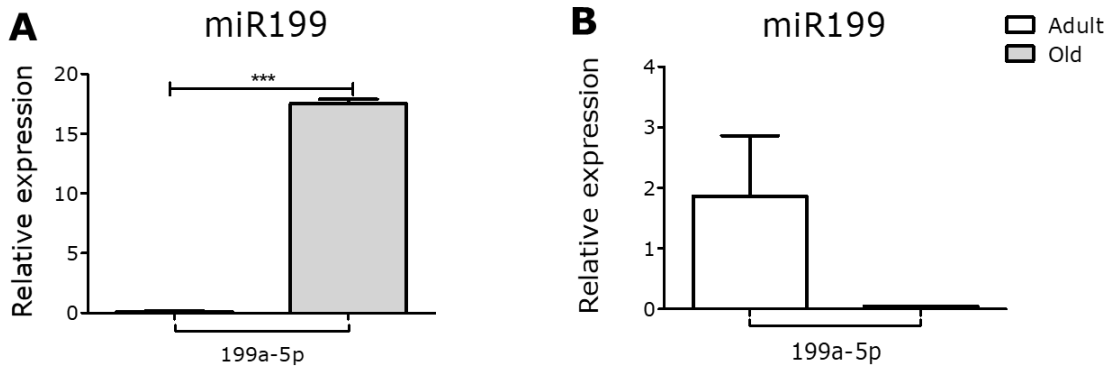

Figure 3.3.5. miR-199a-5p expression is increased in skeletal muscle of old mice, but not the sciatic nerve. The TA and sciatic nerves of adult and old mice were processed for RNA and RT-qPCR for miRs was performed. A) The results showed miR-199a-5p expression is significantly upregulated in the skeletal muscle of old mice as compared to adult mice. B) Expression of miR-199a-5p in sciatic nerves of adult and old mice showed no statistically significant differences, although a non-significant increase in miR-199a-5p expression was observed in adult mice as compared to old mice. Adult – 6 months old; old – 24 months old male C57BL6/J mice. qPCR: Expression relative to Rnu6 is shown. n=3-6. Error bars show SEM, $p < 0.05$ Student's t-test.

We next aimed to determine the effect of age on the expression of some of the miR-199a-5p predicted target genes that were previously determined in the TA muscle of adult and old mice. RT-qPCR analyses showed the expression of miR-199a-5p

predicted target genes and genes associated with processes regulated by these genes during ageing of skeletal muscle. In Nd1, there was a significant downregulation in expression in old mice compared to adult mice (Figure 3.3.6). Expression of predicted target gene, *Pgc-1α*, was not significantly downregulated, in old mice compared to adult mice. Similarly, Hdac9 was shown to be not significant. ER stress related target, Grp78, was not significantly different, and Chop gene expression was similarly not significantly different (Figure 3.3.6). All other targets (Acvr2a, Cav2, Tom20, Gap43, Tgf-β2, Nrf2, Sirt1, Acvr2b, Smarcd1) showed no significant differences.

As miR-199a-5p predicted target genes include genes associated with neuron, and NMJ homeostasis, we also looked at gene expression in the sciatic nerves of adult and old mice. Our results showed a significant increase in mRNA expression of Hdac9 in the sciatic nerve of old mice as compared to adult mice (Figure 3.3.7). Predicted miR-199a-5p target gene, *Pgc-1α*, was not significant, in sciatic nerves of old mice compared to adult mice. Target gene, Grp78, showed no differences in expression, in adult or old sciatic nerves. Gap43 expression was not significantly different compared to controls (Figure 3.3.7).

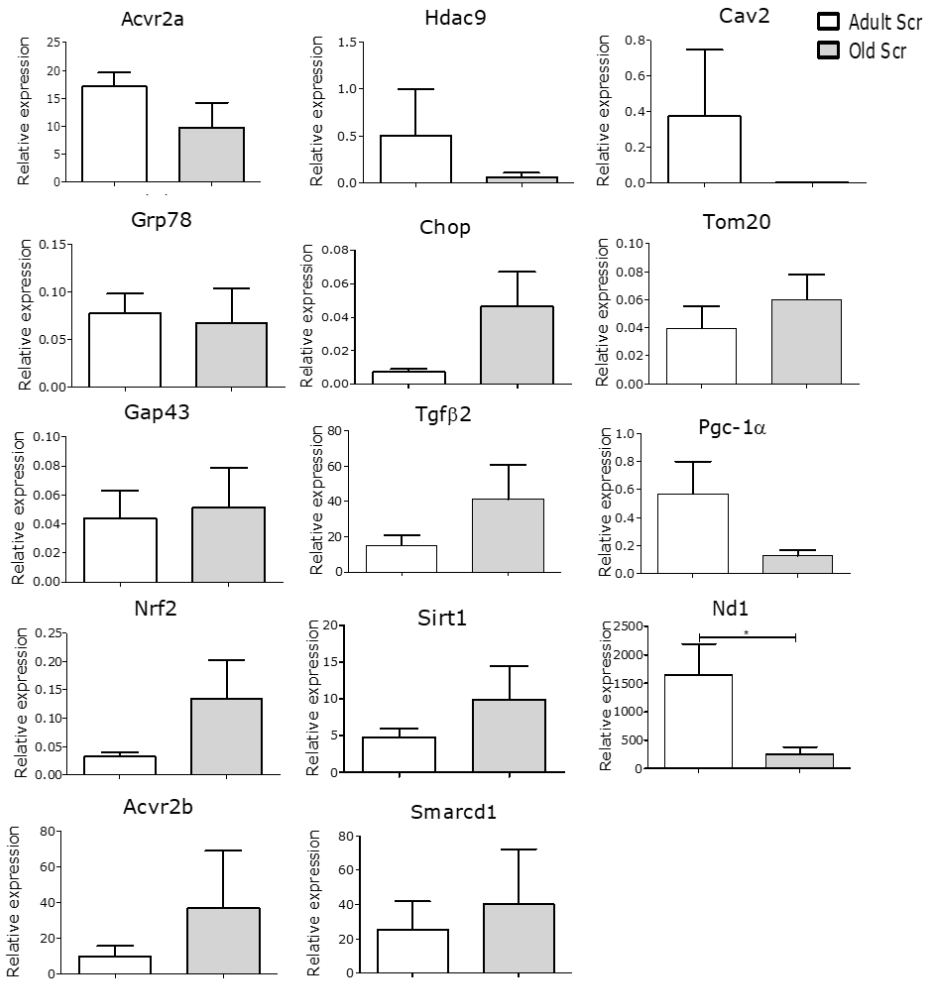

Figure 3.3.6. Nd1, miR-199a-5p predicted target, was differentially expressed in aged skeletal muscle. RT-qPCR of skeletal muscle from adult and old mice show significantly lower mRNA expression of Nd1 in old mice compared to adult mice. Predicted mitochondrial target gene Pgc-1α expression was lower in old mice although not significantly. ER stress genes (Grp78, Chop) showed no significant differences in expression. Adult – 6 months old; old – 24 months old male C57BL6/J mice. qPCR: Expression relative to β2-microglobulin is shown. n=3-6. Error bars show SEM, $p<0.05$ Student's t-test.

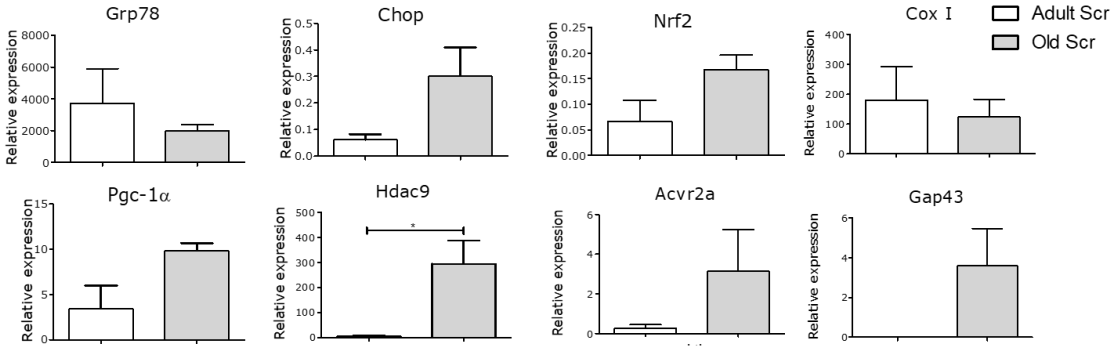

Figure 3.3.7. Hdac9, associated with NMJ, was differentially expressed in aged sciatic nerve. RT-qPCR of sciatic nerves from adult and old mice show significantly increased mRNA expression of Hdac9 in old mice compared to adult mice. Pgc-1α expression was higher in old mice although not significantly. ER stress genes (Grp78, Chop) showed no significant differences in expression, although Chop was noticeably higher in old nerves. Adult – 6 months old; old – 24 months old male C57BL6/J mice. qPCR: Expression relative to β2-microglobulin. n=3-6. Error bars show SEM. * - $p<0.05$ Student's t-test.

3.4 Discussion

This chapter aimed to identify the effect of age on the expression of differentially expressed miRs in human and mice skeletal muscle. We also aimed to determine the predicted targets and pathways that could be potential drivers of the changes to skeletal muscle and NMJ in ageing. Our results showed miR-199a-5p is upregulated in ageing in skeletal muscle among several miRs, and miR-199a-5p is predicted to regulate genes associated with mitochondria, ER stress, autophagy, and neuron regulation. Pathway analyses further show Wnt signalling, neuron regulation, and autophagy as miR-199a-5p-associated target pathways.

3.4.1 miR-199a-5p is upregulated in ageing in humans

The results of the small RNA-seq showed miRs are differentially expressed during ageing (Table 3.3.1, Table 3.3.2). Of the miRs found to be upregulated with ageing, miR-199a-5p was found to be upregulated in aged muscle, but not sciatic nerve. Many miRs have been demonstrated to play key roles in sarcopenia by action through various mechanisms (171), and therefore it was necessary to determine which miRs are affected by ageing. The expression of miR-199a-5p in muscle as shown by heatmap (Figure 3.3.1) clearly demonstrated the expression of miR-199a-5p is affected by age and is upregulated. We have selected several miRs for further

exploration, and as miR-199a-5p was predicted to regulate muscle it was chosen for further inquiry.

3.4.2 miR-199a-5p targets genes associated with ER stress, mitochondria, and neuronal regulation

Next, we aimed to determine the validated and predicted gene targets of miR-199a-5p to determine genes that may be driving the phenotypic changes observed in sarcopenic muscle. The results of this analysis showed genes regulated by miR-199a-5p associated with ER stress and the UPR (Atf6, Chop, Grp78) (267–269). ER stress is associated with sarcopenia (77) and neurodegeneration (270). Also found to be a validated target associated with mitochondria (271) and autophagy (272) was Hif-1α (273). Further targets associated with miR-199a-5p are predicted to regulate neuronal homeostasis (Tgf-β2) (274,275), activin receptor signalling (Acvr1B) (276,277). Also of note were targets associated with autophagy/mitophagy (Becn1) (272) (,). Many of these pathways, such as the UPR, are also involved in extensive crosstalk with other pathways identified here such as mitochondrial and autophagy (278), and ER stress and activin receptors (279). We also found predicted targets that agreed with the validated targets, which included Grp78 and Acvr1b. Other predicted targets that correlated with previously found validated targets included mitochondria (Pgc-1α), neuron (Smarcd1), and Wnt signalling (Wnt2). These data collectively suggest that miR-199a-5p may regulate skeletal muscle and nerve homeostasis through acting on targets corresponding to mitochondria and ER stress pathways and target genes.

3.4.3 miR-199a-5p predicted target genes are associated with neuronal homeostasis and Wnt signalling.

Predicted target genes were next searched in bioinformatics databases to determine target networks that may be regulated by miR-199a-5p. We found miR-199a-5p to be highly correlated with Wnt signalling pathways, autophagy, and neuron regulation (Figure 3.3.4). The results of GO pathway analysis showed the most significant molecular functions associated with miR-199a-5p target genes included tau-protein kinase activity, which has key roles in neurons and neuronal cytoskeleton stabilisation and its dysregulation is associated with Alzheimer's disease (280). Biological processes of target genes of miR-199a-5p determined to be significant were Wnt signalling, apoptosis regulation and neuronal differentiation (Figure 3.3.4). The most

significantly impacted pathways were shown to be related to mTOR signalling, Wnt signalling, and nervous system development. These pathways agree with previous pathway and gene target searches, which further indicates Wnt signalling, and the nervous system are regulated by miR-199a-5p. Activin signalling has been recognised to act alongside the canonical Wnt pathway as a co-activator (281). The results of multiple pathway analyses show overall miR-199a-5p likely regulates Wnt signalling and neuronal homeostasis. The Wnt pathway has been shown previously *in vivo* to be affected by miR-199a-5p in dystrophic muscle, wherein miR-199a-5p was shown to negatively affect myogenic differentiation (252), therefore these data suggest miR-199a-5p dysregulation in ageing may be affecting the homeostasis of the NMJ which could be contributing to degeneration.

3.4.4 miR-199a-5p is upregulated in skeletal muscle during ageing in mice.

Following the information that miR-199a-5p is upregulated in human skeletal muscle, we next aimed to determine the effect of age on miR-199a-5p in skeletal muscle and sciatic nerve of mice. Our results demonstrated miR-199a-5p is significantly upregulated in the skeletal muscle of old mice compared to adult mice as determined by RT-qPCR. The expression of miR-199a-5p was not significantly different in sciatic nerves of old mice compared to adult mice, although the expression was noticeably lower (Figure 3.3.5). This agrees with our human data that shows miR-199a-5p is upregulated in aged skeletal muscle (Table 3.3.2). These data may have been affected by our smaller sample size.

Based on the predicted target genes we had previously identified in human muscle, we next used RT-qPCR to determine expression levels of genes associated with predicted miR-199a-5p targets in adult and old mice in both skeletal muscle and sciatic nerves. Our data showed expression of mitochondrial transport gene encoded by mitochondria (282), Nd1 was significantly reduced in old skeletal muscle compared to adult muscle (Figure 3.3.6). Reduced *ND1* gene content has been correlated with sarcopenia in humans (283). It is believed that mitochondrial mutations and accumulation of defective mitochondria with age are associated with sarcopenia in both humans and rodents (284–286). No other genes were found to demonstrate significantly different expression in skeletal muscle in adult or old mice. In sciatic nerves, Hdac9 was found to be significantly upregulated in old mice compared to adult mice (Figure 3.3.7). The

expression of Hdac9 is associated with denervation episodes (287,288), and is associated with the mTOR, which is associated with miR-199a-5p gene targets (Figure 3.3.4) (289). These data suggest miR-199a-5p regulates Hdac9, which has roles in regulation of reinnervation of muscle endplates, and Hdac9 was shown to inhibit reinnervation in the soleus muscle of mice following nerve transfer (287). Taken together with the data found in published databases, we can conclude miR-199a-5p is upregulated in ageing in skeletal muscle of both humans and mice and is likely a regulator of NMJ interactions by targeting NMJ specific gene targets, ER stress and mitochondria, the dysregulation of which may be a contributing factor in the development of sarcopenia.

Chapter 4 The role of miR-199a-5p in muscle and neuronal homeostasis *in vitro*

4 The role of miR-199a-5p in muscle and neuronal homeostasis *in vitro*

4.1 Introduction

Sarcopenia is defined as age-related loss of muscle mass and muscle function (290) and appears to be almost inevitable, with declining muscle fibres beginning at approximately 50 years of age, and a varied prevalence between 5–13% for people aged 60–70 years and 11–50% for those 80 years and above (36). In addition to skeletal myofibre atrophy associated with ageing, deterioration of the NMJ, the synaptic connection between the motor nerve terminal and the postsynaptic muscle membrane, has been observed with ageing. Human and animal studies have shown axonal denervation, reinnervation and remodelling during ageing as well as NMJ fragmentation with ageing observed in rodent models (291).

Some of these changes are associated with loss of motor units (42,292). Degeneration of axons and motor neurons is a consequence of ageing and results in skeletal muscle atrophy and an abnormal NMJ (42). One of the potential drivers of these NMJ changes are dysregulation of miRs associated with skeletal muscle (293). An individual's initial muscle mass appears to be a critical factor influencing the risk of developing sarcopenia. Muscle mass is dictated by the number of muscle fibres and the size of the fibres. The decline in muscle mass and strength in people after the age of ≈50, appears primarily due to loss of muscle fibres with weakening of the remaining fibres (1,294). Data clearly indicate that in ageing humans and rodents, loss of motor neurons also accompanies the loss of muscle fibres (16,26,295–298), with a 25-50% reduction in the number of α-motor neurons occurring with ageing (299). Progressive loss of muscle mass and function with ageing is also associated with alterations in NMJ morphology, similar to those in neurodegenerative disorders, such as ALS (300–302). NMJ maintenance is a dynamic process: NMJs undergo re-modelling postnatally and NMJs can regenerate following muscle injury, however this process is disrupted during ageing; for example, NMJs in muscle fibres of old mice show a variety of alterations including axonal swelling, sprouting, synaptic detachment, withdrawal of axons from postsynaptic sites and fragmentation of the AChRs (290,303,304).

The reduced interaction between muscle and nerve has been proposed to play a crucial role in the age-related loss of muscle mass and function. However, the

molecular mechanisms underlying NMJ deterioration are not well understood. Most approaches to improve muscle function in older humans/rodents aim to improve the function of the residual muscle fibres through exercise and/or dietary interventions, but no address the mechanistic causes of neuromuscular deterioration. It also remains unknown whether changes occurring in muscle, nerve, or both, initiate the deterioration of neuromuscular interactions in ageing, however it is clear that functional muscle: nerve communication is key to maintaining muscle mass and function. It is therefore important to understand key mechanisms related to neuromuscular deterioration, to design effective therapeutics.

Molecular mechanisms of neuromuscular deterioration are complex, still, factors contributing to neuromuscular deterioration during ageing have been described, such as changes in the expression of neurotrophic factors (87,303,305). Advances in high throughput 'omics' approaches have highlighted significant dysregulation of gene and protein expression in skeletal muscle and nerve during ageing, however functional approaches are still lacking (171,227,306–308). Changes in gene expression and proteins with known roles in neuromuscular homeostasis: Foxo3, Sirt1, Hdac9 and mTOR, Atrogin-1, NGF, BDGF, IGF and TGF-β signalling, as well as others have been associated with muscle and nerve degeneration in sarcopenia (1,87,303,305). Many of these genes are predicated/validated targets of a group of miRs, robust post-transcriptional regulators of gene expression (). The expression of miRs, e.g., miR-378 or miR-143 (205,309) has also been shown to change in muscle and nerve during ageing (82,171,174,300,308).

In humans, miR-199a-5p has also been shown to be upregulated in neurodegenerative disease such as multiple system atrophy, a synucleinopathy (310), as well as ALS (311). Dystrophic muscle has also been associated with elevated miR-199a-5p in human muscle (252,312). Upregulated miR-199a-5p may contribute to NMJ damage and atrophy of the associated skeletal muscle.

The miR-199a-5p family is among miRs predicted and expressed in skeletal muscle as well as in the nerve. The family is comprised of miR-199a (miR-199a-5p (MIMAT0000231) and miR-199a-3p (MIMAT0000232)) and miR-199b (miR-199b-5p (MIMAT0000263) and miR-199b-3p (MIMAT0004563) miRbase, http://www.miRbase.org)). The role of miR-199a-5p specifically has been implicated

in the homeostasis of skeletal and smooth muscle, such as in cell proliferation of human smooth muscle cells through the Wnt pathway (313), upregulation in cardiotoxin models of skeletal muscle regeneration in mice has also been observed, with miR-199a-5p suggested to play a role in development of fibrosis (314). Skeletal muscle also appears to be correlated with miR-199a-5p; sitka deer muscle of aged deer is characterised by upregulated miR-199a-5p, and associated with downregulated ACTN3, a protein component of skeletal muscle Z-discs (315). There also appears to be regulatory roles for miR-199a-5p in cardiopulmonary diseases and age-related disorders. For example, upregulation of miR-199a-5p has been demonstrated in patients with idiopathic pulmonary fibrosis, a disease in which lung transplant is the only option (316), cardiovascular hypertrophy (317), and cancers such as non-small cell lung cancer (318).

The miR-199 family including miR-199a-5p has also been shown to be important in the development of spinal cord in mice (319), and the levels of miR-199a-5p have been correlated with disease progression in multiple sclerosis, suggesting an importance in neurodegeneration (320). A link that has also been observed between miR-199a-5p and osteoarthritis, with the miR playing a negative role in chondrocyte proliferation and survival by way of MAPK4 (321). This suggests a role for miR-199a-5p in nerve, muscle, and cartilage by miR-199a-5p, all three of which play critical roles in skeletal muscle homeostasis. However, the role of miR-199a-5p is regulating neuromuscular homeostasis is unknown.

We hypothesised upregulated miR-199a-5p would negatively regulate myogenesis *in vitro*. To determine the role of miR-199a-5p on myogenesis, *in vitro*, miR-199a-5p mimic overexpression and/or miR inhibitor, antagomiR-199a-5p was used. We aimed to determine the effect of miR-199a-5p on myogenesis in C2C12 myoblasts, and hypertrophy or atrophy in differentiated C2C12 cells using immunostaining. Given the literature supporting the role of miR-199a-5p in neuronal homeostasis, we aimed to assess the effect of miR-199a-5p on neuronal cells. The effects of miR-199a-5p on muscle (C2C12) and nerve (NSC-34) cells (Chapter 5) were investigated to determine myogenic differentiation, size, and area as well as the effect of miR: target interaction through gene expression and protein expression analysis.

4.2 miR-199a-5p *in vitro* materials and methods

4.2.1 Cells and cell culture

In vitro assessments were performed using C2C12 mouse myoblasts (originally derived from satellite cells from the thigh muscle of a 2-month-old female mouse (322)) gifted by Dr Howard Fearnhead (NUIG) and NSC-34 (motor neuron enriched, embryonic mouse spinal cord cells with mouse neuroblastoma, see 5.2.1) cells gifted by Dr Brian McDonagh (NUIG), to assess muscle or nerve, respectively. C2C12 cells are used as a model of skeletal muscle cells and are easily differentiated in culture (323). NSC-34 cells are used in the literature as a relevant model for the study of motor neurons and can be differentiated in culture. The culture conditions and differentiation of NSC-34 cells was taken from published protocols (324).

All cells were seeded before passage number 25, and were cultured in standard growth conditions and in a growth-medium comprised of DMEM hi-glucose supplemented with 10% FBS and 1% penicillin/streptomycin (p/s) (as described in (256)). For cell differentiation assays, C2C12 myoblasts were cultured in DMEM supplemented with 2% HS and 1% p/s using the same growth conditions as previously described in section 2.4.1. For additional *in vitro* assessments in NSC-34 cells, see chapter 5.

4.2.2 miR-199a-5p mimic and inhibitor sequences

All cells used for in vitro experiments (C2C12, NSC34), were transfected with cholesterol-conjugated miR mimics: miR-199a-5p at a final concentration of 100nM, antagomiR-199a-5p (AM-199), or antagomiR scrambled control sequence (Scr) at a final concentration of 200nM as optimised by the Whysall lab (241). Mimics used were chemically modified by the manufacturer with cholesterol (Chl) on passive strands and phosphothioate bonds were included at 5’, and 3’ ends to increase stability. Cholesterol modifications were added by the manufacturer to improve delivery to the cells. All bonds were 2-O-methyl bonds for increased stability.

The sequences were as follows:

Scr- 5'
mC.*.mA.*.mU.mC.mC.mA.mU.mC.mA.mC.mU.mC.mA.mC.mU.mC.mC.mA.mU.
.mC..mA.* .mU.3'-Chl 3'

miR-199a-5p- 5'- miRIDIAN mimic based on mmu-miR-199a-5p MIMAT0000229

antagomiR-199a-5p- 5' mG(*)mA (*)mAmC mAmGmG mUmAmG mUmCmU mGmAmA mCmAmC (*)mU(*) mG(*)mG (*)mG (3'-Chl) 3'

Transfections were performed as described in 2.5.

4.2.3 Cell Counting Kit-8 assay

Cell Counting Kit-8 was used to determine the effect of miR-199a-5p overexpression on C2C12 proliferation. A total of 1000 cells were added to a 96-well plate, 100µl of growth medium was added and allowed to incubate for 4 hours. After 4 hours, half of the samples were to be exposed to hydrogen peroxide (H_2O_2), wells were treated with 1mM H_2O_2 for 10 minutes in a sterile incubator at 37°/5%CO_2. After H_2O_2 treatment if needed, cells were replaced with new medium and treated with miR mimic or antagomiR as described in 2.6.1, and allowed to incubate for 72 hours. After this incubation, a standard curve was plated. 10µl of the CCK-8 assay reagent was added to each well, and the absorbance was read at 450nm on the Hidex microplate reader. Samples were normalised prior to analysis.

4.2.4 ER stress assay

The accumulation and progression of the UPR has been implicated in skeletal muscle health (325,326). Along with skeletal muscle homeostasis, ER stress has also been implicated in the integrity of the NMJ (325). We hypothesised that dysregulated NMJ and skeletal muscle homeostasis may be associated with disrupted ER stress response linked to several miR-199a-5p target genes. Tunicamycin was used to induce ER stress *in vitro,* in order to investigate the effect of stress on C2C12 muscle cells. Tunicamycin has been shown to be an effective inducer of ER stress *in vitro* in hepatocytes and adipocytes (327), as well as in C2C12 cells (328). For ER stress experiments, C2C12 cells were differentiated as described and treated as described in (329); briefly, cells were exposed to tunicamycin for 8 hours at a concentration of 2.5ug/ml, followed by replacement of fresh differentiation medium and Scr and AM-199 treatment was delivered at a concentration of 200nM ml^{-1} of medium, and 100nM ml^{-1} of medium for miR-199a-5p mimic. Following a 48-hour incubation period, MF20 immunostaining and quantification was performed to determine the effect of

miR-199a-5p overexpression and inhibition on C2C12 cells exposed to tunicamycin-induced ER stress.

4.2.5 *In vitro* immunostaining

MF20 immunostaining was performed as previously described 2.7.3 To visualise myosin heavy chain in C2C12 cells. Briefly, C2C12 cells were seeded (50,000 cells/well) into standard 12-well plates (Scr n=4, miR-199a-5p n=4, AM-199 n=4). At ~70% confluency, fresh differentiation medium was added and then miRs were transfected (day 1) and the MF20 staining was performed on day 5 (growth conditions), or day 8 (differentiated myotubes treated on day 5) (Table 2.5.1). Cells were transfected with 200nM of Scr, 100nM of miR-199a-5p, or 200nM AM-199.

MF20 assays were performed by washing the wells in PBS for 5 minutes, next fixing samples in ice-cold MeOH for 5 minutes. Wells were then blocked in 10% HS (in PBS) for 60 minutes at RT on a rocker. Afterwards, primary antibody: MF20 (diluted 1:500 in blocking solution (2% HS)) was added and incubated at RT for 1 hour. Wells were then washed for 5 mins, 3 times in PBS. Next, secondary antibody was added (1:2000 in blocking solution) and incubated at RT in darkness for 45 minutes. Finally, the wells were washed again in PBS and samples were stained with DAPI (1:10,000 in PBS) in darkness for 10 minutes. Images were obtained using the EVOS M5000 and M7000 Imaging Systems. Each group contained 4 replicates and a total of 5 images were taken per well.

4.2.6 RNA isolation

For RNA isolation from C2C12 cells, cells were collected 48 hours after transfection. TRIzol was added and cells were stored at -80° for later RNA processing. RNA was isolated using TRIzol/chloroform standard RNA isolation protocol and RNA purity was assessed on a Nanodrop 2000 spectrophotometer described in 2.9.3

4.2.7 cDNA synthesis and RT-qPCR

Synthesis of cDNA was performed using SuperScript II using 100-500ng RNA. RT-qPCR was performed using miRCURY LNA SYBR Green for miRs (UNISP6: YP00203954, SNORD68: YP00203911, hsa-miR-199a-5p: YP00204494, hsa-miR-199b-5p: YP00204152) and FAST SYBR Green Master Mix for genes. Relative expression was analysed using the delta-delta Ct method and expressed to β2-

microglobulin or S29 (mRNA) and Rnu-6 and/or Snord-61/Snord-68 (miR). A detailed method is provided in 2.10 for cDNA synthesis, and 2.11 for RT-qPCR. Primer sequences for RT-qPCR are listed in Table 2.11.1. List of primer sequences used for qPCR. Housekeeping genes S29, and β2M were used and analysed as described in 2.11.

4.2.8 Protein isolation from C2C12 cells

For protein collection from cells, isolates were collected 48 hours after transfection. Collected isolates were immediately placed in 1X RIPA buffer (Merck 20-188) supplemented with protease inhibitor (1:1000; Sigma P8340) and stored at -80° for later protein quantification and Western blotting.

4.2.9 Protein quantification and Western blot

For protein quantification and Western blot, cells were lysed in 1X RIPA buffer and protein concentrations were calculated using Bradford reagent (Bio Rad 5000006) and BSA standards as described in 2.14. Blotting was performed using protein lysates diluted in Laemmli buffer, and 20μg of protein was run on 8%– 16% polyacrylamide gels. Proteins were transferred to nitrocellulose membranes (GE Life Sciences 10600002) using a semi-dry blotter (Cleaver Scientific). Subsequently, membranes were stained with Ponceau S (0.1 % Ponceau in 5% acetic acid) to visualise and confirm equal protein loading. Membranes were blocked in 5% milk in TBS-T for 1 hour at room temperature, and following, washed 3x10 minutes in TBS-T. Membranes were incubated with primary antibodies (1:750-1:1000 antibodies table listed in supplemental) overnight at 4°C. Membranes were then washed in TBS-T and incubated with fluorescent secondary antibodies; goat anti-rabbit and goat anti-mouse, and images were obtained using Odyssey Fc Imaging system (Li-Cor).

4.2.10 Luciferase assay and reporter constructs

Luciferase assay was performed with the assistance of Dr K. Whysall using protocol as described in Goljanek-Whysall *et al*. 2012 (323). Each experiment had triplicate samples and was carried out four times using two independent plasmid preparations of each reporter. Protein was extracted after transfection, 48 hours later. Luciferase activity was measured using a multilabel counter (Victor2) and normalised to Renilla luciferase. Relative reporter activity for miR treated cells was obtained by normalisation to non-miR-treated WT or mutant constructs, respectively. Statistics

were performed using one-way ANOVA with Dunnett's post-test with $p < 0.05$ considered statistically significant.

4.2.11 Image analysis

Image analyses of MF20 assays were performed as described in Soriano *et al.,* 2017 (256) using ImageJ software, through manually counting nuclei within myotubes for fusion index (fusion index is shown as the percentage of nuclei contained within myotubes to the total number of nuclei in each field of view), and area was calculated using the threshold parameter to obtain the minimum effective area for each condition.

Western blot images were obtained using Odyssey Fc Imaging system (Li-Cor), and quantification was performed using ImageJ and normalised to Ponceau S stain by densitometry of total Ponceau in that sample lane.

Mitochondrial quantification performed using MitoTracker Red was done by quantifying mean fluorescent intensity area of the Red channel and dividing that number by the total number of nuclei present within the image. This was performed with ImageJ and Excel.

4.2.12 Statistical analysis

All data are represented as mean ± SEM. One-way ANOVA was used to compare means of the three groups. A Dunnett's post-test was performed to compare the treatment groups (miR-199a-5p, and AM-199) with the control group (Scr). One-way ANOVA analyses for qPCR, protein and image analysis were performed using GraphPad Prism version 5.03, with p-values ≤ 0.05 considered statistically significant.

4.3 Results

4.3.1 miR-199a-5p regulates myogenesis *in vitro* in C2C12 mouse myoblasts.

To investigate the effect of miR-199a-5p *in vitro*, C2C12 myoblasts were first treated with miR-199a-5p mimic or AM-199 mimic, or scrambled antagomir control (Scr) as described in 2.6.1. Verification of miR-199a-5p upregulation and downregulation by mimic or antagomiR was performed by RT-qPCR for miRs (Figure 4.3.1). The results demonstrated miR-199a-5p treatment results in significant upregulation of miR-199a-

5p in C2C12 cells, further, inhibition by AM-199 resulted in significant downregulation of miR-199a-5p compared to Scr control (Figure 4.3.1).

Immunostaining of treated C2C12 cells with MF20 myosin heavy chain antibody revealed inhibitory effects of miR-199a-5p as compared to Scr controls. Quantification of MF20 immunostaining demonstrated that miR-199a-5p treated C2C12 myoblasts formed smaller myotubes (diameter) with fewer nuclei (fusion index) (Figure 4.3.2). Moreover, miR-199a-5p-treated myoblasts produced very small myotubes containing 1-2 nuclei, although no significant differences were observed in overall myotube area (Figure 4.3.2).

Next, differentiated C2C12 myotubes were treated with miR-199a-5p, AM-199, or Scr control to assess the effect of miR overexpression or inhibition on differentiated C2C12 cells. Immunostaining of treated C2C12 myotubes with MF20 immunostaining revealed inhibitory effects of miR-199a-5p as compared to Scr controls. C2C12 myotubes treated with miR-199a-5p were characterised by smaller myotube diameter as compared to Scr control (Figure 4.3.3). Myotubes treated with AM-199 contained more nuclei (fusion index) compared to miR-199a-5p overexpression (Figure 4.3.3). Further, myotube area was significantly reduced in miR-199a-5p treated myotubes as compared to the Scr control group, with miR-199a-5p overexpression demonstrating a reduced myotube area and thinner myotubes compared to Scr controls but not AM-199 (Figure 4.3.3).

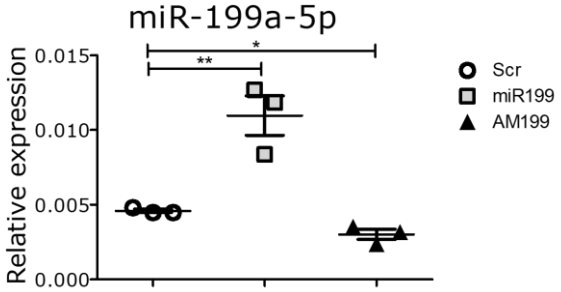

Figure 4.3.1. Treatment of C2C12 myoblasts with miR-199a-5p mimic or AM-199 results in upregulated and downregulated levels of miR-199a-5p, respectively, as compared to Scr control. C2C12 cells were treated with miR-199a-5p mimic or antagomiR-199a-5p, and RNA was isolated 48 hours later. RT-qPCR data showed miR-199a-5p mimic significantly upregulated miR-199a-5p expression, and antagomiR treatment significantly lowered miR-199a-5p expression in C2C12 cells. N= 3, error bars show SEM, expression relative to Rnu-6 is shown. One-way ANOVA with Dunnett's post-test was performed. * $p<0.05$.

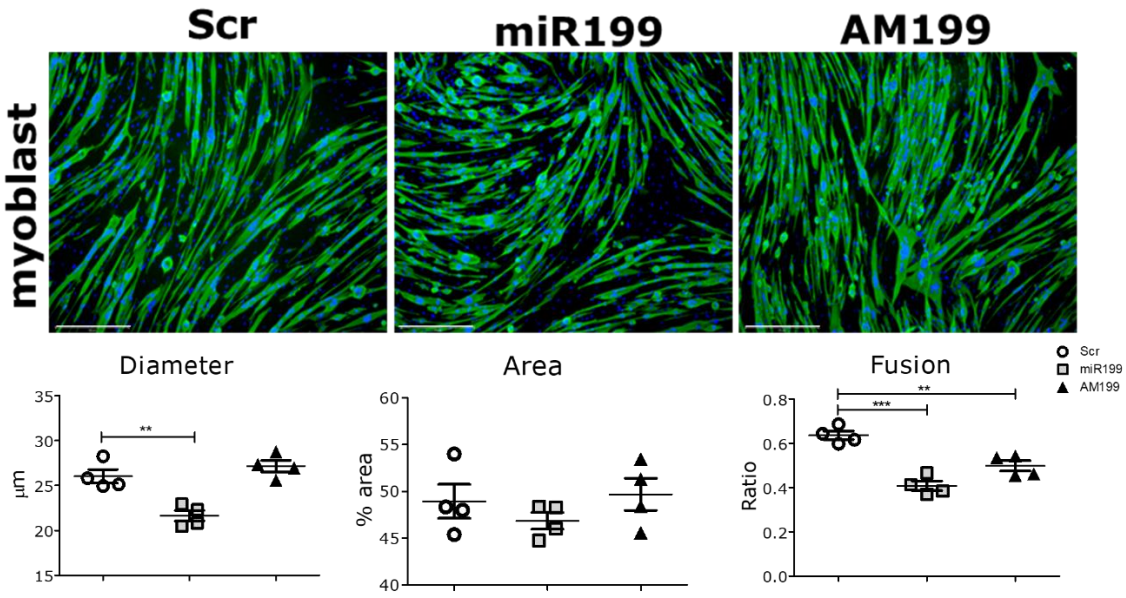

Figure 4.3.2. miR-199a-5p regulates myogenesis in C2C12 mouse myoblasts. C2C12 myoblasts showed decreased diameter size and fusion following treatment with miR-199. Inhibition of miR-199 using AM-199 had no effect on myogenic differentiation as compared to Scr control, as indicated by quantification of MF20 (which detect myosin heavy chain, a myogenesis marker) immunostaining by ImageJ. Representative images are shown, green: MF20, blue: DAPI; n=4. Scr – antagomiR scrambled, miR-199 – miR-199a-5p mimic; AM-199 – antagomiR to miR-199a-5p. Error bars show SEM; * - $p<0.05$. One-way ANOVA with Dunnett's post-test. Scale bar 275 µm.

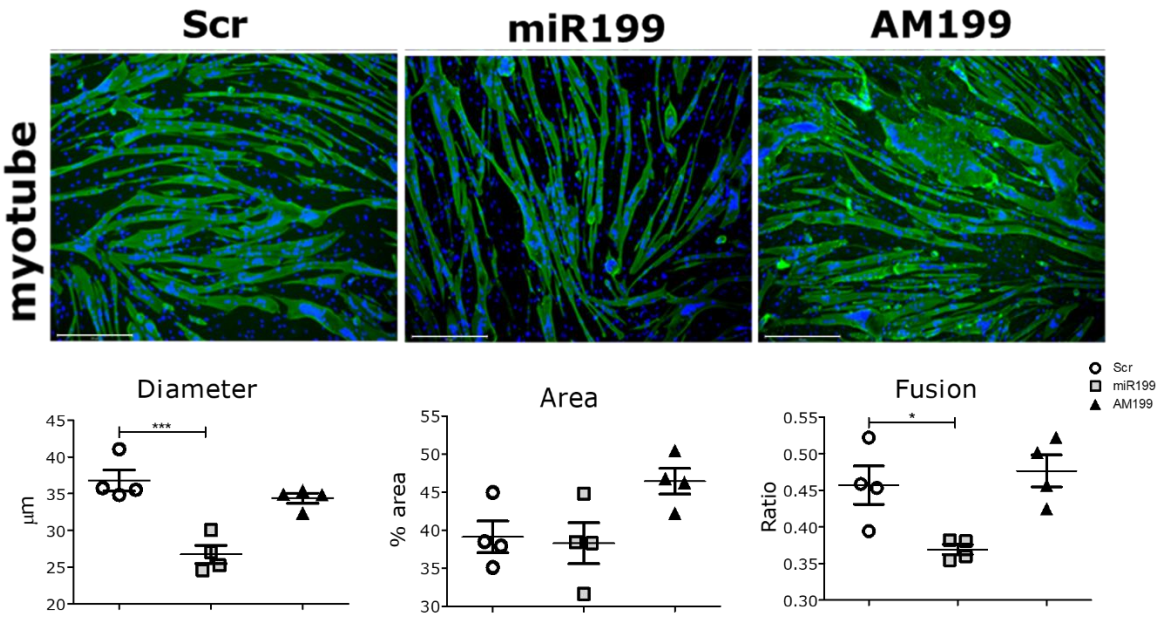

Figure 4.3.3. miR-199a-5p negatively regulates myotube growth. Differentiated C2C12 cells were treated with miR-199, AM-199 or Scr control and then stained with MF20 antibody, which detects myosin heavy chain, a marker of myogenesis. Overexpression of miR-199a-5p resulted in significantly decreased diameter, and fusion index of myotubes as compared to Scr control. Area of myotubes was decreased in myotubes treated with miR-199 mimic as compared to Scr control. Green: MF20, blue: DAPI; n=4. Scr – antagomiR scrambled, miR-199 – miR-199a-5p mimic; AM-199 – antagomiR to miR-199a-5p. Error bars show SEM; * - $p<0.05$. One-way ANOVA with Dunnett's post-test. Scale bar 275 μm.

4.3.2 miR-199a-5p inhibition reduces C2C12 cell number

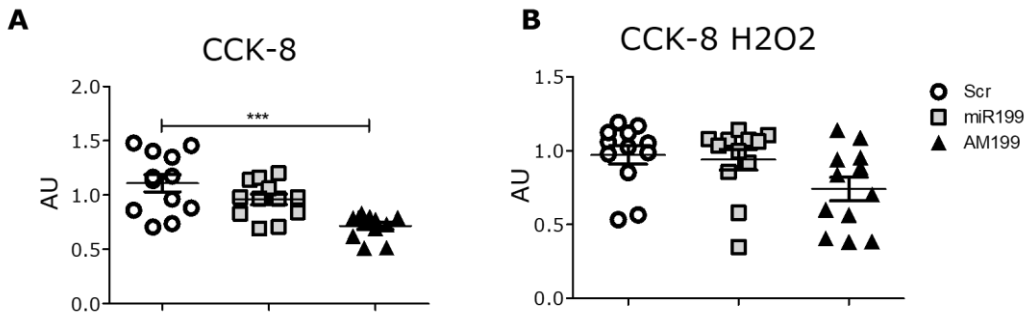

Figure 4.3.4. miR-199a-5p does not affect cell number in the presence of H2O2 but reduces proliferation in growth conditions. Cell Counting Kit-8 (CCK-8) was used to determine the effect of miR-199a-5p on cell number in normal and stressed (H_2O_2 1mM) condition. A) Cell number was reduced with miR-199a-5p inhibition as compared to Scr controls in normal growth conditions. B) Cell number was not affected by miR-199 overexpression or inhibition in the presence of H_2O_2. Arbitrary units shown; n=12. Scr – antagomiR scrambled, miR-199 – miR-199a-5p mimic; AM-199 – antagomiR to miR-199a-5p. Error bars show SEM; * – $p<0.05$. One-way ANOVA with Dunnett's post-test.

4.3.3 miR-199a-5p regulated the expression of ER stress marker, Grp78, in C2C12 cells

To determine mechanism of action of miR-199a-5p, we used target prediction databases to characterise miR-199a-5p target genes. Targets included Grp78 and Atf6 related to ER stress, and these targets are supported by the literature (334–337), as well as our bioinformatic analyses (see 3.3). We therefore explored expression of genes of the three activating arms of the ER stress pathway: *PERK*, *IRE-1α*, and *ATF6*.

The overexpression of miR-199 in C2C12 myoblasts showed moderate downregulation of ATF6 protein levels as compared to Scr controls, however this was not significant (Figure 4.3.5). CHOP protein levels showed a trend towards upregulation following miR-199 treatment, however no significant changes were observed (Figure 4.3.5). A significant increase in levels of ER stress-related protein, GRP78, was observed following miR-199 overexpression as compared to both Scr control and AM-199 treatment was observed (Figure 4.3.5). The mRNA levels of Atf6, Chop and Grp78 were not altered by inhibition or overexpression of miR-199a-

5p, which is not entirely surprising given that miRs can regulate gene expression at protein level without affecting mRNA levels (Figure 4.3.5). Additionally, Xbp1 splicing was analysed as one of the arms of ER stress pathway. Xbp-1 splicing was mildly enhanced following miR-199 inhibition as compared to Scr control, however this was not significant. A variability among the replicates was observed which suggest the need to further explore this aspect of miR-199a-5p function (Figure 4.3.5). Together these data suggests that miR-199a-5p may regulate the PERK arm of the ER stress response through GRP78 upregulation and possible subsequent CHOP activation.

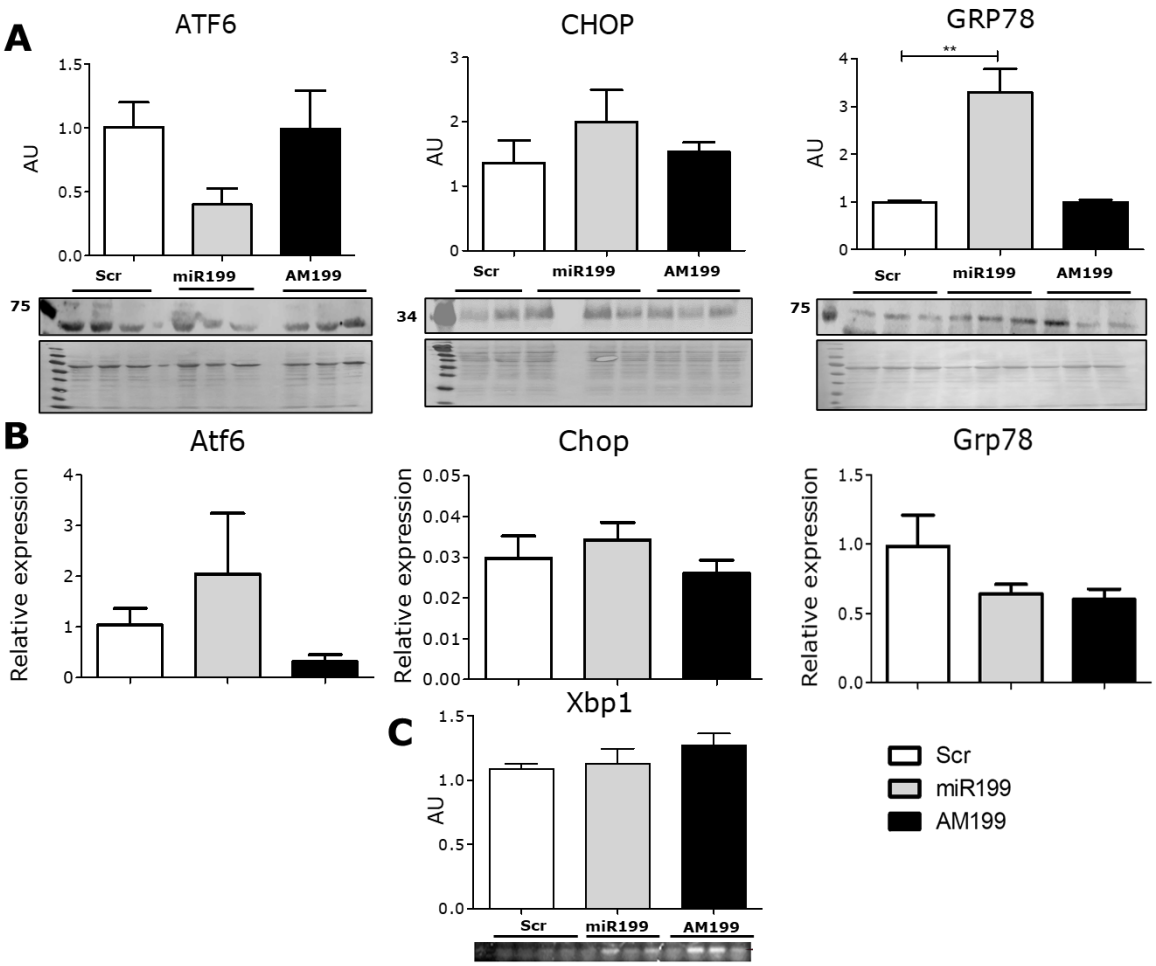

Figure 4.3.5. Overexpression of miR-199 led to increased expression of ER stress-related protein, GRP78 A) C2C12 cells were treated with miR-199a5p, AM-199, or Scr control. Overexpression of miR-199 resulted in significant increase in the protein level of GRP78 compared to both miR inhibition by AM-199, and Scr control. An increase trend was seen in CHOP and decrease in ATF6 protein levels following miR-199 overexpression, although this was not statistically significant. B) No significant changes in relative expression of Atf6, Chop, or Grp78 were observed by qPCR. C) Xbp1 splicing was not altered following miR-199 overexpression or inhibition. Arbitrary units shown for Western blot quantification; qPCR: expression relative to S29 is shown; n=3. Scr – antagomiR scrambled, miR-199 – miR-199a-5p mimic; AM-199 – antagomiR to miR-199a-5p. Error bars show SEM; * – $p<0.05$. One-way ANOVA with Dunnett's post-test.

Next, to further explore the potential regulation of GRP78 and CHOP modulation by miR-199a-5p, C2C12 myoblasts were exposed to tunicamycin as described in 4.2.4. Immunostaining of myoblasts showed higher percentage of myoblasts positively stained for ER stress protein CHOP following miR-199 overexpression and AM-199 treatment led to a decrease in the number of CHOP-positive cells in the presence of tunicamycin as compared to Scr control treated with tunicamycin (Figure 4.3.6).

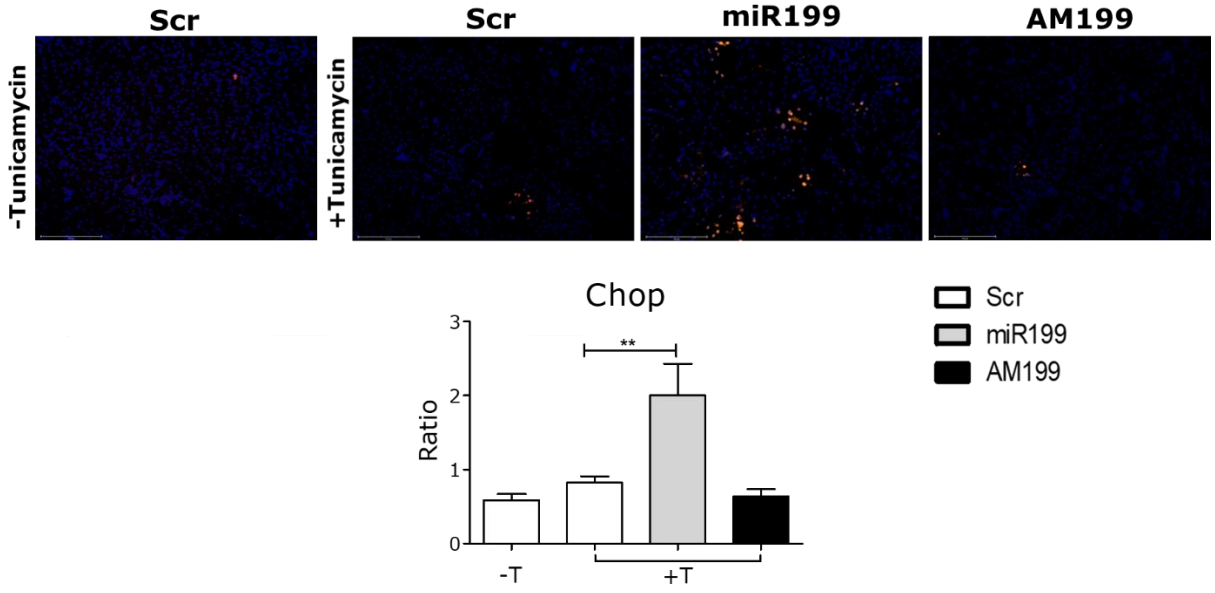

Figure 4.3.6. Overexpression of miR-199a-5p in C2C12 cells results in an increased number of CHOP-positive cells. C2C12 myotubes were exposed to tunicamycin, and then treated with Scr, miR-199a-5p, or AM-199. Quantification of CHOP-expressing cells show tunicamycin significantly upregulated CHOP positive cells with miR-199a-5p treatment. Representative images are shown; red: CHOP, blue: DAPI; n=4. Scr – antagomiR scrambled, miR-199 – miR-199a-5p mimic; AM-199 – antagomiR to miR-199a-5p. Error bars show SEM; * - $p<0.05$. One-way ANOVA with Dunnett's post-test. Scale bar 275µm. Ratio- % cells positive for CHOP.

4.3.4 miR-199a-5p inhibition significantly ameliorates the effects of tunicamycin on C2C12 myotubes

To determine whether miR-199-mediated regulation of proteins related to ER stress, we next investigated whether inhibition of miR-199a-5p may rescue myotube atrophy associated with tunicamycin treatment. C2C12 cells were first treated with tunicamycin to induce ER stress, this resulted in myotube atrophy as quantified by

significantly diminished myotube diameter as compared to Scr control (Figure 4.3.7). MF20 immunostaining and quantification demonstrated that miR-199a-5p, in the presence of tunicamycin, significantly reduced myotube diameter as compared to Scr controls, in the presence of tunicamycin, further, inhibition of miR-199a-5p resulted in significantly increased diameter as compared to Scr controls (Figure 4.3.7). Area was not statistically significantly different between tunicamycin treated groups (Figure 4.3.7). Fusion index was found to be significantly lower in miR-199a-5p treated myotubes as compared to Scr controls, and AM-199 treatment appeared to ameliorate the effects of tunicamycin through preservation of myotube diameter, and fusion (Figure 4.3.7).

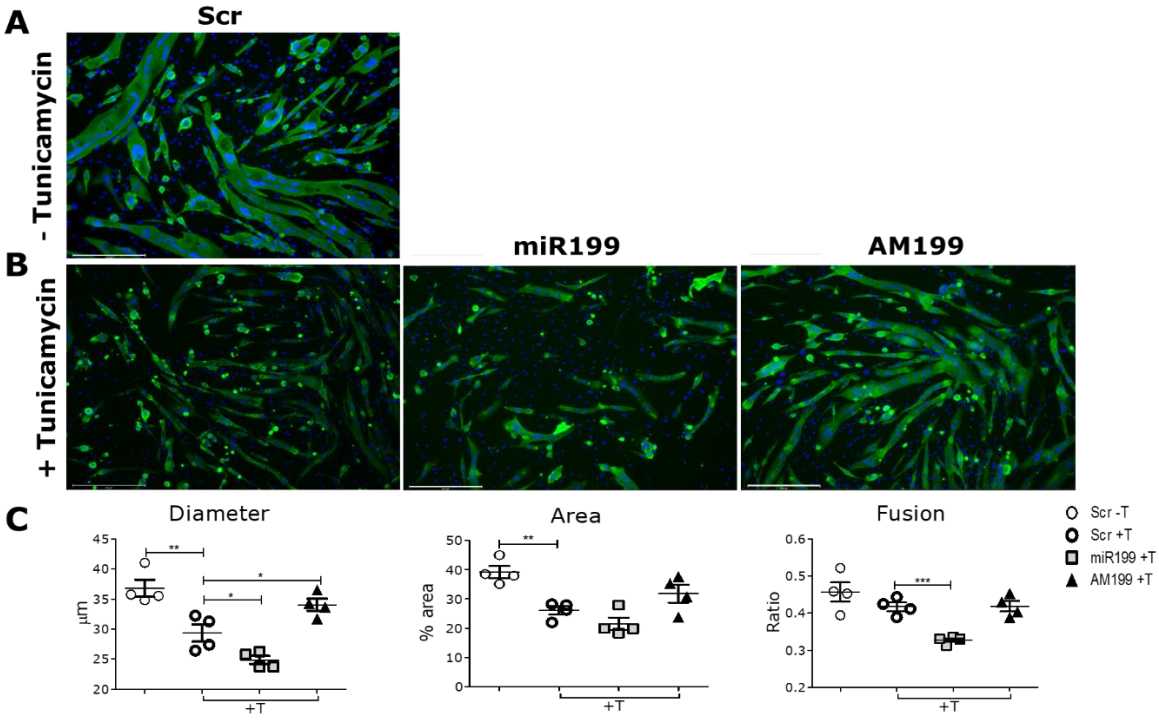

Figure 4.3.7. Inhibition of miR-199a-5p in C2C12 myotubes significantly ameliorated the effect of tunicamycin on diameter. A) C2C12 myotubes were exposed to tunicamycin followed by Scr, miR-199a-5p, or AM-199 treatment, a non-tunicamycin treated Scr control was also used. B) MF20 immunostaining demonstrated that miR-199a-5p enhances negative effects of tunicamycin on myotube diameter and fusion index as compared to Scr control. C) Overexpression of miR-199 in tunicamycin treated cells resulted in significantly reduced myotube diameter and fusion, and AM-199 ameliorated the effects of tunicamycin through preservation of myotube diameter, and fusion. Representative images are shown; green: MF20, blue: DAPI; n=4. Scr – antagomiR scrambled, miR-199 – miR-199a-5p mimic; AM-199 – antagomiR to miR-199a-5p. Error bars show SEM; * - $p<0.05$. One-way ANOVA with Dunnett's post-test. Scale bar 275 µm.

4.3.5 miR-199a-5p did not signifcantly regulate mitochondrial biogenesis

To investigate the effect of miR-199 overexpression or inhibition on mitochondrial function, C2C12 myoblasts were treated with Scr control, miR-199, or AM-199 and next stained with MitoTracker. MitoTracker Red is a fluorescent dye that stains mitochondria in cells and accumulates in mitochondria dependent on membrane potential; it is used to label active mitochondria for quantification on fixed cells (244).

miR-199a-5p treatment led to no significant change in mitochondrial content as compared to Scr controls, whereas inhibition of miR-199a-5p by AM-199 led to increased mitochondrial activity as compared to miR-199a-5p overexpression and Scr controls as determined by quantification of MitoTracker staining (Figure 4.3.8).

Since MitoTracker Red staining indicated a potential enhancement of mitochondrial function in C2C12 myoblasts treated with AM-199, we next investigated mitochondrial function using Seahorse analyser through measuring oxygen consumption rate (OCR) of the cells on a plate-based live cell assay (this experiment was performed with assistance from Ms Maria Borja Gonzalez). Treatment with AM-199 led to improved mitochondrial maximal respiration in C2C12 myoblasts as compared to Scr controls (Figure 4.3.9). miR-199 treatment did not significantly affect OCR when compared to Scr controls.

Together, this suggests that miR-199a-5p inhibition may lead to improved mitochondrial activity. We therefore investigated the expression of genes associated with mitochondrial dynamics and content, as well autophagy including miR targets: Pgc-1α (330), a regulator of mitochondrial biogenesis. Other genes of interest included: *Atg5*, a key autophagy protein that is involved in autophagic vesicle formation as well as mitochondrial quality control after oxidative damage (331); *Lc3b*, a marker of autophagic flux (332); *CoxI*, which is involved in electron transport, and is encoded in the mitochondrial genome, hence considered a marker of mitochondrial content (333); *Tfam*, a mitochondrial protein necessary for ATP production from oxidative phosphorylation (334), and *Nrf2*, which has roles in antioxidant regulation (335).

The expression of mitochondrial marker CoxI, encoded by the mitochondrial genome, and mitochondrial biogenesis marker Pgc-1α, was increased following AM-199 treatment, as compared to Scr controls, however this was not statistically significant

(Figure 4.3.10). Overexpression of miR-199 did not significantly affect expression levels of either CoxI or Pgc-1α compared to Scr controls. miR-199 had no effect on the expression of Atg5, Lc3b, Tfam, or Nrf2 (Figure 4.3.10).

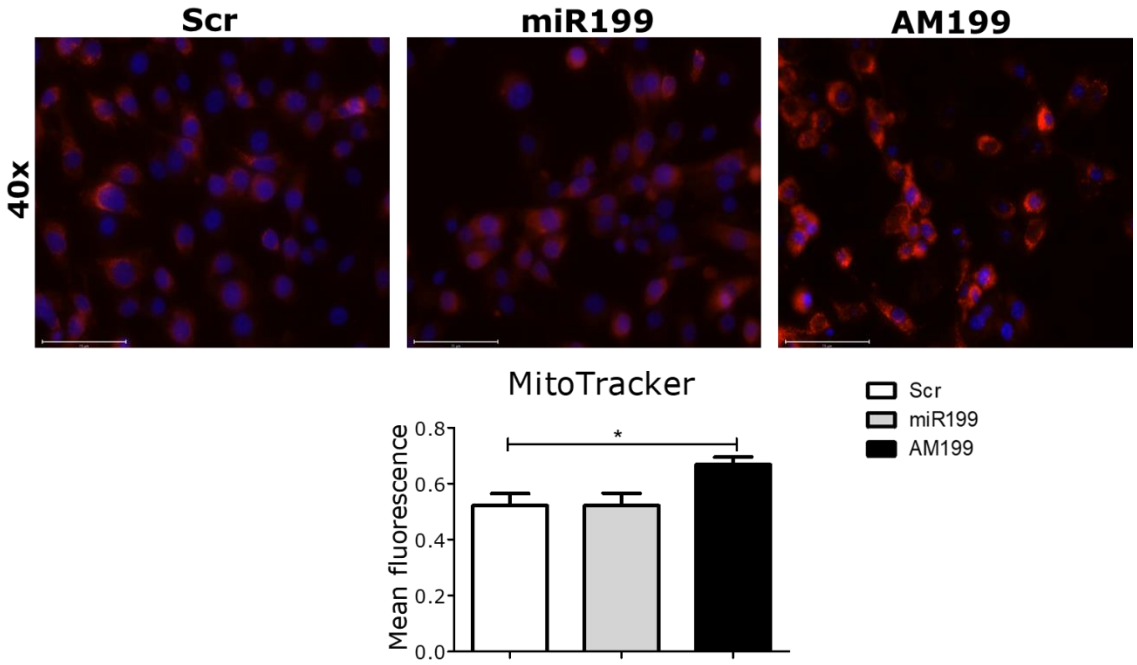

Figure 4.3.8. miR-199 affects mitochondrial activity in C2C12 myoblasts. C2C12 cells were treated with Scr control, miR-199 mimic or AM-199 inhibitor. There was no difference seen between miR-199 overexpression or Scr control. The inhibition of miR-199 by AM-199 resulted in significant increased mean fluorescence compared to both miR overexpression and Scr controls. Representative images are shown red- MitoTracker, blue- DAPI, n=4. Scr – antagomiR scrambled, miR-199 – miR-199a-5p mimic; AM-199 – antagomiR to miR-199a-5p. Error bars show SEM; * - $p<0.05$. One-way ANOVA. Scale 40x- 75µm.

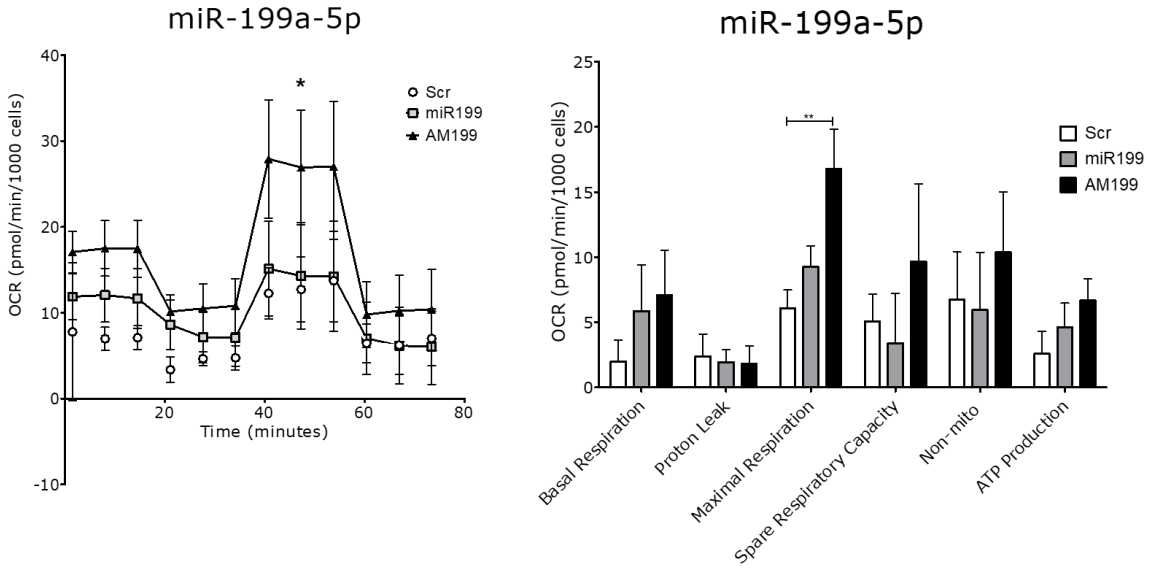

Figure 4.3.9. Inhibition of miR-199a-5p has a positive effect on mitochondrial respiration. Seahorse bioanalysis of mitochondrial function was assessed. AM-199 treatment led to enhanced mitochondrial function. This was specifically seen in parameters of maximal respiration, and spare respiratory capacity in C2C12 myoblasts as compared to Scr controls. Scr – antagomiR scrambled, miR-199 – miR-199a-5p mimic; AM-199 – antagomiR to miR-199a-5p, n=3.

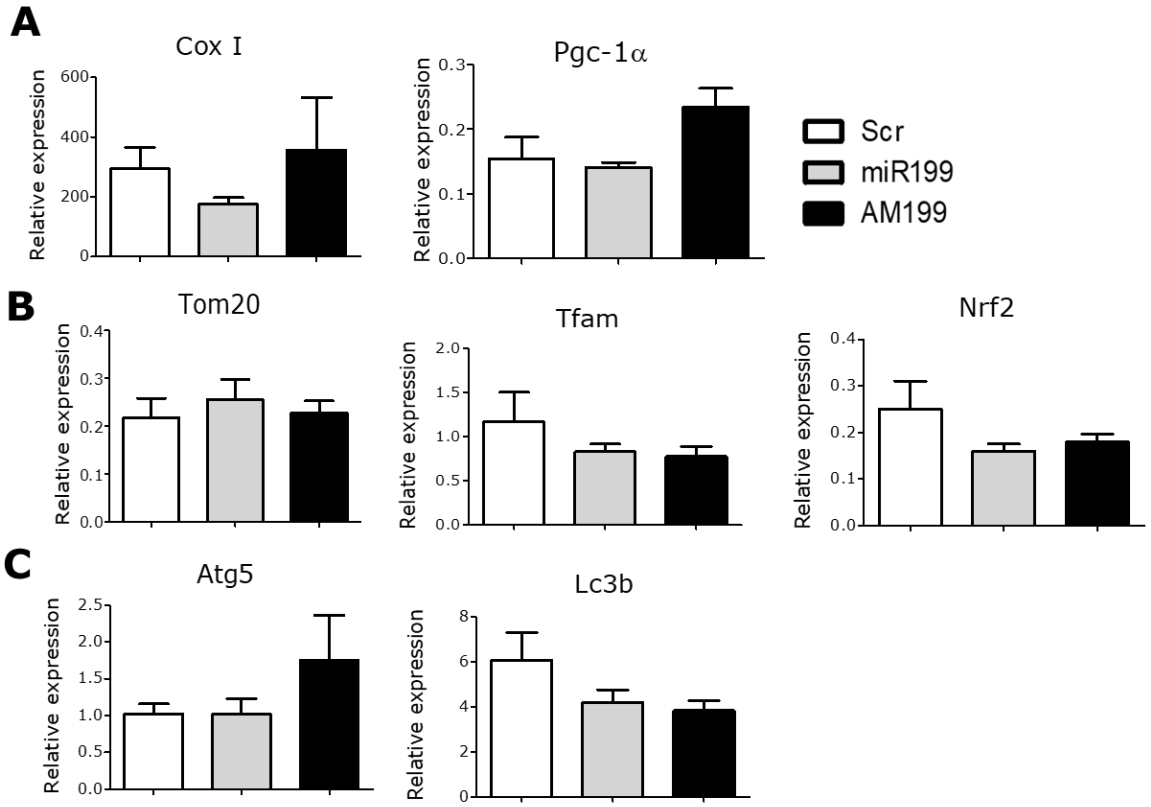

Figure 4.3.10. The expression of mitochondrial biogenesis target, Pgc-1α, was not regulated by miR-199a-5p. A) miR-199 inhibition led to no significant changes in mRNA levels expression of Pgc-1α, CoxI (mitochondrial content marker). miR-199a-5p overexpression did not statistically change Pgc-1α, or CoxI. B) miR-199 had no effect on expression of targets associated with mitochondrial content and dynamics, (Tom20, Tfam, Nrf2) or C) autophagy (Atg5, Lc3b) in C2C12 cells. Expression relative to S29 is shown; n=3. Scr – antagomiR scrambled, miR-199 – miR-199a-5p mimic; AM-199 – antagomiR to miR-199a-5p. Error bars show SEM; * - $p<0.05$. One-way ANOVA with Dunnett's post-test.

4.3.6 miR-199a-5p regulates expression of NMJ-related gene *Gap43 in vitro*

Finally, we explored regulation of genes associated with NMJ homeostasis, including miR-199a-5p targets, Acvr2a, and Hdac9 (336). We also investigated the levels of *GAP43* expression as we found a non-conserved, potentially weak miR-199a-5p binding site in Gap43 3'UTR (see 4.3.7) (Figure 4.3.12). C2C12 cells were treated with miR mimic or inhibitor as described and were assessed on mRNA and protein level by RT-qPCR or western blot, respectively (Figure 4.3.11). Fdz7, a receptor of the Wnt /β-catenin, with roles in developing muscles (323) and target of miR-199a-5p (337) was also investigated, however miR-199a-5p did not affect Fzd7 levels (Figure 4.3.11). Overexpression of miR-199 led to downregulation of NMJ maintenance factor Gap43 on mRNA level, as compared to Scr controls (Figure 4.3.11). Inhibition of miR-199 did not significantly alter mRNA expression levels of Gap43 (Figure 4.3.11). Inhibition of miR-199 in C2C12 myoblasts led to a significant increase in NMJ-associated gene: Hdac9 mRNA levels, as compared to miR-199 overexpression, but not Scr controls; similarly, Acvr2a mRNA level was upregulated following miR-199 inhibition as compared to Scr control and miR-199, although not significantly (Figure 4.3.11).

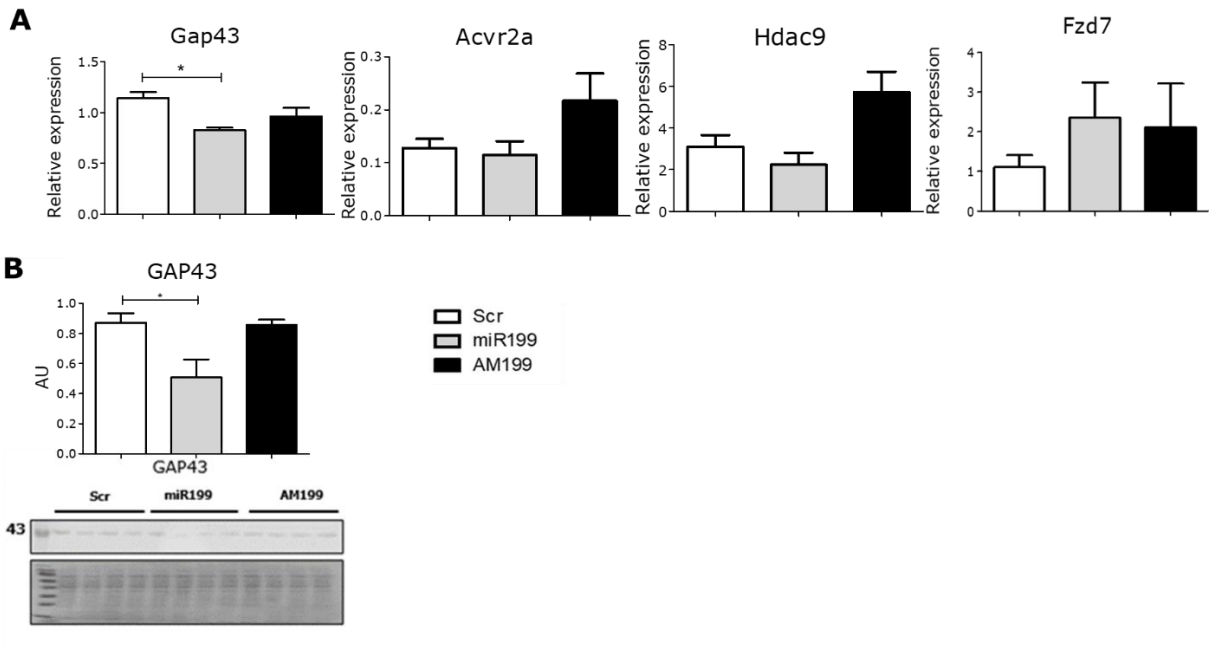

Figure 4.3.11. miR-199 regulates the expression of Gap43 *in vitro*. A) The mRNA levels of Gap43 were significantly lower with miR treatment. Acvr2a was not significantly altered following miR-199 overexpression or inhibition, however a trend towards increase was observed following miR-199 inhibition, as compared to Scr controls. Fzd7 expression was not regulated by miR-199. B) Protein levels of GAP43 were significantly lower following miR-199 overexpression compared to miR-199 inhibition or Scr control. The relative expression of neuron-related gene Gap43 was reduced with miR-199a-5p overexpression compared to Scr control. Expression relative to S29 is shown for mRNA; Western blot and qPCR (n=3). Scr – antagomiR scrambled, miR-199 – miR-199a-5p mimic; AM-199 – antagomiR to miR-199a-5p. Error bars show SEM; * - $p<0.05$. One-way ANOVA with Dunnett's post-test.

4.3.7 miR-199a-5p directly binds to GAP43 3'UTR region

We next generated reporter constructs containing miR-199a-5p binding sites within a dual luciferase reporter vector (323) (this work was done with assistance from Dr Kasia Whysall). The firefly luciferase is fused with the 3'UTR of the target gene containing miR binding site, whereas Renilla luciferase serves as a reference.

Luciferase assay was performed 48 hours after transfection of C2C12 cells with miR-199 or AM199 or Scr control and a miR not predicted to target the genes: miR-378. We focused on Gap43, Grp78, and Hdac9 as these were predicted targets and/or exerted the strongest response to miR-199 treatment. miR-199 downregulated the signal strength in cells treated with Gap43 and Grp78, but not Hdac9 reporter. This

suggests that Gap43 and Grp78, but not Hdac9, are likely a direct target of miR-199 (Figure 4.3.12).

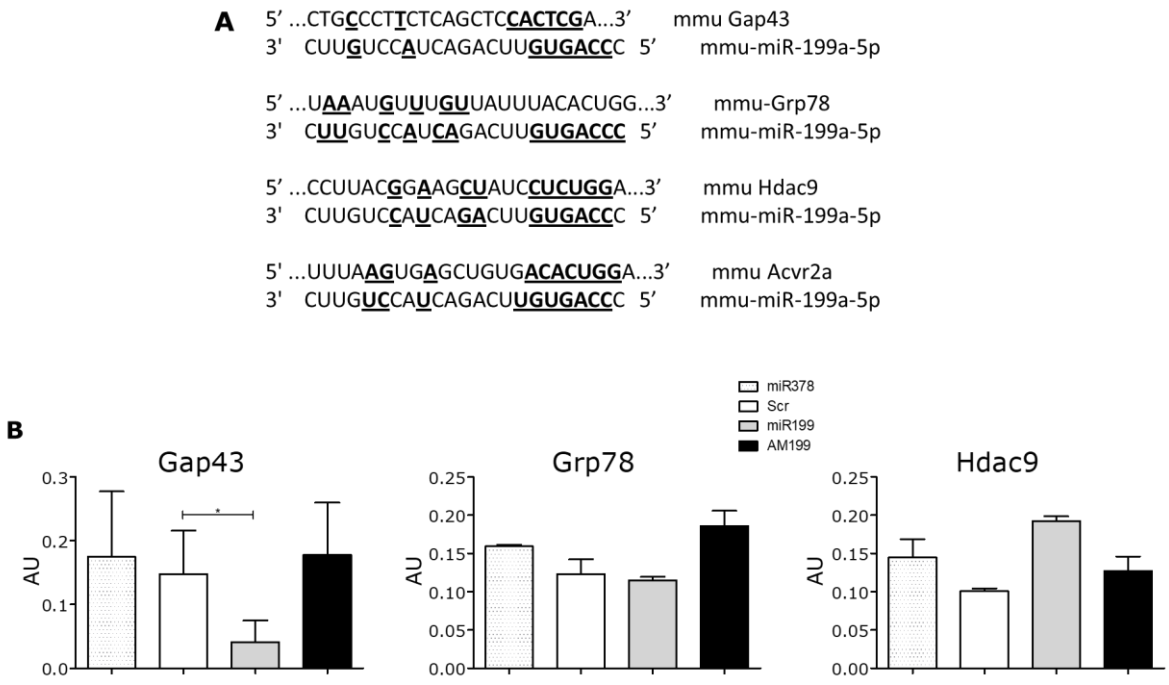

Figure 4.3.12. miR-199a-5p directly binds to its target sites within 3'UTRs of Gap43 and Grp78. A) miR-199a-5p binding sites within its predicted target genes. B. C2C12 were transfected with dual luciferase reporter vector with a 3'UTR sequences containing miR-199 binding site cloned downstream of the firefly luciferase. Gap43 and Grp78 were regulated by miR-199, but not miR-378, overexpression. This suggest miR-199 directly regulates Gap43 and Grp78. Results shown n=3. Error bars show SEM; * - $p<0.05$. One-way ANOVA with Dunnett's post-test.

4.4 Discussion

The aim of this chapter was to examine the effect of miR-199a-5p on cells *in vitro*. Our data indicated that miR-199a-5p overexpression in C2C12 myoblasts and differentiated C2C12 myotubes led to decreased myotube diameter, and decreased myotube fusion. (Figure 4.3.2, Figure 4.3.3). This would suggest upregulated miR-199a-5p inhibits myogenesis during proliferation, and exacerbates atrophy in differentiated myotubes, whereas inhibition of miR-199a-5p resulted in no changes to diameter, fusion or area (Figure 4.3.2, Figure 4.3.3). It should be noted that while we did obtain significantly reduced miR-199a-5p expression with AM199 treatment

(Figure 4.3.1), the reduction in miR-199a-5p expression with antagomiR was not as profound as was observed with miR-199a-5p overexpression. This was likely due in part to limitations encountered related to the small sample size.

The expression of ER stress protein GRP78 on protein level was higher following miR-199a-5p treatment as compared to both Scr controls and miR-199a5-p inhibition in C2C12 cells (Figure 4.3.5). Expression levels of CHOP at protein and mRNA levels were not significantly increased, although there was a non-significant trend towards increase in protein expression levels. However, the number of cells positive for CHOP presence assessed by immunostaining, was significantly higher following miR-199a-5p treatment as compared to both AM-199 treatment as well (Figure 4.3.6), suggesting an ER stress response induction in a proportion of cells following miR-199a-5p treatment. It is not clear why only a proportion of cells responded to miR-199a-5p treatment; however, it may be associated with transfections efficiency of approximately 50-60% as demonstrated in our previous studies (338). The expression levels of NMJ-related protein GAP43 was significantly downregulated with miR-199a-5p overexpression (Figure 4.3.11).

Mitochondria content and function were also assessed in C2C12 cells, MitoTracker staining showed miR-199a-5p inhibition significantly increased mitochondrial activity compared to Scr control and miR-199a-5p overexpression (Figure 4.3.8). The results of miR-199a-5p inhibition also showed increased mRNA expression of Pgc-1α in C2C12 cells. Seahorse analysis of OCR in C2C12 cells showed improvements in mitochondrial maximal respiration with AM-199 administration(Figure 4.3.9).

4.4.1 miR-199a-5p regulates myogenesis *in vitro* in C2C12 mouse myoblasts

Overexpression of miR-199a-5p in C2C12 myoblasts led to a decreased diameter and fusion index, this was also observed in differentiated C2C12 myotubes following miR-199a-5p overexpression (Figure 4.3.2). Inhibition of miR-199a-5p in C2C12 myotubes also led to trending decrease in overall myotube area compared to miR-199a-5p overexpression. Together, these data suggest miR-199a-5p has a negative role in myogenesis, as myotube fusion is a key step in myogenesis (339). Inhibiting miR-199a-5p resulted in increased capability of myotubes to differentiate. This is consistent with previous findings that show miR-199a-5p as a regulator of myogenesis in zebrafish (252). Our results demonstrate that miR-199a-5p inhibits

myogenesis whereas AM-199 has a less pronounced effect, this could be due to transfection efficiency, or could be due to presence of miR-199b-5p, which was not affected by antagomiR to miR-199a-5p. The effect of miR-199a-5p overexpression was more pronounced in myoblasts compared to differentiated myotubes, where inhibition of miR-199a-5p significantly increased myotube diameter and fusion index compared to miR-199a-5p overexpression in myotubes. The expression of miR-199a-5p has been associated with cell-specific differences within muscle, with overexpression of miR-199a-5p promoting myoblast but not myotube proliferation in skeletal muscle in zebrafish (252), suggesting that miR-199a-5p has different roles for muscle during different stages of development as miR function has been shown to be dependent on the overall cellular transcriptome and therefore presence or absence of specific mRNAs within the cells (340). It is possible in adult muscle regeneration, miR-199a-5p expression is altered in the presence of stress. This has implications for muscle regeneration in aged muscle. It has been demonstrated that miR-199a-5p overexpression inhibits macrophage differentiation (341), and this exhibits negative effects on skeletal muscle regeneration (342). Age-related immune dysfunction has been observed and has also been associated with sarcopenia (343). It could therefore be upregulated miR-199a-5p might disrupt immune cell-mediated muscle regeneration by altering macrophage dynamics, which may lead to uncontrolled inflammation and reduced regeneration capacity. Taken collectively, our data suggests miR-199a-5p has different roles during muscle development, and upregulated miR-199a-5p associated with ageing may negatively impact muscle regeneration ultimately contributing to sarcopenia. These data collectively suggest differences between differentiated cells and myoblasts, indicating mature myotubes have different characteristics to myoblasts, and *in vivo* assessment of this miR is important to determine these differences.

Among targets of miR-199a-5p known to regulate satellite cells and their differentiation ability are the Wnt signalling factors (252,313). Inhibition of Wnt-1 has been shown to decrease activation of downstream genes involved in myogenesis (344). The canonical Wnt signalling pathway is more active in foetal myogenesis, and is confined to slow-type myofibres, additionally Wnt molecules released from motor neurons is believed to play a role in NMJ formation and maintenance of the NMJ (345). The Wnt pathways include proteins of the Frizzled class (Fzd), Derailed/Ryk

and RAR-related orphan (ROR) receptors (346). The Frizzled class receptor 7 (FZD7) is a predicted target of miR-199a-5p (337), however our data showed no significant changes with miR overexpression or inhibition (Figure 4.3.11). Muscle specific kinase (MuSK), a member of the ROR family of proteins, has a known role in acetylcholine receptor (AChR) clustering and NMJ maintenance, and MuSK knockout studies result in failure of AChRs to cluster (349). The post-synaptic endplate of the NMJ, is only 0.1% of the myofibre surface, but is composed of millions of AChRs that trigger skeletal muscle contraction (307). This supports further investigation into the NMJ and associated miR-199a-5p targets that could play an important role in neuromuscular maintenance (see 4.4.6). This, in conjunction with Wnt signalling, further highlights the role of miR-199a-5p playing a role in skeletal muscle homeostasis through age-related changes in miR expression that disrupt upstream regulators of myogenesis and/or NMJ maintenance.

4.4.2 miR-199a-5p inhibition reduces C2C12 cell number

We determined that myotube fusion was decreased with overexpression of miR-199a-5p (Figure 4.3.2, Figure 4.3.3). We next aimed to determine the effect of overexpression or inhibition of miR-199a-5p on cell number. Our results indicated inhibition of miR-199a-5p significantly reduced cell number in C2C12 cells in growth conditions, but not in the presence of H_2O_2 induced stress (Figure 4.3.4). This would appear to agree with our fusion data, as the cells must withdraw from the cell cycle in order to fuse into mature myotubes, and therefore we expect fewer cells with AM-199 treatment. As we had observed increased fusion in C2C12 myoblasts and myotubes, it appears that inhibition of miR-199a-5p pushes the cells towards differentiation and fusion.

4.4.3 miR-199a-5p inhibition significantly ameliorates effect of tunicamycin induced myotube atrophy

The dysregulation of the NMJ has been shown to have a role in sarcopenia (298), however it is not known what factors in ageing are responsible for these NMJ changes. Excessive ER stress is a contributor to many age-related disorders, including sarcopenia and neurodegeneration as well as denervation (270,327,347,348). As miR-199a-5p is predicted to target genes associated with NMJ homeostasis, as well as ER stress, we further explored the role of miR-199a-5p in regulation of ER stress

response pathways in a tunicamycin-induced ER stress model. We hypothesised that inhibition of miR-199a-5p would protect C2C12 myotubes from the effect of excessive ER stress and would preserve myotube diameter, myotube area, and fusion index. Tunicamycin is an established ER stress inducer that works by causing an accumulation of unfolded glycoproteins in the ER (349). Tunicamycin treatment resulted in significant reduction in diameter and area of myotubes following tunicamycin treatment and miR-199a-5p overexpression exacerbated this effect (Figure 4.3.7). Inhibition of miR-199a-5p resulted in a partial rescue of tunicamycin-induced phenotype, however this was not significant. Together, these data support a negative role of miR-199a-5p in muscle homeostasis *in vitro*, and its likely regulation of ER stress pathways. These data also suggest inhibiting miR-199a-5p induces a protective type of effect on myotubes in the presence of excess ER stress.

The ageing process results in the accumulation of abnormal and misfolded proteins which then triggers the ER stress response, the prolonged activity of which is thought to promote apoptosis (347). The ER stress response then triggers the UPR by three main sensors: activating transcription factor-6 (ATF6), inositol-requiring protein (IRE) 1α, and protein kinase R (PKR)-like endoplasmic reticulum kinase (PERK) (347). During this process, binding immunoglobulin protein (BiP/GRP78) disassociates from these proteins to bind to the damaged proteins in the ER lumen. Following the release of GRP78, PERK (also known as eukaryotic translation initiation factor 2 alpha kinase 3 (EIF2AK3)) is auto-phosphorylated leading to a cascade of signals including direct phosphorylation of eukaryotic translation initiation factor 2α (eIF2α) and translation of activating transcription factor-4 (ATF4). This induces the pro-apoptotic transcription factor CCAAT enhancer binding protein (C/EBP) homologous protein (CHOP). In rodents, ER stress has been shown to be increased in old rats following a period of disuse. At baseline after disuse, there are elevated levels of ER stress markers Chop and Grp78, however upon reloading, only CHOP overexpression activates the ER stress maladaptive response (348). The multi-armed nature of the maladaptive response is challenging as it remains unclear if miR-199a-5p is working upstream to target a master regulator, or if it is working downstream through a specific arm of the ER stress response as one of its targets (see 3.3). Therefore, it was further necessary to investigate the specific main branches of the UPR to better understand the action of miR-199a-5p within this framework.

4.4.4 miR-199a-5p is predicted to regulate Grp78 associated with ER stress

Grp78 is a predicted target gene of miR-199a-5p. Indeed, Grp78 reporter construct demonstrated potentially direct binding of miR-199a-5p to the miR-199 target site within Grp78 3'UTR (Figure 4.3.12). The expression of Grp78 and the PERK arm (Chop) of ER stress pathway was not significantly activated following mir-199a-5p overexpression in C2C12 (Figure 4.3.5). Immunostaining differentiated C2C12 myotubes using CHOP antibody after exposure to tunicamycin demonstrated that the overexpression of miR-199a-5p in C2C12 myotubes resulted in a significant increase in number of cells positive for CHOP (Figure 4.3.6). Others have suggested a basal level of ER stress yields a mild protective effect, called ER hormesis (347). Western blot of protein isolates probed for CHOP did not significantly show increased expression with miR-199a-5p overexpression. Additionally, qPCR analysis also showed increased trend towards significance in Chop expression with miR-199a-5p overexpression. This is similar to what was observed in CHOP protein expression by quantified by Western blot. Taken together with what we observed in GRP78 Western blot, suggests miR-199 has an effect on ER stress. Although miRs canonically act through downregulation of gene expression, some have been shown to upregulate gene expression. It has been reported miR-mediated upregulation is selective, and specific to RNA sequence context, and other RNA binding proteins (350). In this study, predicted target of miR-199a-5p: Grp78 was upregulated following miR-199a-5p overexpression and seemed to bind to Grp78 target site within 3'UTR (Figure 4.3.5, Figure 4.3.12). We hypothesis that miR-199a-5p either regulates Grp78 through upregulating gene expression or regulates upstream regulator of Grp78, such as IGF-1 receptor signalling (351), which has an overall stronger effect on Grp78 expression than miR-199a-5p itself. Insulin signalling was further observed to be an associated predicted pathway of miR-199a-5p.

There are three main ER stress sensors, one of which PERK, upregulates CHOP expression. Another sensing pathway is the ATF6 pathway; and two *ATF6* genes exist: *ATF6α*, and *ATF6β* (352). Following sensing misfolded proteins in the ER, ER chaperone protein GRP78 dissociates from ATF6 as well as the other sensors, which allows interaction with irregular proteins. GRP78 was significantly upregulated following miR-199a-5p overexpression as compared to both miR inhibition, and Scr control (Figure 4.3.6). This effect was not observed in gene expression analysis by

qPCR. To analyse the effect of the miR treatment on the ER protein ATF6, Western blot was performed, the results of which demonstrated ATF6 protein expression was not significantly reduced with miR-199a-5p overexpression (Figure 4.3.6). Another arm of the UPR involves activation of IRE1α, which activates splicing of a 26-base intron from XBP1 mRNA through its ER activity. This generates transcription factor sXBP1, the XBP1-unspliced/XBP1-spliced ratio correlates with the expression level of expressed proteins in order to adapt the folding capacity of the ER and is a type of protein folding quality control (353). In the present study, miR-199 did not regulate Xbp1 splicing suggesting that this arm of ER stress response is not activated in the presence of miR-199 (Figure 4.3.6).

The present study demonstrates miR-199a-5p is regulates ER stress response through Grp78 and potentially CHOP expression regulation with other UPR-associated proteins not affected by miR-199a-5p. CHOP expression is upregulated upon activation of PERK, which undergoes activation following the release of GRP78 in the presence of ER stress. Processes that are affected by this arm of the UPR include maintenance of muscle mass, autophagy, antioxidant response and mitochondrial biogenesis (354). The IRE1α arm was not affected as there were no changes to Xbp1 splicing. The ATF6 arm of the was not significantly affected by miR-199a-5p, although there was a slight affect as protein expression was noticeably reduced with miR-199a-5p overexpression, but as ATF6 is a predicted target this makes sense. Levels of CHOP expression have been shown to be elevated in skeletal muscle with sciatic nerve transection (354).

One of the consequences of the maladaptive ER response is disrupted mitochondrial homeostasis (278). CHOP inhibits the expression of Bcl-2 proteins, which have roles in mitochondrial dynamics (355,356). Mitochondrial dysfunction is associated with ageing, muscle loss, and NMJ dysfunction (42,73,284,357), and it is likely miR-199a-5p impacts mitochondria through one of its predicted targets like Pgc-1α, or indirectly through regulating ER stress response (358).

4.4.5 miR-199a-5p did not significantly regulate mitochondrial biogenesis

ER stress has been proposed to regulate mitochondrial dynamics (355). The effect of miR-199a-5p on mitochondrial function *in vitro* was assessed in C2C12 cells first to

determine the effect of miR-199a-5p overexpression. Dysregulation of mitochondrial homeostasis is highly implicated in sarcopenia pathogenesis, possibly due to progressive denervation and reinnervation that occurs in ageing and leads to impaired motor control and muscle atrophy (359).

MitoTracker staining was used to measures mitochondrial membrane potential and is indicative of live mitochondria, and in the present study, C2C12 myoblasts were treated with miR-199a-5p, AM-199, or Scr control, and then stained with MitoTracker red. miR-199a-5p inhibition resulted in increased mitochondrial activity (Figure 4.3.8).

Maximal respiration and OCR of mitochondria in C2C12 cells was assessed using a Seahorse bioanalyser, a plate-based live cell assay that allows monitoring of the OCR in real time. Inhibition of miR-199a-5p resulted in increased OCR compared to both miR-199a-5p overexpression and Scr control (Figure 4.3.9). Further, maximal respiration, basal respiration, respiratory capacity, non-mitochondrial respiration, and ATP production were not significantly increased with AM-199 treatment. These data agree with MitoTracker data, suggesting increased mitochondrial function following miR-199a-5p inhibition. Mitochondria are key for not only cellular energy, but also ROS signalling, Ca^{2+} regulation, and apoptosis, and reduced mitochondrial function has consequences on skeletal muscle during ageing (359). Mitochondria-associated genes were assessed to further investigate the mitochondrial changes observed with miR-199a-5p inhibition. Mitochondrial respiratory chain component (360), CoxI, was upregulated although not significantly with miR-199a-5p inhibition. Master regulator of energy metabolism and regulator of mitochondrial biogenesis (361), Pgc1-α, was significantly upregulated following miR-199a-5p inhibition (Figure 4.3.10). These data correspond to the mitochondrial effects that were observed with miR inhibition in C2C12 cells stained with MitoTracker. Other mitochondrial genes and autophagy related genes showed no changes with either miR-199a-5p overexpression or inhibition.

Together, these data suggest that miR-199a-5p might influence skeletal muscle homeostasis through regulating mitochondrial dynamics, ER stress response. Others have shown miR-199a-5p expression is linked to ER stress (269,362). ER stress generates pro-apoptotic signals that likely have a mitochondrial-specific effects

disrupting mitochondrial homeostasis (355). A link between reduced mitochondrial function and NMJ disruption has been observed in rat models of sarcopenia (286), and mitochondrial function is known to be affected by ER stress (278). It has also been demonstrated that ageing muscle produces ROS (42) and abnormal ROS levels are believed to contribute to neurodegeneration and NMJ disruption by damaging mitochondria (363). Autophagy has been described as a potential mediator in this process, as inhibited autophagy in ageing is linked with increased oxidative stress in addition to mitochondrial dysfunction and NMJ damage (162). Taken together upregulated miR-199a-5p in ageing may play a role in sarcopenic developments by contributing to uncontrolled ER stress signalling that leads to mitochondrial dysfunction and subsequent NMJ instability.

4.4.6 miR-199a-5p regulates expression of NMJ-related gene *Gap43 in vitro*

Denervation contributes to the loss of muscle observed in ageing and disease and has been demonstrated to have negative consequences for skeletal muscle (70,174,325). The NMJ is composed of a pre-synaptic terminal, synaptic cleft, and post-synaptic membrane and the synapse itself works in an all- or- none fashion, meaning muscle contraction can only occur if the endplate potential reaches a specific threshold allowing the opening of calcium channels (364). The NMJ has been shown in mice to fragment with age, which may be secondary to the degeneration of skeletal muscle fibres although this is not yet clear. In humans, evidence suggests changes in endplate morphology and remodelling of the NMJ precedes loss of motor units, and may be muscle fibre-type specific, and further the main causes of age-associated NMJ dysfunction include inflammation, mitochondrial dysfunction and oxidative stress and neurodegeneration (365). GAP43 is a neuronal protein associated with growth and nerve terminal plasticity and appears critical to NMJ (366). Additionally, ER stress-induced apoptosis is associated with GAP43 (367) and GAP43 is expressed in skeletal muscle cells, satellite cells and isolated mouse muscle fibres (368).

4.4.7 miR-199a-5p directly binds to GAP43 3'UTR

In the present study, miR-199a-5p was demonstrated to directly bind to a predicted miR-199a-5p target site within Gap43 3'UTR (Figure 4.3.12). miR-199a-5p overexpression in C2C12 cells resulted in significantly reduced expression of Gap43

(Figure 4.3.11). Other NMJ-specific gene targets were investigated in C2C12 cells, including Hdac9, which is highly expressed in innervated muscle and is involved in myogenin regulation and regulation of denervation dependent genes (287,369). Furthermore, Acvr2a, which interacts with skeletal muscle *via* myostatin and is a member of the TGF-β family, has a role in synaptic function at the NMJ (275,277). Acvr2a was upregulated in AM-199 treated C2C12 cells, although this was not significant. A significant increase in Hdac9 expression was seen with AM-199 administration as compared to miR-199a-5p overexpression was observed in C2C12 cells (Figure 4.3.11). Acvr2a and Hdac9 predicted target sites did not seem to be functional in our study (Figure 4.3.11), suggesting that these genes may not be directly regulated by miR-199a-5p.

The NMJ is highly associated with skeletal muscle health and the maintenance of skeletal muscle (42,291,298,365,370) and a dysregulated NMJ may play a role in denervation with ageing. Other studies in rats demonstrate age-associated disuse atrophy is more destructive in older animals than young, and older animals have a basal level of NMJ remodelling and denervation, which is suggestive of defective NMJ transmission. Our results indicate a potential role for miR-199a-5p in the regulation of NMJ homeostasis.

Chapter 5 The role of miR-199a-5p in maintaining neuronal homeostasis *in vitro* in NSC-34 neuron-like cells.

5 The role of miR-199a-5p in maintaining neuronal homeostasis *in vitro* in NSC-34 neuron-like cells

5.1 Introduction

Age-related muscle atrophy is associated with neuromuscular interactions deterioration and denervation (298). The loss of contractile function and the associated atrophy progressively reduces muscle function and results in increased risk of frailty and falls and increased risk of morbidity and mortality. Denervation contributes to mobility impairment in advanced age, and ultimately results in accelerated atrophy by increased disuse (359). Motor units, composed of single neurons and the associated innervated muscle fibres, are key to controlling muscular commands from the brain to muscular action, and ageing is associated with loss of motor units and decreased muscular performance (296,371). Further complicating matters, the ageing of the neuromuscular system is not uniform across all individuals or sexes (371). For example, one study has shown elite female masters athletes (44-83 years old) experience a reduction in motor unit firing rates that was not seen in males (372). Other studies have demonstrated age-related differences between females and male muscular performance, that might be influenced by neuromuscular health, including greater myofibre atrophy and size variance as well as disproportionate type II fibre atrophy in females (373). Sarcopenia is thought to be partially caused by muscle fibre denervation and motor neuron apoptosis and the neurological component to sarcopenia is not well understood (299).

The peripheral nervous system is affected by age, and the changes occur along the whole length of the neural pathway, terminating at the NMJ. The ageing process in humans affects the NMJ through progressive motor neuron loss and subsequent maladaptive peripheral nerve sprouting, and associated reductions in endocrine and paracrine production of IGF-1, which is associated with axonal sprouting (299). Other studies have shown age-related changes to axon regeneration and sprouting after age-associated disease such as stroke in mice (374), and in humans ageing has been associated with downregulated GAP43 (375). There are also anatomical structural changes observed in older human adults, including synaptic cleft widening, junctional fold degeneration and increased acetylcholine receptors (299). Increased oxidative stress and dysfunction of satellite cells has been correlated with muscle fibre loss

from motor unit remodelling (371). Strength and power losses that correspond to ageing are progressive in nature and strength loss seen is typically ≈10% per year starting at 40-50 years of age, and contraction speeds and maximal torque are reduced with advanced age, although there appears to be differences in muscle groups (371). This implicates the neurological contribution to age-related muscle loss, in muscular power, contraction speed, and motor unit stability, although the primary cause for these changes is not well understood. The neurodevelopmental disorder, Rett syndrome, which causes disruptions to motor coordination, is associated with upregulated miR-199a-5p (376) which directly acts on the Akt signalling pathway (377,378).

As miR-199a-5p is predicted to regulate NMJ-associated genes, miR-199a-5p was investigated in motor neuron-like NSC-34 cells, which are a hybrid cell line of neuroblastoma and mouse motorneuron-enriched spinal cord cells from 12-14 day embryonic mice (379). We aimed to determine the effect of miR-199a-5p on motor neuron-like differentiated NSC-34 cells *in vitro* by using miR-199a-5p overexpression, miR-199a-5p inhibition by AM-199 or Scr control, and then assessed at the RNA and protein level as was performed on C2C12 cells. We hypothesised miR-199a-5p overexpression would result in lower expression of NMJ-proteins, and would negative impact mitochondrial content.

5.2 Materials and methods

5.2.1 Cells and cell culture

NSC-34 (motor neuron enriched, embryonic mouse spinal cord cells with mouse neuroblastoma) cells were gifted by Dr Brian McDonagh (NUIG). All cells were cultured in standard growth conditions (see 2.5) and in a growth-medium comprised of DMEM supplemented with 10% FBS and 1% p/s as described in 2.4.2.

5.2.2 NSC-34 cell differentiation

For cell differentiation assays, NSC-34 cells were cultured in 10% DMEM, 1% p/s as described for growth; differentiation assays were performed with DMEM and 3% HS as described in 2.4.2, and the differentiation protocol was taken from Maier *et al*. (324).

5.2.3 Cell Counting Kit-8 assay

Cell Counting Kit-8 was used to determine the effect of miR-199a-5p overexpression on NSC-34 cell number. A total of 1000 cells were added to a 96-well plate, 100µl of growth medium was added and allowed to incubate for 4 hours. After 4 hours, half of the samples were to be exposed to hydrogen peroxide (H_2O_2) to invoke oxidative stress, wells were treated with 1mM H_2O_2 for 10 minutes in a sterile incubator at 37°/5% CO_2. After H_2O_2 treatment if needed, cells were replaced with new medium and treated with miR mimic or antagomiR as described in 2.6, and allowed to incubate for 72 hours. After this incubation, a standard curve was plated. 10µl of the CCK-8 assay reagent was added to each well, and the absorbance was read at 450nm on the Hidex microplate reader and samples were normalised before analysis.

5.2.4 miR-199a-5p transfection

Cells were transfected with cholesterol-conjugated miR mimics: miR-199a-5p, antagomiR-199a-5p, or scrambled control sequence (miRIDIAN) at a final concentration of 200nM as described in 2.6. and determined previously by Whysall lab (241).

The sequences used in transfection:

Scr- 5'- CUCGUUCCUGGUCGUCACCAGU-3'

miR-199a-5p- 5'- miRIDIAN mimic (Horizon Discovery) based on mmu-miR-199a-5p MIMAT0000229

antagomiR-199a-5p- 5'- GAACAGGUAGUCUGAACACUGGG-3'

5.2.5 Immunostaining of NSC-34 cells

βIII Tubulin staining was performed on differentiated NSC-34 cells to assess the effect of miR-199a-5p on neurite growth. For NSC-34 cells, the protocol for βIII Tubulin staining was performed as described in 2.7.5. Briefly, samples were fixed in methanol for 5 minutes. Before being washed in PBS again for 3 minutes. After this, samples were blocked and then the primary antibody – βIII Tubulin (1:750 in 2% blocking solution) was added and allowed to incubate for 2 hours. The cells were then washed in PBS and the secondary antibody, anti-Rat (1:2000 in 2% blocking solution) was added and incubated for 60 minutes covered at room temperature. The samples

were washed in PBS, covered before being stained with DAPI. Finally, samples were washed in PBS, before being imaged with the EVOS microscope imaging system.

5.2.6 RNA collection from NSC-34 cells

For RNA collection from NSC-34 cells, isolates were collected 48 hours after transfection. Collection of isolates was performed by immediately placing in TRIzol and stored at -80° for later RNA processing. RNA was isolated using TRIzol/chloroform standard RNA isolation protocol and RNA purity was assessed on a Nanodrop 2000 spectrophotometer as described in 2.9.3

5.2.7 cDNA synthesis and RT-qPCR from NSC-34 cells

Synthesis of cDNA was performed using SuperScript II (100-500ng RNA) as described in 2.10. RT-qPCR was performed using miRCURY LNA SYBR Green for miRs (UNISP6 YP00203954, SNORD68 YP00203911, hsa-miR-199a-5p YP00204494, hsa-miR-199b-5p YP00204152) and FAST SYBR Green Master Mix. Relative expression was to β2M or S29 (mRNA) and Rnu-6 and/or Snord-61/Snord-68 (miR) was calculated using the delta-delta Ct method and the changes in relative expression were analysed. Primer sequences for RT-qPCR are listed in Table 2.11.1. The protocol for RT-qPCR is located in 2.11

5.2.8 Protein isolation from NSC-34 cells

Protein was isolated from NSC-34 cells as described in 2.13. In brief, the cells were collected 48 hours after transfection. Collected isolates were immediately placed in 1X RIPA buffer supplemented with protease inhibitor (1:1000) and stored at -80° for later protein quantification and Western blotting as described in 2.14.

5.2.9 Protein quantification and Western blot

For protein quantification and Western blot, cells were lysed in 1X RIPA buffer and protein concentrations were calculated using Bradford reagent and BSA standards as described in 2.14. Blotting was performed using protein lysates diluted in Laemmli buffer, and 20μg of protein was run on 8%– 16% polyacrylamide gels as described in 2.14. Proteins were transferred to nitrocellulose membranes using a semi-dry blotter. Subsequently, membranes were stained with Ponceau S (0.1 % Ponceau in 5% acetic acid) to visualise and confirm equal protein loading. Membranes were blocked in 5% milk in TBS-T for 1 hour at RT, and following, washed in TBS-T. Membranes were

incubated with primary antibodies (1:750-1:1000 antibodies table listed in 2.7.1) overnight at 4°C. Membranes were then washed in TBS-T and incubated with fluorescent secondary antibodies; goat anti-rabbit and goat anti-mouse depending on primary species, and images were obtained using Odyssey Fc imaging system.

5.2.10 Image analysis

Image analyses of βIII tubulin assays were performed as described using ImageJ software. Images were created using the EVOS microscope imaging system. The EVOS M5000, and EVOS M7000 systems were used for imaging. Fluorescence microscopy for immunostaining was also performed using these systems, and utilised the EVOS GFP light cube (AMEP4951), EVOS DAPI light cube (AMEP4950), or EVOS Cy5 light cube (AMEP4956). At least 5 images were taken per each well (n=4). Images were exported as TIF files. Image analysis of differentiated NSC-34 cells was performed using ImageJ and the free plugin NeuriteTracer to trace the outgrowing neurites from differentiated cells. The outputs were then analysed in Microsoft Excel and then graphed with GraphPad Prism (version 5.03). Western blot images were obtained using Odyssey Fc imaging system (Li- Cor), and quantification was performed using ImageJ and normalised to Ponceau S stain by densitometry of total Ponceau in that sample lane as described in 2.14.4

5.2.11 Statistical analysis

All data are represented as mean ± SEM. One-way ANOVA was used to compare means of the three groups. A Dunnett's post-test was performed to compare the treatment groups (miR-199a-5p, and AM-199) with the control group (Scr). One-way ANOVA analyses for qPCR, protein and image analysis were performed using GraphPad Prism (version 5.03), with p-values < 0.05 considered statistically significant.

5.3 Results

5.3.1 miR-199a-5p does not regulate neurite growth in NSC-34 cells

NSC-34 cells were first treated with miR-199a-5p mimic, miR-199a-5p inhibitor (AM-199), or Scr control, to overexpress miR-199a-5p. Transfection of miR-199a-5p demonstrated miR-199a-5p treatment upregulated miR-199a-5p expression as determined by RT-qPCR (Figure 5.3.1).

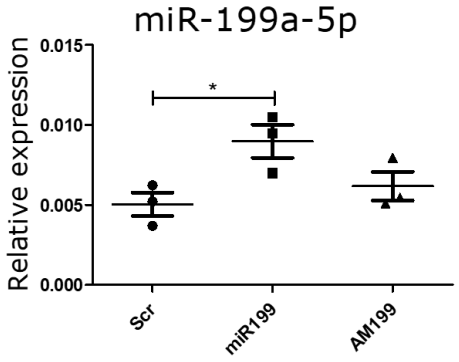

Figure 5.3.1. Treatment of NSC-34 cells with miR-199a-5p mimic results in upregulated level of miR-199a-5p as compared to Scr control. NSC-34 cells were treated with miR-199a-5p mimic or AM199, and RNA was isolated 48 hours later. RT-qPCR data showed miR-199a-5p mimic significantly upregulated miR-199a-5p expression, compared to Scr control. Treatment with AM199 did not significantly reduce miR-199a-5p expression. N= 3, error bars show SEM, expression relative to Snord68 is shown. One-way ANOVA with Dunnett's post-test was performed. *$p<0.05$.

After differentiation and treatment, the cells were immunostained with βIII tubulin, a microtubule element that is used as a marker of neurons. Next, the neurites were measured to determine the effect of miR overexpression or inhibition on the number and length of neurites. miR-199a-5p overexpression increased neurite length compared to Scr control, however when compared to the number of neurites present, miR-199a-5p overexpression resulted in fewer overall neurites present compared to Scr control. Compared to Scr control, AM-199 treated cells were also characterised by fewer neurites (Figure 5.3.2). It must be noted that the efficiency of differentiation of NSC-34 cells following published protocols was very poor and the nature of NSC-34 cells (neuroblastoma) necessitate careful interpretation of these results, especially given upregulation of ER response in cancer cells overall (380), additionally the transfection efficacy of AM199 treatment was observed to be poor (Figure 5.3.1).

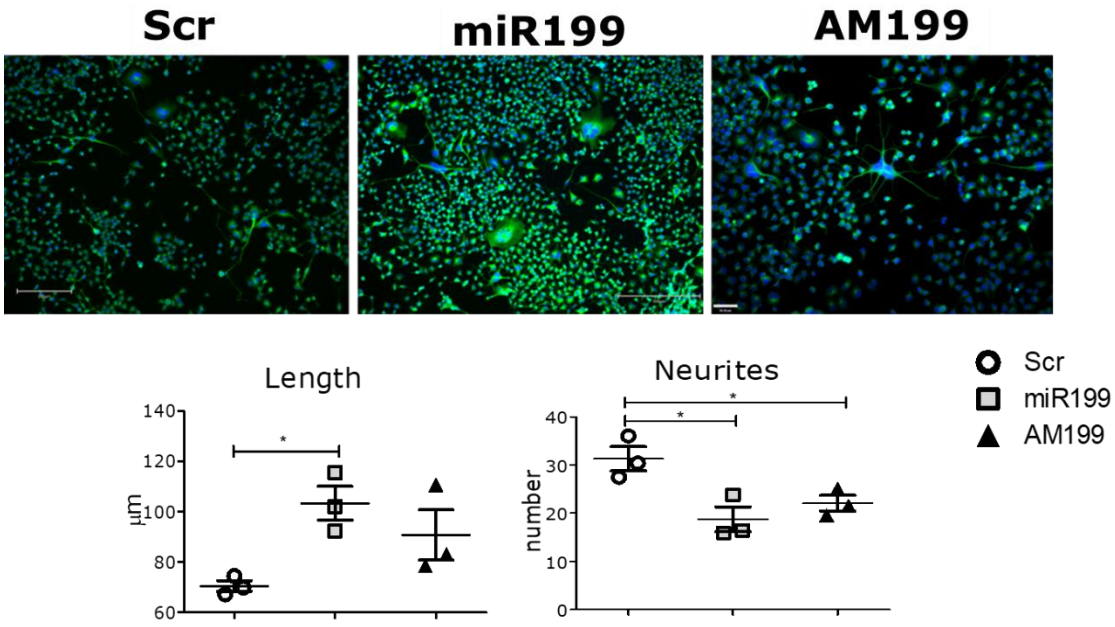

Figure 5.3.2 NSC-34 neurite length and number are affected by miR-199a-5p overexpression. NSC-34 neurite length is affected by miR-199a-5p mimic or inhibitor as compared to control, but miR-199a-5p overexpression or inhibition reduces total number of neurites. NSC-34 cells were differentiated and treated with miR-199 mimic, AM-199, or Scr control and then stained against βIII tubulin. The quantification demonstrated either miR-199a-5p overexpression or inhibition resulted in increased length of neurites compared to Scr control. When assessed for number of neurites present in each treatment group, the results showed miR-199a-5p overexpression significantly reduced the total number of neurites as compared to both Scr control and AM-199. The inhibition of miR-199a-5p by AM-199 resulted in a significant reduction in neurites as compared to Scr control. Representative images are shown; green: βIII tubulin, blue: DAPI; n=4. Scr – antagomiR scrambled, miR-199 – miR-199a-5p mimic; AM-199 – antagomiR to miR-199a-5p. Error bars show SEM; * - $p<0.05$. One-way ANOVA with Dunnett's post-test. Scale bar 300 μm.

5.3.2 miR-199a-5p affects the expression of genes associated with ER stress response in NSC-34 cells

The effect of miR-199a-5p in NSC-34 cells was investigated to determine its effect on the ER stress response. NSC-34 cells were treated as described in 2.6, and the expression of ER stress related proteins were assessed by Western blot. We also examined the effect of miR-199a-5p overexpression and inhibition on NSC-34 cell number during normal and stressed conditions using the Cell Counting Kit-8 assay. Our results demonstrated that in growth conditions, there was no effect with either miR-199a-5p overexpression or inhibition, however in the presence of H2O2, miR-

199a-5p inhibition resulted in increased cell number as compared to Scr controls (Figure 5.3.3).

Following miR-199a-5p overexpression, protein levels of CHOP were significantly upregulated as compared to Scr controls (Figure 5.3.4). This was consistent with CHOP protein levels being downregulated with AM-199 treatment, although this effect was not significant (Figure 5.3.4). Next, following miR-199a-5p overexpression, mRNA levels of Chop were upregulated, as compared to Scr control although this was not statistically significant (Figure 5.3.4).

The protein levels of another ER stress marker, GRP78, were significantly upregulated following miR-199a-5p overexpression when compared to Scr controls. Protein levels of GRP78 were significantly lower following AM-199 treatment as compared to miR-199a-5p overexpression. miR-199a-5p overexpression also led to increased levels of Grp78 mRNA, as assessed by RT-qPCR, when compared to both Scr control and AM-199 (Figure 5.3.4**Error! Reference source not found.**). ATF6 expression was not regulated by either miR-199a-5p overexpression or inhibition (Figure 5.3.4).

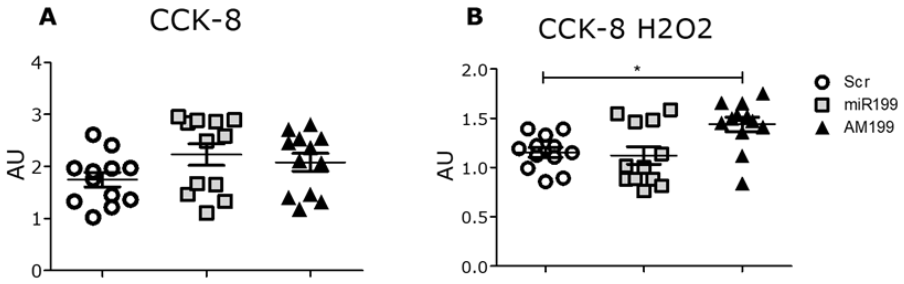

Figure 5.3.3. miR-199a-5p inhibition increases number of NSC-34 cells in the presence of H_2O_2. Cell Counting Kit-8 was used to determine the effect of miR-199a-5p on cell count in normal and stressed (H_2O_2 1mM) condition. A) Cell number was unchanged with miR-199a-5p inhibition or overexpression as compared to Scr controls. B) Cell number was increased in NSC-34 cells treated with AM-199 in the presence of H_2O_2 as compared to Scr controls. Arbitrary units shown; n=12. Scr – antagomiR scrambled, miR-199 – miR-199a-5p mimic; AM-199 – antagomiR to miR-199a-5p. Error bars show SEM; * – $p<0.05$. One-way ANOVA with Dunnett's post-test.

The role of miR-199a-5p in muscle and *neuronal homeostasis in vitro* in NSC-34 neuron-like cells

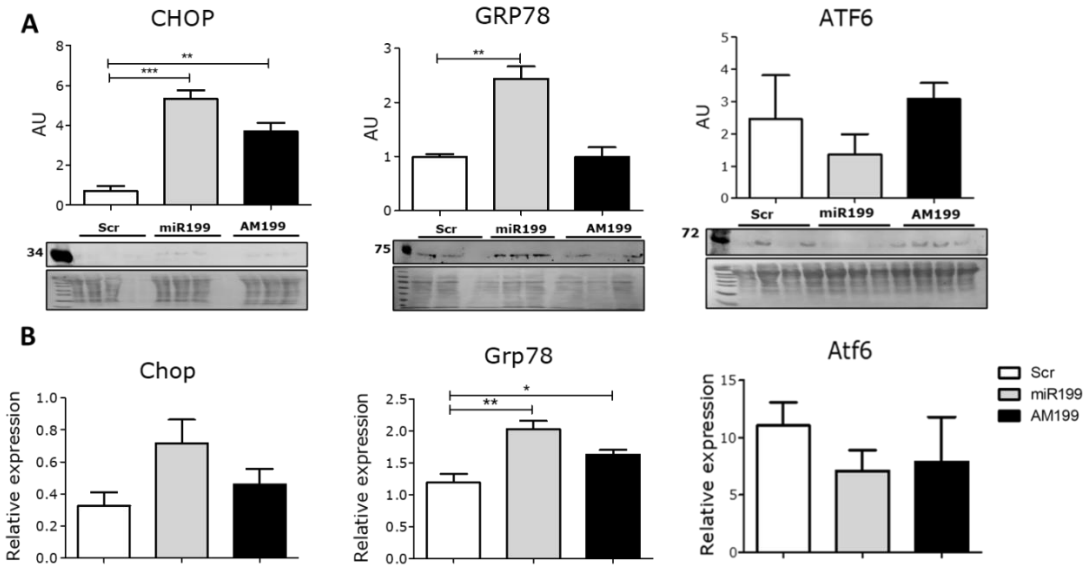

Figure 5.3.4. miR-199a-5p affects the expression of genes associated with ER stress in NSC-34 cells. A) Overexpression of miR-199a-5p in NSC-34 cells resulted in significantly increased expression of CHOP and GRP78, when compared to Scr control. No significant changes were observed following miR-199a-5p inhibition. miR-199a-5p had no effect on ATF6 protein levels. B) The levels of Chop mRNA was not significantly increased, following miR-199a-5p overexpression. The expression of Grp78 was increased following miR-199a-5p overexpression when compared to both Scr control, whereas Atf6 mRNA levels were not affected by miR-199a-5p mimic or AM-199. Scr – antagomiR scrambled, miR-199 – miR-199a-5p mimic; AM-199 – antagomiR to miR-199a-5p. Error bars show SEM; * - $p<0.05$ Arbitrary units shown for Western blot quantification; qPCR: expression relative to S29 is shown; n=3. Error bars show SEM; * – $p<0.05$ One-way ANOVA with Dunnett's post-test.

5.3.3 miR-199a-5p regulates the expression of GAP43 *in vitro* in NSC-34 cells.

To determine the effect of miR-199 on the expression of NMJ-specific proteins in NSC-34 cells, NSC-34 cells were treated as described in 2.6, and then protein and RNA isolates were assessed by western blot and RT-qPCR, respectively to determine the effect on NMJ-related proteins (Figure 5.3.5)

GAP43 is expressed in developing and regenerating neurons. Inhibition of miR-199a-5p resulted in significantly increased protein levels of GAP43, as compared to miR-199a-5p overexpression as well as Scr controls in NSC-34 cells. GAP43 increased levels following miR-199a-5p inhibition are consistent with higher length on neurites observed (Figure 5.3.2), however, the reason for the discrepancy of the effect of miR-199a-5p on neurite length without an increase in GAP43 levels is unclear. Other

The role of miR-199a-5p in muscle and *neuronal homeostasis in vitro* in NSC-34 neuron-like cells

NMJ-specific targets expressed in motor neurons, Hdac9 (381), and Acvr2a (276), were not regulated by miR-199a-5p overexpression or inhibition (Figure 5.3.5).

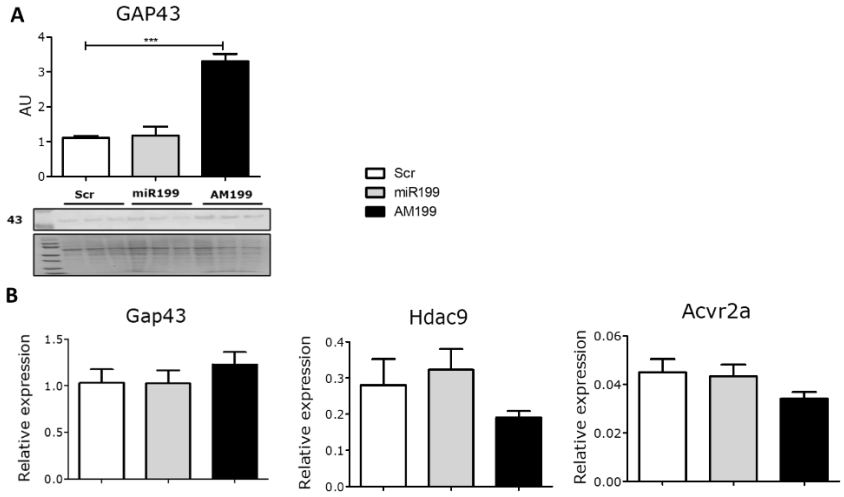

Figure 5.3.5. miR-199a-5p affects NMJ-related protein GAP43 in NSC-34 cells. NSC-34 cells were treated with miR-199a-5p overexpression, inhibition by AM-199, or Scr control. A) Protein expression levels of GAP43 in NSC-34 cells treated with miR-199a-5p inhibitor were significantly higher compared to miR-199 overexpression as well as Scr controls. B) Gap43 mRNA levels did not show significant changes. Other NMJ-related targets, Hdac9, and Acvr2a showed no significant differences. Scr – antagomiR scrambled, miR-199 – miR-199a-5p mimic; AM-199 – antagomiR to miR-199a-5p. Arbitrary units shown for Western blot quantification; qPCR: expression relative to S29 is shown; n=3. Scr – antagomiR scrambled, miR-199 – miR-199a-5p mimic; AM-199 – antagomiR to miR-199a-5p. Error bars show SEM; * – $p<0.05$. One-way ANOVA with Dunnett's post-test.

5.3.4 miR-199a-5p regulates the expression of mitochondria-and-autophagy-associated genes in NSC-34 cells.

The effects of miR-199a-5p overexpression or inhibition on mitochondrial and autophagy proteins and genes were investigated next in NSC-34 cells by western blot and RT-qPCR. Among miR-199a-5p predicted target genes are *Pgc1-α* (330), and *Hif-1α* (273), which are associated with mitochondria. We therefore examined the expression of *Tomm20*, a mitochondrial gene encoded by nuclear genome, as well as CoxI, a mitochondrial gene encoded by mitochondrial genome. The levels of Tom20 mRNA were not statistically significantly increased following miR-199a-5p inhibition as compared to miR overexpression, and CoxI levels were not affected (Figure 5.3.6). Consistently, miR-199a-5p did not regulate the expression of Pgc-1α, a transcription factor regulating mitochondrial biogenesis, however, miR-199a-5p overexpression led

to decreased levels of Nrf2, a transcription factor involved in regulating oxidative stress. To determine whether autophagy is regulated by miR-199a-5p in NSC-34, we analysed the expression of Lc3b and Atg5—inhibition of miR-199a-5p led to increased levels of Atg5 as compared to Scr controls. No change was seen to Atg5 mRNA expression with miR-199a-5p overexpression (Figure 5.3.6).

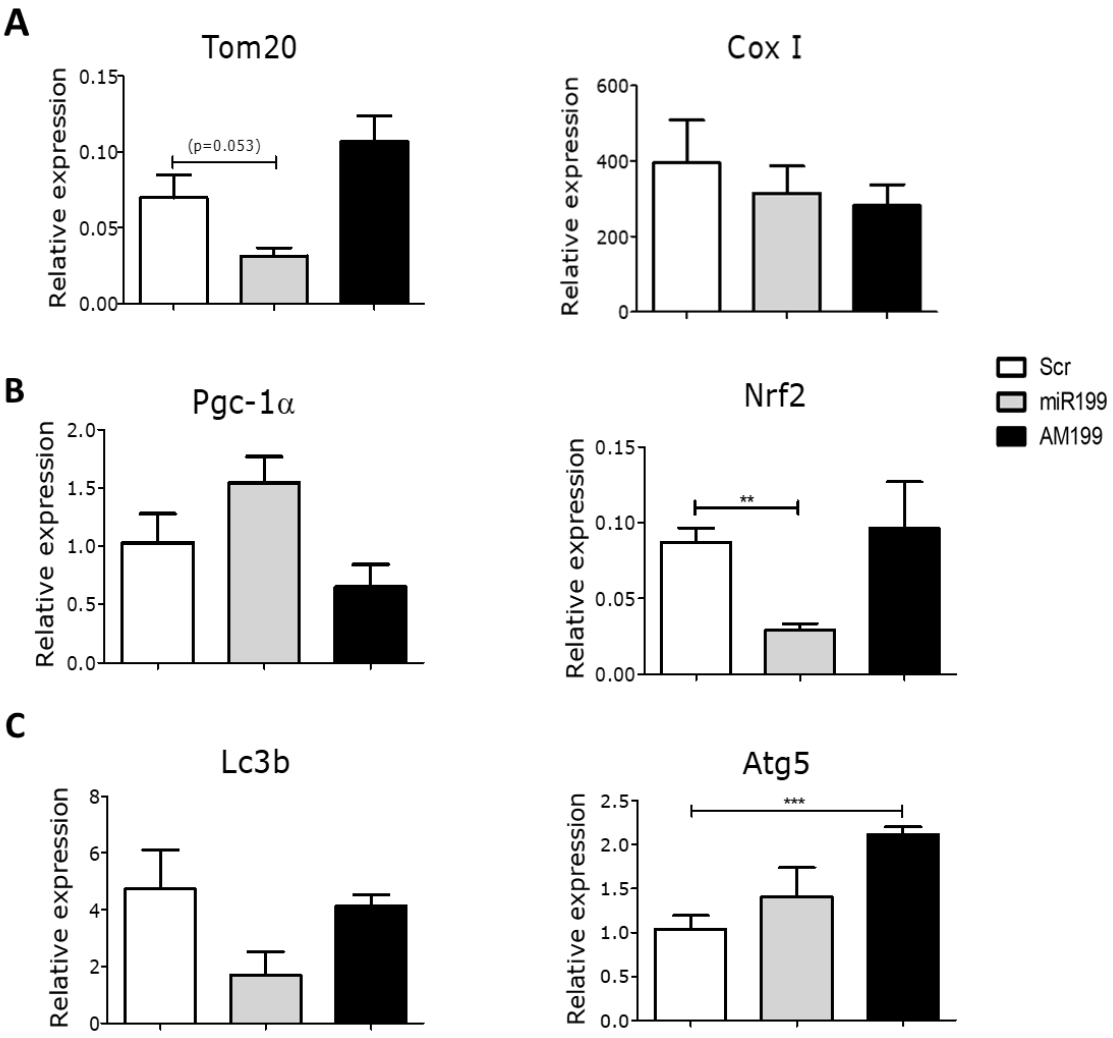

Figure 5.3.6. miR-199a-5p regulates the expression of mitochondrial and autophagy-associated genes in NSC-34 cells. A) mRNA levels of Tom20 were not significantly changed with miR-199a-5p inhibition or miR-199a-5p overexpression as assessed by RT-qPCR. Expression levels of CoxI were not different between any group. B) mRNA expression levels of mitochondrial biogenesis marker Pgc-1α were unaffected by either miR-199a-5p overexpression or inhibition. miR-199a-5p overexpression led to decreased levels of Nrf2 mRNA expression compared to Scr control. C) mRNA levels of autophagy protein Lc3b showed no significant changes, and mRNA expression of Atg5 was significantly higher with miR-199a-5p inhibition as compared to Scr controls. Scr – antagomiR scrambled, miR-199 – miR-199a-5p mimic; AM-199 – antagomiR to miR-199a-5p. qPCR: expression relative to S29 is

shown; n=3. Error bars show SEM; * – $p<0.05$. One-way ANOVA with Dunnett's post-test.

5.4 Discussion

The aim of this chapter was to examine the effect of miR-199a-5p on nerve cells *in vitro*. The resulting effect of miR-199a-5p on NSC-34 cells was investigated and cells were treated with miR-199a-5p mimic, AM-199 or Scr control. In skeletal muscle cells, miR-199a-5p regulated the expression of ER stress-, NMJ-, and some mitochondria-related genes. Since miR-199a-5p is expressed in neural tissue (382,383) and has been shown to have a function in the context of Rett syndrome (253), and sarcopenia is associated with NMJ degeneration, the role of miR-199a-5p in a motor neuron model was investigated. ER stress-, mitochondria-, and NMJ-related genes were studied in NSC-34 cells to further elucidate the link between mitochondria and potentially dysfunctional NMJ, as impaired axonal mitochondrial function is associated with axon degeneration (384). The aim of this chapter was to determine whether miR-199a-5p regulates ER stress, and mitochondrial dynamics and could therefore contribute to the degeneration of NMJ during ageing. We first treated NSC-34 cells, and miR-199a-5p overexpression was significant (Figure 5.3.1), it was observed that, like C2C12 cells, the AM199 treatment was not as powerful as miR overexpression.

NSC-34 cells are a hybrid cell line generated by fusing neuroblastoma with mouse motor neuron-enriched spinal cord cells, and they are used as experimental models. The usefulness of these cells in different models, however, appears to be limited (379,385), and miR-199a-5p has a role in both tumour repression and promotion, making its interaction with the hybrid cell line potentially problematic. However, these cells have been shown to be utilised in neurodegeneration models, and therefore were used in these experiments (324). A study of NSC-34 cells as a model for amyotrophic lateral sclerosis (ALS), showed NSC-34 cells demonstrated poor differentiation capabilities, and Ca^{2+} signalling, which are critical for ALS *in vitro* models (385). ALS patient samples have demonstrated upregulated miR-199a-5p expression (386).

The hybrid nature of these cells is a serious limitation of this chapter and data, and although the results here are indicative of miR-199a-5p functions in motor neuron cells, it cannot be directly translated into the function of miR-199 in motor neurons *in vivo*. One concern is tumour-specific mitochondria variants are observed in many cancers including neuroblastoma (387). Further, the UPR and ER stress has a complex role within cancer, due to apoptosis-resistant cancer cells, and potential tumour-promoting activity of the UPR in cancer (388). Despite the limitations, the results demonstrate a potential role of miR-199 in regulating function in motor neurons.

5.4.1 miR-199a-5p overexpression or inhibition affects differentiated neurites in NSC-34 cells

NSC-34 cells were differentiated and treated with miR-199a-5p mimic or antagomiR, and the differentiated neurites were then stained against βIII tubulin and then measured and counted (Figure 5.3.2), and we found miR overexpression increased neurite length. This appears to be paradoxical, as overexpression or inhibition would not drive neurite outgrowth with any specificity. However, it is possible miR transfections were not as efficient and miR levels were not strongly changed. The result of neurite number however, indicated a lower number of neurites with miR-199a-5p overexpression, as compared to Scr control (Figure 5.3.2). We further observed in NSC-34 cells, miR-199a-5p inhibition increased cell number in the presence of H_2O_2. The inhibition of miR-199a-5p by AM-199 also significantly lowered the number of neurites although not to the degree seen with miR-199a-5p overexpression. However, similar effects of miR-199a-5p and AM-199 treatment were previously observed in another study, suggesting a potential feedback loop existence (252). Additionally, miR-199a-5p overexpression significantly increased miR-199a-5p levels compared to Scr controls, however AM199 treatment was observed to not be as effective in these cells and did not significantly reduce miR-199a-5p expression (Figure 5.3.1).

5.4.2 miR-199a-5p affects the levels of ER stress-related proteins in NSC-34 cells

The link between ER stress and miR-199a-5p was assessed in NSC-34 cells. Data from section 4.3.3 demonstrates that in C2C12 cells, miR-199a-5p regulated the expression of ER stress-related proteins: CHOP as well as GRP78. We first examined

the effect of miR-199a-5p overexpression and inhibition on the proliferation of NSC-34 cells, and our results demonstrated no changes present in normal growth conditions, but during the presence of stress, inhibition of miR-199a-5p resulted in increased cell number as compared to Scr controls (Figure 5.3.3). When assessed at the protein level, NSC-34 cells showed CHOP protein expression was significantly upregulated with miR-199a-5p overexpression in NSC-34 cells. Chop mRNA expression was upregulated similar to the results seen in Western blot, although not significantly (Figure 5.3.4). GRP78, has critical functions in endogenous mechanisms of neuroprotection, potentially by inhibition of apoptosis, although, this is likely not the main cause of neurodegeneration (389). CHOP transcription factor has been linked to ER-stress induced apoptosis, as well as mitochondrial-mediated autophagy (80). CHOP-linked ER stress has been linked with neurodegeneration and demyelination in multiple sclerosis, and the knowledge of CHOP as a regulator of apoptosis acting on the mitochondrial membrane (80,390). Increased CHOP expression has been shown to downregulate BCL2, an apoptotic regulator localised to the mitochondrial membrane (80). A study of spinal cord injury in rats demonstrate GRP78 and CHOP upregulation are correlated with ER-stress related apoptosis within the early stages of injury, and delivery of nerve growth factor decreased levels of CHOP, GRP78 and also increased the expression of GAP43 (367). These data highlight the link between ER stress and apoptosis of neurons. To determine further how ER stress is affecting neuronal homeostasis and given the knowledge of apoptosis at the NMJ, however, future investigation of the effects of miR-199a-5p on the ER stress pathway in the context of motor neurons are needed in more appropriate *in vitro* models.

5.4.3 miR-199a-5p effects GAP43 in NSC-34 cells

To determine whether miR-199a-5p regulates NMJ homeostasis through regulation of NMJ-related genes in motor neuron-like NSC-34 cells, in addition to C2C12 cells, we next established if miR-199a-5p regulated neuronal growth protein, GAP43. miR-199a-5p overexpression on GAP43 protein expression was not significant compared to Scr control (Figure 5.3.5), however inhibition of miR-199a-5p significantly increased protein expression of GAP43 compared to Scr control. Relative mRNA expression levels of Gap43 were not significantly influenced by overexpression or inhibition, although there was a non-significant increase in expression levels of Gap43

with miR-199a-5p inhibition. Other targets with NMJ activity: HDAC9 and ACVR2a were not regulated by miR-199a-5p.

Differentiated NSC-34 cells demonstrate increased expression of neuronal markers, including GAP43 (324). GAP43 is located throughout the neuron but is more concentrated at the axon terminal and appears to be critical for nerve sprouting at the NMJ and is likewise upregulated with nerve regeneration (366). Literature supports the role of miR-199a-5p in regulation of neuron injury, with miR-199a-5p overexpression facilitating ROS production and apoptosis *in vitro* (391). The overexpression of miR-199a-5p has been associated with oxygen-glucose deprivation/reoxygenation injury in murine neurons, and the results of a study on overexpression of miR-199a-5p in mouse neurons demonstrated reduced Nrf2 expression levels, and a significant increase in Nrf2 expression levels with miR-199a-5p inhibition (391). *Nrf2* is a regulator of the adaptive response to oxidants, and increased Nrf2 activity is associated with protection from oxidative damage *in vivo* (335,392). The authors of this study reported increased Nrf2 signalling is beneficial to neuron survival through resistance to oxidative stress and apoptosis (391). This agrees with other reports that demonstrate inhibition of miR-199a-5p reduces apoptosis of neuronal cells following spinal cord injury (393).

Other studies of miR-199a-5p suggest it is highly involved in apoptosis, as downregulation of miR-199a-5p reduces high glucose-induced apoptosis and ROS generation in pancreatic β-cells (394), and inhibition of miR-199a-5p has also been shown to protect cardiomyocytes against hypoxia-induced apoptosis (395). Others have reported similar protective effects on inhibiting miR-199a-5p in cardiomyocytes exposed to uncontrolled hypoxia-induced ER stress arising from congenital heart disease (396) The abnormal metabolic environment resulting from hypoxic conditions initiates ER stress responses and can lead to apoptosis. The results in 5.3.2 demonstrate significant increased ER stress with miR-199a-5p overexpression in NSC-34 cells, which therefore may be driving cell neuron cell apoptosis and a subsequent decline in the NMJ as results of the current study demonstrate inhibiting miR-199 promotes expression of GAP43, which is critical to NMJ function.

5.4.4 miR-199a-5p regulates the expression of mitochondrial-, oxidative stress-, and autophagy-associated genes in NSC-34 cells

As the results of miR-199a-5p overexpression pointed towards increased ER stress and altered NMJ-specific targets, it was next necessary to investigate the role of mitochondria in this process as previous literature supports a role in mitochondrial dysfunction through ER stress and neurodegeneration (355,359,384,397,398). The results of the present study indicated miR-199a-5p inhibition significantly increased mRNA expression of mitochondrial membrane protein, Tom20 by RT-qPCR. Central regulator of energy metabolism, Pgc-1α stimulates expression of nuclear genes encoding for mitochondrial proteins (361). The present study demonstrated that miR-199a-5p overexpression or inhibition had no significant effect on relative expression of Pgc-1α. Similarly, Cox1, a component of the electron transport chain, and mitochondrial enzyme, showed no significant differences at mRNA levels following miR-199a-5p expression regulation. Mitochondrial dysfunction is common to neuromuscular disease and upregulated miR-199a-5p was found to be associated with differentially expressed mitochondrial pathways such as mitochondrial translation in multiple sclerosis patients (399). Mitochondrial dysfunction in neurons yields altered Ca^{2+} signalling, oxidative stress, and apoptosis, and as neurons are dependent on mitochondria for Ca^{2+} signalling and ATP production, aberrant mitochondria can be localised to the axons (400). Changes in mitochondria such as fragmentation (401), and abnormal cristae (402), have been detected in neurological disorders such as Huntington's Disease (402). The increases in Tom20 mRNA expression and Nrf2 expression with miR-199a-5p inhibition in the present study are similar to that seen in GAP43 protein expression levels, which agree with inhibition of miR-199a-5p promoting beneficial effects on cells *in vitro,* by potentially maintaining homeostasis of mitochondrial transport proteins (402), and oxidative stress proteins (391) as well as axon regeneration (403). Gap43 is also associated with the regeneration of nerves following injury; neural injuries induce neurons to release neurotrophic factors, which can stimulate proteins such as GAP43 to encourage regeneration and promote neuroprotection (404).

There also exists a known role between the UPR and ER stress and autophagy, and there may be an important role for miR-199 in their regulation (278). The crosstalk between ER stress and mitochondrial dysfunction observed with ageing and disease

indicates a potential role for mitochondrial influence on the negative effects seen with miR-199a-5p related upregulation. Selective mitochondrial autophagy controls the quality and number of mitochondria, and the mitochondria themselves are believed to be involved both autophagosome biogenesis and autophagic flux (405). The present study assessed autophagy regulator Atg5 by RT-qPCR and miR-199a-5p overexpression did not significantly increase Atg5 expression, although miR-199a-5p inhibition significantly increased Atg5 expression compared to Scr control. Upon induction of autophagy, Atg5 drives the formation of autophagosomes (406). Atg5 has been identified as a target of miR-199a-5p and was demonstrated to prevent myocardial hypertrophy by regulating autophagy of myocardial cells through the Atg5-miR-199a-5p pathway, in which miR-199 overexpression inhibits autophagy (251). This link also exits in ageing and neurodegeneration, as mitochondria-specific autophagy protects neurons by eliminating damaged mitochondria and controlling ROS and neuron apoptosis (272).

In the present study, mRNA levels of autophagic flux marker LC3B, the best characterised isoform of LC3 (332), were found increased with miR-199a-5p inhibition, although not significantly (Figure 5.3.6). While it was observed Lc3b mRNA expression was lower, although not significantly as compared to Scr controls, and therefore may be regulated by miR-199a-5p, however a Western blot or autophagy flux reporter assay would be needed to determine if miR-199a-5p is driving changes in autophagic flux. During autophagy, autophagosome formation (Figure 1.5.1) involves cytosolic LC3 (LC3-I) is conjugated to phosphatidylethanolamine to bind the resulting (LC3-II) to the autophagosome, which then joins to the lysosome to form the autolysosome (407). Simultaneously, LC3-II is degraded by lysosomal proteases, and the degradation rate is correlated to autophagic flux, thus the ratio between LC3BI/II is indicative of autophagy be correlating autophagosome number to autophagy (332). This study demonstrated miR-199a-5p inhibition did not significantly increase mRNA expression of Lc3b compared to Scr control.

Other studies have identified miR-199a-5p as a negative regulator of autophagy as demonstrated by inhibited LC3B expression (317). Defective autophagy is associated with fragmented NMJ morphology and NMJ instability resulting in increased denervation. A possible mechanism for this in mice is oxidative stress resulting from

mitochondrial dysfunction leads to further defective mitochondria and NMJ damage by neuron apoptosis (162). Nrf2 mRNA levels with miR-199a-5p overexpression demonstrated significantly reduced levels of relative expression compared to Scr control. This agrees with the observed miR-199a-5p overexpression reducing mitochondrial content in both the NSC-34 cells as well as C2C12 cells (Figure 4.3.8). This suggests potentially controlling miR-199a-5p upregulation could be beneficial to neuromuscular health by controlling rampant ER stress that ultimately damages localised mitochondria potentially through preventing neuron apoptosis at the NMJ.

Chapter 6 The role of miR-199a-5p in muscle and neuronal homeostasis *in vivo*.

6 The role of miR-199 in muscle and neuronal homeostasis *in vivo*

6.1 Introduction

Sarcopenia, the age-related progressive loss of skeletal muscle mass and function (disease classification: ICD-10-CM), results in frailty, decline in strength and decrease in quality of life of older people. Humans lose skeletal muscle at a rate of 1-2% per year from the approximate age of fifty (408). The reduction in muscle mass and strength in older people is underpinned by progressive pathophysiological changes, which ultimately perturb the maintenance of muscle homeostasis. Changes in skeletal muscles during ageing show considerable similarities between human and rodents (409). Among proposed mechanisms of sarcopenia, are progressive myofibre atrophy (with type II muscle fibres potentially more susceptible to atrophy than type I fibres), alterations in satellite cell biology and therefore defective regeneration, adipose tissue infiltration and chronic inflammation have been proposed (82,84,85,208,410). The remaining muscle fibres of older mammals are characterised by decreased strength, increased susceptibility to damage and impaired regeneration, when compared to muscles of younger adults (84). Changes in miR, mRNA and protein expression have been described in ageing muscle (85,90,158,168). Our group has shown that restoring physiological levels of specific miRs can improve myofibre size and muscle force, however comprehensive studies on the role of miRs in sarcopenia are needed. Sarcopenia is associated with increased risk of death and impairment in the aged population (411). However, given that sarcopenia is an age-related loss of skeletal muscle associated with systemic changes during ageing, a suitable *in vivo* model must be used to study the effects of interventions on skeletal muscle, in addition to *in vitro* studies (412). The mouse model of ageing will use male and female C57BL6/J mice: adult (3 months old) and old (24 -26 months old – muscle loss is significant at this age) mice. Ageing affects multiple tissues and is a complex process from a mechanistic point of view. Old mice are the simplest and best model of ageing among mouse models (248). Other models, such as progeroid mice, Zmpste24-/- , Polg mutants, Nfkb1-/- or Terc-/- mice provide an advantage of accelerated ageing, however the mechanisms leading to muscle loss in these models are associated with a given mutation, rather than the process of ageing, and changes in muscle in these models do not always recapitulate all/most aspects of human muscle ageing. Therefore, aged mice are the most appropriate mouse model to study ageing.

Humans and mice have up to 78.5% gene homology (412), and congruencies in human and rodent musculoskeletal anatomy make them robust models for investigating the mechanisms driving sarcopenia in the aged organism (413). Given the changes we observed in C2C12 muscle cells and NSC-34 neuron-like cells with miR-199a-5p overexpression, we next aimed to determine the effect of miR-199a-5p overexpression or inhibition *in vivo* to better understand the potential mechanisms behind miR-199a-5p influence on skeletal muscle and neuromuscular homeostasis in ageing and disease. Other studies have demonstrated mouse models of sarcopenia can be affected by miR administration (160,171,205,290,414–416). Dysregulated miR-199a-5p in dystrophic muscle has been observed in zebrafish, mdx mice, and human Duchenne's muscular dystrophy biopsies (252), although the effect in skeletal muscle in ageing is not known. Predicted and validated targets (please see Chapter 3) of miR-199a-5p, our *in vitro* data on miR-199a-5p function, as well as current literature suggests both muscle (417) and nerve (418), are affected by dysregulated miR-199a-5p, therefore we used a mouse model of miR-199 overexpression to validate the effect of miR-199a-5p on neuromuscular homeostasis.

This chapter aimed to determine the effect of miR-199a-5p overexpression and miR-199a-5p inhibition on muscle size, force and weight, as NMJ morphology *in vivo* in mice. Additionally, we investigated the effect of miR-199a-5p on mRNA and protein expression levels of ER stress-, mitochondria-, and NMJ-related genes in mouse skeletal muscle—pathways regulated by miR-199a-5p in our *in vitro* data (see Chapters 4 and 5). We hypothesised miR-199a-5p overexpression would reduce muscle size and muscle force, and inhibiting miR-199a-5p would preserve muscle.

6.2 Materials and methods

6.2.1 Animals

C57Bl/6 male mice (young mice ~5-months old; old mice ~23 months old at start of treatment) obtained from Charles River UK. Experiments were performed in accordance with UK Home Office guidelines under the UK Animals (Scientific Procedures) Act 1986 and received ethical approval from the University of Liverpool Animal Welfare and Ethical Review Body (HPRA Licence AE19125/P091, reviewed by ACREC and AWB, NUIG.)

All animals were fed *ad libitum* and remained on a 12-hr light-dark cycle under specific pathogen-free conditions. To manipulate miR-199a-5p levels, mice were injected with cholesterol-modified: Scr control, miR mimic, or antagomiR mimic, at a concentration of 2mg/kg bodyweight two times during the experimental period (days 1, 10). For the regeneration experiments mice were injected three times (day 1, 8, 15). The dosing was established in a previous study: Goljanek-Whysall *et al*. (160). The antagomiR does not bind to the miR permanently and downregulation for expression is not always detected by qPCR despite inhibition of its function.

All mimics were delivered intravenously by tail vein as described in 2.15.4. Mice were euthanised by cervical dislocation 3-weeks after the first injection. For regeneration experiments, mice were euthanised 4-weeks after the first treatment. Tissues were immediately collected and either frozen at -80 for later sample processing (RNA and protein isolation) (2.15.2, 2.9) or placed in Cryomatrix/OCT and snap frozen in isopentane for histology (2.15.2). IV injections were performed by Dr K. Whysall.

6.2.2 Mimic and inhibitor sequences used *in vivo*

The following miR sequences were used *in vivo*:

Scr Control- 5' mC.*.mA.*.mU.mC.mC.mA.mU.mC.mA.mC.mU.mC.mA.mC.mU.mC.mC.mA.mU.*.mC.*.mA.* .mU.3'-Chl 3'

miR-199a-5p- 5’- miRIDIAN mimic based on mmu-miR-199a-5p MIMAT0000229

antagomiR-199a-5p- 5' mG(*)mA (*)mAmC mAmGmG mUmAmG mUmCmU mGmAmA mCmAmC (*)mU(*) mG(*)mG (*)mG (3'-Chl) 3'

Chl—Cholesterol

M—2-O’ methyl bonds

(*)—phosphothiate bonds

A detailed description of miR delivery *in vivo* can be found in 2.15.4.

6.2.3 Muscle histology

For muscle histology, sections (8-10 µm thickness taken from the mid-belly of the tibialis anterior (TA) muscle) were taken at –20°C and mounted on glass slides. Slides were then rinsed in PBS and fixed in ice-cold methanol for 5 minutes. Sections were taken either as transverse cross-sections for myofibre size analysis (WGA) or longitudinally for NMJ visualisation (2.8).

To determine the effect of miR-199a-5p on myofibre size, sections were first air-dried for 3 minutes, blocked for 10 minutes at RT in blocking solution containing PBS and 10% HS. Slides were next washed in PBS and incubated in fluorescein-labelled wheat germ agglutinin (WGA; 5µg/ml) diluted 1:2000 in PBS and 4′,6-diamidino-2-phenylindole (DAPI, 1 µg/ml) for 30 minutes covered at RT. Finally, slides were washed 3 times in PBS before mounting cover slips with non-fluorescing mounting medium, hydromount.

For NMJ visualisation, sections were prepared similar to cross-sections before being blocked in a blocking solution (1% Triton-X, 4% bovine serum albumin, 1% HS) for 2 hours at RT. Slides were next incubated with primary antibodies: synaptic vesicle glycoprotein-2 (SV2; 1:50) and neurofilament (2H3; 1:50) overnight at 4°C and all antibodies were diluted in a 10% blocking solution. Slides were next washed 3 times in PBS for 5 minutes and then incubated in secondary antibody (1:1000) for 2 hours at RT covered from light. Slides were next washed 3 times in PBS again and then again incubated for 1 hour at RT to visualise the acetylcholine receptor (α-Bungarotoxin; 1:500), before being rinsed in PBS for 5 minutes and then cover slips mounted with hydromount.

6.2.4 Muscle function analysis

Muscle function analysis was performed on the extensor digitorum longus (EDL) muscle via peroneal nerve stimulation as described and performed previously in (419). In short, the distal tendon of the EDL was attached to the lever or a servomotor (Aurora Scientific). The EDL muscles were stimulated electrically to contract at muscle optimal length (Lo) and optimal stimulation voltage (10 V). This was performed at 2-minute intervals for 300 milliseconds with a 0.2 millisecond pulse width to determine maximum isometric tetanic force (Po). Lo was determined with a series of 1 Hz stimulations and set at the length that generated maximum force. The

frequency increases went from 10 to a max of 300 Hz in 50 Hz increments. Po was identified when the maximum force reached a plateau. Muscle fibre length (Lf) and weight of EDL muscles were measured *ex vivo*. Specific Po (mN/mm2) was calculated by dividing Po by total fibre cross-sectional area. Force measurements were performed by Dr K. Whysall.

6.2.5 RNA isolation and cDNA synthesis

Frozen muscle tissue was processed for RNA as described in 2.9. RNA was isolated using TRIzol/chloroform standard RNA isolation protocol and RNA purity was assessed on a Nanodrop 2000 spectrophotometer as described in 2.9. Synthesis of cDNA was performed using SuperScript II (100-500ng RNA) or miScript RT II (100ng RNA).

6.2.6 Real-time qPCR and PCR

Real-time qPCR was performed using miScript SYBR Green Master Mix for miRs (UNISP6 YP00203954, SNORD68 YP00203911, hsa-miR-199a-5pa-5p YP00204494, hsa-miR-199a-5pb-5p YP00204152) and FAST SYBR Green Master Mix. Relative expression was to β2-microblobulin or S29 (mRNA) and Rnu-6 and/or Snord-61/Snord-68 (miR) and was calculated using delta-delta Ct method; changes in relative expression were analysed. Primer sequences are listed in Table 2.11.1. The protocol for RT-qPCR is listed in 2.11.

Standard PCR for Xbp1 was performed using Readymix REdTaq PCR reactive mix. Samples were analysed by electrophoresis on a 2% agarose gel (1% w/v in Tris-acetate-EDTA buffer) complemented with SYBR Safe DNA gel stain (1:10,000), and then visualised using the Odyssey Fc imaging system.

6.2.7 Protein isolation and Western blot

Muscle tissue was processed as described in 2.12.1. Protein was isolated and Western blotting was performed as described in 2.14. Briefly, homogenised in RIPA buffer and protein concentrations were calculated using Bradford reagent using BSA standards. Blotting was performed using protein lysates diluted in Laemmli buffer, and 20-30μg of protein was run on 8%– 16% polyacrylamide gels. Proteins were transferred to nitrocellulose membranes using a semi-dry blotter. Subsequently,

membranes were stained with Ponceau S (0.1 % Ponceau in 5% acetic acid) to visualise and confirm equal protein loading. Membranes were blocked in 5% milk in TBS-T for 1 hour at room temperature, and following, washed 3x10 minutes in TBS-T. Membranes were incubated with primary antibodies (1:750-1:1000 antibodies table listed in 2.7.1) overnight at 4°C. Membranes were then washed in TBS-T and incubated with fluorescent secondary antibodies; goat anti-rabbit and goat anti-mouse dependent on primary antibody, and images were obtained using Odyssey Fc imaging system. Quantification was performed using ImageJ and normalised to Ponceau S stain by densitometry of total Ponceau in that sample lane.

6.2.8 Barium chloride injections for muscle regeneration *in vivo*.

A mouse model of muscle regeneration was used by first injuring the right gastrocnemius of the mouse with 1.2% barium chloride ($BaCL_2$) suspended in sterile PBS. The gastrocnemius was injured by intramuscular injection, of 30µl into the right muscle under gas anaesthesia. Animals were given intramuscular injection of buprenorphine was administered at 0.05mg/kg BW immediately after IM injection. All tissues were collected immediately after euthanasia, and snap frozen with liquid nitrogen and OCT for histology or stored at -80°C for future use. Experiments were performed in accordance with UK Home Office guidelines under the UK Animals (Scientific Procedures) Act 1986 and received ethical approval from the University of Liverpool Animal Welfare and Ethical Review Body (HPRA Licence AE19125/P091, reviewed by ACREC and AWB, NUIG.).

6.2.9 Image analysis

Images were created using the EVOS microscope imaging system using 10X or 40X magnification. The EVOS M5000, and EVOS M7000 systems were used for imaging. Fluorescence microscopy for immunostaining was also performed using the EVOS GFP light cube (AMEP4951), EVOS DAPI light cube (AMEP4950), or EVOS Cy5 light cube (AMEP4956). Images were exported as TIF files as single or merged channels. WGA Image analysis was performed using ImageJ and the macro ‘Tissue Geometry Stats’ (https://biii.eu/tissue-cell-segmentation) to semi-automatically quantify minimal Feret’s diameter of WGA immunostained images (2.8.1). The minimal Feret’s diameter is defined as the closest possible distance between the two

parallel tangents of the muscle fibre (420). Values below 20µm were excluded to minimise artifacts.

Results were analysed in Microsoft Excel and then graphed with GraphPad Prism (Prism version 5.03 software package for Windows). Western blot images were obtained using Odyssey Fc imaging system (Li- Cor), and quantification was performed using ImageJ and normalised to Ponceau S stain by densitometry of total Ponceau in that sample lane as described in 2.14.

6.2.10 Statistical analysis

All data are represented as mean ± SEM. For three or more groups, one-way ANOVA were performed using Prism version 5.03 software package for Windows (GraphPad Software, www.graphpad.com). The power analysis was performed as described in Goljanek-Whysall *et al.* (160). One-way ANOVA was used to compare three groups and can be used to detect statistical differences with normally distributed data with relatively small sample sizes. Further, Dunnett's post-test was selected to compare the results of treatments against the Scr control, to determine the effect of miR-199a-5p overexpression or inhibition against the control Scr sequence. Student's t test was used to compare two groups. All data are presented; p-values ≤ 0.05 considered statistically significant. Statistics are discussed in detail in 2.17.

6.3 Results

6.3.1 miR-199 has little effect on myofibre size *in vivo*

Muscle was first collected from treated young and old mice, and RT-qPCR for miR-199a-5p was performed to determine the effectiveness of miR overexpression and inhibition (Figure 6.3.1). Our results showed miR-199a-5p overexpression in miR treated young and old mice. AM-199 treatment resulted in reduced expression of miR-199a-5p (Figure 6.3.1), however, these results were not significant. Next, gross changes in body and muscle weights in young and old mice treated with Scr control, miR-199a-5p mimic, or antagomiR-199 were analysed. Old mice showed an increase in bodyweight overall as compared to adult mice (Figure 6.3.2). Raw muscle weights showed QUAD muscle was significantly lower in old mice compared to young mice. miR-199a-5p overexpression had no effect on GAS, TA, or EDL muscle (Figure

6.3.3). As a ratio of bodyweight, the QUAD was also observed to be significantly smaller in old Scr control mice as compared to young Scr control mice when taken as a percentage of whole bodyweight (Figure 6.3.4). The GAS also was observed to be significantly smaller in old mince compared to young mice, and further miR-199a-5p overexpression in old mice resulted in significantly smaller GAS muscle as compared to Scr controls (Figure 6.3.4). Muscle of the TA and EDL of young and old mice showed no significant differences in weight as a ratio of bodyweight. Myofibre size analysis by minimum Feret's diameter revealed a minimal decrease in myofibre size following miR-199a-5p overexpression and increase in myofibre size following miR-199a-5p inhibition in TA of old mice (Figure 6.3.5).

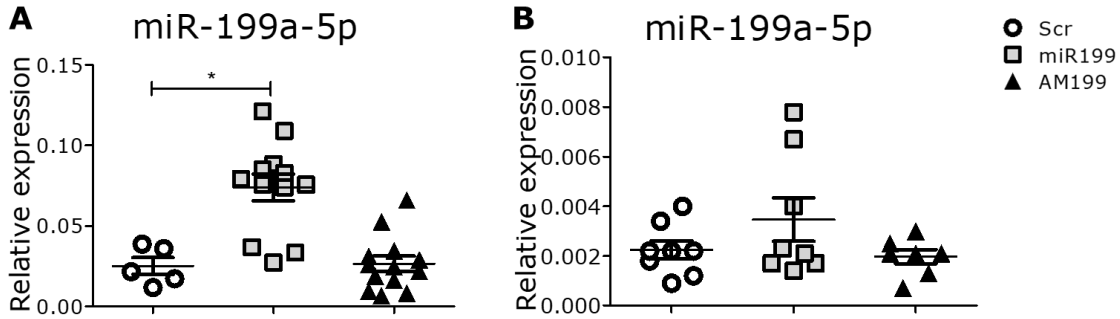

Figure 6.3.1. miR-199a-5p mimic and inhibitor delivery to muscle. Mimic for miR-199a-5p, AM-199, and Scr control were delivered to the muscle by intravenous injection. A) Young muscle shows miR-199a-5p overexpression with miR delivery. AM-199 delivery not as powerful. B) Old mice demonstrated miR-199a-5p overexpression exhibited similar miR delivery and miR-199a-5p inhibition in old mice. qPCR: expression relative to S29 is shown; n=(4). Scr – antagomiR scrambled, miR-199- miR-199a-5p – mimic; AM-199 – antagomiR to miR-199a-5p. Error bars show SEM; * - $p<0.05$; one-way ANOVA, Dunnett's post-test; (young mice ~5-months old; old mice ~23 months old).

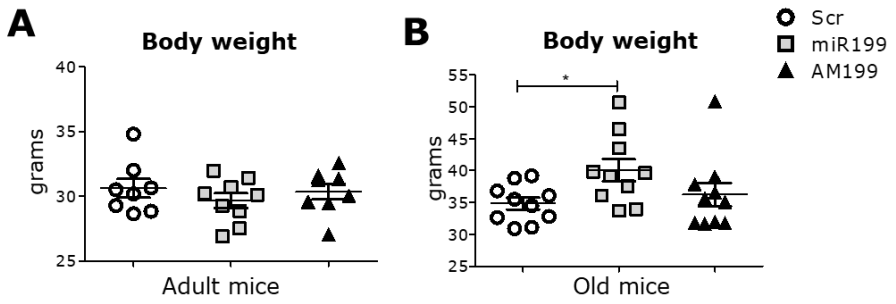

Figure 6.3.2. miR-199a-5p overexpression does not regulate muscle weight *in vivo in* young mice, but increased weight in old mice. Young and old mice were treated with miR-199a-5p mimic, inhibitor, or Scr control, and body weight and the weight of lower limb muscles were measured. A) Overexpression of miR-199a-5p resulted in no significant increase in bodyweight in young mice. B) A significant increase in bodyweight was observed in old mice overexpressing miR-199a-5p compared to control. Scr – antagomiR scrambled, miR-199– miR-199a-5p mimic; AM-199 – antagomiR to miR-199a-5p. Error bars show SEM; * - p<0.05; one-way ANOVA, Dunnett's post-test; n=(8) (young mice ~5-months old; old mice ~23 months old).

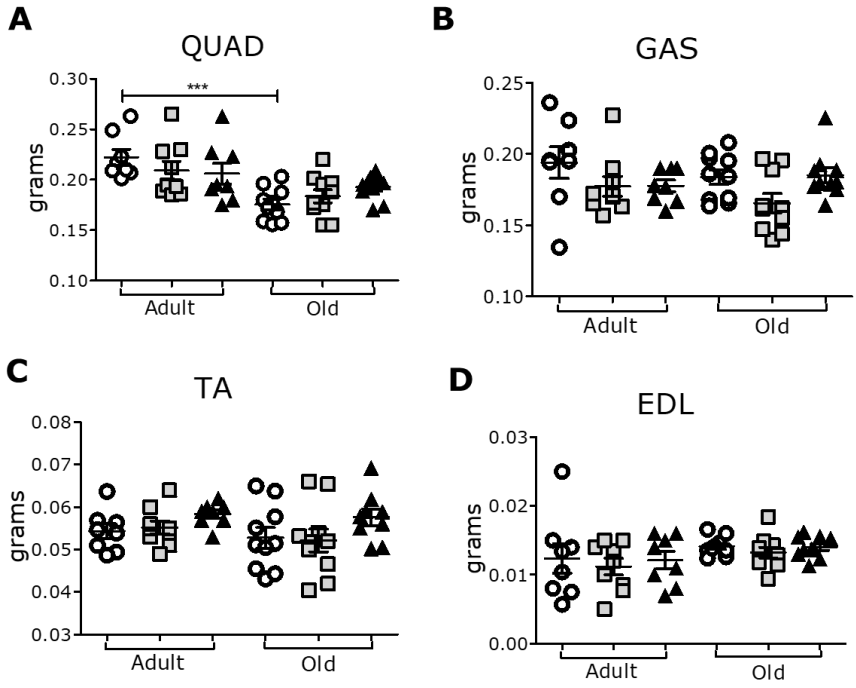

Figure 6.3.3. miR-199a-5p has a minimal effect on muscle weight *in vivo*. A) Raw muscle weights showed in old mice, miR-199a-5p downregulated muscle weight in the QUAD muscle as compared to Scr control. Raw EDL muscle weights showed no changes. Scr – antagomiR scrambled, miR-199 – miR-199a-5p mimic; AM-199 – antagomiR to miR-199a-5p. Error bars show SEM; * - p<0.05; one-way ANOVA, Dunnett's post-test; n=(8) (young mice ~5-months old; old mice ~23 months old).

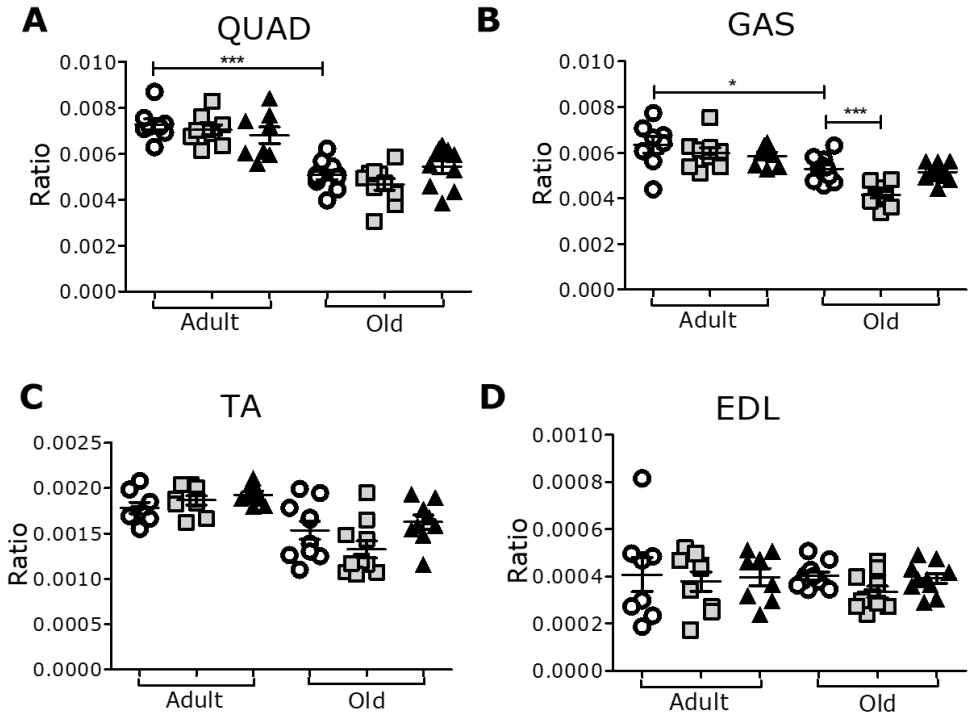

Figure 6.3.4. miR-199a-5p has a minimal effect on muscle weight *in vivo* when bodyweight is considered. Young and old mice were treated with Scr control, miR-199a-5p mimic or AM-199. Results showed: A) as a ratio of bodyweight, the QUAD was found to be significantly lower in old age Scr control as compared to young Scr. B) In the GAS, miR-199a-5p overexpression significantly lowered muscle size as a ratio of total bodyweight when compared to Scr control. Old mice further showed smaller GAS muscle compared to young mice. C) TA muscles showed no differences as a ratio of bodyweight. D) EDL muscle showed no differences as a ratio of bodyweight. Scr – antagomiR scrambled, miR-199– miR-199a-5p mimic; AM-199 – antagomiR to miR-199a-5p. Error bars show SEM; * - $p<0.05$; one-way ANOVA, Dunnett's post-test; n=(8) (young mice ~5-months old; old mice ~23 months old).

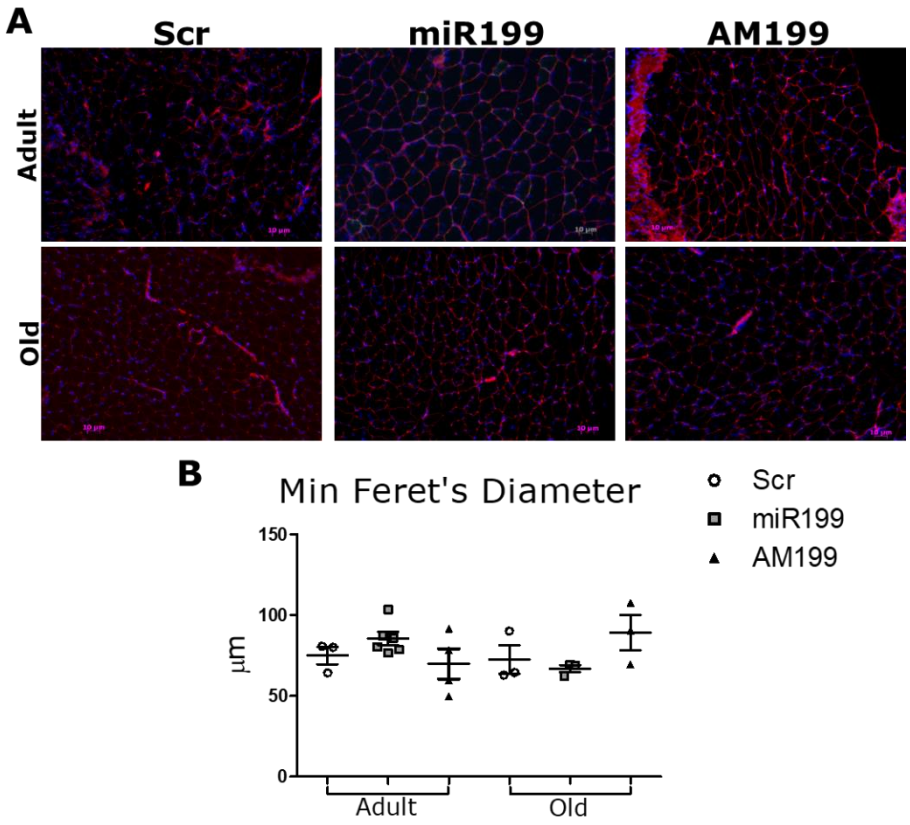

Figure 6.3.5. miR-199a-5p has little effect on myofibre size *in vivo*. Young and old mice were treated with miR-199a-5p mimic, inhibitor, or Scr control. WGA immunostaining of cross sections of TA muscle revealed that overexpression or inhibition of miR-199a-5p resulted in no significant changes to myofibre cross-sectional area as measured by minimal Feret's diameter. Scr – antagomiR scrambled, miR-199 – miR-199a-5p mimic; AM-199 – antagomiR to miR-199a-5p. Error bars show SEM; * - $p<0.05$; one-way ANOVA, Dunnett's post-test; (young mice ~5-months old; old mice ~23 months old).

6.3.2 miR-199a-5p inhibition leads to increased specific and maximum EDL force *in vivo*.

We next aimed to determine functional changes in muscle force following manipulation of miR-199a-5p expression. Muscle forces were examined *in vivo* in EDL muscles through stimulation of the peroneal nerve. Muscle of old mice were characterised by decreased maximum and specific force, as expected (Figure 6.3.6). miR-199a-5p overexpression or inhibition did not result in significant changes in maximum or specific force of EDL of young mice as compared to Scr control (Figure 6.3.6). In miR-treated mice, two groups were visible within the group showing one group exhibiting lower force and the other group exhibiting unchanged force. In old mice, miR inhibition by AM-199 led to a significant increase, as compared to old Scr control mice, in maximum and specific force (Figure 6.3.6). Overall, the increase of muscle force following miR-199a-5p inhibition is consistent with maximum and specific force in old mice.

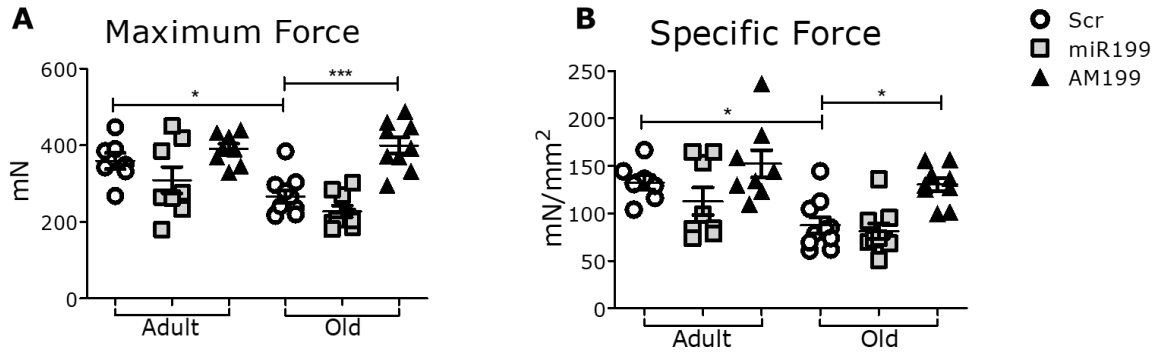

Figure 6.3.6. miR-199a-5p inhibition improves maximum and specific force *in vivo* in EDL of old mice. A) Overexpression of miR-199a-5p in young mice did not significantly reduce maximum force as compared to Scr young mice. Treatment with miR-199a-5p resulted in half the group exhibiting no change and the other half exhibiting lower, although not significantly, force. Old mice were observed to be weaker than young mice, and miR-199a-5p inhibition significantly improved force. B) Specific force measurements showed old mice were weaker than young mice. Specific force of AM-199 treated old mice were significantly upregulated as compared to old Scr controls. Scr – antagomiR scrambled, miR-199 – miR-199a-5p mimic; AM-199 – antagomiR to miR-199a-5p. Error bars show SEM; * - $p<0.05$; one-way ANOVA, Dunnett's post-test; n=(8-10) (young mice ~5-months old; old mice ~23 months old).

6.3.3 miR-199a-5p disrupts NMJ morphology *in vivo*.

The NMJ is the key site of transmission of action potentials in motor neurons into skeletal muscle contraction. We therefore looked at the longitudinal axis of the TA muscle and utilised immunostaining of the acetylcholine receptor (α-Bungarotoxin), as well as synaptic vesicle glycoprotein-2 (SV2) and neurofilament (2H3) to assess the morphology of the NMJ site following miR-199a-5p overexpression or inhibition. Overexpression of miR-199a-5p created observable differences in NMJ structure in both young and old mice. The traditional 'pretzel-like' appearance of the NMJ site that is present in healthy young Scr controls was altered with miR-199a-5p overexpression in young mice. In old mice, disrupted NMJs were observed in Scr control-treated mice and miR-199a-5p-treated mice (Figure 6.3.7). The presence of fragmented NMJ was indicated by the appearance of small islands within the NMJ that were inconsistent with the usual pretzel-like shape of the healthy NMJ, in addition to fragmentation, disrupted NMJ resulted in a rounded bunched-like appearance. The treatment with miR-199a-5p in young mice lead to increased incidence of abnormal NMJ morphology, and in old mice, miR-199a-5p similarly resulted in an increase in the number of NMJs with abnormal normal morphology as compared to old control mice as shown by confocal microscopy (Figure 6.3.9). We were unable to statistically quantify partial of full denervation due to small number of samples with preserved nerve, however observations of limited number of samples using confocal microscopy indicates that denervation was observed in sections of old control and old AM199 mice. miR-199a-5p led to increased number of sections with partial denervation and fragmentation observed in both young and old mice, in addition to morphological changes of NMJ as compared to young control (Figure 6.3.9).

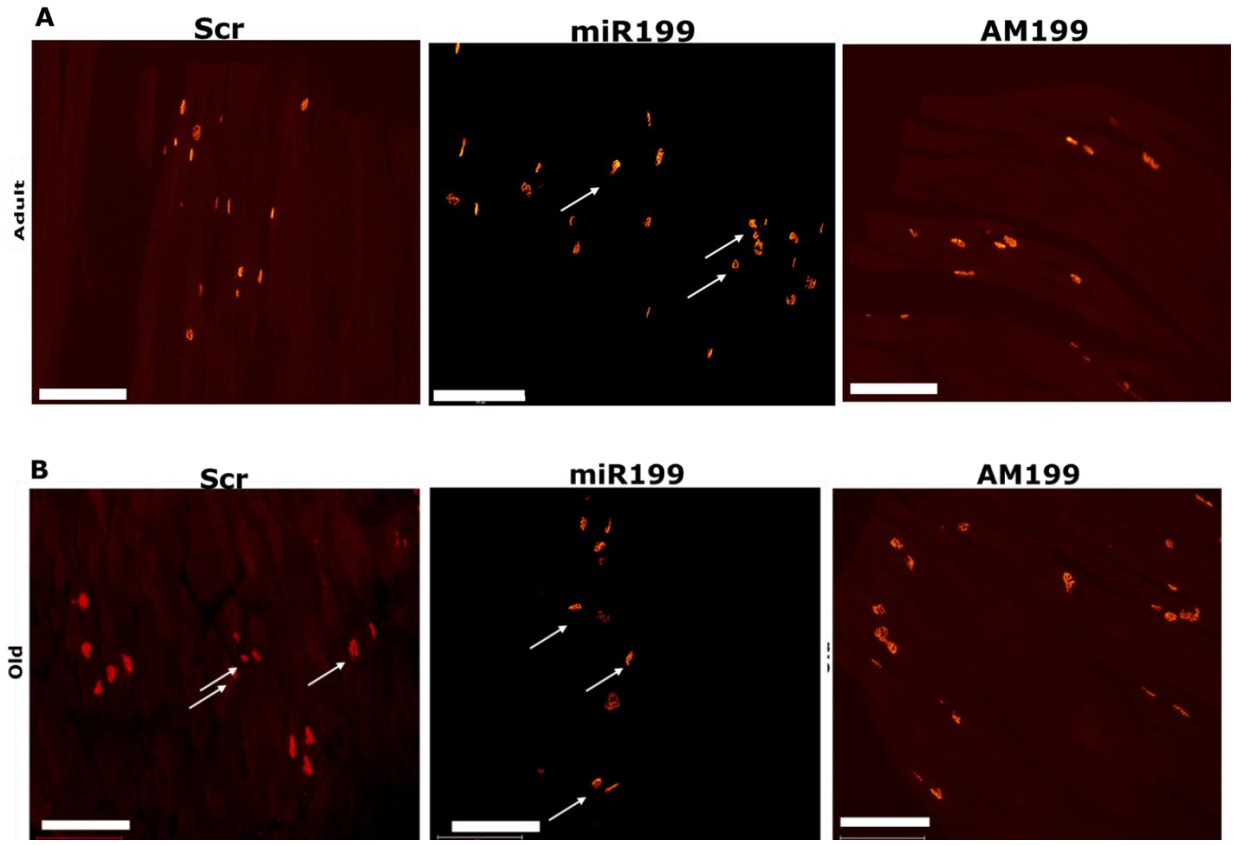

Figure 6.3.7. miR-199a-5p regulates neuromuscular morphology *in vivo*. Immunostaining of NMJ of mouse TA muscle treated with miR-199a-5p mimic, miR-199a-5p inhibitor or Scr control showed miR-199a-5p overexpression led to NMJ disruption as shown by increased fragmentation and 'island' formation. Instances of abnormal NMJ morphology were more frequent in miR-199a-5p treated mice. Representative images are shown; red: α-bungarotoxin, arrows denote abnormal NMJ. Scr – antagomiR scrambled, miR-199 – miR-199a-5p mimic; AM-199 – antagomiR to miR-199a-5p. Scale bar 275 µm, n=(87 young, 76 old) (young mice ~5-months old; old mice ~23 months old).

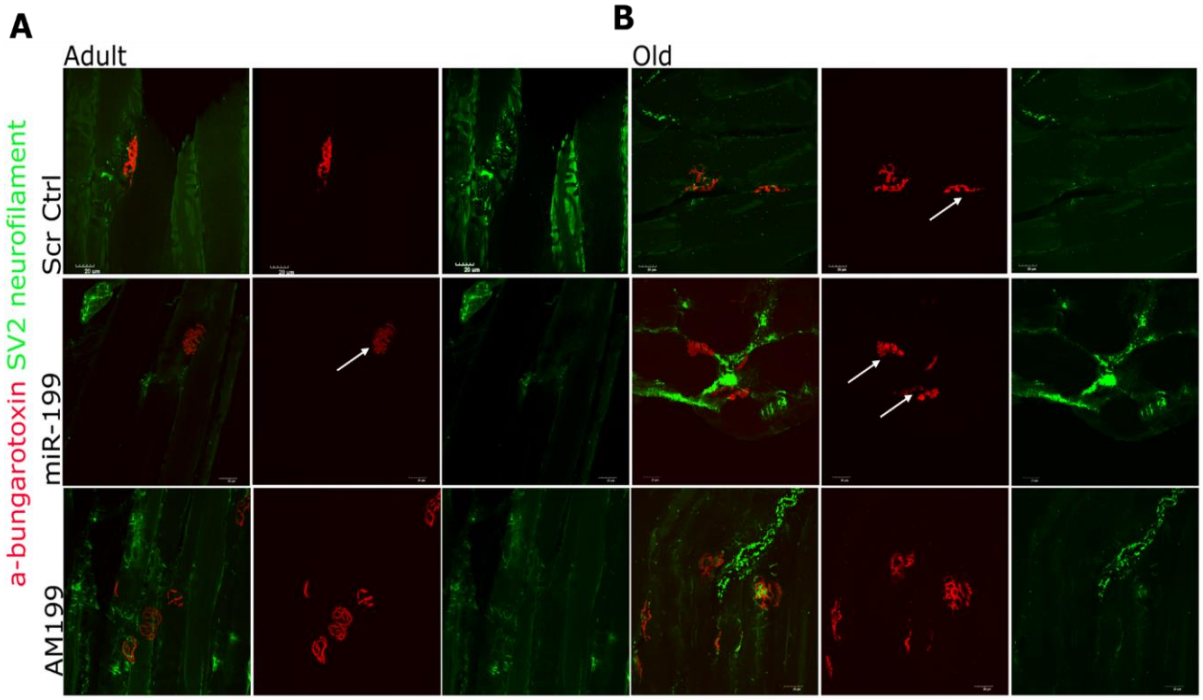

Figure 6.3.8. miR-199a-5p regulates NMJ morphology *in vivo*. Immunostaining of NMJ of mouse TA muscle treated with miR-199a-5p mimic, miR-199a-5p inhibitor or Scr control and subsequent confocal imaging indicated the presence of abnormal NMJs (indicated with white arrows) showing fragmented and bunched appearance as opposed to the traditional 'pretzel-like' shape, in addition to partial denervation as indicated by no SV2 signal. Scr – antagomiR scrambled, miR-199 – miR-199a-5p mimic; AM-199 – antagomiR to miR-199a-5p. Scale bar 20µm. (young mice ~5-months old; old mice ~23 months old).

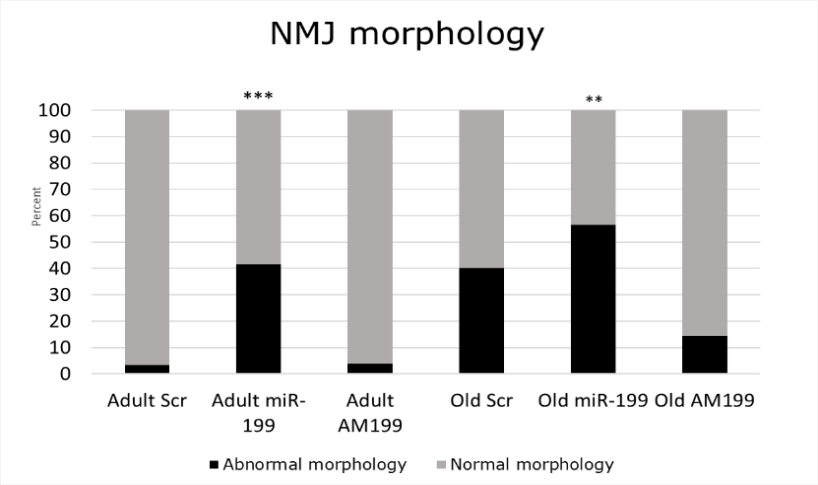

Figure 6.3.9. Quantification of NMJ morphology shows miR-199a-5p contributes to abnormal morphology. Young and old mice demonstrated significantly increased instances of abnormal morphology with overexpression of miR-199a-5p. Young X^2 (1, N = 87) = 3.841, p = 0.00005. Old X^2 (1, N = 76) = 10.159, p = 0.006. Scr – antagomiR scrambled, miR-199 – miR-199a-5p mimic; AM-199 – antagomiR to miR-199a-5p. (young mice ~5-months old; old mice ~23 months old).

6.3.4 miR-199a-5p regulates expression of genes associated with ER stress *in vivo*.

Data from 4.3.3, 5.3.2 demonstrated ER stress related proteins are affected by miR-199a-5p. We therefore investigated the effect of miR-199a-5p overexpression or inhibition on ER stress-related genes *in vivo*, to determine which potential branch of the ER stress response, (PERK, IRE1, or ATF6) is activated by miR-199a-5p. We therefore first looked at the PERK branch. CHOP functions downstream of PERK (347), and mRNA expression of Chop was significantly upregulated in TA muscle from old mice as compared to young mice, and miR-199a-5p overexpression in young mice led to upregulation of Chop mRNA levels, as compared to young Scr controls. In old mice, miR-199a-5p overexpression did not further elevate Chop mRNA levels and AM-199 had no effect on Chop mRNA levels (Figure 6.3.10). Consistently, CHOP protein levels were upregulated following miR-199a-5p overexpression in young and old mice, as compared to relevant controls (Figure 6.3.10).

Grp78 mRNA levels were elevated in young mice following miR-199a-5p overexpression, however GRP78 protein levels were not upregulated in young mice following miR-199a-5p overexpression (Figure 6.3.10). GRP78 protein levels were

however elevated following miR-199a-5p overexpression in old mice (Figure 6.3.10). Inhibition of miR-199a-5p did not regulate GRP78 mRNA or protein levels in young mice (Figure 6.3.10). ATF6 protein expression was significantly downregulated with miR-199a-5p treatment in young mice as compared to Scr controls. No changes in ATF6 protein expression were seen in old mice. To assess the IRE1 branch of the ER stress response, we looked at Xbp1 spliced (Xbp1s) which functions downstream of IRE1. No differences between treatment group and controls were observed in standard PCR for Xbp1, and further, no changes to mRNA expression of Xbp1 were demonstrated as assessed by RT-qPCR , although miR-199a-5p treated groups demonstrated noticeably increased expression as compared to Scr controls although this was not significant (Figure 6.3.10).

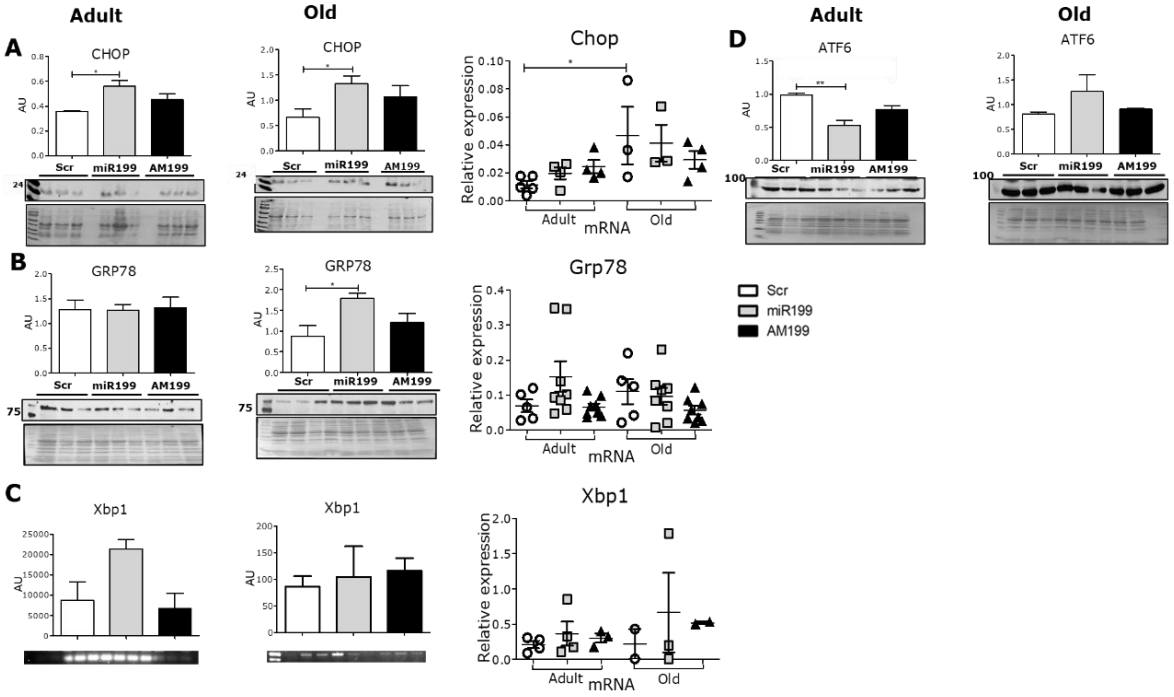

Figure 6.3.10. miR-199a-5p regulates some ER stress genes *in vivo*. Mice were treated with miR-199a-5p mimic, inhibitor, or Scr control. A) Overexpression of miR-199a-5p resulted in significant increase in protein expression of CHOP in both young and old mice compared to Scr controls. RT-qPCR showed miR-199a-5p upregulated Chop mRNA expression in old mice as compared to young mice. B) Treatment with miR-199a-5p led to no change in protein expression of GRP78 in young mice. In old mice, overexpression of miR-199a-5p resulted in increased GRP78 protein expression as compared to Scr controls. RT-qPCR demonstrated Grp78 mRNA expression was upregulated in young mice treated with miR-199a-5p as compared to Scr controls, although not significantly C) Xbp1s was not significantly altered by miR-199a-5p treatment in either young or old mice as quantified by PCR, although there was a trend increase in expression in miR-199a-5p treated groups. RT-qPCR showed no changes to Xbp1 mRNA expression with miR-199a-5p treatment. D) ER stress protein ATF6 expression was significantly downregulated with miR-199a-5p treatment in young mice as compared to Scr controls. Scr – antagomiR scrambled, miR-199– miR-199a-5p mimic; AM-199 – antagomiR to miR-199a-5pa-5p. Arbitrary units shown for Western blot (n=3) and PCR quantification, RT-qPCR/PCR (n=3-4); qPCR: expression relative to S29 is shown; n=(3-8). Scr – antagomiR scrambled, miR-199 – miR-199a-5p mimic; AM-199 – antagomiR to miR-199a-5p. Error bars show SEM; * - $p<0.05$; one-way ANOVA, Dunnett's post-test; (young mice ~5-months old; old mice ~23 months old).

6.3.5 miR-199a-5p does not regulate mitochondrial biogenesis but regulates autophagy *in vivo.*

The effects of miR-199a-5p overexpression or inhibition on mitochondrial proteins and genes were next investigated *in vivo* by western blot and RT-qPCR. Tom20 mitochondrial gene encoded by nuclear genome, showed no significant differences in protein expression as quantified by western blot, mRNA expression levels of Tom20 similarly showed no significant differences (Figure 6.3.11). Nrf2 (Nuclear factor erythroid 2-related factor 2) antioxidant transcription factor which has also been reported to be involved in mitochondrial biogenesis was also investigated (421,422). Inhibition of miR-199a-5p resulted in increased expression levels of Nrf2 mRNA in muscle of young and old (not significantly) mice, as compared to the relevant controls (Figure 6.3.11). Nrf2 protein levels were not consistently altered, however activated NRF2 is relocated into the nucleus, hence western blot on nuclear fraction would be needed to confirm a potential activation or deactivation of NRF2 by miR-199a-5p. However, the levels of Nd1 mRNA, a gene encoded by mitochondrial genome, were significantly downregulated in muscle of old mice as compared to young mice (Figure 6.3.11). Among miR-199a-5p predicted target genes are Pgc1-α which is associated with mitochondrial biogenesis (361). Surprisingly, in young mice, miR-199a-5p inhibition led to significantly lower mRNA expression of Pgc-1α as compared to Scr control. In old mice, no changes were observed with either miR-199a-5p overexpression or inhibition (Figure 6.3.11). A western blot analysis would be required to confirm the effects of miR-199a-5p on Pgc-1α activation.

As we had previously observed changes in autophagy markers with miR-199a-5p treatment in NSC-34 cells (5.3.4) miR-199a-5p regulates the expression of mitochondria-and-autophagy-associated genes in NSC-34 cells. We next aimed to determine the effect of miR-199a-5p *in vivo*. P62 is an adapter protein that is required for delivery of cargo to the autophagosome and is modulated by oxidative stress *via* Nrf2 (160). miR-199a-5p overexpression or inhibition in muscle of young mice did not have any effects on p62 protein expression, however miR-199a-5p overexpression in muscle of old mice led to decreased p62 protein levels; interestingly the levels of NRF2 protein were elevated in muscle of old mice treated with miR-199a-5p mimic, supporting the regulatory role of miR-199a-5p on regulating the p62:Nrf2 axis. LC3-II is a marker of autophagy and is associated with autophagic flux (332). Lc3b

mRNA expression was found to be lower in old mice overall as compared to young mice, although not significantly (Figure 6.3.12). RT-qPCR analysis of Lc3b mRNA demonstrated downregulation of Lc3b expression in young mice following miR-199a-5p inhibition and a trend towards upregulation in old mice following miR-199a-5p overexpression. Protein expression of LC3BII/I ratio demonstrated no significant differences in young mice, however old mice demonstrated significantly increased protein levels of LC3BII/I ratio (Figure 6.3.12).

ATG5 is an autophagy protein that is part of the ATG12 conjugation system and has key roles in autophagic vesicle formation (423). ATG5 protein levels were significantly lower with miR-199a-5p overexpression in young mice as compared to Scr controls. Old mice showed a similar trend in downregulation of ATG5 protein expression as compared to Scr controls although this was not significant (Figure 6.3.12). Together, these data suggest that miR-199a-5p may regulate autophagy. Mitophagy, a mitochondria-associated autophagy, could be downregulated as a result as well, which could potentially be associated with increased mitochondrial content, an effect of miR-199a-5p inhibition in muscle of old mice.

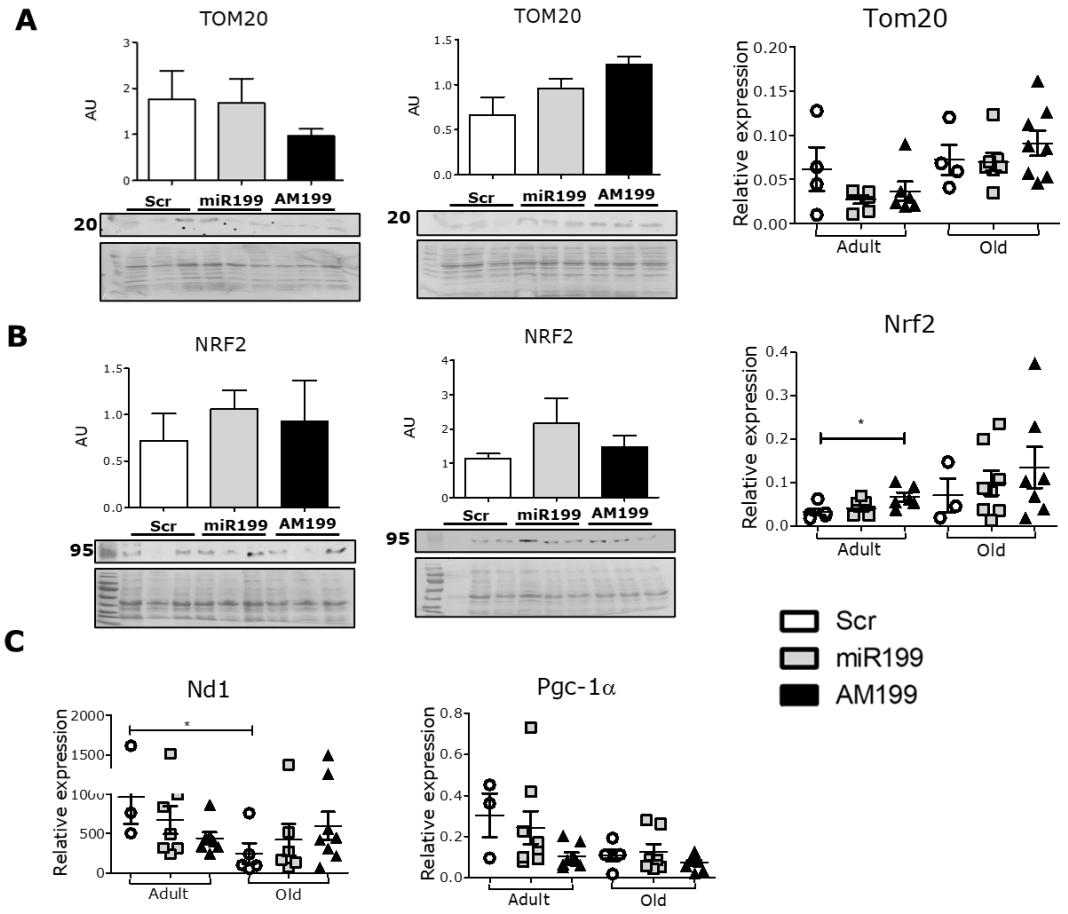

Figure 6.3.11. miR-199a-5p does not regulate the expression of mitochondrial-associated genes *in vivo*. Mice were treated with miR-199a-5p mimic, inhibitor, or Scr control, and TA muscles were isolated for western blot and RT-qPCR. A) Overexpression of miR-199a-5p resulted in no significant changes to protein expression of TOM20 as quantified by western blot. No changes to mRNA expression of Tom20 were observed by RT-qPCR. B) Overexpression of miR-199a-5p led to no significant changes in mRNA expression or protein expression of Nrf2 in young and old mice. C) miR-199a-5p inhibition led to significantly reduced mRNA expression of Nd1 in young mice but not old mice. Similarly, mRNA expression of Pgc-1α was significantly reduced with miR-199a-5p inhibition in young mice, however, this was not seen in old mice. Relative expression to S29. Scr – antagomiR scrambled, miR-199a-5p – miR-199a-5p mimic; AM-199 – antagomiR to miR-199a-5p. Error bars show SEM; * - $p<0.05$; one-way ANOVA, Dunnett's post-test; n=(8-10) (young mice ~5-months old; old mice ~23 months old).

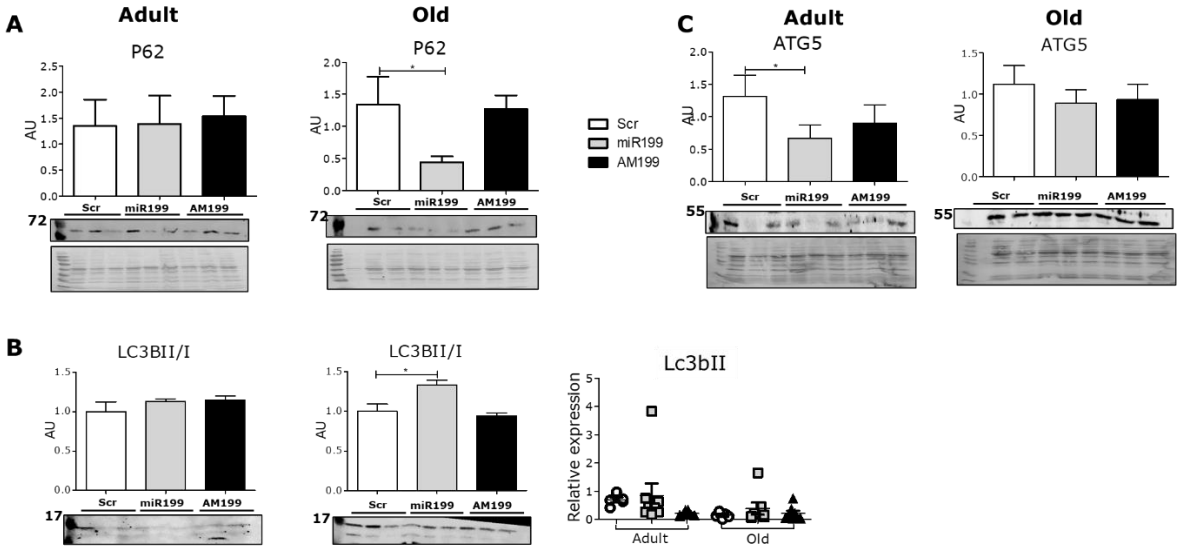

Figure 6.3.12. miR-199a-5p regulates the expression of autophagy-associated proteins *in vivo*. Mice were treated with miR-199a-5p mimic, inhibitor, or Scr control, and TA muscles were isolated for western blot. A) Overexpression of miR-199a-5p resulted in no significant changes to protein expression of p62 in young mice as quantified by Western blot. Inhibition of miR-199a-5p in old mice led to significantly increased protein expression of p62 as compared to miR-199a-5p overexpression as quantified by Western blot. B) Lc3bII was not significantly affected by miR overexpression or inhibition. C) ATG5 protein levels were significantly lower in young mice treated with miR-199a-5p as compared to Scr controls. Scr – antagomiR scrambled, miR-199a-5p – miR-199a-5p mimic; AM-199 – antagomiR to miR-199a-5p. Error bars show SEM; * - $p<0.05$; one-way ANOVA, Dunnett's post-test; Western blot n=3, qPCR n=(8-10) (young mice ~5-months old; old mice ~23 months old).

6.3.6 miR-199a-5p regulates the expression of GAP43 *in vivo.*

We next aimed to determine the effect of miR-199a-5p overexpression and inhibition on NMJ-related genes in muscle *in vivo*. Young and old mice were treated with miR-199a-5p mimic, AM-199, or Scr control and TA muscles were isolated and processed for RT-qPCR and/or western blotting. The expression of GAP43 mRNA showed no significant changes in either young or old mice following miR-199a-5p level regulation (Figure 6.3.13). However, overexpression of miR-199a-5p resulted in lower levels of GAP43 protein, and inhibition of miR-199a-5p resulted in higher levels of GAP43 protein in TA of young mice as compared to young Scr control (Figure 6.3.13). These effects were not observed in muscle of old mice. Relative mRNA expression of predicted miR-199a-5p, NMJ-associated target, Acvr2a was

significantly increased in old Scr control mice as compared to young Scr control mice (Figure 6.3.13). Another NMJ-associated predicted target gene, Hdac9, showed no significant changes to mRNA expression following miR treatment in young mice, a non-significant increase in expression was observed with AM-199 treatment. Old mice showed no significant differences between any group (Figure 6.3.13). Together these data suggest that miR-199a-5p is more effective in regulating NMJ-associated genes in muscle of young, but not old mice possibly due to other changes associated with ageing that may be altering these mechanics. This is consistent with observed phenotype of NMJ morphology, as we have shown overexpression of miR-199a-5p disturbs normal NMJ shape, and inhibition of miR-199a-5p appears to somewhat preserve the normal NMJ morphology (Figure 6.3.9). Further, as the inhibition of miR-199a-5p was associated with preservation of muscle force, yet we observed no considerable changes to muscle size and the changes seen in GAP43 expression, it makes sense the main driver behind these changes would be related to the NMJ.

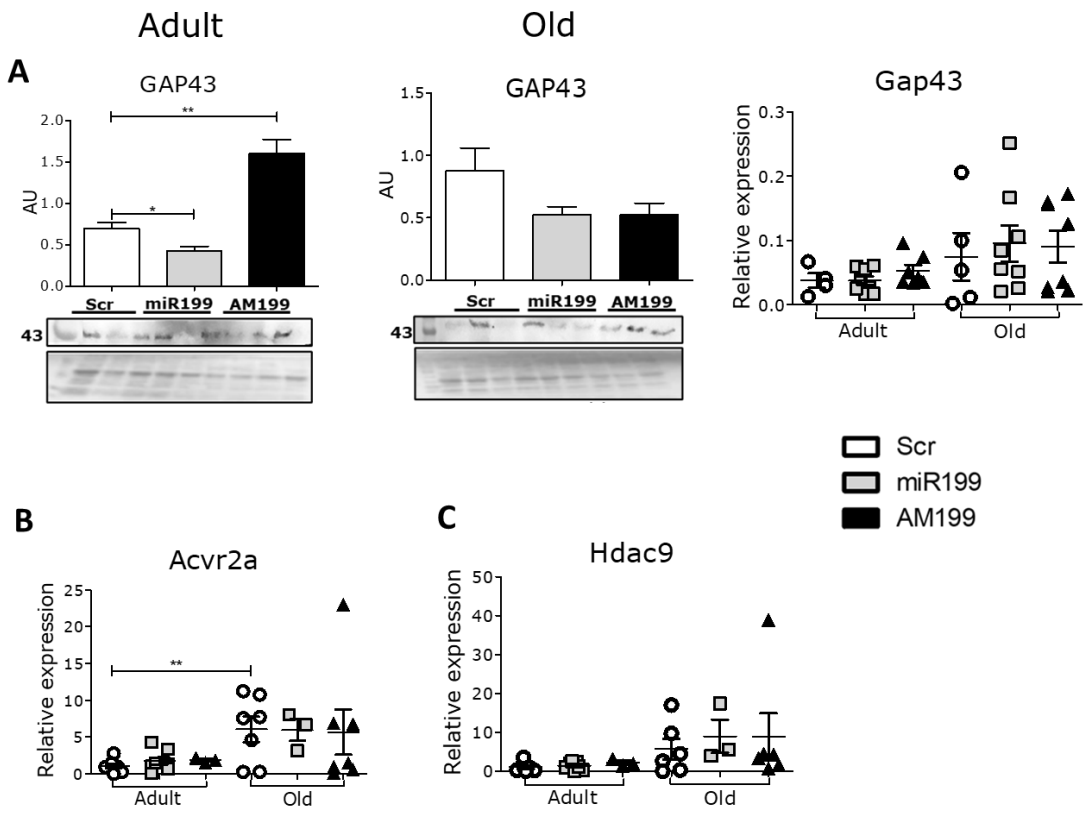

Figure 6.3.13. miR-199a-5p regulates the expression of GAP43 *in vivo*. Mice were treated with miR-199a-5p mimic, inhibitor, or Scr control, and TA muscles were isolated for western blot and RT-qPCR. A) Overexpression of miR-199a-5p resulted in significantly lowered protein expression of GAP43 in young mice, miR-199a-5p inhibition resulted in a significant increase in GAP43 protein expression as compared to Scr controls. No changes to mRNA expression of Gap43 were observed by RT-qPCR in either young or old mice, although a trend towards increase in Gap43 expression was observed with AM-199 in young mice as compared to Scr controls. B) miR-199a-5p overexpression or inhibition resulted in no changes to Acvr2a mRNA in young or old mice. Old mice showed significant increase in Acvr2z mRNA expression when compared to Scr controls. C) Relative mRNA expression of Hdac9 was not observed to be different between any of the groups in both young and old mice, although old mice overall showed higher levels of expression in all groups. Relative expression to S29. Scr – antagomiR scrambled, miR-199 – miR-199a-5p mimic; AM-199 – antagomiR to miR-199a-5p. Error bars show SEM; * - $p<0.05$; one-way ANOVA, Dunnett's post-test; Western blot n=(3), RT-qPCR n=(4-8), (young mice ~5-months old; old mice ~23 months old).

6.3.7 miR-199a-5p does not affect muscle regeneration *in vivo*.

As miR-199a-5p was upregulated in old human muscle (3.3.1), and in mice (3.3.4) and is predicted to regulate targets associated with muscle regeneration, we additionally utilised a $BaCl_2$ model of muscle injury to determine the effect of miR-199a-5p overexpression on mRNA expression of muscle regeneration specific targets *in vivo*. Our results demonstrated no significant change to gross muscle weight or bodyweight in either young or old mice (Figure 6.3.14). When muscle was compared as a ratio of total bodyweight, there were no significant differences observed in the QUAD, GAS, or TA muscle. EDL muscles showed significantly higher weights in AM-199 treated mice as compared to Scr controls when bodyweight was considered (Figure 6.3.15). Muscle size was also found to be unaffected by mir-199a-5p overexpression in young mice or miR-199a-5p inhibition in old mice during muscle regeneration (Figure 6.3.16).

Maximum force of the EDL muscle was found to not be affected by miR-199a-5p overexpression in young mice or inhibition in old mice (Figure 6.3.17). Specific force of the EDL was also not changed (Figure 6.3.17). This is not surprising given we had not observed any changes to muscle weights.

We also investigated the expression of predicted targets of miR-199a-5p that we found that were related to myogenesis (3.3.2). RT-qPCR results of predicted targets Acvr2b, Smarcd1, Jun, and Sirt1 showed no changes in mRNA expression in either young or old mice. Overexpression of miR-199a-5p did not affect mRNA expression with injury in any gene target investigated (Figure 6.3.18).

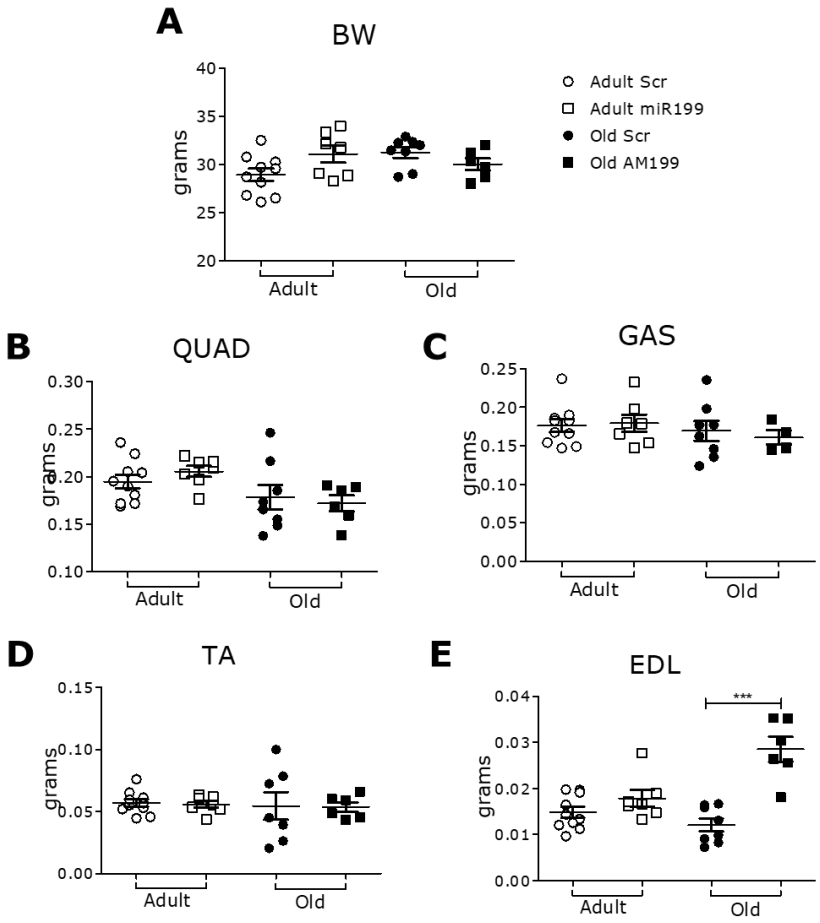

Figure 6.3.14. miR-199a-5p does not significantly affect bodyweight or muscle weight during regeneration. Young and old mice were injured in the right gastrocnemius with 1.2% $BaCl_2$ and then treated with miR-199a-5p mimic (young mice) or AM-199 (old mice). A) Bodyweight was not changed with miR overexpression. B) QUAD muscles were not affected. C) GAS muscle was found to be unchanged. D) TA muscle also showed no changes between groups. E) Muscle of the EDL was found to be significantly higher with miR-199a-5p inhibition in old mice. Scr – antagomiR scrambled, miR-199a-5p – miR-199a-5p mimic; AM-199 – antagomiR to miR-199a-5p. Error bars show SEM; * - $p<0.05$; Student's t-test; n=(6-10), (young mice ~6-months old; old mice ~24 months old).

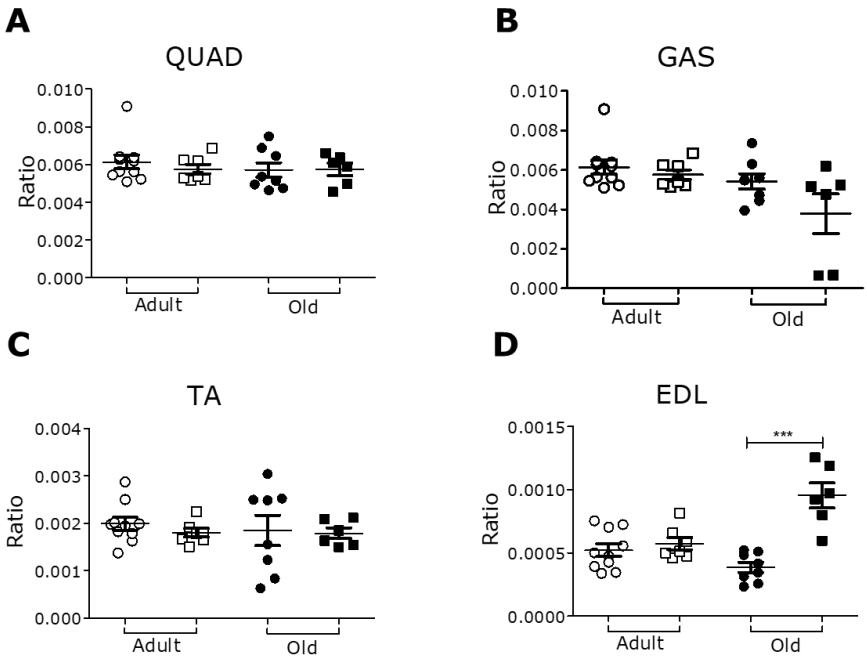

Figure 6.3.15. miR-199a-5p has a minimal effect on muscle weight *in vivo* during muscle regeneration when bodyweight is considered. Young and old mice were injured in the right gastrocnemius with 1.2% $BaCl_2$ and then treated with miR-199a-5p mimic (young mice) or AM-199 (old mice). A) QUAD muscles were not affected by miR-199a-5p during regeneration when bodyweight is considered. B) GAS muscle was found to be unchanged. C) TA muscle also showed no changes between groups. D) Muscle of the EDL was found to be significantly higher with miR-199a-5p inhibition in old mice when bodyweight is considered. Scr – antagomiR scrambled, miR-199a-5p – miR-199a-5p mimic; AM-199 – antagomiR to miR-199a-5p. Error bars show SEM; * - $p<0.05$; Student's t-test; n=(6-10), (young mice ~6-months old; old mice ~24 months old).

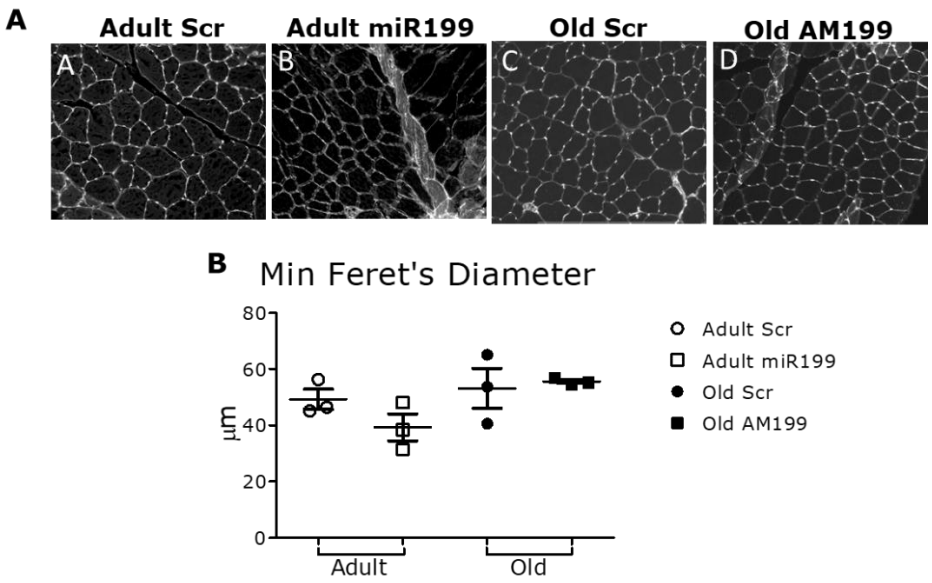

Figure 6.3.16. miR-199a-5p has no effect on myofibre size during muscle regeneration *in vivo*. Young mice were treated with miR-199a-5p mimic or Scr control, and old mice were treated with miR-199a-5p inhibitor or Scr control. A) WGA immunostaining of cross sections of TA muscle revealed that miR-199a-5p resulted in no significant changes to myofibre CSA as measured by B) minimal Feret's diameter during muscle regeneration. Scr – antagomiR scrambled, miR-199a-5p – miR-199a-5p mimic; AM-199 – antagomiR to miR-199a-5p. Error bars show SEM; * - $p<0.05$; one-way ANOVA, Dunnett's post-test; (young mice ~5-months old; old mice ~23 months old).

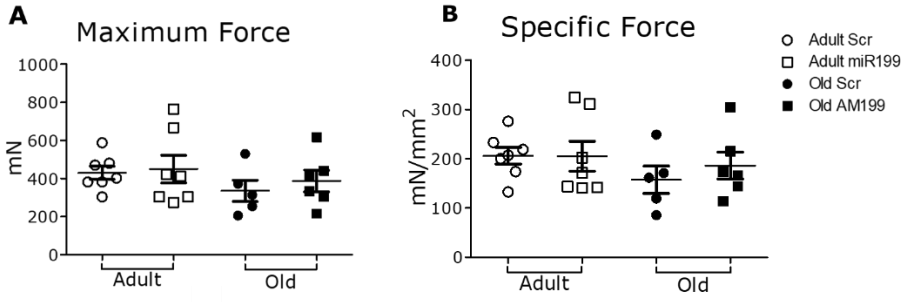

Figure 6.3.17. Maximum and specific forces were not affected by miR-199a-5p during muscle regeneration *in vivo*. Young and old mice were injured in the right gastrocnemius with 1.2% $BaCl_2$ and then treated with miR-199a-5p mimic (young mice) or AM-199 (old mice). A) Maximum forces were not affected by overexpression or inhibition of miR-199a-5p. B) Specific force of the EDL was also not affected by miR overexpression or inhibition. Scr – antagomiR scrambled, miR-199a-5p – miR-199a-5p mimic; AM-199 – antagomiR to miR-199a-5p. Error bars show SEM; * - $p<0.05$; Student's t-test; n=(6-10), (young mice ~6-months old; old mice ~24 months old).

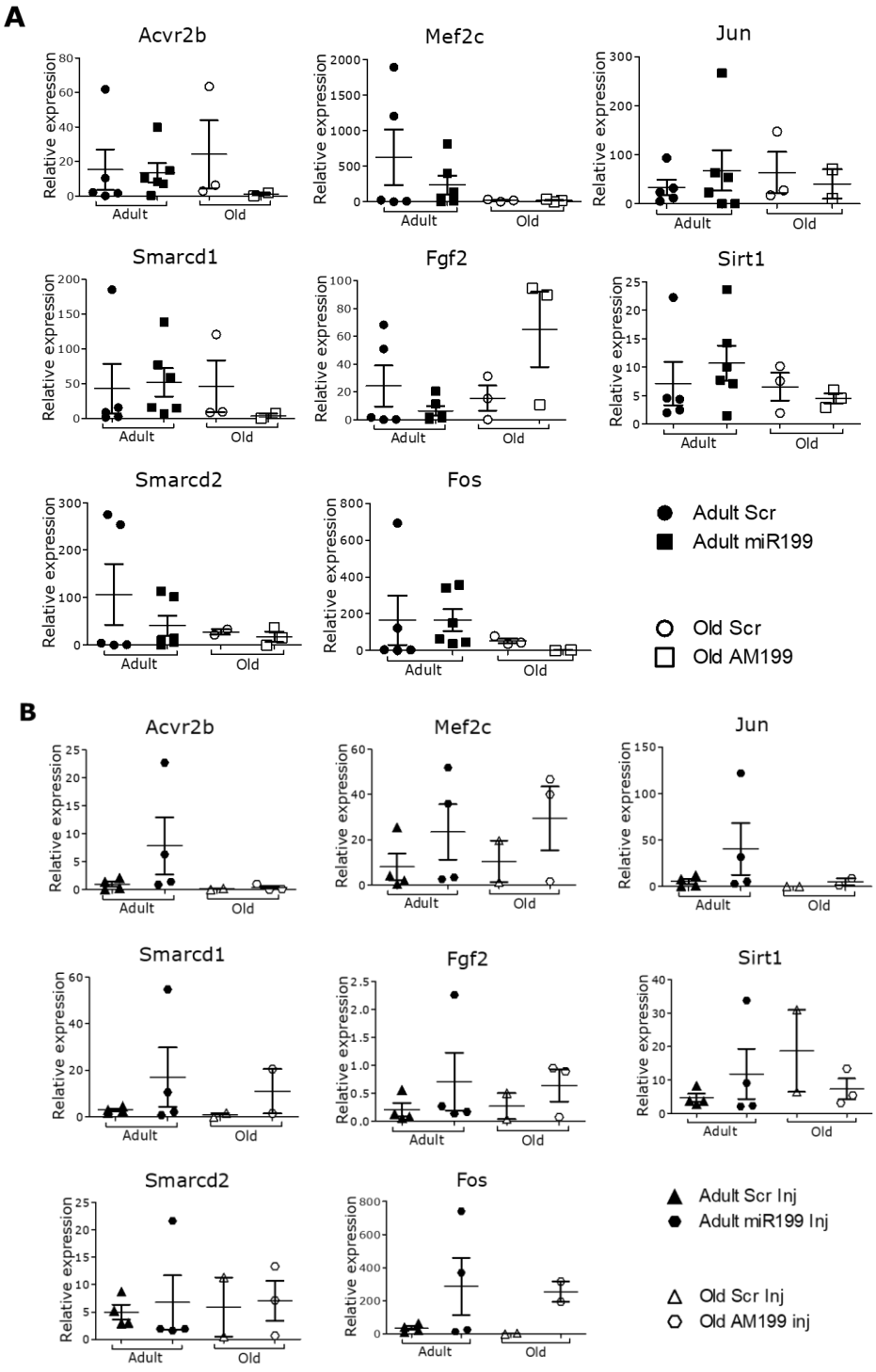

Figure 6.3.18. miR-199a-5pa-5p does not significantly affect muscle regeneration *in vivo*. A) Predicted targets of miR-199a-5p associated with muscle regeneration: Acvr2b, Smarcd1, Smarcd2, Jun, Sirt1, Mef2c, Fgf2, and Fos, showed no changes in mRNA expression with miR-199a-5p overexpression. B) No changes were seen in either young or old mice and the presence of injury did not significantly affect expression of any of the targets investigated. Relative expression to S29. Scr – antagomiR scrambled, miR-199 – miR-199a-5p mimic; AM-199 – antagomiR to miR-199a-5p. Error bars show SEM; * - $p<0.05$; one-way ANOVA, Dunnett's post-test; RT-qPCR n=(4-8), (young mice ~6-months old; old mice ~24 months old).

6.3.8 Age changes the expression of some NMJ-related genes *in vivo* in sciatic nerve.

As we had discovered NMJ-associated genes were altered with miR-199a-5p overexpression, and given the changes to the NMJ with ageing, we next wanted to determine the effect of ageing on the sciatic nerve in vivo, to investigate the effect on mRNA levels of previous gene targets previously examined in muscle and nerve cells in aged mice (4.3.6, 5.3.3). RT-qPCR of sciatic nerve samples showed miR-199a-5p overexpression in mice treated with miR-199a-5p mimic, and inhibition with mice treated with AM-199 in sciatic (Figure 6.3.19).

Sciatic nerves were taken from young and old mice and RT-qPCR was performed to determine mRNA expression changes of some of the selected genes we had previously investigated *in vitro* and *in vivo* that occur in aged mice. We looked at ER stress-related genes, Grp78, and Chop. The results showed no significant differences, although Chop expression higher in old mice sciatic nerve compared to young mice nerves (Figure 6.3.20). Mitochondria-associated genes showed no significant expression changes in old sciatic nerves compared to young sciatic nerves in Nrf2, CoxI, or Pgc-1α. The expression of NMJ related gene, Hdac9 in the sciatic nerve was significantly upregulated in old mice when compared to young mice (Figure 6.3.20). Other NMJ-related genes previously investigated, Acvr2a, and Gap43 showed non-significant increases in old mice sciatic nerves.

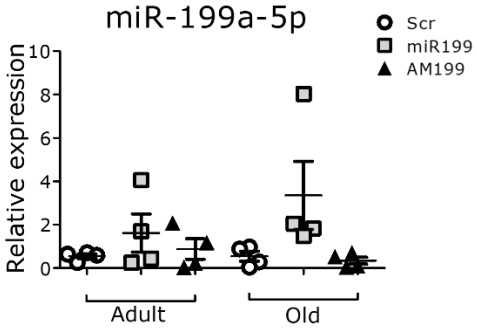

Figure 6.3.19. miR-199a-5p expression in sciatic nerve *in vivo*. Delivery of miRs in young and old mice did not result in increased expression of miR-199a-5p in the sciatic nerve as quantified by RT-qPCR. Relative expression to S29. Scr – antagomiR scrambled, miR-199a-5p – miR-199a-5p mimic; AM-199 – antagomiR to miR-199a-5p. Error bars show SEM; * - $p<0.05$; one-way ANOVA, Dunnett's post-test; RT-qPCR n=(4), (young mice ~5-months old; old mice ~23 months old).

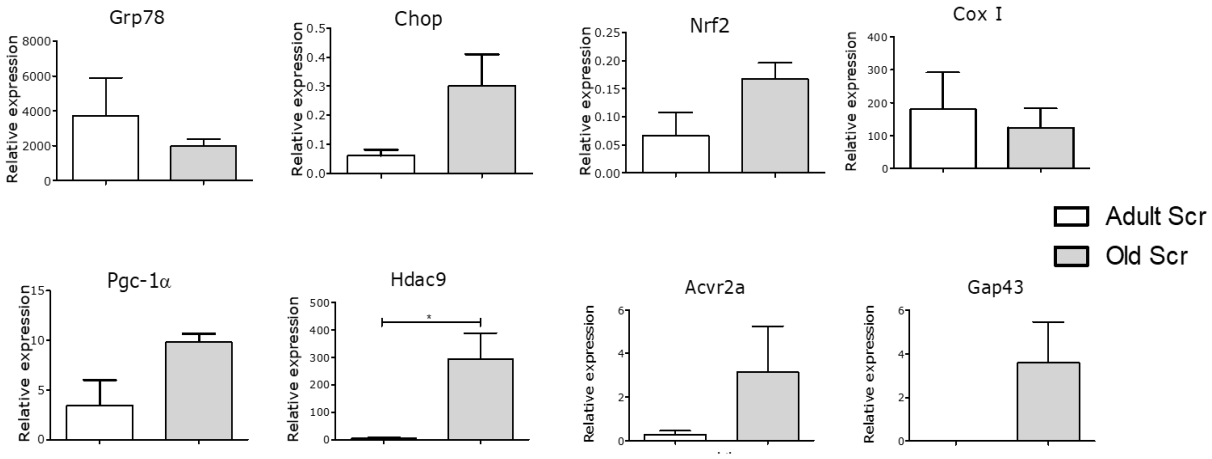

Figure 6.3.20. Age changes the expression of some NMJ-related genes *in vivo* in sciatic nerves. The sciatic nerves of young and old mice were processed for RT-qPCR and changes in expression demonstrated no changes to mRNA expression of Grp78, or Chop were observed although a non-significant increase in Chop expression was observed in old sciatic nerves. Mitochondrial-associated genes, Nrf2, CoxI, and Pgc-1α showed no significant changes in old nerves. Young mice showed significant changes in mRNA expression of Hdac9 in sciatic nerves of old mice compared to young sciatic nerves. Acvr2a and Gap43 showed non-significant increased expression in old sciatic nerves. Relative expression to S29. Error bars show SEM; * - $p<0.05$ Student's t-test, n=(3).

6.4 Discussion

The aim of this chapter was to examine the effect of miR-199a-5p on neuromuscular homeostasis during ageing *in vivo*. The effect of miR-199a-5p on skeletal muscle and neuromuscular interactions was assessed in young and old mice treated with miR-199a-5p mimic, AM-199 or Scr control. We had previously determined that miR-199a-5p is upregulated in ageing (Chapter 3), and in primary skeletal muscle cells. miR-199a-5p regulated the expression of ER stress-, NMJ-, and mitochondria-related genes. Since miR-199a-5p is increased in ageing and the increase of miR-199a-5p is associated with changes in NMJ morphology, ER stress and mitochondrial dysfunction, we aimed to validate the effect of miR-199a-5p in aged and young mice to provide pre-clinical evidence for potential therapeutic modulation of miR-199a-5p expression. We first aimed to treat the mice with miR mimic, and antagomiR, and we observed that overexpression of miR-199a-5p was significant in young mice (Figure 6.3.1), although inhibition of miR-199a-5p by AM199 was shown to be unsuccessful in significantly reducing the expression of miR-199a-5p. In old mice, we further

observed similarly, that AM199 treatment was insufficient to significantly reduce the expression of miR-199a-5p compared to old controls. These data therefore present a strong limitation to the *in vivo* results. Future optimisation of treatment doses and delivery will be required to elucidate an optimal dose for AM199 treatment.

6.4.1 miR-199a-5p had little effect on myofibre size *in vivo.*

The impact of miR-199a-5p on myofibre size was assessed *in vivo*, using young and old mice treated with miR-199a-5p mimic, AM-199, or Scr control. Our results demonstrated young muscles of the lower limbs, as well as overall bodyweight were not affected by miR-199a-5p overexpression, however this was different in old mice. Old mice showed a significant increase in bodyweight with miR-199a-5p overexpression when compared to Scr controls (Figure 6.3.2). QUAD muscles showed significantly lowered muscle weight in old mice compared to young mice (Figure 6.3.3). The QUAD and GAS muscles were also observed to be smaller in older Scr control mice compared to young Scr control mice, and the GAS was observed to be smaller in old mice treated with miR-199a-5p when the muscle was assessed as a ratio of total bodyweight (Figure 6.3.4).

There is little known about the role of miR-199a-5p in skeletal muscle, however it has been demonstrated to have a negative role in myogenesis in zebrafish, and it has been suggested this is accomplished in part through the WNT signalling pathway, a pathway with roles in satellite cell homeostasis (252). The increase in bodyweight with miR-199a-5p overexpression in old mice appears to conflict with the loss of muscle that was observed in old mice treated with miR-199a-5p mimics, however this may be due to increased adiposity in old mice contributing to overall greater body mass, however this was not tested in these animals. The accumulation of intramuscular fat mass with ageing has been previously observed and has been referred to and defined as ‘sarcopenic obesity’ and is characterised by increased body mass and decreased muscle mass (424). This could explain the reasoning for increased bodyweight, yet with smaller muscles seen in old mice.

The ageing process appears to have a significant impact overall on the muscle mass of GAS and QUAD, which both showed less muscle in old mice (Figure 6.3.4). This might also be accounted for by overall increase in mass seen with ageing that is not necessarily due to muscle weight. We hypothesised, miR-199a-5p inhibition would

have an effect on maintaining size compared to controls, although this was not significantly changed, and there may not have been a strong enough effect to fully preserve the muscle. As we observed AM199 efficiency to be not as strong particularly in old mice.

Analysis of the cross-sectional area of the muscle showed no significant changes in fibre size as quantified by minimal Feret's diameter (Figure 6.3.5). These data taken together with the decreases in muscle size that were observed suggest the muscle mass is overall not greatly reduced with miR-199a-5p overexpression in aged mice.

6.4.2 miR-199a-5p inhibition leads to increased specific and maximum EDL force *in vivo.*

We next looked at whether these changes seen in muscle mass would affect muscle force *in vivo*. Maximum force measurements showed decreased maximum force in old mice as compared to young mice (Figure 6.3.6). In old mice, miR-199a-5p inhibition resulted in significantly increased maximum force as compared to Scr controls (Figure 6.3.6). Specific EDL force measurements, which considers the cross-sectional area of the muscle, similarly showed a significant reduction in specific force in old mice as compared to young mice. (Figure 6.3.6). These data together suggests that miR-199a-5p inhibition preserves force of the muscle. When considering the effect of miR-199a-5p on NMJ morphology, we also observed a partial preservation of NMJ shape. These data in conjunction with the force data suggests potentially inhibition of miR-199a-5p preserves muscle force through preservation of the NMJ.

As mentioned, miR-199a-5p directly targets the Wnt pathway, and this has consequences on NMJ maintenance (425). Human NMJs in ageing are not yet well understood, although they are smaller and simpler than rodent NMJ, however it is believed that ageing results in shallower folds in the post-synapse and there is a loss of active zones along the motor axon terminal (426). Further, ageing skeletal muscle in rats have demonstrated age-related changes in NMJ stability (427). Old mice also have shown that preservation of the NMJ by IGF-1 administration to motor neurons resulted in larger, more intact, complex NMJs with significantly improved specific force compared to aged controls (428). Interestingly, the authors of this study also noted no changes to old muscle (EDL) size or weight, despite the observed functional improvements to force. These data suggest that NMJ stability plays a key role in

maintaining force capabilities in ageing. Our data shows inhibiting miR-199a-5p results in significant improvements to maximal and specific force. Further our data agrees with the lack of significantly altered muscle fibre size, yet with in an increase in force with miR-199a-5p inhibition. These collectively supports the idea miR-199a-5p disrupts the NMJ which leads to the negative effects seen in muscle force production seen with old age. This ultimately suggests overall miR-199a-5p may negatively affect muscle *via* nerve and NMJ dysregulation with ageing.

6.4.3 miR-199a-5p disrupts NMJ morphology *in vivo*

As we had established miR-199a-5p had effects on NMJ-specific genes *in vitro,* and we had seen increased force production with miR-199a-5p inhibition in old mice, we next wanted to determine the effect of miR-199a-5p on the NMJ *in vivo* in young and old mice. Longitudinal sections were taken of the TA muscle of young and old mice treated with miR-199a-5p, AM-199 or Scr control and acetylcholine receptor (α-Bungarotoxin), synaptic vesicle glycoprotein-2 (SV2) and neurofilament (2H3) proteins were stained to assess NMJ morphology. Overexpression of miR-199a-5p led to increased fragmentation of the NMJ in both young and old mice (Figure 6.3.7). The NMJ is traditionally described in mice as being pretzel-shaped, and the post-synaptic muscle membrane is characterised by extensive folding that extends into the sarcoplasm (364). The ageing rodent NMJ is characterised by morphological changes including post-synaptic site fragmentation, and decreased junctional folds, as well as reduced active zones and reduced AChR at the post-synaptic site (426). The aged NMJ begins to degenerate in ageing, and begins with axon thinning, non-specific sprouting that does not interface with the muscle, and appearance of ‘blebbing’ at the nerve terminal and axon. This ultimately leads to denervation and axon retraction (426). Our data show old mice and young mice both had instances of NMJ fragmentation, but miR-199a-5p treated mice showed increased instances of fragmentation and island formation at the NMJ (Figure 6.3.8) there was significantly more instances of abnormal NMJ with miR-199a-5p overexpression as compared to Scr controls (Figure 6.3.9). Fragmentation and morphological changes were also increased overall in old mice, although this was more apparent in miR-199a-5p treated NMJs.

The involvement of miR-199a-5p in neurodegeneration is documented (253,391,393); for example, miR-199a-5pa-5p has been implicated in the development of Alzheimer's disease by decreasing Neuritin, a synaptic maintenance neurotrophic factor (254). While our data only semi-quantifies the extent of the NMJ fragmentation, it demonstrates and agrees with our other data that suggests miR-199a-5p upregulation ultimately leads to NMJ instability which has negative effects on skeletal muscle. Our *in vivo* data shows miR-199a-5p inhibition increased maximum and specific force in older mice, and this would agree with the morphological changes that were observed in old mice treated with miR-199a-5p. While these changes agree with one another, we next wanted to determine the potential mechanisms behind these effects to determine what might be a driving factor behind these alterations.

6.4.4 miR-199a-5p may regulate the expression of genes associated with ER stress *in vivo*.

Our previous data in C2C12 (Figure 4.3.5, Figure 4.3.6) and NSC-34 cells (Figure 5.3.4) demonstrated miR-199a-5p regulated some ER-stress related proteins and genes. Expression of GRP78 protein was significantly increased in C2C12 and NSC-34 cells, and CHOP expression was elevated in C2C12 cells, and was significantly increased in NSC-34 cells. Therefore, we wanted to determine if miR-199a-5p would regulate ER-stress-related genes and proteins *in vivo* in young and old mice.

Our findings showed miR-199a-5p overexpression significantly increased protein expression levels of CHOP in both young and old mice as compared to Scr controls. Expression of Chop mRNA was significantly upregulated in miR-199a-5p treated young mice compared to Scr controls, Chop was also observed to be upregulated with age compared to young mice (Figure 6.3.10). Protein expression of GRP78 was not significantly changed with either miR-199a-5p overexpression or inhibition in young mice, however miR-199a-5p treated old mice showed moderately increased levels of GRP78 protein expression compared to Scr controls (Figure 6.3.10); increased Grp78 mRNA expression as compared to Scr controls, which is consistent with what we have observed in both C2C12 and NSC-34 cells. Old mice did not show any significant differences in Grp78 mRNA expression (Figure 6.3.10).

It has been suggested that the accumulation of misfolded proteins, and elevated ER stress, is an inevitable part of the ageing process (429), and it has further also been

demonstrated that age-related ER stress might not be directly responsible for anabolic resistance leading to sarcopenia in mice (430). Old mice have demonstrated elevated CHOP expression upon reloading after a period hindlimb unloading to mimic disuse atrophy (348). The authors of this study observed old mice to experience greater ER stress, lower force production, and higher expression of genes associated with NMJ denervation and inactivity, yet with no change to protein synthesis mechanics. They also noted increased expression of autophagy markers at baseline and upon reloading in old mice (348). Increased Chop and Grp78 is associated with activated PERK arm of the ER stress response and elevated CHOP is associated with inhibition of myogenic differentiation through repression of MyoD (354). The increased expression of CHOP has been associated with apoptosis of neurons and progression of neurodegeneration (270,431,432). Our data shows CHOP is upregulated with miR-199a-5p overexpression *in vivo* in both young and old mice. We have also demonstrated CHOP protein expression is upregulated with miR-199a-5p overexpression in NSC-34 cells (significantly) (Figure 5.3.4), and (Figure 4.3.5), together with what was observed in vivo, these data suggest miR-199a-5p overexpression activates the Chop pathway which could ultimately lead to apoptosis of motor neurons at the NMJ and further instability.

In our study, the reductions to muscle weight observed were not associated with smaller myofibres (Figure 6.3.5) .We also determined the effect of miR-199a-5p inhibition in old mice resulted in great force production as measured by maximum and specific force of the EDL. These data, taken into consideration with the data showing here that ER stress protein, CHOP, is upregulated with miR-199a-5p overexpression i*n vivo* indicates the negative effect on muscle of miR-199a-5p might be working on the motor neuron level by ER stress contributing to NMJ instability and degeneration. This instability at the NMJ could lead to denervation episodes and faulty reinnervation, which would contribute to defective muscle innervation and a potential exacerbation of sarcopenic changes. Interestingly, mitochondrial dysfunction is linked to ER stress and neurodegeneration (433). Furthermore, ageing mitochondria are associated with NMJ degeneration (359). Therefore, we wanted to determine the role of miR-199a-5p overexpression on mitochondria.

6.4.5 miR-199a-5p does not regulate mitochondrial biogenesis but regulates autophagy *in vivo*.

We next aimed to determine if the changes in expression of mitochondrial proteins and genes that were observed with miR-199a-5p overexpression *in vitro* (4.3.5, 5.3.4), would be also observed *in vivo*. We first looked at the effect of miR-199a-5p on TOM20, a mitochondrial membrane protein with a key role in protein transport (434), NRF2, a regulator of redox homeostasis with demonstrated effect on skeletal muscle (392), in young and old mice. Our results showed no significant changes in expression at protein level of TOM20, although in old mice, there was a noticeable trend increase towards upregulation in old mice treated with AM-199 (Figure 6.3.11); there were no differences between treatment groups in either young or old mice when assessing Tom20 mRNA levels. We next looked at *Nd1*, a gene involved in electron transport implicated in neurodegenerative and nerve diseases (282), and *Pgc-1α*, a key regulator of energy metabolism with roles in aged skeletal muscle and neurons (361,435,436) (Figure 6.3.11). Our results showed Nd1 mRNA expression was reduced although not significantly in young mice treated with AM-199 as compared to Scr control. Old mice showed significantly lower Nd1 mRNA expression as compared to young. In old mice, there was a significant upregulation in relative mRNA expression with miR-199a-5p inhibition as compared to Scr control. Similarly, mRNA expression of Pgc-1α also was significantly reduced with AM-199 treatment as compared to Scr controls in young mice, whereas old mice did not show any differences.

The results here overall indicated miR-199a-5p has different effects in young and old mice. Others have demonstrated Pgc-1α has a complex role in aged muscle. In transgenic mice overexpression of Pgc-1α resulted in less fatigable muscle in old age, but at the expense of decreased strength in the EDL. They also observed old mice overexpressing Pgc-1α had increased trabecular bone loss compared to old wild-type mice (435), which indicates a balance needed to maintain musculoskeletal homeostasis in ageing. Upregulation of Pgc-1α in neurons has also been shown to have a protective effect in NSC-34 cells and transgenic mice (436). We show here that miR-199a-5p overexpression did lower expression of both Nd1 and Pgc-1α mRNA expression compared to control although it was not significant. Aged mice have demonstrated lower expression of Pgc-1α compared to young mice (437), which agrees with our data.

As autophagy targets are predicted to be regulated by miR-199a-5p, we next looked at protein expression of autophagy protein, p62, which is the selective cargo carrier for autophagic degradation of misfolded proteins and is key to selective mitochondrial autophagy (mitophagy) (438). Our results showed p62 expression in young mice was not affected by miR-199a-5p overexpression or inhibition, however, old mice treated with AM-199 demonstrated increased mRNA expression of p62 as compared to miR-199a-5p overexpression (Figure 6.3.12). Increased p62 protein expression is generally associated with inhibition of autophagy (439). However, aberrant p62 expression is associated with neurodegenerative disease, and inhibition of p62 is associated with decreased mitophagy (440). Further, low expression levels of p62 protein have been demonstrated to lead to neuropathological changes (441). It has also been demonstrated loss of p62 function leads to neurodegeneration and an Alzheimer-and ALS-like phenotype (442). Taken along with our data, it appears miR-199a-5p does not directly regulate mitochondria directly but may participate in autophagic processes. We further observed in old mice increased LC3BII/I ratio in mice treated with miR-199a-5p, this data agrees with the data we observed in p62 protein levels, as, both p62, and LC3 are frequently used to measure autophagic flux, and reduced levels of p62 are associated with increased LC3BII/I expression (443). It is important to note LC3B does not necessarily indicate flux of autophagy but can indicate autophagic sequestration and/or inhibition of autophagosome clearance (444), therefore upregulated LC3BII/I could indicate increased presence of autophagosome formation; however, it does not necessarily indicate increased autophagy. However, we also observed in old mice significantly decreased expression of p62, which indicates induction of autophagy (443). The role of p62 is complex in neurodegeneration, but the absence of p62 has been observed in childhood-onset neurodegenerative disease patient fibroblasts and this has been linked to mitophagy. Further, zebrafish models of ALS have demonstrated p62 knockdown results in abnormal motor behaviour and abnormal motor neurons (445).

This however appears to occur differentially in old muscle compared to young muscle. This is not entirely surprising, as ageing brings along with it many dysregulated systems required for neuromuscular homeostasis such as abnormal mitophagy, accumulation of mitochondrial DNA damage and respiratory chain defect, metabolic disturbance, pro-apoptotic signalling, and oxidative stress (285), and

therefore more investigation is warranted to determine the specific changes that might be driving this; however, it could be that old adult muscle has much higher expression of miR-199a-5p and so miR-199a-5p overexpression in old mice elicits a less drastic effect.

6.4.6 miR-199a-5p regulates the expression of GAP43 *in vivo*.

We next looked at the effect of miR-199a-5p overexpression and inhibition on NMJ-related genes in muscle *in vivo*. The expression of neuronal regeneration protein GAP43 demonstrated significantly reduced protein expression in young mice overexpressing miR-199a-5p; a trend towards downregulation with miR-199a-5p overexpression was observed in old mice (Figure 6.3.13), further Gap43 mRNA expression levels demonstrated no changes in either young or old mice (Figure 6.3.13). These data agree with previous findings in cells that demonstrates inhibition of miR-199a-5p results in increased protein expression of GAP43 (Figure 4.3.11, Figure 5.3.5). Relative mRNA expression of predicted miR-199a-5p, NMJ-associated target, Acvr2a was observed to be significantly upregulated in old Scr mice as compared to Scr controls in young mice. Another NMJ-associated gene, Hdac9 showed no significant changes in young or old mice differences between any group, although it was observed that Hdac9 was upregulated overall compared to young mice (Figure 6.3.13).

In young mice, GAP43 protein expression, was increased with AM-199 treatment as compared to miR-199a-5p overexpression, although this effect was not seen in old mice. A similar trend was observed in Gap43 mRNA expression in young mice. AM-199 treated mice showed increased expression, although not significantly. As old mice have demonstrated to show increased instances of denervation and regeneration (298,426), it could be that the effect is much more pronounced in young mice. The expression of GAP43 has been shown to be critical to the stability and maintenance of axonal outgrowth *in vivo* especially after injury (446). Further it has been suggested that GAP43 may function alongside cytoskeletal proteins to maintain presynaptic structures (447). Given we have shown miR-199a-5p is associated with increased instances of NMJ morphological change as well as downregulation of GAP43 protein expression in young mice overexpressing miR-199a-5p, it is possible upregulated

miR-199a-5p with age increases NMJ instability by downregulating key synaptic and neuronal proteins.

We also shown increased mRNA expression of Acvr2a in old mice compared to young mice (Figure 6.3.13). We observed mRNA expression of Acvr2a to be upregulated in old mice. Dysregulation of the Wnt pathway also may inhibit Acvr2a signalling, and as miR-199a-5p is predicted to target Wnt signalling, miR-199a-5p may affect Acvr2a *via* dysregulated Wnt regulation (252,313). Hdac9 is associated with reinnervation (287), and is also linked to the canonical Wnt pathway (448). These data collectively suggest that miR-199a-5p overexpression reduces the expression of NMJ-associated possibly through altering Wnt signalling, the downstream effect of which is altered synaptic transmission and muscle weakness. Overall, these findings consistently show *in vivo*, young mice are much more sensitive to changes in miR expression than old mice. This is possibly due to the increased instances of homeostatic disruption throughout the body seen in old age that might therefore blunt these miR responses to fine-tuning genetic expression.

6.4.7 miR-199a-5p does not affect muscle regeneration *in vivo*.

As we had previously identified predicted targets associated with myogenesis (see 3.3), we used an in vivo model of muscle injury in young and old mice to determine the effect of miR-199a-5p overexpression or inhibition on the regeneration of skeletal muscle (GAS) in mice. We used miR-199a-5p overexpression to upregulate miR-199a-5p during muscle regeneration in young mice, and miR-199a-5p inhibitor (AM-199) in old mice to determine if inhibiting miR-199a-5p in old skeletal muscle would preserve muscle mass during regeneration.

Our results showed no significant differences with miR-199a-5p overexpression or inhibition on bodyweight muscle regeneration in either young or old mice (Figure 6.3.14), and further there were no changes to gross muscle weight (Figure 6.3.14). Increases in weight of muscle of the EDL as a ratio of total bodyweight in old mice was observed (Figure 6.3.15). We further observed no changes to myofibre size as quantified by minimum Feret's diameter of the cross-sectional area (Figure 6.3.16).

Finally, and as expected given there were no changes to muscle weight, there were no changes in maximum or specific force of the EDL (Figure 6.3.17). We also investigated mRNA expression levels of predicted myogenic targets of miR-199a-5p

(Figure 6.3.18). We observed no significant differences in any gene assessed. This in conjunction with muscle data suggests that miR-199a-5pa-5p may affect muscle *via* the nerve and/or neuronal components of the neuromuscular junction, as we have not observed any changes to myogenic specific targets *in vivo*.

6.4.8 Age changes the expression of some NMJ-related genes *in vivo* in sciatic nerves.

We had observed through bioinformatics () miR-199a-5p is upregulated during ageing. We also wanted to determine if ageing affected the gene expression of some of the genes we have previously studied *in vitro* and *in vivo*. ER stress-related genes, Grp78, and Chop. showed no significant differences, although Chop expression was somewhat increased in old mice compared to young mice (Figure 6.3.20). Mitochondria-associated genes, Nrf2, CoxI, or Pgc-1α, showed no significant expression changes in old sciatic nerves compared to young sciatic nerves. The expression of NMJ related gene, Hdac9 was significantly upregulated in old mice when compared to young mice (Figure 6.3.20). Other NMJ-related genes previously investigated, Acvr2a, and Gap43 showed non-significant increases in old sciatic nerves. These data show ageing increased the expression of Hdac9 significantly, and increased the expression of Chop, Nrf2, and Pgc-1α, although these were not significant increases. The increased of expression of genes in sciatic nerve during ageing has been studied and linked to the development of sarcopenia (449). Others have demonstrated upregulated Hdac9 is significant after injury in young mice, but this is not observed in old mice, however Hdac9 has also been shown to be elevated in uninjured older mice (450). Our results appear to agree with others that demonstrate increased expression of Hdac9 with age in the sciatic nerve.

Chapter 7 Discussion

7 Discussion

The overall findings of miR-199a-5p role in skeletal muscle and ageing demonstrated the following main conclusions:

- Upregulated miR-199a-5p in adult mice may result in increased ER stress *via* GRP78, and lower GAP43 levels, leading to a disrupted NMJ.
- Inhibition of miR-199a-5p ameliorated the effects of tunicamycin on myotubes *in vitro*.
- miR-199a-5p did not regulate muscle regeneration *in vivo*.
- Inhibition of miR-199a-5p potentially preserves the NMJ morphology which is key to muscle function, however the mechanism remains unresolved.
- Force improvements observed *in vivo* potentially due to preserved NMJ. (451)

We aimed to determine the effect of miR dysregulation on skeletal muscle in the context of sarcopenia. We hypothesised restoring levels of miRs to physiological levels would improve muscle mass and strength by re-balancing the activity of the molecular networks regulating muscle homeostasis. We performed small RNA-seq to determine differentially expressed miRs in ageing, and we selected miR-199a-5p as one of the miRs found to be upregulated in ageing, and we investigated miR-199a-5p *in vitro* and *in vivo.* First, miR-199a-5p was upregulated in ageing in both human myoblasts and mice muscle. Sarcopenia, and other age-related musculoskeletal disorders are believed to be influenced by dysregulation of miRs (82,290,414). As we had determined that miR-199a-5p was upregulated in ageing, we wanted to determine which potential targets of miR-199a-5p could be affected that would contribute towards sarcopenia. We therefore looked in muscle cells and neuron-like cells and determined neuronal protein GAP43 to be negatively regulated by miR-199a-5p. We performed luciferase assay and determined Gap43 to be a target of miR-199a-5p. Further, ER stress was predicated to be regulated by miR-199a-5p and we found upregulated ER stress marker GRP78 with miR-199a-5p overexpression, and in C2C12 cells, we further observed inhibition of miR-199a-5p protected myotubes against ER stress induced atrophy. We next looked at miR-199a-5p overexpression and inhibition *in vivo*, and we observed that while miR-199a-5p did not regulate muscle regeneration, overexpression resulted in disruptive morphological changes to the NMJ. Further, inhibition of miR-199a-5p preserved force of the EDL muscle.

Taken together, these data suggest miR-199a-5p is upregulated in ageing and may contribute to the progression of sarcopenia by disturbing the NMJ.

Sarcopenia is believed to be influenced by dysregulation of mitochondria (283–285), autophagy (452,453), the neuromuscular junction (303), and ER stress (347). Further, mitochondria, ER stress, and autophagy have all been shown to engage in extensive crosstalk during homeostasis and in the presence of disease, and thus examining them together would bring insight into miR-mediated muscle loss (278,405). Age-associated alterations in NMJ have been linked to dysregulation of mitochondrial autophagy, ER stress, and oxidative stress (325,359,363,365), which ultimately has been shown to lead to sarcopenia (89,286,303,454). (313)(266)(455)Assessing miR-199a-5p overexpression *in vitro,* (456)it would be next important to investigate this effect in humans, using primary human myoblasts to determine the effect of miR-199a-5p overexpression on fusion and myotube size. As we did not observe miR-199a-5p to regulate muscle regeneration *in vivo*, it would be important next to investigate miR-199a-5p in the context of other forms of regeneration, such as denervation-reinnervation. Defective reinnervation negatively impacts the health of the NMJ. (364)Alterations to NMJ morphology in other diseases, such as *mdx* mice, have been shown to be significantly weaker as measured by reduced muscle torque and increased neuromuscular transmission failure (457). In our study, we were unable to successfully visualise the nerve in some samples, however we did notice expected denervation present in old mice. Ageing is associated with continuous, progressive denervation and re-innervation at the NMJ (365), and therefore it could be miR-199a-5p upregulation in ageing negatively impacts these re-innervation episodes and prevents a full recapitulation of the NMJ following denervation. (346)

We observed NMJ morphological changes in addition to force changes. This suggests miR-199a-5p is expressed in neurons, so we investigated proteins associated with NMJ maintenance. As we determined miR-199a-5p targeted Gap43, upregulation of miR-199a-5p with ageing would therefore lead to downregulation of Gap43 which would agree with what we observed *in vitro* and *in vivo*. We did not observe changes in Gap43 expression at the mRNA level, this could be explained by the nature of miRs as a fine-tuning mechanisms of gene expression at the post-transcriptional level (250), and miR-responses can range from small changes in gene expression to regulation of networks, based on context (458), and thus it would not be surprising to

see much more subtle changes in mRNA expression and as we had determined that miR-199a-5p inhibition was less powerful in old mice, this would agree with the less drastic changes in mRNA expression observed in Gap43 *in vitro* and *in vivo*.

While dysregulated nerve sprouting and defective re-innervation following injury could explain some of the irregularities observed in NMJ morphology, it does not fully explain the fragmentation and loss of force. Future work in this would involve investigation into other NMJ-specific proteins such as Agrin, which is released by axon terminals and activates MuSK, which is crucial to each step in NMJ formation and maintenance in adulthood (459). Interestingly, Wnt receptors have been shown to activate MuSK, by binding at Frizzled-like domains, as miR-199a-5p is predicated to target both Wnt and FZD proteins, it will be necessary to determine if miR-199a-5p expression is associated with these NMJ proteins *in vivo*. It would also be beneficial to visualise the NMJ *in vivo* in Thy1-YFP mice which express yellow fluorescent protein (YFP) at high levels in motor neurons and can be used to precisely identify the NMJ and the presence or absence of denervation.

The presence of rampant ER stress has been implicated in ageing (348), and is associated as well with neurodegeneration and NMJ dysfunction (325,460,461). We had determined ER stress related genes were predicted to be regulated by miR-199a-5p, and we found (462)(347)upregulated GRP78 *in vitro* and *in vivo*, which is associated with increased ER stress (463), which would agree with upregulated CHOP protein that was observed. Evidence has shown that some miRs may upregulate gene expression and this has been shown in ER stress related to cancer, such as let-7e-5p, which has been shown to upregulate expression of GRP78 and CHOP in cancer cells (464). It could also be that miR-199a-5p is regulating some part of the PI3K/Akt pathway, which is an upstream regulator of GRP78 (465). We had observed through bioinformatics that miR-199a-5p is predicted to regulate transmembrane receptor protein tyrosine kinases (Figure 3.3.4), and these are key to the PI3K/Akt pathway (466). Therefore, it would be important to investigate the potential upstream regulators of Grp78. It is still unclear if ER stress is a contributing factor to the disruptions we observed at the NMJ or if it is a result of this disruption, and there exists a link between ER stress and NMJ function, therefore better understanding of the ER stress response with miR-199a-5p upregulation will be helpful in precisely determining the mechanism of NMJ abnormality that was observed.

It is believed the ER stress response is underpinned by mitochondria and autophagy crosstalk, (278). We had identified autophagy and mitochondria targets predicted to be regulated by miR-199a-5p (). In addition, mitochondria (355) and autophagy (467) dysfunction are linked to neurodegeneration and are associated with ageing and sarcopenia (284,468). *Pgc-1α* is known as the major regulator of mitochondrial biogenesis (361) and was predicted to be a target of miR-199a-5p, although we did not observe significant differences *in vitro* or *in vivo*. Recent evidence supports the role of Nrf2 in mitochondrial biogenesis and is associated with Pgc1-α (422), however despite noticing increased activity in the mitochondria in C2C12 cells, this does not necessarily mean mitochondrial biogenesis is improved (422), and we did not observe biogenesis to be altered. Future work requires assessment of(469) mitochondrial morphology as it has been demonstrated mitochondrial cristae are altered with age (73,470), it would be beneficial to utilise electron microscopy to visualise the mitochondria of young and old mice overexpressing miR-199a-5p to determine their morphological characteristics, as irregular mitochondria been associated with NMJ dysfunction (359). Autophagy is also highly associated with mitochondria (469), and further defective autophagy is recognised to play a role in the ER stress response (278). Impaired autophagy is also associated with degeneration of the NMJ (162). We noticed no significant changes to autophagy-related targets investigated *in vitro*, however *in vivo*, we observed autophagic carrier protein, p62, protein levels to be downregulated in old mice treated with miR-199a-5p overexpression, and LC3BII/I protein levels to be significantly upregulated with miR-199a-5p overexpression. This relationship is consistent with what has been observed in the literature, as decreased p62 would indicate increased autophagy *via* increased degradation of itself, and increased LC3BII/I conversion would indicate increased autophagosome production (443). This would indicate in our study that miR-199a-5p overexpression is increasing autophagy, however, despite p62/LC3 being used to determine autophagic flux, it is not possible to determine this based off protein expression levels as there is no ‘flux’ present (443). Further, it could be that increased LC3BII/I from miR-199a-5p overexpression may not necessarily mean increased autophagy but may indicate increased autophagosome formation without autophagic degradation. Future work would require utilising an autophagy flux assay to determine actual flux in autophagy as opposed to a singular point in time.

Interestingly, p62 has been shown to be required for neurodifferentiation, and is also involved in mitophagy, further irregular p62 expression has been associated with neurodegeneration (440). Downregulation of p62 has been demonstrated to hinder neuronal differentiation, as well as respiratory chain function and energy metabolism, thus linking p62 to mitochondria (471). Therefore, the next targets to investigate would be direct mitophagy effectors such as PINK1, BNIP3, and FUNDC1 (472).(472)(473)(389) Motor neuron death is associated with ER stress and stalled autophagy, so investigating these targets in the context of miR-199a-5p will help to better clarify the potential connection between the overexpression of this miR and the differences in ER stress and autophagy protein levels that we observed with miR-199a-5p manipulation *in vitro* and *in vivo.* It will be necessary to observe these effects within the context of the neuromuscular niche, and we would aim to determine if miR-199a-5p upregulation with age disturbs mitophagy, resulting in aberrant mitochondria, through dynamics, morphology, or mtDNA changes leading to NMJ dysfunction. It would be important determine if local NMJ mitochondria are affected, and whether they play an active role in denervation. Unfortunately, we did not have muscle samples with intact NMJ to further investigate this, however future work would be interesting to involve labelling of sections with Nav1.5 antibody, a marker of denervation (359), and investigate if miR-199a-5p upregulates denervation-responsive genes such as: MuSK involved in synapse formation (459), NCAM, involved in neuronal function and mediated by RTK/protein tyrosine kinases, (predicted pathway of miR-199a-5p; Figure 3.3.4), inhibitors of which affect neuronal growth (474), and RUNX1, involved in neuronal differentiation (475).

We did not observe miR-199a-5p inhibition to significantly improve muscle regeneration after injury in old mice. This was not unexpected given that we had observed little changes to muscle despite the significant changes we had observed *in vitro* with miR-199a-5p inhibition and in force production *in vivo*. Further, we observed no significant changes to mRNA expression of myogenic predicted targets of miR-199a-5p. We surmise the effect observed in muscle force increase would occur as a result of a preserved NMJ with miR-199a-5p inhibition. In summary, there is evidence that miR-199a-5p upregulation has a negative role in skeletal muscle, and that miR-199a-5p upregulation affects skeletal muscle differently in ageing. Although we observed muscle force preservation in ageing with miR-199a-5p inhibition, there

remains questions of underlying molecular pathways affected by this in ageing, and whether a miR199a-5p-based therapeutic would be beneficial in preserving muscle during ageing or other disorders associated with disrupted neuromuscular homeostasis. The ageing process is a multifactorial process involving multiple interlinking changes at the cellular level that manifest in physiological changes. The results presented here identify miR-199a-5p, whose expression is altered with age, as a key regulator of pathways directly involved in age-related skeletal muscle atrophy.

7.1 Strengths and weaknesses

The strengths in this work are the demonstration of upregulated miR-199a-5p in ageing, this was demonstrated in humans and in mice. Targets of miR-199a-5p include several that are implicated in sarcopenia such as mitochondria, and ER stress. The main limitation in this study was only female participants were used for muscle sample collection, and therefore it would be critical to assess male human primary myoblasts to further explore this topic. Further, in this study we only performed small-RNA seq on myoblasts and not the whole muscle, therefore, we would next aim to investigate this on whole muscle in females and males. The *in vitro* experiments demonstrated upregulated GRP78, which potentially involves miR-199a-5p in the PERK arm of the ER stress response and demonstrated inhibition of miR-199a-5p in the presence of tunicamycin-induced ER stress preserved myotube size. However, a serious limitation of this work is the efficacy of transfection, particularly the antagomiR in both *in vitro* and *in vivo* work. We used antagomiR to miR-199a-5p, however the levels of miR-199b-5p could still be present in cells. As these miRs have the same seed sequence, it could be that the AM-199 treatment was diluted. Further, the differentiation of the NSC-34 cells was poor, and therefore a better motor neuron model would be important to further understand the role of miR-199a-5p in motor neurons. Similar to in vivo data obtained, the transfection efficiency of AM199 in NSC-34 cells was also observed to be weaker compared to miR-199a-5p overexpression. Future work optimising the AM199 concentration *in vivo* will be needed to determine the optimal dosing concentrations to significantly affect miR-199a-5p inhibition.

In vivo, we found morphological changes with overexpression of miR-199a-5p, which potentially implicates its role in neuronal homeostasis. This idea is supported in part

by the reduction in GAP43 expression with miR-199a-5p treatment witnessed in adult mice. However, a limitation of this work was the lack of histological samples that were usable, as such, we were unable to fully visualise the nerve and therefore we were not able to fully determine denervation. Further, as observed *in vitro*, AM-199 treatment may have been diluted by presence of miR-199b-5p.

While this work demonstrates a potential role for miR-199a-5p in the development of sarcopenia, through upregulation during ageing and subsequent NMJ disruption, the role of miR-199a-5p in sarcopenia, and NMJ homeostasis requires further exploration to precisely determine mechanisms. Future work that would be critical next would be an assessment of mitophagy targets (*i.e.*, Pink1, Bnip3, and Fundc1), and mitochondrial dynamic regulators (*i.e.*, Fis1, Drp1, Opa1, and Mfn1/Mfn2) as we had observed inhibition of miR-199a-5p increased mitochondrial activity, although this does not mean necessarily increased biogenesis or function. It is key to understanding the role of miR-199a-5p in sarcopenia, as mitochondrial regulation is considered a hallmark of ageing (468).

As we had also determined Gap43 as a target of miR-199a-5p, it would next be important to further explore the NMJ as Gap43 is implicated in neurodegeneration (404). We next would aim to explore the localised area surrounding the NMJ to determine if there are specific effect localised to the NMJ, to assess this, it would be useful to utilise immunostaining of Gap43, and denervation markers such as neural cell adhesion molecule (NCAM) which has been used as a marker of denervation in skeletal muscle (476). Denervation is highly implicated in NMJ change with ageing, (298,425), and miRs control of NMJ and denervation-reinnervation of muscle is associated with sarcopenia pathogenesis (414). Better understanding the NMJ and the role of miR-199a-5p would further elucidate if this miR is able to contribute to sarcopenia. Presently, the remains much to be explained to determine if miR-199a-5p has a therapeutic role in the treatment of sarcopenia. There is evidence the NMJ is a key contributor to sarcopenia (477), and therefore controlling NMJ homeostasis could provide protection against denervation and muscle loss.

In conclusion, upregulated miR-199a-5p may contribute to the development of sarcopenia by altering the morphology of the NMJ, resulting in decreased force production capabilities. Additionally, upregulated miR-199a-5p associated with

ageing may drive ER stress which may further compromise the NMJ and subsequently contribute to the development and progression of sarcopenia, although more work is needed to precisely determine the role of miR-199a-5p in the development of sarcopenia, and whether this is a viable therapeutic target.

Chapter 8 References

8 References

1. Mukund K, Subramaniam S. Skeletal muscle: A review of molecular structure and function, in health and disease. Wiley Interdiscip Rev Syst Biol Med [Internet]. 2020 Jan 1 [cited 2021 Sep 21];12(1). Available from: /pmc/articles/PMC6916202/

2. Dave HD, Shook M, Varacallo M. Anatomy, Skeletal Muscle. StatPearls [Internet]. 2021 Sep 5 [cited 2022 Oct 7]; Available from: https://www.ncbi.nlm.nih.gov/books/NBK537236/

3. Argilés JM, Campos N, Lopez-Pedrosa JM, Rueda R, Rodriguez-Mañas L. Skeletal Muscle Regulates Metabolism via Interorgan Crosstalk: Roles in Health and Disease. J Am Med Dir Assoc. 2016 Sep 1;17(9):789–96.

4. Associate Degree Nursing Physiology Review [Internet]. [cited 2022 Nov 23]. Available from: https://www.austincc.edu/apreview/PhysText/Muscle.html

5. Tajsharghi H. Thick and Thin Filament Gene Mutations in Striated Muscle Diseases. Int J Mol Sci [Internet]. 2008 Jul [cited 2022 Nov 7];9(7):1259. Available from: /pmc/articles/PMC2635722/

6. Gao QQ, McNally EM. The Dystrophin Complex: structure, function and implications for therapy. Compr Physiol [Internet]. 2015 Jul 7 [cited 2023 Mar 10];5(3):1223. Available from: /pmc/articles/PMC4767260/

7. Salvage SC, Jackson AP, Huang CLH. Structure and Function of Skeletal Muscle. Encyclopedia of Bone Biology. 2019 Jan 1;34–49.

8. 10.2 Skeletal Muscle - Anatomy and Physiology 2e | OpenStax [Internet]. [cited 2022 Oct 7]. Available from: https://openstax.org/books/anatomy-and-physiology-2e/pages/10-2-skeletal-muscle

9. McCuller C, Jessu R, Callahan AL. Physiology, Skeletal Muscle. StatPearls [Internet]. 2022 Mar 25 [cited 2022 Nov 22]; Available from: https://www.ncbi.nlm.nih.gov/books/NBK537139/

10. Calderón JC, Bolaños P, Caputo C. The excitation–contraction coupling mechanism in skeletal muscle. Biophys Rev [Internet]. 2014 Mar [cited 2022 Oct 10];6(1):133. Available from: /pmc/articles/PMC5425715/

References

11. Slater CR. The Structure of Human Neuromuscular Junctions: Some Unanswered Molecular Questions. Int J Mol Sci [Internet]. 2017 Oct 19 [cited 2022 Nov 28];18(10). Available from: /pmc/articles/PMC5666864/

12. Neuromuscular junction: Parts, structure and steps | Kenhub [Internet]. [cited 2022 Nov 28]. Available from: https://www.kenhub.com/en/library/anatomy/the-neuromuscular-junction-structure-and-function

13. Omar A, Marwaha K, Bollu PC. Physiology, Neuromuscular Junction. StatPearls [Internet]. 2022 May 8 [cited 2022 Nov 25]; Available from: https://www.ncbi.nlm.nih.gov/books/NBK470413/

14. Purves D, Augustine GJ, Fitzpatrick D, Katz LC, LaMantia AS, McNamara JO, et al. Acetylcholine. 2001 [cited 2022 Nov 28]; Available from: https://www.ncbi.nlm.nih.gov/books/NBK11143/

15. Normal neuromuscular junction [Internet]. [cited 2022 Nov 28]. Available from: https://ykhoa.org/d/image.htm?imageKey=NEURO/62694

16. Talbot J, Maves L. Skeletal muscle fiber type: using insights from muscle developmental biology to dissect targets for susceptibility and resistance to muscle disease. Wiley Interdiscip Rev Dev Biol [Internet]. 2016 Jul 1 [cited 2022 Oct 10];5(4):518. Available from: /pmc/articles/PMC5180455/

17. Weiss A, McDonough D, Wertman B, Acakpo-Satchivi L, Montgomery K, Kucherlapati R, et al. Organization of human and mouse skeletal myosin heavy chain gene clusters is highly conserved. Proc Natl Acad Sci U S A [Internet]. 1999 Mar 16 [cited 2022 Nov 28];96(6):2958–63. Available from: https://www.pnas.org/doi/abs/10.1073/pnas.96.6.2958

18. Brzeska H, Korn ED. Regulation of class I and class II myosins by heavy chain phosphorylation. Journal of Biological Chemistry [Internet]. 1996 Jul 19 [cited 2022 Nov 28];271(29):16983–6. Available from: http://www.jbc.org/article/S0021925818312833/fulltext

19. Schiaffino S, Reggiani C. Myosin isoforms in mammalian skeletal muscle. J Appl Physiol (1985) [Internet]. 1994 [cited 2022 Nov 28];77(2):493–501. Available from: https://pubmed.ncbi.nlm.nih.gov/8002492/

20. Harrison BC, Allen DL, Leinwand LA. IIb or not IIb? Regulation of myosin heavy chain gene expression in mice and men. Skelet Muscle [Internet]. 2011 Feb 1 [cited 2022 Nov 28];1(1):1–9. Available from: https://link.springer.com/articles/10.1186/2044-5040-1-5

21. Tajsharghi H, Darin N, Rekabdar E, Kyllerman M, Wahlström J, Martinsson T, et al. Mutations and sequence variation in the human myosin heavy chain IIa gene (MYH2). European Journal of Human Genetics 2005 13:5 [Internet]. 2005 Mar 2 [cited 2022 Nov 29];13(5):617–22. Available from: https://www.nature.com/articles/5201375

22. Pegoraro E, Gavassini BF, Borsato C, Melacini P, Vianello A, Stramare R, et al. MYH7 gene mutation in myosin storage myopathy and scapulo-peroneal myopathy. Neuromuscular Disorders. 2007 Apr;17(4):321–9.

23. Melkonian EA, Schury MP. Biochemistry, Anaerobic Glycolysis. StatPearls [Internet]. 2022 Aug 8 [cited 2022 Nov 29]; Available from: https://www.ncbi.nlm.nih.gov/books/NBK546695/

24. Scott W, Stevens J, Binder-Macleod SA. Human Skeletal Muscle Fiber Type Classifications. Phys Ther [Internet]. 2001 Nov 1 [cited 2022 Nov 29];81(11):1810–6. Available from: https://academic.oup.com/ptj/article/81/11/1810/2857618

25. Dunn J, Grider MH. Physiology, Adenosine Triphosphate. StatPearls [Internet]. 2022 Feb 17 [cited 2022 Nov 29]; Available from: https://www.ncbi.nlm.nih.gov/books/NBK553175/

26. Polla B, D'Antona G, Bottinelli R, Reggiani C. Respiratory muscle fibres: specialisation and plasticity. Thorax [Internet]. 2004 Sep 1 [cited 2022 Oct 10];59(9):808–17. Available from: https://thorax.bmj.com/content/59/9/808

27. Motor Units and Muscle Receptors (Section 3, Chapter 1) Neuroscience Online: An Electronic Textbook for the Neurosciences | Department of

Neurobiology and Anatomy - The University of Texas Medical School at Houston [Internet]. [cited 2022 Nov 29]. Available from: https://nba.uth.tmc.edu/neuroscience/m/s3/chapter01.html

28. Ørtenblad N, Nielsen J, Boushel R, Söderlund K, Saltin B, Holmberg HC. The muscle fiber profiles, mitochondrial content, and enzyme activities of the exceptionally well-trained arm and leg muscles of elite cross-country skiers. Front Physiol. 2018 Aug 2;9(AUG):1031.

29. Romero NB, Mezmezian M, Fidziańska A. Main steps of skeletal muscle development in the human: Morphological analysis and ultrastructural characteristics of developing human muscle. Handb Clin Neurol. 2013 Jan 1;113:1299–310.

30. Sambasivan R, Tajbakhsh S. Skeletal muscle stem cell birth and properties. Semin Cell Dev Biol. 2007 Dec 1;18(6):870–82.

31. Kim JH, Jin P, Duan R, Chen EH. Mechanisms of myoblast fusion during muscle development. Curr Opin Genet Dev [Internet]. 2015 Jun 1 [cited 2022 Oct 11];32:162. Available from: /pmc/articles/PMC4508005/

32. Lehka L, Rędowicz MJ. Mechanisms regulating myoblast fusion: A multilevel interplay. Semin Cell Dev Biol. 2020 Aug 1;104:81–92.

33. Soares RJ, Cagnin S, Chemello F, Silvestrin M, Musaro A, de Pitta C, et al. Involvement of microRNAs in the regulation of muscle wasting during catabolic conditions. J Biol Chem [Internet]. 2014 Aug 8 [cited 2018 Dec 12];289(32):21909–25. Available from: http://www.ncbi.nlm.nih.gov/pubmed/24891504

34. Drummond MJ, McCarthy JJ, Sinha M, Spratt HM, Volpi E, Esser KA, et al. Aging and microRNA expression in human skeletal muscle: a microarray and bioinformatics analysis. Physiol Genomics [Internet]. 2011 May 1 [cited 2018 Sep 13];43(10):595–603. Available from: http://www.ncbi.nlm.nih.gov/pubmed/20876843

35. Ali S, Garcia JM. Sarcopenia, cachexia and aging: diagnosis, mechanisms and therapeutic options - a mini-review. Gerontology [Internet]. 2014 [cited 2018

Sep 10];60(4):294–305. Available from: http://www.ncbi.nlm.nih.gov/pubmed/24731978

36. Sakuma K, Aoi W, Yamaguchi A. Molecular mechanism of sarcopenia and cachexia: recent research advances. Pflugers Arch [Internet]. 2017 Jun 19 [cited 2018 Sep 10];469(5–6):573–91. Available from: http://link.springer.com/10.1007/s00424-016-1933-3

37. Liang R, Rimmelé P, Bigarella CL, Yalcin S, Ghaffari S. Evidence for AKT-independent regulation of FOXO1 and FOXO3 in haematopoietic stem and progenitor cells. Cell Cycle [Internet]. 2016 Mar 18 [cited 2023 Mar 13];15(6):861. Available from: /pmc/articles/PMC4845935/

38. Eijkelenboom A, Burgering BMT. FOXOs: signalling integrators for homeostasis maintenance. Nature Reviews Molecular Cell Biology 2013 14:2 [Internet]. 2013 Jan 17 [cited 2023 Mar 13];14(2):83–97. Available from: https://www.nature.com/articles/nrm3507

39. Sandri M, Barberi L, Bijlsma AY, Blaauw B, Dyar KA, Milan G, et al. Signalling pathways regulating muscle mass in ageing skeletal muscle. The role of the IGF1-Akt-mTOR-FoxO pathway. Biogerontology [Internet]. 2013 Jun 19 [cited 2018 Sep 11];14(3):303–23. Available from: http://link.springer.com/10.1007/s10522-013-9432-9

40. Scicchitano BM, Dobrowolny G, Sica G, Musarò A. Molecular Insights into Muscle Homeostasis, Atrophy and Wasting. Curr Genomics [Internet]. 2018 Jan 1 [cited 2022 Oct 11];19(5):356. Available from: /pmc/articles/PMC6030854/

41. Yoshida T, Delafontaine P. Mechanisms of IGF-1-Mediated Regulation of Skeletal Muscle Hypertrophy and Atrophy. Cells 2020, Vol 9, Page 1970 [Internet]. 2020 Aug 26 [cited 2022 Nov 29];9(9):1970. Available from: https://www.mdpi.com/2073-4409/9/9/1970/htm

42. Sakellariou GK, Lightfoot AP, Earl KE, Stofanko M, McDonagh B. Redox homeostasis and age-related deficits in neuromuscular integrity and function. J Cachexia Sarcopenia Muscle [Internet]. 2017 Dec 1 [cited 2022 Jul 7];8(6):881. Available from: /pmc/articles/PMC5700439/

43. Altun M, Besche HC, Overkleeft HS, Piccirillo R, Edelmann MJ, Kessler BM, et al. Muscle wasting in aged, sarcopenic rats is associated with enhanced activity of the ubiquitin proteasome pathway. J Biol Chem [Internet]. 2010 Dec 17 [cited 2022 Oct 11];285(51):39597–608. Available from: https://pubmed.ncbi.nlm.nih.gov/20940294/

44. Thoma A, Lightfoot AP. NF-kB and Inflammatory Cytokine Signalling: Role in Skeletal Muscle Atrophy. Adv Exp Med Biol [Internet]. 2018 [cited 2022 Oct 11];1088:267–79. Available from: https://pubmed.ncbi.nlm.nih.gov/30390256/

45. Rybalka E, Timpani CA, Debruin DA, Bagaric RM, Campelj DG, Hayes A. The Failed Clinical Story of Myostatin Inhibitors against Duchenne Muscular Dystrophy: Exploring the Biology behind the Battle. Cells [Internet]. 2020 Dec 10 [cited 2020 Dec 11];9(12):2657. Available from: https://www.mdpi.com/2073-4409/9/12/2657

46. Scimeca M, Piccirilli E, Mastrangeli F, Rao C, Feola M, Orlandi A, et al. Bone Morphogenetic Proteins and myostatin pathways: Key mediator of human sarcopenia. J Transl Med. 2017 Feb 15;15(1).

47. Masiero E, Sandri M. Autophagy inhibition induces atrophy and myopathy in adult skeletal muscles. Autophagy [Internet]. 2010 Feb 16 [cited 2022 Oct 11];6(2):307–9. Available from: https://pubmed.ncbi.nlm.nih.gov/20104028/

48. Grumati P, Bonaldo P. Autophagy in Skeletal Muscle Homeostasis and in Muscular Dystrophies. Cells 2012, Vol 1, Pages 325-345 [Internet]. 2012 Jul 26 [cited 2022 Dec 1];1(3):325–45. Available from: https://www.mdpi.com/2073-4409/1/3/325/htm

49. Li P, Ma Y, Yu C, Wu S, Wang K, Yi H, et al. Autophagy and Aging: Roles in Skeletal Muscle, Eye, Brain and Hepatic Tissue. Front Cell Dev Biol [Internet]. 2021 Oct 28 [cited 2022 Dec 1];9:752962. Available from: /pmc/articles/PMC8581214/

50. Xia Q, Huang X, Huang J, Zheng Y, March ME, Li J, et al. The Role of Autophagy in Skeletal Muscle Diseases. Front Physiol. 2021 Mar 25;12:291.

51. Wohlgemuth SE, Seo AY, Marzetti E, Lees HA, Leeuwenburgh C. Skeletal muscle autophagy and apoptosis during aging: effects of calorie restriction and life-long exercise. Exp Gerontol [Internet]. 2010 Feb [cited 2018 Sep 13];45(2):138–48. Available from: http://www.ncbi.nlm.nih.gov/pubmed/19903516

52. McCarthy JJ, Esser KA. Anabolic and catabolic pathways regulating skeletal muscle mass. Curr Opin Clin Nutr Metab Care [Internet]. 2010 [cited 2022 Oct 11];13(3):230. Available from: /pmc/articles/PMC2877703/

53. Hain BA, Narasimhan A, Ballinger TJ, Guise TA, Waning DL. Cancer-associated muscle dysfunction. Encyclopedia of Bone Biology. 2020 Jun 26;379–89.

54. Xu M, Chen X, Chen D, Yu B, Huang Z. FoxO1: a novel insight into its molecular mechanisms in the regulation of skeletal muscle differentiation and fiber type specification. Oncotarget [Internet]. 2017 Feb 2 [cited 2023 Mar 13];8(6):10662. Available from: /pmc/articles/PMC5354690/

55. Yoon MS. mTOR as a Key Regulator in Maintaining Skeletal Muscle Mass. Front Physiol [Internet]. 2017 [cited 2018 Sep 11];8:788. Available from: http://www.ncbi.nlm.nih.gov/pubmed/29089899

56. Walston JD. Sarcopenia in older adults. Curr Opin Rheumatol [Internet]. 2012 Nov [cited 2019 Jan 17];24(6):623–7. Available from: http://www.ncbi.nlm.nih.gov/pubmed/22955023

57. Kim Y, Triolo M, Hood DA. Impact of Aging and Exercise on Mitochondrial Quality Control in Skeletal Muscle. Oxid Med Cell Longev. 2017;2017.

58. Ziaaldini MM, Marzetti E, Picca A, Murlasits Z. Biochemical Pathways of Sarcopenia and Their Modulation by Physical Exercise: A Narrative Review. Front Med (Lausanne) [Internet]. 2017 Oct 4 [cited 2019 May 22];4:167. Available from: http://journal.frontiersin.org/article/10.3389/fmed.2017.00167/full

59. Kalyani RR, Corriere M, Ferrucci L. Age-related and disease-related muscle loss: the effect of diabetes, obesity, and other diseases. Lancet Diabetes

Endocrinol [Internet]. 2014 Oct [cited 2018 Sep 10];2(10):819–29. Available from: http://www.ncbi.nlm.nih.gov/pubmed/24731660

60. Schiaffino S, Dyar KA, Ciciliot S, Blaauw B, Sandri M. Mechanisms regulating skeletal muscle growth and atrophy. FEBS J [Internet]. 2013 Sep 1 [cited 2022 Oct 11];280(17):4294–314. Available from: https://onlinelibrary.wiley.com/doi/full/10.1111/febs.12253

61. Kitajima Y, Yoshioka K, Suzuki N. The ubiquitin-proteasome system in regulation of the skeletal muscle homeostasis and atrophy: From basic science to disorders. Journal of Physiological Sciences [Internet]. 2020 Sep 16 [cited 2022 Nov 30];70(1):1–12. Available from: https://jps.biomedcentral.com/articles/10.1186/s12576-020-00768-9

62. Yang W, Hu P. Skeletal muscle regeneration is modulated by inflammation. J Orthop Translat [Internet]. 2018 Apr 1 [cited 2022 Oct 11];13:25. Available from: /pmc/articles/PMC5892385/

63. Morgan J, Partridge T. Skeletal muscle in health and disease. Dis Model Mech [Internet]. 2020 Feb 1 [cited 2020 Feb 13];13(2):dmm042192. Available from: http://dmm.biologists.org/lookup/doi/10.1242/dmm.042192

64. Fu X, Wang H, Hu P. Stem cell activation in skeletal muscle regeneration. Cellular and Molecular Life Sciences [Internet]. 2015 May 1 [cited 2022 Dec 1];72(9):1663. Available from: /pmc/articles/PMC4412728/

65. Laumonier T, Menetrey J. Muscle injuries and strategies for improving their repair. Journal of Experimental Orthopaedics 2016 3:1 [Internet]. 2016 Jul 22 [cited 2022 Oct 17];3(1):1–9. Available from: https://link.springer.com/articles/10.1186/s40634-016-0051-7

66. Ruffell D, Mourkioti F, Gambardella A, Kirstetter P, Lopez RG, Rosenthal N, et al. A CREB-C/EBPβ cascade induces M2 macrophage-specific gene expression and promotes muscle injury repair. Proc Natl Acad Sci U S A [Internet]. 2009 Oct 10 [cited 2023 Mar 13];106(41):17475. Available from: /pmc/articles/PMC2762675/

67. Fukada S ichiro, Higashimoto T, Kaneshige A. Differences in muscle satellite cell dynamics during muscle hypertrophy and regeneration. Skelet Muscle [Internet]. 2022 Dec 1 [cited 2022 Dec 1];12(1):1–10. Available from: https://skeletalmusclejournal.biomedcentral.com/articles/10.1186/s13395-022-00300-0

68. Kaczmarek A, Kaczmarek M, Ciałowicz M, Clemente FM, Wolański P, Badicu G, et al. The Role of Satellite Cells in Skeletal Muscle Regeneration—The Effect of Exercise and Age. Biology (Basel) [Internet]. 2021 Oct 1 [cited 2022 Dec 1];10(10). Available from: /pmc/articles/PMC8533525/

69. Forcina L, Cosentino M, Musarò A. Mechanisms Regulating Muscle Regeneration: Insights into the Interrelated and Time-Dependent Phases of Tissue Healing. Cells [Internet]. 2020 May 22 [cited 2022 Dec 1];9(5). Available from: /pmc/articles/PMC7290814/

70. Wong A, Garcia SM, Tamaki S, Striedinger K, Barruet E, Hansen SL, et al. Satellite cell activation and retention of muscle regenerative potential after long-term denervation. Stem Cells [Internet]. 2021 Mar 1 [cited 2022 Oct 11];39(3):331–44. Available from: https://onlinelibrary.wiley.com/doi/full/10.1002/stem.3316

71. Mitochondria - Physiopedia [Internet]. [cited 2022 Dec 1]. Available from: https://www.physio-pedia.com/Mitochondria

72. Xu Z, Zhang D, He X, Huang Y, Shao H. Transport of Calcium Ions into Mitochondria. Curr Genomics [Internet]. 2016 Apr 18 [cited 2022 Dec 1];17(3):215. Available from: /pmc/articles/PMC4869008/

73. Hood DA, Memme JM, Oliveira AN, Triolo M. Maintenance of Skeletal Muscle Mitochondria in Health, Exercise, and Aging. Annu Rev Physiol [Internet]. 2019 Feb 10 [cited 2019 Nov 25];81(1):19–41. Available from: https://www.annualreviews.org/doi/10.1146/annurev-physiol-020518-114310

74. Peterson CM, Johannsen DL, Ravussin E. Skeletal muscle mitochondria and aging: A review. J Aging Res. 2012;2012.

75. Terman A, Kurz T, Navratil M, Arriaga EA, Brunk UT. Mitochondrial Turnover and aging of long-lived postmitotic cells: The mitochondrial-lysosomal axis theory of aging. Antioxid Redox Signal [Internet]. 2010 Feb 15 [cited 2022 Dec 2];12(4):503–35. Available from: https://www.liebertpub.com/doi/10.1089/ars.2009.2598

76. Sousa-Victor P, Gutarra S, García-Prat L, Rodriguez-Ubreva J, Ortet L, Ruiz-Bonilla V, et al. Geriatric muscle stem cells switch reversible quiescence into senescence. Nature 2014 506:7488 [Internet]. 2014 Feb 12 [cited 2022 Oct 17];506(7488):316–21. Available from: https://www.nature.com/articles/nature13013

77. Deldicque L. Endoplasmic reticulum stress in human skeletal muscle: Any contribution to sarcopenia? Front Physiol. 2013 Sep 3;4 SEP:236.

78. Rayavarapu S, Coley W, Nagaraju K. Endoplasmic Reticulum Stress in Skeletal Muscle Homeostasis and Disease. Curr Rheumatol Rep [Internet]. 2012 Jun [cited 2022 Dec 2];14(3):238. Available from: /pmc/articles/PMC3587844/

79. Deldicque L, Hespel P, Francaux M. Endoplasmic reticulum stress in skeletal muscle: Origin and metabolic consequences. Exerc Sport Sci Rev [Internet]. 2012 Jan [cited 2022 Dec 2];40(1):43–9. Available from: https://journals.lww.com/acsm-essr/Fulltext/2012/01000/Endoplasmic_Reticulum_Stress_in_Skeletal_Muscle_.8.aspx

80. Hu H, Tian M, Ding C, Yu S. The C/EBP homologous protein (CHOP) transcription factor functions in endoplasmic reticulum stress-induced apoptosis and microbial infection. Vol. 10, Frontiers in Immunology. Frontiers Media S.A.; 2019.

81. Henchcliffe C, Beal FM. Mitochondrial biology and oxidative stress in Parkinson disease pathogenesis. Nat Clin Pract Neurol [Internet]. 2008 [cited 2022 Dec 5];4(11):600–9. Available from: https://pubmed.ncbi.nlm.nih.gov/18978800/

82. Brown DM, Goljanek-Whysall K. MicroRNAs: Modulators of the underlying pathophysiology of sarcopenia? Ageing Research Reviews. 2015.

83. Cruz-Jentoft AJ, Baeyens JP, Bauer JM, Boirie Y, Cederholm T, Landi F, et al. Sarcopenia: European consensus on definition and diagnosis: Report of the European Working Group on Sarcopenia in Older People. Age Ageing [Internet]. 2010 Jul 1 [cited 2018 Sep 6];39(4):412–23. Available from: https://academic.oup.com/ageing/article-lookup/doi/10.1093/ageing/afq034

84. Brooks S v., Faulkner JA. Contraction-induced injury: recovery of skeletal muscles in young and old mice. https://doi.org/101152/ajpcell19902583C436 [Internet]. 1990 [cited 2022 Oct 17];258(3 27-3). Available from: https://journals.physiology.org/doi/10.1152/ajpcell.1990.258.3.C436

85. McDonagh B, Sakellariou GK, Smith NT, Brownridge P, Jackson MJ. Differential cysteine labeling and global label-free proteomics reveals an altered metabolic state in skeletal muscle aging. J Proteome Res [Internet]. 2014 Nov 7 [cited 2022 Oct 17];13(11):5008–21. Available from: https://pubs.acs.org/doi/full/10.1021/pr5006394

86. Valdez G, Tapia JC, Kang H, Clemenson GD, Gage FH, Lichtman JW, et al. Attenuation of age-related changes in mouse neuromuscular synapses by caloric restriction and exercise. Proc Natl Acad Sci U S A [Internet]. 2010 Aug 17 [cited 2022 Oct 17];107(33):14863–8. Available from: https://www.pnas.org/doi/abs/10.1073/pnas.1002220107

87. Larsson L, Degens H, Li M, Salviati L, Lee Y il, Thompson W, et al. Sarcopenia: Aging-related loss of muscle mass and function. Physiol Rev [Internet]. 2019 Jan 1 [cited 2022 Oct 17];99(1):427–511. Available from: https://journals.physiology.org/doi/10.1152/physrev.00061.2017

88. Hettwer S, Lin S, Kucsera S, Haubitz M, Oliveri F, Fariello RG, et al. Injection of a Soluble Fragment of Neural Agrin (NT-1654) Considerably Improves the Muscle Pathology Caused by the Disassembly of the Neuromuscular Junction. PLoS One [Internet]. 2014 Feb 10 [cited 2022 Oct 17];9(2):e88739. Available from: https://journals.plos.org/plosone/article?id=10.1371/journal.pone.0088739

89. Bütikofer L, Zurlinden A, Bolliger MF, Kunz B, Sonderegger P. Destabilization of the neuromuscular junction by proteolytic cleavage of agrin results in precocious sarcopenia. The FASEB Journal [Internet]. 2011 Dec 1 [cited 2022 Oct 17];25(12):4378–93. Available from: https://onlinelibrary.wiley.com/doi/full/10.1096/fj.11-191262

90. Soares RJ, Cagnin S, Chemello F, Silvestrin M, Musaro A, de Pitta C, et al. Involvement of MicroRNAs in the regulation of muscle wasting during catabolic conditions. Journal of Biological Chemistry [Internet]. 2014 Aug 8 [cited 2022 Oct 17];289(32):21909–25. Available from: http://www.jbc.org/article/S002192582033132X/fulltext

91. Markofski MM, Dickinson JM, Drummond MJ, Fry CS, Fujita S, Gundermann DM, et al. Effect of age on basal muscle protein synthesis and mTORC1 signaling in a large cohort of young and older men and women. Exp Gerontol [Internet]. 2015 May [cited 2018 Sep 11];65:1–7. Available from: http://www.ncbi.nlm.nih.gov/pubmed/25735236

92. Nelson G, Kucheryavenko O, Wordsworth J, von Zglinicki T. The senescent bystander effect is caused by ROS-activated NF-κB signalling. Mech Ageing Dev. 2018 Mar 1;170:30–6.

93. Baar MP, Perdiguero E, Muñoz-Cánoves P, de Keizer PL. Musculoskeletal senescence: a moving target ready to be eliminated. Curr Opin Pharmacol. 2018 Jun 1;40:147–55.

94. Baker DJ, Wijshake T, Tchkonia T, Lebrasseur NK, Childs BG, van de Sluis B, et al. Clearance of p16Ink4a-positive senescent cells delays ageing-associated disorders. Nature 2011 479:7372 [Internet]. 2011 Nov 2 [cited 2022 Oct 17];479(7372):232–6. Available from: https://www.nature.com/articles/nature10600

95. Hu Z, Klein JD, Mitch WE, Zhang L, Martinez I, Wang XH. MicroRNA-29 induces cellular senescence in aging muscle through multiple signaling pathways. Aging (Albany NY) [Internet]. 2014 [cited 2022 Oct 17];6(3):160. Available from: /pmc/articles/PMC4012934/

96. Bu H, Wedel S, Cavinato M, Jansen-Dürr P. MicroRNA Regulation of Oxidative Stress-Induced Cellular Senescence. Oxid Med Cell Longev [Internet]. 2017 [cited 2023 Mar 30];2017. Available from: /pmc/articles/PMC5448073/

97. MAURO A. SATELLITE CELL OF SKELETAL MUSCLE FIBERS. J Biophys Biochem Cytol [Internet]. 1961 Feb 1 [cited 2022 Oct 17];9(2):493–5. Available from: http://rupress.org/jcb/article-pdf/9/2/493/1078104/493.pdf

98. Verdijk LB, Koopman R, Schaart G, Meijer K, Savelberg HHCM, van Loon LJC. Satellite cell content is specifically reduced in type II skeletal muscle fibers in the elderly. Am J Physiol Endocrinol Metab [Internet]. 2007 Jan [cited 2022 Oct 17];292(1). Available from: https://pubmed.ncbi.nlm.nih.gov/16926381/

99. Kadi F, Charifi N, Henriksson J. The number of satellite cells in slow and fast fibres from human vastus lateralis muscle. Histochem Cell Biol [Internet]. 2006 Jul 8 [cited 2022 Oct 17];126(1):83–7. Available from: https://link.springer.com/article/10.1007/s00418-005-0102-0

100. Collins CA, Zammit PS, Ruiz AP, Morgan JE, Partridge TA. A Population of Myogenic Stem Cells That Survives Skeletal Muscle Aging. Stem Cells [Internet]. 2007 Apr 1 [cited 2022 Oct 17];25(4):885–94. Available from: https://academic.oup.com/stmcls/article/25/4/885/6402187

101. Brack AS, Rando TA. Intrinsic changes and extrinsic influences of myogenic stem cell function during aging. Stem Cell Rev [Internet]. 2007 Sep 15 [cited 2022 Oct 17];3(3):226–37. Available from: https://link.springer.com/article/10.1007/s12015-007-9000-2

102. Blau HM, Cosgrove BD, Ho ATV. The central role of muscle stem cells in regenerative failure with aging. Nature Medicine 2015 21:8 [Internet]. 2015 Aug 6 [cited 2022 Oct 17];21(8):854–62. Available from: https://www.nature.com/articles/nm.3918

103. Thalacker-Mercer AE, Dell'Italia LJ, Cui X, Cross JM, Bamman MM. Differential genomic responses in old vs. young humans despite similar levels of modest muscle damage after resistance loading. Physiol Genomics

[Internet]. 2010 Feb [cited 2022 Oct 17];40(3):141–9. Available from: https://journals.physiology.org/doi/10.1152/physiolgenomics.00151.2009

104. Mcardle A, Dillmann WH, Mestril R, Faulkner JA, Jackson MJ. Overexpression of HSP70 in mouse skeletal muscle protects against muscle damage and age‐related muscle dysfunction; Overexpression of HSP70 in mouse skeletal muscle protects against muscle damage and age‐related muscle dysfunction. The FASEB Journal. 2003;

105. Jejurikar SS, Henkelman EA, Cederna PS, Marcelo CL, Urbanchek MG, Kuzon WM. Aging increases the susceptibility of skeletal muscle derived satellite cells to apoptosis. Exp Gerontol. 2006 Sep 1;41(9):828–36.

106. Bortoli S, Renault V, Eveno E, Auffray C, Butler-Browne G, Piétu G. Gene expression profiling of human satellite cells during muscular aging using cDNA arrays. Gene. 2003 Dec 4;321(1–2):145–54.

107. Mccarthy JJ, Mula J, Miyazaki M, Erfani R, Garrison K, Farooqui AB, et al. Effective fiber hypertrophy in satellite cell-depleted skeletal muscle. Development [Internet]. 2011 Sep 1 [cited 2022 Oct 17];138(17):3657–66. Available from: https://journals.biologists.com/dev/article/138/17/3657/44631/Effective-fiber-hypertrophy-in-satellite-cell

108. Fry CS, Lee JD, Mula J, Kirby TJ, Jackson JR, Liu F, et al. Inducible depletion of satellite cells in adult, sedentary mice impairs muscle regenerative capacity without affecting sarcopenia. Nature Medicine 2014 21:1 [Internet]. 2014 Dec 15 [cited 2022 Oct 17];21(1):76–80. Available from: https://www.nature.com/articles/nm.3710

109. Natarajan A, Lemos DR, Rossi FM v. Cell Cycle Fibro/adipogenic progenitors: A double-edged sword in skeletal muscle regeneration. 2010 [cited 2022 Oct 17]; Available from: https://www.tandfonline.com/action/journalInformation?journalCode=kccy20

110. Rodeheffer MS. Tipping the scale: muscle versus fat. Nature Cell Biology 2010 12:2 [Internet]. 2010 Jan 17 [cited 2022 Oct 17];12(2):102–4. Available from: https://www.nature.com/articles/ncb0210-102

111. Mendias CL, Gumucio JP, Davis ME, Bromley CW, Davis CS, Brooks S v. Transforming growth factor-beta induces skeletal muscle atrophy and fibrosis through the induction of atrogin-1 and scleraxis. Muscle Nerve [Internet]. 2012 Jan 1 [cited 2022 Oct 17];45(1):55–9. Available from: https://onlinelibrary.wiley.com/doi/full/10.1002/mus.22232

112. Jun J il, Lau LF. Cellular senescence controls fibrosis in wound healing. Aging (Albany NY) [Internet]. 2010 [cited 2022 Oct 17];2(9):627. Available from: /pmc/articles/PMC2984611/

113. Uezumi A, Ikemoto-Uezumi M, Tsuchida K. Roles of nonmyogenic mesenchymal progenitors in pathogenesis and regeneration of skeletal muscle. Front Physiol. 2014;5 FEB:68.

114. Ambros V. microRNAs: tiny regulators with great potential. Cell [Internet]. 2001 Dec 28 [cited 2022 Oct 11];107(7):823–6. Available from: https://pubmed.ncbi.nlm.nih.gov/11779458/

115. Plotnikova O, Baranova A, Skoblov M. Comprehensive Analysis of Human microRNA–mRNA Interactome. Front Genet. 2019 Oct 8;10:933.

116. Hammond SM. An overview of microRNAs. Adv Drug Deliv Rev [Internet]. 2015 Jun 29 [cited 2022 Oct 11];87:3–14. Available from: https://pubmed.ncbi.nlm.nih.gov/25979468/

117. Friedman RC, Farh KKH, Burge CB, Bartel DP. Most mammalian mRNAs are conserved targets of microRNAs. Genome Res [Internet]. 2009 Jan [cited 2022 Dec 5];19(1):92–105. Available from: https://pubmed.ncbi.nlm.nih.gov/18955434/

118. Fazi F, Nervi C. MicroRNA: basic mechanisms and transcriptional regulatory networks for cell fate determination. Cardiovasc Res [Internet]. 2008 Sep 1 [cited 2022 Dec 7];79(4):553–61. Available from: https://academic.oup.com/cardiovascres/article/79/4/553/346393

119. Winter J, Jung S, Keller S, Gregory RI, Diederichs S. Many roads to maturity: microRNA biogenesis pathways and their regulation. Nature Cell Biology 2009

11:3 [Internet]. 2009 [cited 2022 Oct 17];11(3):228–34. Available from: https://www.nature.com/articles/ncb0309-228

120. Wahid F, Shehzad A, Khan T, Kim YY. MicroRNAs: Synthesis, mechanism, function, and recent clinical trials. Biochimica et Biophysica Acta (BBA) - Molecular Cell Research [Internet]. 2010 Nov 1 [cited 2019 Jan 18];1803(11):1231–43. Available from: https://www.sciencedirect.com/science/article/pii/S0167488910001837

121. Bartel DP. MicroRNAs: Genomics, Biogenesis, Mechanism, and Function. Cell. 2004.

122. O'Brien J, Hayder H, Zayed Y, Peng C. Overview of microRNA biogenesis, mechanisms of actions, and circulation. Front Endocrinol (Lausanne). 2018 Aug 3;9(AUG):402.

123. Medley JC, Panzade G, Zinovyeva AY. microRNA strand selection: Unwinding the rules. Wiley Interdiscip Rev RNA [Internet]. 2021 May 1 [cited 2022 Dec 6];12(3):e1627. Available from: https://onlinelibrary.wiley.com/doi/full/10.1002/wrna.1627

124. Kuo WT, Yu SY, Li SC, Lam HC, Chang HT, Chen WS, et al. MicroRNA-324 in Human Cancer: miR-324-5p and miR-324-3p Have Distinct Biological Functions in Human Cancer. Anticancer Res [Internet]. 2016 Oct 1 [cited 2022 Dec 6];36(10):5189–96. Available from: https://pubmed.ncbi.nlm.nih.gov/27798879/

125. Wang X. Composition of seed sequence is a major determinant of microRNA targeting patterns. Bioinformatics [Internet]. 2014 May 5 [cited 2022 Dec 6];30(10):1377. Available from: /pmc/articles/PMC4016705/

126. Annese T, Tamma R, de Giorgis M, Ribatti D. microRNAs Biogenesis, Functions and Role in Tumor Angiogenesis. Front Oncol. 2020 Nov 27;10:2610.

127. Westholm JO, Lai EC. Mirtrons: microRNA biogenesis via splicing. Biochimie [Internet]. 2011 Nov [cited 2022 Dec 6];93(11):1897. Available from: /pmc/articles/PMC3185189/

128. Wahl MC, Will CL, Lührmann R. The spliceosome: design principles of a dynamic RNP machine. Cell [Internet]. 2009 Feb 20 [cited 2022 Dec 6];136(4):701–18. Available from: https://pubmed.ncbi.nlm.nih.gov/19239890/

129. Yang JS, Lai EC. Dicer-independent, Ago2-mediated microRNA biogenesis in vertebrates. Cell Cycle [Internet]. 2010 Nov 15 [cited 2022 Dec 6];9(22):4455–60. Available from: https://pubmed.ncbi.nlm.nih.gov/21088485/

130. Ghanbarian H, Aghamiri S, Eftekhary M, Wagner N, Wagner KD. Small Activating RNAs: Towards the Development of New Therapeutic Agents and Clinical Treatments. Cells [Internet]. 2021 Mar 1 [cited 2023 Mar 13];10(3):1–13. Available from: /pmc/articles/PMC8001863/

131. Triulzi T, Iorio M V., Tagliabue E, Casalini P, Triulzi T, Iorio M V., et al. microRNA: New Players in Metastatic Process. Oncogene and Cancer - From Bench to Clinic [Internet]. 2013 Jan 24 [cited 2023 Mar 13]; Available from: https://www.intechopen.com/chapters/42295

132. Wilczynska A, Bushell M. The complexity of miRNA-mediated repression. Cell Death Differ [Internet]. 2015 Jan 1 [cited 2022 Dec 7];22(1):22. Available from: /pmc/articles/PMC4262769/

133. Rouya C, Siddiqui N, Morita M, Duchaine TF, Fabian MR, Sonenberg N. Human DDX6 effects miRNA-mediated gene silencing via direct binding to CNOT1. RNA [Internet]. 2014 [cited 2022 Dec 7];20(9):1398. Available from: /pmc/articles/PMC4138323/

134. Ramchandran R, Chaluvally-Raghavan P. miRNA-Mediated RNA Activation in Mammalian Cells. Adv Exp Med Biol [Internet]. 2017 [cited 2022 Dec 7];983:81–9. Available from: https://pubmed.ncbi.nlm.nih.gov/28639193/

135. Ørom UA, Nielsen FC, Lund AH. MicroRNA-10a Binds the 5′UTR of Ribosomal Protein mRNAs and Enhances Their Translation. Mol Cell. 2008 May 23;30(4):460–71.

136. Vaschetto LM. miRNA activation is an endogenous gene expression pathway. RNA Biol [Internet]. 2018 Jun 3 [cited 2022 Dec 7];15(6):826. Available from: /pmc/articles/PMC6152443/

137. Goljanek-Whysall K, Sweetman D, Münsterberg AM. microRNAs in skeletal muscle differentiation and disease. Clin Sci [Internet]. 2012 Dec 1 [cited 2022 Oct 7];123(11):611–25. Available from: /clinsci/article/123/11/611/68980/microRNAs-in-skeletal-muscle-differentiation-and

138. Munsterberg AE, Lassar AB. Combinatorial signals from the neural tube, floor plate and notochord induce myogenic bHLH gene expression in the somite. Development [Internet]. 1995 Mar 1 [cited 2022 Oct 17];121(3):651–60. Available from: https://journals.biologists.com/dev/article/121/3/651/38480/Combinatorial-signals-from-the-neural-tube-floor

139. van Rooij E, Liu N, Olson EN. MicroRNAs flex their muscles. Trends Genet [Internet]. 2008 Apr [cited 2022 Oct 17];24(4):159–66. Available from: https://pubmed.ncbi.nlm.nih.gov/18325627/

140. Small EM, O'Rourke JR, Moresi V, Sutherland LB, McAnally J, Gerard RD, et al. Regulation of PI3-kinase/Akt signaling by muscle-enriched microRNA-486. Proc Natl Acad Sci U S A [Internet]. 2010 Mar 2 [cited 2022 Oct 17];107(9):4218–23. Available from: https://www.pnas.org/doi/abs/10.1073/pnas.1000300107

141. McCarthy JJ, Esser KA. MicroRNA-1 and microRNA-133a expression are decreased during skeletal muscle hypertrophy. J Appl Physiol (1985) [Internet]. 2007 Jan [cited 2022 Oct 17];102(1):306–13. Available from: https://pubmed.ncbi.nlm.nih.gov/17008435/

142. Callis TE, Deng Z, Chen JF, Wang DZ. Muscling Through the microRNA World. https://doi.org/103181/0709-MR-237 [Internet]. 2008 Feb 1 [cited 2022 Oct 17];233(2):131–8. Available from: https://journals.sagepub.com/doi/abs/10.3181/0709-mr-237

143. Goljanek-Whysall K, Sweetman D, Abu-Elmagd M, Chapnik E, Dalmay T, Hornstein E, et al. MicroRNA regulation of the paired-box transcription factor Pax3 confers robustness to developmental timing of myogenesis. Proc Natl

Acad Sci U S A [Internet]. 2011 Jul 19 [cited 2022 Oct 17];108(29):11936–41. Available from: https://www.pnas.org/doi/abs/10.1073/pnas.1105362108

144. Cheung TH, Quach NL, Charville GW, Liu L, Park L, Edalati A, et al. Maintenance of muscle stem-cell quiescence by microRNA-489. Nature 2012 482:7386 [Internet]. 2012 Feb 23 [cited 2022 Oct 17];482(7386):524–8. Available from: https://www.nature.com/articles/nature10834

145. Crist CG, Montarras D, Pallafacchina G, Rocancourt D, Cumano A, Conway SJ, et al. Muscle stem cell behavior is modified by microRNA-27 regulation of Pax3 expression. Proc Natl Acad Sci U S A [Internet]. 2009 Aug 11 [cited 2022 Oct 20];106(32):13383–7. Available from: https://www.pnas.org/doi/abs/10.1073/pnas.0900210106

146. Saccone V, Consalvi S, Giordani L, Mozzetta C, Barozzi I, Sandoná M, et al. HDAC-regulated myomiRs control BAF60 variant exchange and direct the functional phenotype of fibro-adipogenic progenitors in dystrophic muscles. Genes Dev [Internet]. 2014 Apr 15 [cited 2022 Oct 20];28(8):841–57. Available from: http://genesdev.cshlp.org/content/28/8/841.full

147. Mok GF, Lozano-Velasco E, Maniou E, Viaut C, Moxon S, Wheeler G, et al. Mir-133-mediated regulation of the hedgehog pathway orchestrates embryo myogenesis. Development (Cambridge) [Internet]. 2018 Jun 1 [cited 2022 Oct 20];145(12). Available from: https://journals.biologists.com/dev/article/145/12/dev159657/48436/miR-133-mediated-regulation-of-the-Hedgehog

148. Goljanek-Whysall K, Mok GF, Alrefaei AF, Kennerley N, Wheeler GN, Münsterberg A. myomiR-dependent switching of BAF60 variant incorporation into Brg1 chromatin remodeling complexes during embryo myogenesis. Development [Internet]. 2014 Sep 1 [cited 2022 Oct 20];141(17):3378–87. Available from: https://journals.biologists.com/dev/article/141/17/3378/46329/myomiR-dependent-switching-of-BAF60-variant

149. van Rooij E, Quiat D, Johnson BA, Sutherland LB, Qi X, Richardson JA, et al. A family of microRNAs encoded by myosin genes governs myosin expression

and muscle performance. Dev Cell [Internet]. 2009 Nov 17 [cited 2022 Oct 20];17(5):662. Available from: /pmc/articles/PMC2796371/

150. Nakasa T, Ishikawa M, Shi M, Shibuya H, Adachi N, Ochi M. Acceleration of muscle regeneration by local injection of muscle-specific microRNAs in rat skeletal muscle injury model. J Cell Mol Med [Internet]. 2010 Oct 1 [cited 2022 Oct 20];14(10):2495–505. Available from: https://onlinelibrary.wiley.com/doi/full/10.1111/j.1582-4934.2009.00898.x

151. D'Souza WN, Douangpanya J, Mu S, Jaeckel P, Zhang M, Maxwell JR, et al. Differing roles for short chain fatty acids and GPR43 agonism in the regulation of intestinal barrier function and immune responses. PLoS One [Internet]. 2017 Jul 1 [cited 2022 Oct 20];12(7):e0180190. Available from: https://journals.plos.org/plosone/article?id=10.1371/journal.pone.0180190

152. Ultimo S, Zauli G, Martelli AM, Vitale M, McCubrey JA, Capitani S, et al. Influence of physical exercise on microRNAs in skeletal muscle regeneration, aging and diseases. Oncotarget [Internet]. 2018 Mar 3 [cited 2022 Oct 20];9(24):17220. Available from: /pmc/articles/PMC5908319/

153. Chen LH, Chiou GY, Chen YW, Li HY, Chiou SH. microRNA and aging: A novel modulator in regulating the aging network. Ageing Res Rev. 2010 Nov 1;9(SUPPL.):S59–66.

154. Choi SW, Lee JY, Kang KS. miRNAs in stem cell aging and age-related disease. Mech Ageing Dev. 2017 Dec 1;168:20–9.

155. Güller I, Russell AP. MicroRNAs in skeletal muscle: their role and regulation in development, disease and function. J Physiol [Internet]. 2010 Nov 1 [cited 2022 Oct 20];588(21):4075–87. Available from: https://onlinelibrary.wiley.com/doi/full/10.1113/jphysiol.2010.194175

156. Kim JY, Park YK, Lee KP, Lee SM, Kang TW, Kim HJ, et al. Genome-wide profiling of the microRNA-mRNA regulatory network in skeletal muscle with aging. Aging (Albany NY) [Internet]. 2014 [cited 2022 Oct 20];6(7):524. Available from: /pmc/articles/PMC4153621/

157. Hitachi K, Tsuchida K. Role of microRNAs in skeletal muscle hypertrophy. Front Physiol [Internet]. 2014;4:408. Available from: http://journal.frontiersin.org/article/10.3389/fphys.2013.00408/abstract

158. Soriano-Arroquia A, House L, Tregilgas L, Canty-Laird E, Goljanek-Whysall K. The functional consequences of age-related changes in microRNA expression in skeletal muscle. Biogerontology [Internet]. 2016 Jun 27 [cited 2019 Dec 11];17(3):641–54. Available from: http://link.springer.com/10.1007/s10522-016-9638-8

159. Bloch SAA, Donaldson AVJ, Lewis A, Banya WAS, Polkey MI, Griffiths MJD, et al. MiR-181a: A potential biomarker of acute muscle wasting following elective high-risk cardiothoracic surgery. Crit Care [Internet]. 2015 Apr 7 [cited 2020 May 11];19(1):147. Available from: http://ccforum.com/content/19/1/147

160. Goljanek-Whysall K, Soriano-Arroquia A, McCormick R, Chinda C, McDonagh B. miR-181a Regulates p62/SQSTM1, Parkin and Protein DJ-1 Promoting Mitochondrial Dynamics in Skeletal Muscle Ageing. bioRxiv. 2019 Oct 16;805176.

161. Borja-Gonzalez M, Casas-Martinez JC, McDonagh B, Goljanek-Whysall K. Aging Science Talks: The role of miR-181a in age-related loss of muscle mass and function. Transl Med Aging. 2020;4:81–5.

162. Carnio S, LoVerso F, Baraibar MA, Longa E, Khan MM, Maffei M, et al. Autophagy Impairment in Muscle Induces Neuromuscular Junction Degeneration and Precocious Aging. Cell Rep. 2014 Sep 11;8(5):1509–21.

163. García-Prat L, Martínez-Vicente M, Perdiguero E, Ortet L, Rodríguez-Ubreva J, Rebollo E, et al. Autophagy maintains stemness by preventing senescence. Nature 2016 529:7584 [Internet]. 2016 Jan 6 [cited 2022 Oct 20];529(7584):37–42. Available from: https://www.nature.com/articles/nature16187

164. Masiero E, Agatea L, Mammucari C, Blaauw B, Loro E, Komatsu M, et al. Autophagy Is Required to Maintain Muscle Mass. Cell Metab. 2009 Dec 2;10(6):507–15.

165. Cuthbertson D, Smith K, Babraj J, Leese G, Waddell T, Atherton P, et al. Anabolic signaling deficits underlie amino acid resistance of wasting, aging muscle. FASEB J [Internet]. 2005 Mar [cited 2022 Oct 20];19(3):1–22. Available from: https://pubmed.ncbi.nlm.nih.gov/15596483/

166. Rennie MJ. Anabolic resistance in critically ill patients. Crit Care Med [Internet]. 2009 [cited 2022 Oct 20];37(SUPPL. 10). Available from: https://journals.lww.com/ccmjournal/Fulltext/2009/10001/Anabolic_resistance_in_critically_ill_patients.15.aspx

167. Camera DM, Ong JN, Coffey VG, Hawley JA. Selective modulation of microRNA expression with protein ingestion following concurrent resistance and endurance exercise in human skeletal muscle. Front Physiol. 2016 Mar 7;7(MAR):87.

168. Drummond MJ, McCarthy JJ, Fry CS, Esser KA, Rasmussen BB. Aging differentially affects human skeletal muscle microRNA expression at rest and after an anabolic stimulus of resistance exercise and essential amino acids. Am J Physiol Endocrinol Metab [Internet]. 2008 Dec [cited 2022 Oct 20];295(6):1333–40. Available from: https://journals.physiology.org/doi/10.1152/ajpendo.90562.2008

169. Margolis LM, Lessard SJ, Ezzyat Y, Fielding RA, Rivas DA. Circulating MicroRNA Are Predictive of Aging and Acute Adaptive Response to Resistance Exercise in Men. The Journals of Gerontology: Series A [Internet]. 2017 Oct 1 [cited 2022 Oct 20];72(10):1319–26. Available from: https://academic.oup.com/biomedgerontology/article/72/10/1319/2640248

170. Nielsen S, Scheele C, Yfanti C, Åkerström T, Nielsen AR, Pedersen BK, et al. Muscle specific microRNAs are regulated by endurance exercise in human skeletal muscle. J Physiol [Internet]. 2010 Oct 15 [cited 2022 Oct 20];588(20):4029–37. Available from: https://onlinelibrary.wiley.com/doi/full/10.1113/jphysiol.2010.189860

171. Sannicandro AJ, Soriano-Arroquia A, Goljanek-Whysall K. micro(RNA)-managing muscle wasting. J Appl Physiol [Internet]. 2019 Apr 11 [cited 2019

May 15];japplphysiol.00961.2018. Available from: https://www.physiology.org/doi/10.1152/japplphysiol.00961.2018

172. Dubinsky AN, Dastidar SG, Hsu CL, Zahra R, Djakovic SN, Duarte S, et al. Let-7 Coordinately Suppresses Components of the Amino Acid Sensing Pathway to Repress mTORC1 and Induce Autophagy. Cell Metab. 2014 Oct 7;20(4):626–38.

173. Rippo MR, Olivieri F, Monsurrò V, Prattichizzo F, Albertini MC, Procopio AD. MitomiRs in human inflamm-aging: A hypothesis involving miR-181a, miR-34a and miR-146a. Exp Gerontol. 2014 Aug 1;56:154–63.

174. de Gasperi R, Hamidi S, Harlow LM, Ksiezak-Reding H, Bauman WA, Cardozo CP. Denervation-related alterations and biological activity of miRNAs contained in exosomes released by skeletal muscle fibers. Scientific Reports 2017 7:1 [Internet]. 2017 Oct 16 [cited 2022 Oct 20];7(1):1–11. Available from: https://www.nature.com/articles/s41598-017-13105-9

175. Koutsoulidou A, Mastroyiannopoulos NP, Furling D, Uney JB, Phylactou LA. Expression of miR-1, miR-133a, miR-133b and miR-206 increases during development of human skeletal muscle. BMC Dev Biol [Internet]. 2011 Jun 7 [cited 2022 Oct 20];11(1):1–9. Available from: https://bmcdevbiol.biomedcentral.com/articles/10.1186/1471-213X-11-34

176. Beuvink I, Kolb FA, Budach W, Garnier A, Lange J, Natt F, et al. A novel microarray approach reveals new tissue-specific signatures of known and predicted mammalian microRNAs. Nucleic Acids Res [Internet]. 2007 Apr 1 [cited 2022 Oct 20];35(7):e52–e52. Available from: https://academic.oup.com/nar/article/35/7/e52/1084140

177. Sempere LF, Freemantle S, Pitha-Rowe I, Moss E, Dmitrovsky E, Ambros V. Expression profiling of mammalian microRNAs uncovers a subset of brain-expressed microRNAs with possible roles in murine and human neuronal differentiation. Genome Biol [Internet]. 2004 Feb 16 [cited 2022 Oct 20];5(3):1–11. Available from: https://link.springer.com/articles/10.1186/gb-2004-5-3-r13

178. Mishima Y, Abreu-Goodger C, Staton AA, Stahlhut C, Shou C, Cheng C, et al. Zebrafish miR-1 and miR-133 shape muscle gene expression and regulate sarcomeric actin organization. Genes Dev [Internet]. 2009 Mar 3 [cited 2022 Oct 20];23(5):619. Available from: /pmc/articles/PMC2658521/

179. Fernandes T, Nakamuta JS, Magalhães FC, Roque FR, Lavini-Ramos C, Schettert IT, et al. Exercise training restores the endothelial progenitor cells number and function in hypertension: Implications for angiogenesis. J Hypertens [Internet]. 2012 [cited 2022 Oct 20];30(11):2133–43. Available from: https://journals.lww.com/jhypertension/Fulltext/2012/11000/Exercise_training_restores_the_endothelial.14.aspx

180. Russell AP, Lamon S, Boon H, Wada S, Güller I, Brown EL, et al. Regulation of miRNAs in human skeletal muscle following acute endurance exercise and short-term endurance training. J Physiol [Internet]. 2013 Sep 1 [cited 2022 Oct 20];591(18):4637–53. Available from: https://onlinelibrary.wiley.com/doi/full/10.1113/jphysiol.2013.255695

181. Panguluri SK, Bhatnagar S, Kumar A, McCarthy JJ, Srivastava AK, Cooper NG, et al. Genomic Profiling of Messenger RNAs and MicroRNAs Reveals Potential Mechanisms of TWEAK-Induced Skeletal Muscle Wasting in Mice. PLoS One [Internet]. 2010 Jan 19 [cited 2022 Oct 20];5(1):e8760. Available from: https://journals.plos.org/plosone/article?id=10.1371/journal.pone.0008760

182. Duran BODS, Fernandez GJ, Mareco EA, Moraes LN, Salomão RAS, Gutierrez De Paula T, et al. Differential microRNA Expression in Fast- and Slow-Twitch Skeletal Muscle of Piaractus mesopotamicus during Growth. PLoS One [Internet]. 2015 Nov 3 [cited 2022 Oct 20];10(11):e0141967. Available from: https://journals.plos.org/plosone/article?id=10.1371/journal.pone.0141967

183. Lee DE, Brown JL, Rosa ME, Brown LA, Perry RA, Wiggs MP, et al. microRNA-16 Is Downregulated During Insulin Resistance and Controls Skeletal Muscle Protein Accretion. J Cell Biochem [Internet]. 2016 Aug 1

[cited 2022 Oct 20];117(8):1775–87. Available from: https://onlinelibrary.wiley.com/doi/full/10.1002/jcb.25476

184. Ye L, Zuo Y, Chen F, Peng Q, Lu X, Wang G, et al. miR-18a-3p and Its Target Protein HuR May Regulate Myogenic Differentiation in Immune-Mediated Necrotizing Myopathy. Front Immunol [Internet]. 2022 Jan 5 [cited 2022 Oct 24];12. Available from: /pmc/articles/PMC8766969/

185. Sayed D, He M, Hong C, Gao S, Rane S, Yang Z, et al. MicroRNA-21 is a downstream effector of AKT that mediates its antiapoptotic effects via suppression of fas ligand. Journal of Biological Chemistry [Internet]. 2010 Jun 25 [cited 2022 Oct 20];285(26):20281–90. Available from: http://www.jbc.org/article/S0021925818497050/fulltext

186. Wada S, Kato Y, Okutsu M, Miyaki S, Suzuki K, Yan Z, et al. Translational suppression of atrophic regulators by MicroRNA-23a integrates resistance to skeletal muscle atrophy. Journal of Biological Chemistry [Internet]. 2011 Nov 4 [cited 2022 Oct 20];286(44):38456–65. Available from: http://www.jbc.org/article/S002192582050690X/fulltext

187. Russell AP, Wada S, Vergani L, Hock MB, Lamon S, Léger B, et al. Disruption of skeletal muscle mitochondrial network genes and miRNAs in amyotrophic lateral sclerosis. Neurobiol Dis [Internet]. 2013 Jan 1 [cited 2018 Dec 12];49:107–17. Available from: https://www.sciencedirect.com/science/article/pii/S0969996112003026

188. Hudson MB, Woodworth-Hobbs ME, Zheng B, Rahnert JA, Blount MA, Gooch JL, et al. miR-23a is decreased during muscle atrophy by a mechanism that includes calcineurin signaling and exosome-mediated export. Am J Physiol Cell Physiol [Internet]. 2014 Mar 15 [cited 2022 Oct 20];306(6):551–8. Available from: https://journals.physiology.org/doi/10.1152/ajpcell.00266.2013

189. Guan L, Hu X, Liu L, Xing Y, Zhou Z, Liang X, et al. bta-miR-23a involves in adipogenesis of progenitor cells derived from fetal bovine skeletal muscle. Scientific Reports 2017 7:1 [Internet]. 2017 Mar 3 [cited 2022 Oct 20];7(1):1–12. Available from: https://www.nature.com/articles/srep43716

190. Wang M, Liu W, Jiao J, Li J, Wang C, Zhang L. Expression Profiling of mRNAs and Long Non-Coding RNAs in Aged Mouse Olfactory Bulb. Sci Rep [Internet]. 2017 Dec 1 [cited 2022 Oct 20];7(1). Available from: https://pubmed.ncbi.nlm.nih.gov/28522862/

191. Chen X, Huang Z, Chen D, Yang T, Liu G. Role of microRNA-27a in myoblast differentiation. Cell Biol Int [Internet]. 2014 Feb 1 [cited 2022 Oct 20];38(2):266–71. Available from: https://onlinelibrary.wiley.com/doi/full/10.1002/cbin.10192

192. Crist CG, Montarras D, Pallafacchina G, Rocancourt D, Cumano A, Conway SJ, et al. Muscle stem cell behavior is modified by microRNA-27 regulation of Pax3 expression. Proc Natl Acad Sci U S A [Internet]. 2009 Aug 11 [cited 2022 Oct 20];106(32):13383–7. Available from: https://www.pnas.org/doi/abs/10.1073/pnas.0900210106

193. Ling YH, Sui MH, Zheng Q, Wang KY, Wu H, Li WY, et al. miR-27b regulates myogenic proliferation and differentiation by targeting Pax3 in goat. Scientific Reports 2018 8:1 [Internet]. 2018 Mar 2 [cited 2022 Oct 20];8(1):1–12. Available from: https://www.nature.com/articles/s41598-018-22262-4

194. Yu Y, Du H, Wei S, Feng L, Li J, Yao F, et al. Adipocyte-Derived Exosomal MiR-27a Induces Insulin Resistance in Skeletal Muscle Through Repression of PPARγ. Theranostics [Internet]. 2018 [cited 2022 Oct 20];8(8):2171–88. Available from: https://pubmed.ncbi.nlm.nih.gov/29721071/

195. Winbanks CE, Wang B, Beyer C, Koh P, White L, Kantharidis P, et al. TGF-beta regulates miR-206 and miR-29 to control myogenic differentiation through regulation of HDAC4. J Biol Chem [Internet]. 2011 Apr 22 [cited 2022 Oct 20];286(16):13805–14. Available from: https://pubmed.ncbi.nlm.nih.gov/21324893/

196. Wei W, He HB, Zhang WY, Zhang HX, Bai JB, Liu HZ, et al. miR-29 targets Akt3 to reduce proliferation and facilitate differentiation of myoblasts in skeletal muscle development. Cell Death & Disease 2013 4:6 [Internet]. 2013 Jun 13 [cited 2022 Oct 20];4(6):e668–e668. Available from: https://www.nature.com/articles/cddis2013184

197. Deng Z, He Y, Yang X, Shi H, Shi A, Lu L, et al. MicroRNA-29: A Crucial Player in Fibrotic Disease. Mol Diagn Ther [Internet]. 2017 Jun 1 [cited 2022 Oct 20];21(3):285–94. Available from: https://link.springer.com/article/10.1007/s40291-016-0253-9

198. Hu Z, Klein JD, Mitch WE, Zhang L, Martinez I, Wang XH. MicroRNA-29 induces cellular senescence in aging muscle through multiple signaling pathways. Aging (Albany NY) [Internet]. 2014 [cited 2022 Oct 20];6(3):160. Available from: /pmc/articles/PMC4012934/

199. Wang L, Zhou L, Jiang P, Lu L, Chen X, Lan H, et al. Loss of miR-29 in Myoblasts Contributes to Dystrophic Muscle Pathogenesis. Molecular Therapy. 2012 Jun 1;20(6):1222–33.

200. Galimov A, Merry TL, Luca E, Rushing EJ, Mizbani A, Turcekova K, et al. MicroRNA-29a in Adult Muscle Stem Cells Controls Skeletal Muscle Regeneration During Injury and Exercise Downstream of Fibroblast Growth Factor-2. Stem Cells [Internet]. 2016 Mar 1 [cited 2022 Oct 20];34(3):768–80. Available from: https://academic.oup.com/stmcls/article/34/3/768/6407566

201. Sato S, Ogura Y, Kumar A. TWEAK/Fn14 signaling axis mediates skeletal muscle atrophy and metabolic dysfunction. Front Immunol. 2014;5(JAN):18.

202. Zhang D, Wang X, Li Y, Zhao L, Lu M, Yao X, et al. Thyroid hormone regulates muscle fiber type conversion via miR-133a1. Journal of Cell Biology [Internet]. 2014 Dec 22 [cited 2022 Oct 20];207(6):753–66. Available from: www.jcb.org/cgi/doi/10.1083/jcb.201406068JCB753

203. Nie Y, Sato Y, Wang C, Yue F, Kuang S, Gavin TP. Impaired exercise tolerance, mitochondrial biogenesis, and muscle fiber maintenance in miR-133a–deficient mice. The FASEB Journal [Internet]. 2016 Nov 1 [cited 2022 Oct 20];30(11):3745–58. Available from: https://onlinelibrary.wiley.com/doi/full/10.1096/fj.201600529R

204. Boettger T, Wüst S, Nolte H, Braun T. The miR-206/133b cluster is dispensable for development, survival and regeneration of skeletal muscle. Skelet Muscle [Internet]. 2014 Dec 12 [cited 2022 Oct 20];4(1):1–13. Available from: https://link.springer.com/articles/10.1186/s13395-014-0023-5

205. Soriano-Arroquia A, Mccormick R, Molloy AP, Mcardle A, Goljanek-Whysall K. Age-related changes in miR-143-3p:Igfbp5 interactions affect muscle regeneration. Aging Cell [Internet]. 2016 Apr 1 [cited 2022 Oct 20];15(2):361–9. Available from: https://onlinelibrary.wiley.com/doi/full/10.1111/acel.12442

206. McCarthy JJ. MicroRNA-206: The skeletal muscle-specific myomiR. Biochimica et Biophysica Acta (BBA) - Gene Regulatory Mechanisms. 2008 Nov 1;1779(11):682–91.

207. McCarthy JJ, Esser KA, Peterson CA, Dupont-Versteegden EE. Evidence of MyomiR network regulation of β-myosin heavy chain gene expression during skeletal muscle atrophy. Physiol Genomics [Internet]. 2009 Nov [cited 2022 Oct 20];39(3):219–26. Available from: https://journals.physiology.org/doi/10.1152/physiolgenomics.00042.2009

208. Williams AH, Valdez G, Moresi V, Qi X, McAnally J, Elliott JL, et al. MicroRNA-206 delays ALS progression and promotes regeneration of neuromuscular synapses in mice. Science [Internet]. 2009 Dec 11 [cited 2022 Oct 20];326(5959):1549–54. Available from: https://pubmed.ncbi.nlm.nih.gov/20007902/

209. Dey BK, Gagan J, Dutta A. miR-206 and -486 Induce Myoblast Differentiation by Downregulating Pax7. Mol Cell Biol [Internet]. 2011 Jan 11 [cited 2022 Oct 20];31(1):203–14. Available from: https://journals.asm.org/doi/10.1128/MCB.01009-10

210. Liu N, Williams AH, Maxeiner JM, Bezprozvannaya S, Shelton JM, Richardson JA, et al. microRNA-206 promotes skeletal muscle regeneration and delays progression of Duchenne muscular dystrophy in mice. J Clin Invest [Internet]. 2012 Jun 1 [cited 2022 Oct 20];122(6):2054–65. Available from: http://www.jci.org

211. van Rooij E, Sutherland LB, Qi X, Richardson JA, Hill J, Olson EN. Control of stress-dependent cardiac growth and gene expression by a microRNA. Science [Internet]. 2007 Apr 27 [cited 2022 Oct 20];316(5824):575–9. Available from: https://pubmed.ncbi.nlm.nih.gov/17379774/

212. Zhang D, Li Y, Yao X, Wang H, Zhao L, Jiang H, et al. miR-182 Regulates Metabolic Homeostasis by Modulating Glucose Utilization in Muscle. Cell Rep. 2016 Jul 19;16(3):757–68.

213. Gan Z, Rumsey J, Hazen BC, Lai L, Leone TC, Vega RB, et al. Nuclear receptor/microRNA circuitry links muscle fiber type to energy metabolism. J Clin Invest [Internet]. 2013 Jun 3 [cited 2022 Oct 20];123(6):2564–75. Available from: https://pubmed.ncbi.nlm.nih.gov/23676496/

214. Xu S, Linher-Melville K, Yang BB, Wu D, Li J. Micro-RNA378 (miR-378) Regulates Ovarian Estradiol Production by Targeting Aromatase. Endocrinology [Internet]. 2011 Oct 1 [cited 2022 Oct 20];152(10):3941–51. Available from: https://academic.oup.com/endo/article/152/10/3941/2457290

215. Zeng P, Han W, Li C, Li H, Zhu D, Zhang Y, et al. miR-378 attenuates muscle regeneration by delaying satellite cell activation and differentiation in mice. Acta Biochim Biophys Sin (Shanghai) [Internet]. 2016 Sep 1 [cited 2022 Oct 20];48(9):833–9. Available from: https://academic.oup.com/abbs/article/48/9/833/2236686

216. Small EM, O'Rourke JR, Moresi V, Sutherland LB, McAnally J, Gerard RD, et al. Regulation of PI3-kinase/Akt signaling by muscle-enriched microRNA-486. Proc Natl Acad Sci U S A [Internet]. 2010 Mar 2 [cited 2022 Oct 20];107(9):4218–23. Available from: https://www.pnas.org/doi/abs/10.1073/pnas.1000300107

217. Kloosterman WP, Steiner FA, Berezikov E, de Bruijn E, van de Belt J, Verheul M, et al. Cloning and expression of new microRNAs from zebrafish. Nucleic Acids Res [Internet]. 2006 May 1 [cited 2022 Oct 20];34(9):2558–69. Available from: https://academic.oup.com/nar/article/34/9/2558/2401677

218. Wang XY, Chen XL, Huang ZQ, Chen DW, Yu B, He J, et al. MicroRNA-499-5p regulates porcine myofiber specification by controlling Sox6 expression. animal [Internet]. 2017 Dec 1 [cited 2022 Oct 20];11(12):2268–74. Available from: https://www.cambridge.org/core/journals/animal/article/microrna4995p-regulates-porcine-myofiber-specification-by-controlling-sox6-expression/ED638CE0E4A415A34091321F953724BC

219. Aoi W, Naito Y, Mizushima K, Takanami Y, Kawai Y, Ichikawa H, et al. The microRNA miR-696 regulates PGC-1α in mouse skeletal muscle in response to physical activity. Am J Physiol Endocrinol Metab [Internet]. 2010 Apr [cited 2022 Oct 20];298(4):799–806. Available from: https://journals.physiology.org/doi/10.1152/ajpendo.00448.2009

220. Wang H, Shi L, Liang T, Wang B bin, Wu WJ, Su G, et al. MiR-696 Regulates C2C12 Cell Proliferation and Differentiation by Targeting CNTFRα. Int J Biol Sci [Internet]. 2017 Jan 1 [cited 2022 Oct 20];13(4):413. Available from: /pmc/articles/PMC5436562/

221. Shinde S, Bhadra U. A complex genome-MicroRNA interplay in human mitochondria. Biomed Res Int. 2015;2015.

222. Carrer M, Liu N, Grueter CE, Williams AH, Frisard MI, Hulver MW, et al. Control of mitochondrial metabolism and systemic energy homeostasis by microRNAs 378 and 378*. Proc Natl Acad Sci U S A [Internet]. 2012 Sep 18 [cited 2022 Oct 21];109(38):15330–5. Available from: https://www.pnas.org/doi/abs/10.1073/pnas.1207605109

223. Iwayama T, Steele C, Yao L, Dozmorov MG, Karamichos D, Wren JD, et al. PDGFRα signaling drives adipose tissue fibrosis by targeting progenitor cell plasticity. Genes Dev [Internet]. 2015 Jun 1 [cited 2022 Oct 21];29(11):1106–19. Available from: http://genesdev.cshlp.org/content/29/11/1106.full

224. Glass D, Roubenoff R. Recent advances in the biology and therapy of muscle wasting. Ann N Y Acad Sci [Internet]. 2010 Nov 1 [cited 2018 Sep 6];1211(1):25–36. Available from: http://doi.wiley.com/10.1111/j.1749-6632.2010.05809.x

225. Morvan F, Rondeau JM, Zou C, Minetti G, Scheufler C, Scharenberg M, et al. Blockade of activin type II receptors with a dual anti-ActRIIA/IIB antibody is critical to promote maximal skeletal muscle hypertrophy. Proc Natl Acad Sci U S A [Internet]. 2017 Nov 21 [cited 2022 Oct 21];114(47):12448–53. Available from: https://www.pnas.org/doi/abs/10.1073/pnas.1707925114

226. Passey SL, Hansen MJ, Bozinovski S, McDonald CF, Holland AE, Vlahos R. Emerging therapies for the treatment of skeletal muscle wasting in chronic obstructive pulmonary disease. Pharmacol Ther. 2016 Oct 1;166:56–70.

227. Kemp GJ, Birrell F, Clegg PD, Cuthbertson DJ, de Vito G, van Dieën JH, et al. Developing a toolkit for the assessment and monitoring of musculoskeletal ageing. Age Ageing [Internet]. 2018 Sep 1 [cited 2022 Oct 21];47(suppl_4):iv1–19. Available from: https://academic.oup.com/ageing/article/47/suppl_4/iv1/5091975

228. Blondal T, Jensby Nielsen S, Baker A, Andreasen D, Mouritzen P, Wrang Teilum M, et al. Assessing sample and miRNA profile quality in serum and plasma or other biofluids. Methods. 2013 Jan 1;59(1):S1–6.

229. Siracusa J, Koulmann N, Banzet S. Circulating myomiRs: a new class of biomarkers to monitor skeletal muscle in physiology and medicine [Internet]. Journal of Cachexia, Sarcopenia and Muscle Wiley Blackwell; Feb 1, 2018 p. 20–7. Available from: http://doi.wiley.com/10.1002/jcsm.12227

230. van Rooij E, Kauppinen S. Development of microRNA therapeutics is coming of age. EMBO Mol Med [Internet]. 2014 Jul [cited 2019 Jan 20];6(7):851–64. Available from: http://www.ncbi.nlm.nih.gov/pubmed/24935956

231. Chakraborty C, Sharma AR, Sharma G, Lee SS. Therapeutic advances of miRNAs: A preclinical and clinical update. J Adv Res [Internet]. 2021 Feb 1 [cited 2022 Dec 7];28:127. Available from: /pmc/articles/PMC7753224/

232. Miravirsen works against hepatitis C virus. BMJ [Internet]. 2013 Apr 3 [cited 2022 Oct 21];346. Available from: https://www.bmj.com/content/346/bmj.f2069

233. Chakraborty C, Sharma AR, Sharma G, Doss CGP, Lee SS. Therapeutic miRNA and siRNA: Moving from Bench to Clinic as Next Generation Medicine. Mol Ther Nucleic Acids. 2017 Sep 15;8:132–43.

234. van der Ree MH, van der Meer AJ, van Nuenen AC, de Bruijne J, Ottosen S, Janssen HL, et al. Miravirsen dosing in chronic hepatitis C patients results in decreased microRNA-122 levels without affecting other microRNAs in plasma.

Aliment Pharmacol Ther [Internet]. 2016 Jan 1 [cited 2022 Oct 21];43(1):102–13. Available from: https://onlinelibrary.wiley.com/doi/full/10.1111/apt.13432

235. Bouchie A. First microRNA mimic enters clinic. Nat Biotechnol [Internet]. 2013 [cited 2022 Oct 21];31(7):577. Available from: https://pubmed.ncbi.nlm.nih.gov/23839128/

236. Liang L, He X. A narrative review of microRNA therapeutics: understanding the future of microRNA research. Precis Cancer Med [Internet]. 2021 Dec 30 [cited 2022 Dec 8];4(0). Available from: https://pcm.amegroups.com/article/view/6620/html

237. Rupaimoole R, Slack FJ. MicroRNA therapeutics: towards a new era for the management of cancer and other diseases. 2017 [cited 2018 Oct 15];16(3):203–22. Available from: https://www.nature.com/articles/nrd.2016.246

238. van Rooij E, Purcell AL, Levin AA. Developing MicroRNA therapeutics. Circ Res. 2012;110(3):496–507.

239. Yaffe D, Saxel O. Serial passaging and differentiation of myogenic cells isolated from dystrophic mouse muscle. Nature 1977 270:5639 [Internet]. 1977 Dec 1 [cited 2022 Oct 4];270(5639):725–7. Available from: https://www.nature.com/articles/270725a0

240. Blau HM, Pavlath GK, Hardeman EC, Chiu CP, Silberstein L, Webster SG, et al. Plasticity of the Differentiated State. Science (1979) [Internet]. 1985 Nov 15 [cited 2022 Oct 4];230(4727):758–66. Available from: https://www.science.org/doi/10.1126/science.2414846

241. Bardell DA. microRNA:target interactions in tendinopathy. 2021;

242. Maity B, Sheff D, Fisher RA. Immunostaining: Detection of Signaling Protein Location in Tissues, Cells and Subcellular Compartments. Methods Cell Biol. 2013 Jan 1;113:81–105.

243. Ahn KH, Kim S, Yang M, Lee DW. A Pillar-Based High-Throughput Myogenic Differentiation Assay to Assess Drug Safety. Molecules [Internet]. 2021 Oct 1 [cited 2022 Oct 6];26(19). Available from: https://pubmed.ncbi.nlm.nih.gov/34641349/

244. Clutton G, Mollan K, Hudgens M, Goonetilleke N. A Reproducible, Objective Method Using MitoTracker® Fluorescent Dyes to Assess Mitochondrial Mass in T Cells by Flow Cytometry. Cytometry [Internet]. 2019 Apr 1 [cited 2022 Oct 5];95(4):450. Available from: /pmc/articles/PMC6461488/

245. Sieber-Blum M, Schnell L, Grim M, Hu YF, Schneider R, Schwab ME. Characterization of epidermal neural crest stem cell (EPI-NCSC) grafts in the lesioned spinal cord. Molecular and Cellular Neuroscience. 2006 May 1;32(1–2):67–81.

246. T042-TECHNICAL BULLETIN NanoDrop Spectrophotometers. [cited 2022 Oct 5]; Available from: www.nanodrop.com

247. Stael S, Miller LP, Fernández-Fernández ÁD, van Breusegem F. Detection of Damage-Activated Metacaspase Activity by Western Blot in Plants. Methods in Molecular Biology [Internet]. 2022 [cited 2022 Oct 5];2447:127–37. Available from: https://link.springer.com/protocol/10.1007/978-1-0716-2079-3_11

248. Kõks S, Dogan S, Tuna BG, González-Navarro H, Potter P, Vandenbroucke RE. Mouse models of ageing and their relevance to disease. Mech Ageing Dev. 2016 Dec 1;160:41–53.

249. Motulsky H. Analyzing Data with GraphPad Prism. 1999 [cited 2023 Jan 11]; Available from: www.graphpad.com

250. Singh G, Storey KB. MicroRNA Cues from Nature: A Roadmap to Decipher and Combat Challenges in Human Health and Disease? Cells [Internet]. 2021 Dec 1 [cited 2022 Oct 29];10(12). Available from: /pmc/articles/PMC8699674/

251. Wu XC, Yuan CF, He YM, Zhou ZY, Luo Y, Yang MT, et al. [Chikusetsu saponin Ⅳa ameliorates myocardial hypertrophy of rats through regulating expression of miR199a-5p/Atg5]. Zhongguo Zhong Yao Za Zhi [Internet]. 2021 Oct 1 [cited 2022 Oct 29];46(19):5064–71. Available from: https://pubmed.ncbi.nlm.nih.gov/34738402/

252. Alexander MS, Kawahara G, Motohashi N, Casar JC, Eisenberg I, Myers JA, et al. MicroRNA-199a is induced in dystrophic muscle and affects WNT

signaling, cell proliferation, and myogenic differentiation. Cell Death Differ. 2013;20(9):1194–208.

253. Tsujimura K, Irie K, Nakashima H, Egashira Y, Fukao Y, Fujiwara M, et al. miR-199a Links MeCP2 with mTOR Signaling and Its Dysregulation Leads to Rett Syndrome Phenotypes. Cell Rep. 2015 Sep 22;12(11):1887–901.

254. Song D, Li G, Hong Y, Zhang P, Zhu J, Yang L, et al. miR-199a decreases Neuritin expression involved in the development of Alzheimer's disease in APP/PS1 mice. Int J Mol Med [Internet]. 2020 Jul 1 [cited 2022 Dec 27];46(1):384. Available from: /pmc/articles/PMC7255456/

255. Dobrowolny G, Martone J, Lepore E, Casola I, Petrucci A, Inghilleri M, et al. A longitudinal study defined circulating microRNAs as reliable biomarkers for disease prognosis and progression in ALS human patients. Cell Death Discov [Internet]. 2021 Jun 1 [cited 2023 May 8];7(1). Available from: https://pubmed.ncbi.nlm.nih.gov/33431881/

256. Soriano-Arroquia A, Clegg PD, Molloy AP, Goljanek-Whysall K. Preparation and Culture of Myogenic Precursor Cells/Primary Myoblasts from Skeletal Muscle of Adult and Aged Humans. J Vis Exp [Internet]. 2017 Feb 16 [cited 2022 Jul 27];2017(120):55047. Available from: /pmc/articles/PMC5408649/

257. Fowler EK, Bradley T, Moxon S, Chapman T. Divergence in Transcriptional and Regulatory Responses to Mating in Male and Female Fruitflies. Sci Rep [Internet]. 2019 Dec 1 [cited 2023 Jan 12];9(1). Available from: https://pubmed.ncbi.nlm.nih.gov/31695054/

258. Prüfer K, Stenzel U, Dannemann M, Green RE, Lachmann M, Kelso J. PatMaN: rapid alignment of short sequences to large databases. Bioinformatics [Internet]. 2008 Jul [cited 2023 Jan 12];24(13):1530–1. Available from: https://pubmed.ncbi.nlm.nih.gov/18467344/

259. Love MI, Huber W, Anders S. Moderated estimation of fold change and dispersion for RNA-seq data with DESeq2. Genome Biol [Internet]. 2014 Dec 5 [cited 2023 Jan 12];15(12). Available from: https://pubmed.ncbi.nlm.nih.gov/25516281/

260. Ge SX, Son EW, Yao R. iDEP: an integrated web application for differential expression and pathway analysis of RNA-Seq data. BMC Bioinformatics [Internet]. 2018 Dec 19 [cited 2023 Jan 12];19(1). Available from: https://pubmed.ncbi.nlm.nih.gov/30567491/

261. Metsalu T, Vilo J. ClustVis: a web tool for visualizing clustering of multivariate data using Principal Component Analysis and heatmap. Nucleic Acids Res [Internet]. 2015 [cited 2023 Jan 12];43(W1):W566–70. Available from: https://pubmed.ncbi.nlm.nih.gov/25969447/

262. Benjamini Y, Drai D, Elmer G, Kafkafi N, Golani I. Controlling the false discovery rate in behavior genetics research. Behavioural brain research [Internet]. 2001 Nov 8 [cited 2023 Jan 12];125(1–2):279–84. Available from: https://pubmed.ncbi.nlm.nih.gov/11682119/

263. Kanakis I, Alameddine M, Folkes L, Moxon S, Myrtziou I, Ozanne SE, et al. Small-rna sequencing reveals altered skeletal muscle micrornas and snornas signatures in weanling male offspring from mouse dams fed a low protein diet during lactation. Cells [Internet]. 2021 [cited 2023 Jan 12];10(5). Available from: /pmc/articles/PMC8150574/

264. Huang HY, Lin YCD, Cui S, Huang Y, Tang Y, Xu J, et al. miRTarBase update 2022: an informative resource for experimentally validated miRNA-target interactions. Nucleic Acids Res [Internet]. 2022 Jan 7 [cited 2022 Dec 30];50(D1):D222–30. Available from: https://pubmed.ncbi.nlm.nih.gov/34850920/

265. Nixon KCJ, Rousseau J, Stone MH, Sarikahya M, Ehresmann S, Mizuno S, et al. A Syndromic Neurodevelopmental Disorder Caused by Mutations in SMARCD1, a Core SWI/SNF Subunit Needed for Context-Dependent Neuronal Gene Regulation in Flies. Am J Hum Genet. 2019 Apr 4;104(4):596–610.

266. von Maltzahn J, Chang NC, Bentzinger CF, Rudnicki MA. Wnt Signaling in Myogenesis. Trends Cell Biol [Internet]. 2012 Nov [cited 2022 Dec 27];22(11):602. Available from: /pmc/articles/PMC3479319/

267. Yu Z, Wang AM, Adachi H, Katsuno M, Sobue G, Yue Z, et al. Macroautophagy Is Regulated by the UPR–Mediator CHOP and Accentuates the Phenotype of SBMA Mice. PLoS Genet [Internet]. 2011 Oct [cited 2022 Dec 20];7(10). Available from: /pmc/articles/PMC3192827/

268. Ahmadi A, Khansarinejad B, Hosseinkhani S, Ghanei M, Mowla SJ. miR-199a-5p and miR-495 target GRP78 within UPR pathway of lung cancer. Gene. 2017 Jul 15;620:15–22.

269. Su SF, Chang YW, Andreu-Vieyra C, Fang JY, Yang Z, Han B, et al. miR-30d, miR-181a and miR-199a-5p cooperatively suppress the endoplasmic reticulum chaperone and signaling regulator GRP78 in cancer. Oncogene 2013 32:39 [Internet]. 2012 Oct 22 [cited 2022 Dec 20];32(39):4694–701. Available from: https://www.nature.com/articles/onc2012483

270. Lindholm D, Wootz H, Korhonen L. ER stress and neurodegenerative diseases. Cell Death & Differentiation 2006 13:3 [Internet]. 2006 Jan 6 [cited 2022 Jul 20];13(3):385–92. Available from: https://www.nature.com/articles/4401778

271. Semenza GL. Hypoxia-Inducible Factor 1: Regulator of Mitochondrial Metabolism and Mediator of Ischemic Preconditioning. Biochim Biophys Acta [Internet]. 2011 Jul [cited 2023 Jan 2];1813(7):1263. Available from: /pmc/articles/PMC3010308/

272. Tekirdag KA, Ozturk DG, Gozuacik D. Alteration in Autophagic-lysosomal Potential During Aging and Neurological Diseases: The microRNA Perspective. Curr Pathobiol Rep [Internet]. 2013 Dec 1 [cited 2022 Nov 22];1(4):247–61. Available from: https://link.springer.com/article/10.1007/s40139-013-0031-x

273. Wang Y, Dai YX, Wang SQ, Qiu MK, Quan ZW, Liu Y bin, et al. miR-199a-5p inhibits proliferation and induces apoptosis in hemangioma cells through targeting HIF1A. Int J Immunopathol Pharmacol [Internet]. 2018 Jan 1 [cited 2022 Nov 19];31. Available from: https://journals.sagepub.com/doi/10.1177/0394632017749357

274. Meyers EA, Kessler JA. TGF-β Family Signaling in Neural and Neuronal Differentiation, Development, and Function. Cold Spring Harb Perspect Biol

[Internet]. 2017 [cited 2022 Dec 30];9(8). Available from: /pmc/articles/PMC5538418/

275. Bill W. TGF-beta: A retrograde signaling molecule involved in the formation of neuromuscular junctions in C. elegans. Front Neurosci. 2010;4.

276. Albertson RC, Payne-Ferreira TL, Postlethwait J, Yelick PC. Zebrafish acvr2a and acvr2b exhibit distinct roles in craniofacial development. Developmental Dynamics [Internet]. 2005 Aug 1 [cited 2022 Dec 9];233(4):1405–18. Available from: https://onlinelibrary.wiley.com/doi/full/10.1002/dvdy.20480

277. Bhattacharya TK, Shukla R, Chatterjee RN, Bhanja SK. Comparative analysis of silencing expression of myostatin (MSTN) and its two receptors (ACVR2A and ACVR2B) genes affecting growth traits in knock down chicken. Scientific Reports 2019 9:1 [Internet]. 2019 May 24 [cited 2022 Nov 14];9(1):1–13. Available from: https://www.nature.com/articles/s41598-019-44217-z

278. Senft D, Ronai ZA. UPR, autophagy, and mitochondria crosstalk underlies the ER stress response. Trends Biochem Sci [Internet]. 2015 Mar 1 [cited 2022 Nov 21];40(3):141–8. Available from: http://www.cell.com/article/S0968000415000031/fulltext

279. Gariballa N, Ali BR. Endoplasmic Reticulum Associated Protein Degradation (ERAD) in the Pathology of Diseases Related to TGFβ Signaling Pathway: Future Therapeutic Perspectives. Front Mol Biosci [Internet]. 2020 Oct 29 [cited 2023 Jan 2];7. Available from: /pmc/articles/PMC7658374/

280. Martin L, Latypova X, Wilson CM, Magnaudeix A, Perrin ML, Yardin C, et al. Tau protein kinases: Involvement in Alzheimer's disease. Ageing Res Rev [Internet]. 2013 [cited 2023 Jan 2];12:289–309. Available from: www.elsevier.com/locate/arr

281. Tsuchida K, Nakatani M, Hitachi K, Uezumi A, Sunada Y, Ageta H, et al. Activin signaling as an emerging target for therapeutic interventions. Cell Communication and Signaling [Internet]. 2009 Jun 18 [cited 2023 Jan 2];7(1):1–11. Available from: https://biosignaling.biomedcentral.com/articles/10.1186/1478-811X-7-15

282. MT-ND1 mitochondrially encoded NADH dehydrogenase 1 [Homo sapiens (human)] - Gene - NCBI [Internet]. [cited 2022 Dec 28]. Available from: https://www.ncbi.nlm.nih.gov/gene/4535

283. Shah VO, Scariano J, Waters D, Qualls C, Morgan M, Pickett G, et al. Mitochondrial DNA deletion and sarcopenia. Genet Med [Internet]. 2009 Mar [cited 2023 Jan 2];11(3):147. Available from: /pmc/articles/PMC3737247/

284. Coen PM, Musci R V., Hinkley JM, Miller BF. Mitochondria as a target for mitigating sarcopenia. Frontiers in Physiology. 2019.

285. Rygiel KA, Picard M, Turnbull DM. The Journal of Physiology The ageing neuromuscular system and sarcopenia: a mitochondrial perspective. J Physiol [Internet]. 2016 [cited 2019 May 22];594:4499–512. Available from: https://physoc.onlinelibrary.wiley.com/doi/pdf/10.1113/JP271212

286. Ibebunjo C, Chick JM, Kendall T, Eash JK, Li C, Zhang Y, et al. Genomic and Proteomic Profiling Reveals Reduced Mitochondrial Function and Disruption of the Neuromuscular Junction Driving Rat Sarcopenia. 2013 [cited 2018 Nov 7]; Available from: http://mcb.asm.org/

287. Macpherson PCD, Farshi P, Goldman D. Dach2-Hdac9 signaling regulates reinnervation of muscle endplates. Development (Cambridge) [Internet]. 2015 Dec 1 [cited 2022 Nov 14];142(23):4038–48. Available from: /pmc/articles/PMC4712835/

288. Klingl YE, Pakravan D, van den Bosch L. Opportunities for histone deacetylase inhibition in amyotrophic lateral sclerosis. Br J Pharmacol [Internet]. 2021 Mar 1 [cited 2023 Jan 2];178(6):1353–72. Available from: https://onlinelibrary.wiley.com/doi/full/10.1111/bph.15217

289. Castets P, Ham DJ, Rüegg MA. The TOR Pathway at the Neuromuscular Junction: More Than a Metabolic Player? Front Mol Neurosci. 2020 Aug 28;13:162.

290. Cannataro R, Carbone L, Petro JL, Cione E, Vargas S, Angulo H, et al. Sarcopenia: Etiology, Nutritional Approaches, and miRNAs. Int J Mol Sci

[Internet]. 2021 Sep 1 [cited 2022 Jun 29];22(18):22. Available from: /pmc/articles/PMC8466275/

291. Iyer SR, Shah SB, Lovering RM. The Neuromuscular Junction: Roles in Aging and Neuromuscular Disease. Int J Mol Sci [Internet]. 2021 Aug 1 [cited 2022 Jul 19];22(15). Available from: https://pubmed.ncbi.nlm.nih.gov/34360831/

292. Delbono O, Rodrigues ACZ, Bonilla HJ, Messi ML. The Emerging Role of the Sympathetic Nervous System in Skeletal Muscle Motor Innerfvation and Sarcopenia. Ageing Res Rev [Internet]. 2021 May 1 [cited 2022 Jul 7];67:101305. Available from: /pmc/articles/PMC8049122/

293. Wang L, Zhang L. Emerging Roles of Dysregulated MicroRNAs in Myasthenia Gravis. Front Neurosci [Internet]. 2020 May 21 [cited 2022 Jun 9];14. Available from: /pmc/articles/PMC7253668/

294. Roubenoff R, Hughes VA. Sarcopenia: Current Concepts. J Gerontol A Biol Sci Med Sci [Internet]. 2000 Dec 1 [cited 2018 Sep 6];55(12):M716–24. Available from: https://academic.oup.com/biomedgerontology/article-lookup/doi/10.1093/gerona/55.12.M716

295. Schiaffino S, Reggiani C. Fiber types in Mammalian skeletal muscles. Physiol Rev [Internet]. 2011 Oct [cited 2022 Oct 10];91(4):1447–531. Available from: https://journals.physiology.org/doi/10.1152/physrev.00031.2010

296. Manini TM, Hong SL, Clark BC. Aging and muscle: a neuron's perspective. Curr Opin Clin Nutr Metab Care [Internet]. 2013 Jan [cited 2022 Nov 15];16(1):21–6. Available from: /pmc/articles/PMC3868452/

297. Pratt J, de Vito G, Narici M, Boreham C. Neuromuscular Junction Aging: A Role for Biomarkers and Exercise. The Journals of Gerontology: Series A [Internet]. 2021 Mar 31 [cited 2022 Jul 14];76(4):576–85. Available from: https://academic.oup.com/biomedgerontology/article/76/4/576/5896490

298. Bao Z, Cui C, Chow SKH, Qin L, Wong RMY, Cheung WH. AChRs Degeneration at NMJ in Aging-Associated Sarcopenia–A Systematic Review. Front Aging Neurosci. 2020 Dec 10;12:454.

299. Kwon YN, Yoon SS. Sarcopenia: Neurological Point of View. J Bone Metab [Internet]. 2017 [cited 2022 Nov 15];24(2):83. Available from: /pmc/articles/PMC5472802/

300. Park KHJ. Mechanisms of Muscle Denervation in Aging: Insights from a Mouse Model of Amyotrophic Lateral Sclerosis. Aging Dis [Internet]. 2015 [cited 2022 Jul 15];6(5):380. Available from: /pmc/articles/PMC4567220/

301. McCormick R, Goljanek-Whysall K. MicroRNA Dysregulation in Aging and Pathologies of the Skeletal Muscle. Int Rev Cell Mol Biol. 2017 Jan 1;334:265–308.

302. Morley JE. Pharmacologic Options for the Treatment of Sarcopenia. Calcif Tissue Int [Internet]. 2016 Apr 23 [cited 2019 Sep 5];98(4):319–33. Available from: http://link.springer.com/10.1007/s00223-015-0022-5

303. Ham DJ, Börsch A, Lin S, Thürkauf M, Weihrauch M, Reinhard JR, et al. The neuromuscular junction is a focal point of mTORC1 signaling in sarcopenia. Nat Commun [Internet]. 2020 Dec 1 [cited 2022 Jul 7];11(1). Available from: /pmc/articles/PMC7481251/

304. Vasilaki A, Richardson A, van Remmen H, Brooks S v, Larkin L, McArdle A, et al. Role of nerve-muscle interactions and reactive oxygen species in regulation of muscle proteostasis with ageing. J Physiol [Internet]. 2017 Oct 15 [cited 2018 Oct 1];595(20):6409–15. Available from: http://www.ncbi.nlm.nih.gov/pubmed/28792061

305. Lin IH, Chang JL, Hua K, Huang WC, Hsu MT, Chen YF. Skeletal muscle in aged mice reveals extensive transformation of muscle gene expression. BMC Genet [Internet]. 2018 Dec 8 [cited 2018 Nov 5];19(1):55. Available from: https://bmcgenet.biomedcentral.com/articles/10.1186/s12863-018-0660-5

306. Wilkinson DJ, Piasecki M, Atherton PJ. The age-related loss of skeletal muscle mass and function: Measurement and physiology of muscle fibre atrophy and muscle fibre loss in humans. Ageing Res Rev [Internet]. 2018 [cited 2018 Sep 6];47:123–32. Available from: https://doi.org/10.1016/j.arr.2018.07.005

307. Su J, Ekman C, Oskolkov N, Lahti L, Ström K, Brazma A, et al. A novel atlas of gene expression in human skeletal muscle reveals molecular changes associated with aging. Skelet Muscle [Internet]. 2015 [cited 2018 Nov 6];5:35. Available from: http://www.ncbi.nlm.nih.gov/pubmed/26457177

308. Jung HJ, Lee KP, Kwon KS, Suh Y. MicroRNAs in Skeletal Muscle Aging: Current Issues and Perspectives. Vol. 74, Journals of Gerontology - Series A Biological Sciences and Medical Sciences. Oxford University Press; 2019. p. 1008–14.

309. Proctor CJ, Goljanek-Whysall K. Using computer simulation models to investigate the most promising microRNAs to improve muscle regeneration during ageing. Scientific Reports 2017 7:1 [Internet]. 2017 Sep 26 [cited 2022 Oct 24];7(1):1–12. Available from: https://www.nature.com/articles/s41598-017-12538-6

310. Noronha O, Mesarosovo L, Anink JJ, Iyer A, Aronica E, Mills JD. Differentially Expressed miRNAs in Age-Related Neurodegenerative Diseases: A Meta-Analysis. Genes (Basel) [Internet]. 2022 Jun 9 [cited 2022 Aug 3];13(6):1034. Available from: /pmc/articles/PMC9222420/

311. Banack SA, Dunlop RA, Cox PA. An miRNA fingerprint using neural-enriched extracellular vesicles from blood plasma: towards a biomarker for amyotrophic lateral sclerosis/motor neuron disease. Open Biol [Internet]. 2020 [cited 2022 Dec 13];10(6). Available from: /pmc/articles/PMC7333885/

312. Sharma M, Juvvuna PK, Kukreti H, McFarlane C. Mega roles of microRNAs in regulation of skeletal muscle health and disease. Frontiers in Physiology. 2014.

313. Gheinani AH, Burkhard FC, Rehrauer H, Fournier CA, Monastyrskaya K. MicroRNA MiR-199a-5p regulates smooth muscle cell proliferation and morphology by targeting WNT2 signaling pathway. Journal of Biological Chemistry [Internet]. 2015 Mar 13 [cited 2020 Sep 30];290(11):7067–86. Available from: https://pubmed.ncbi.nlm.nih.gov/25596533/

314. Wang Y, Lu J, Liu Y. Skeletal Muscle Regeneration in Cardiotoxin-Induced Muscle Injury Models. Int J Mol Sci [Internet]. 2022 Nov 2 [cited 2022 Dec 13];23(21):13380. Available from: /pmc/articles/PMC9657523/

315. Jia B, Liu Y, Li Q, Zhang J, Ge C, Wang G, et al. Altered miRNA and mRNA Expression in Sika Deer Skeletal Muscle with Age. Genes 2020, Vol 11, Page 172 [Internet]. 2020 Feb 6 [cited 2022 Aug 3];11(2):172. Available from: https://www.mdpi.com/2073-4425/11/2/172/htm

316. Shi L, Han Q, Hong Y, Li W, Gong G, Cui J, et al. Inhibition of miR-199a-5p rejuvenates aged mesenchymal stem cells derived from patients with idiopathic pulmonary fibrosis and improves their therapeutic efficacy in experimental pulmonary fibrosis. Stem Cell Res Ther [Internet]. 2021 Dec 1 [cited 2022 Aug 10];12(1). Available from: /pmc/articles/PMC7905557/

317. Li Z, Song Y, Liu L, Hou N, An X, Zhan D, et al. miR-199a impairs autophagy and induces cardiac hypertrophy through mTOR activation. Cell Death & Differentiation 2017 24:7 [Internet]. 2015 Jul 10 [cited 2022 Nov 22];24(7):1205–13. Available from: https://www.nature.com/articles/cdd201595

318. Yang X, Zheng Y, Tan J, Tian R, Shen P, Cai W, et al. MiR-199a-5p–HIF-1α-STAT3 Positive Feedback Loop Contributes to the Progression of Non-Small Cell Lung Cancer. Front Cell Dev Biol. 2021 Feb 18;8:1931.

319. Zhao B, Huang M, Bai Y, Fan C, Fan Y, Jin Y. Identification of differentially expressed miRNAs in mouse spinal cord development. Acta Biochim Biophys Sin (Shanghai) [Internet]. 2015 Mar 1 [cited 2022 Aug 3];47(3):224–9. Available from: https://academic.oup.com/abbs/article/47/3/224/1754871

320. Martinez B, Peplow P. MicroRNAs in blood and cerebrospinal fluid as diagnostic biomarkers of multiple sclerosis and to monitor disease progression. Neural Regen Res [Internet]. 2020 Apr 1 [cited 2022 Aug 3];15(4):606. Available from: /pmc/articles/PMC6975152/

321. Lu H, Yang Y, Ou S, Qi Y, Li G, He H, et al. The silencing of miR-199a-5p protects the articular cartilage through MAPK4 in osteoarthritis. Ann Transl

Med [Internet]. 2022 May [cited 2022 Aug 9];10(10):601–601. Available from: /pmc/articles/PMC9201181/

322. Diokmetzidou A, Tsikitis M, Nikouli S, Kloukina I, Tsoupri E, Papathanasiou S, et al. Strategies to Study Desmin in Cardiac Muscle and Culture Systems. Methods Enzymol. 2016 Jan 1;568:427–59.

323. Goljanek-Whysall K, Pais H, Rathjen T, Sweetman D, Dalmay T, Münsterberg A. Regulation of multiple target genes by miR-1 and miR-206 is pivotal for C2C12 myoblast differentiation. J Cell Sci [Internet]. 2012 Aug 1 [cited 2023 Jan 13];125(15):3590–600. Available from: https://journals.biologists.com/jcs/article/125/15/3590/32411/Regulation-of-multiple-target-genes-by-miR-1-and

324. Maier O, Böhm J, Dahm M, Brück S, Beyer C, Johann S. Differentiated NSC-34 motoneuron-like cells as experimental model for cholinergic neurodegeneration. Neurochem Int [Internet]. 2013 Jun 1 [cited 2019 Feb 22];62(8):1029–38. Available from: https://www.sciencedirect.com/science/article/pii/S0197018613001010?via%3Dihub

325. Walter LA, Blake LP, Gallot YS, Arends CJ, Sozio RS, Onifer SM, et al. Effect of Denervation on XBP1 in Skeletal Muscle and the Neuromuscular Junction. Int J Mol Sci [Internet]. 2021 Jan 1 [cited 2022 Jul 11];23(1). Available from: https://pubmed.ncbi.nlm.nih.gov/35008595/

326. He S, Fu T, Yu Y, Liang Q, Li L, Liu J, et al. IRE1α regulates skeletal muscle regeneration through myostatin mRNA decay. J Clin Invest [Internet]. 2021 Sep 9 [cited 2022 Jul 11];131(17). Available from: /pmc/articles/PMC8409588/

327. Abdullahi A, Stanojcic M, Parousis A, Patsouris D, Jeschke MG. Modeling Acute ER stress in vivo and in vitro. Shock [Internet]. 2017 Apr 1 [cited 2022 Oct 25];47(4):506. Available from: /pmc/articles/PMC5348263/

328. Quan X, Wang J, Liang C, Zheng H, Zhang L. Melatonin inhibits tunicamycin-induced endoplasmic reticulum stress and insulin resistance in skeletal muscle cells. Biochem Biophys Res Commun. 2015 Aug 7;463(4):1102–7.

329. Kennedy D, Samali A, Jäger R. Methods for studying ER stress and UPR markers in human cells. Methods in Molecular Biology [Internet]. 2015 [cited 2023 Mar 21];1292:3–18. Available from: https://link.springer.com/protocol/10.1007/978-1-4939-2522-3_1

330. Zeng N, Huang YQ, Yan YM, Hu ZQ, Zhang Z, Feng JX, et al. Diverging targets mediate the pathological role of miR-199a-5p and miR-199a-3p by promoting cardiac hypertrophy and fibrosis. Mol Ther Nucleic Acids. 2021 Dec 3;26:1035–50.

331. Ye X, Zhou XJ, Zhang H. Exploring the Role of Autophagy-Related Gene 5 (ATG5) Yields Important Insights Into Autophagy in Autoimmune/Autoinflammatory Diseases. Front Immunol [Internet]. 2018 Oct 17 [cited 2022 Dec 15];9(OCT):2334. Available from: /pmc/articles/PMC6199349/

332. Hwang HJ, Ha H, Lee BS, Kim BH, Song HK, Kim YK. LC3B is an RNA-binding protein to trigger rapid mRNA degradation during autophagy. Nature Communications 2022 13:1 [Internet]. 2022 Mar 17 [cited 2022 Dec 12];13(1):1–17. Available from: https://www.nature.com/articles/s41467-022-29139-1

333. Hu YD, Pang HZ, Li DS, Ling SS, Lan D, Wang Y, et al. Analysis of the cytochrome c oxidase subunit 1 (COX1) gene reveals the unique evolution of the giant panda. Gene. 2016 Nov 5;592(2):303–7.

334. Bonawitz ND, Clayton DA, Shadel GS. Initiation and Beyond: Multiple Functions of the Human Mitochondrial Transcription Machinery. Mol Cell. 2006 Dec 28;24(6):813–25.

335. Ma Q. Role of Nrf2 in Oxidative Stress and Toxicity. Annu Rev Pharmacol Toxicol [Internet]. 2013 Jan [cited 2022 Nov 21];53:401. Available from: /pmc/articles/PMC4680839/

336. TargetscanHuman 7.2: predicted miRNA targets of miR-199-5p [Internet]. [cited 2022 Dec 16]. Available from: https://www.targetscan.org/cgi-bin/targetscan/vert_72/targetscan.cgi?species=Mouse&gid=&mir_sc=&mir_c=&mir_nc=&mir_vnc=&mirg=miR-199a-5p

337. Song J, Gao L, Yang G, Tang S, Xie H, Wang Y, et al. MiR-199a Regulates Cell Proliferation and Survival by Targeting FZD7. PLoS One [Internet]. 2014 Oct 14 [cited 2022 Jul 21];9(10):110074. Available from: /pmc/articles/PMC4196968/

338. Giakoumaki I, Pollock N, Aljuaid T, Sannicandro AJ, Alameddine M, Owen E, et al. Postnatal Protein Intake as a Determinant of Skeletal Muscle Structure and Function in Mice—A Pilot Study. International Journal of Molecular Sciences 2022, Vol 23, Page 8815 [Internet]. 2022 Aug 8 [cited 2022 Aug 30];23(15):8815. Available from: https://www.mdpi.com/1422-0067/23/15/8815/htm

339. Jeong J, Conboy IM. Phosphatidylserine directly and positively regulates fusion of myoblasts into myotubes. Biochem Biophys Res Commun [Internet]. 2011 Oct 10 [cited 2022 Nov 1];414(1):9. Available from: /pmc/articles/PMC3195849/

340. Wang J, Yang LZ, Zhang JS, Gong JX, Wang YH, Zhang CL, et al. Effects of microRNAs on skeletal muscle development. Gene. 2018 Aug 20;668:107–13.

341. Lin HS, Gong JN, Su R, Chen MT, Song L, Shen C, et al. miR-199a-5p inhibits monocyte/macrophage differentiation by targeting the activin A type 1B receptor gene and finally reducing C/EBPα expression. J Leukoc Biol [Internet]. 2014 Dec 1 [cited 2022 Dec 19];96(6):1023–35. Available from: https://onlinelibrary.wiley.com/doi/full/10.1189/jlb.1A0514-240R

342. Saclier M, Yacoub-Youssef H, Mackey AL, Arnold L, Ardjoune H, Magnan M, et al. Differentially activated macrophages orchestrate myogenic precursor cell fate during human skeletal muscle regeneration. Stem Cells [Internet]. 2020 Feb [cited 2022 Dec 19];31(2):384–96. Available from: https://air.unimi.it/handle/2434/735659

343. Zhang X, Li H, He M, Wang J, Wu Y, Li Y. Immune system and sarcopenia: Presented relationship and future perspective. Exp Gerontol. 2022 Jul 1;164:111823.

344. Singh GB, Cowan DB, Wang DZ. Tiny Regulators of Massive Tissue: MicroRNAs in Skeletal Muscle Development, Myopathies, and Cancer Cachexia. Front Oncol. 2020 Nov 23;10:2647.

345. Kuroda K, Kuang S, Taketo MM, Rudnicki MA. Canonical Wnt signaling induces BMP-4 to specify slow myofibrogenesis of fetal myoblasts. Skelet Muscle [Internet]. 2013 Dec 5 [cited 2022 Dec 19];3(1):1–13. Available from: https://skeletalmusclejournal.biomedcentral.com/articles/10.1186/2044-5040-3-5

346. Boëx M, Messéant J, Bauché S, Fontaine B, Legay C, Strochlic L. Regulation of mammalian neuromuscular junction formation and maintenance by Wnt signaling. Curr Opin Physiol. 2018 Aug 1;4:88–95.

347. Gallot YS, Bohnert KR. Confounding Roles of ER Stress and the Unfolded Protein Response in Skeletal Muscle Atrophy. Int J Mol Sci [Internet]. 2021 Mar 1 [cited 2022 Jul 21];22(5):1–18. Available from: /pmc/articles/PMC7961896/

348. Baehr LM, West DWD, Marcotte G, Marshall AG, de Sousa LG, Baar K, et al. Age-related deficits in skeletal muscle recovery following disuse are associated with neuromuscular junction instability and ER stress, not impaired protein synthesis. Aging (Albany NY) [Internet]. 2016 [cited 2022 Jul 12];8(1):127. Available from: /pmc/articles/PMC4761718/

349. Oslowski CM, Urano F. Measuring ER stress and the unfolded protein response using mammalian tissue culture system. Methods Enzymol [Internet]. 2011 [cited 2022 Nov 14];490(C):71. Available from: /pmc/articles/PMC3701721/

350. Orang AV, Safaralizadeh R, Kazemzadeh-Bavili M. Mechanisms of miRNA-Mediated Gene Regulation from Common Downregulation to mRNA-Specific Upregulation. Int J Genomics [Internet]. 2014 [cited 2023 Jan 17];2014. Available from: /pmc/articles/PMC4142390/

351. Pfaffenbach KT, Pong M, Morgan TE, Wang H, Ott K, Zhou B, et al. GRP78/BiP is a Novel Downstream Target of IGF-1 Receptor Mediated

Signaling. J Cell Physiol [Internet]. 2012 Dec [cited 2023 Jan 17];227(12):3803. Available from: /pmc/articles/PMC3421054/

352. Kadowaki H, Nishitoh H. Signaling Pathways from the Endoplasmic Reticulum and Their Roles in Disease. Genes (Basel) [Internet]. 2013 Sep [cited 2022 Nov 2];4(3):306. Available from: /pmc/articles/PMC3924831/

353. Hetz C. The unfolded protein response: controlling cell fate decisions under ER stress and beyond. Nature Reviews Molecular Cell Biology 2012 13:2 [Internet]. 2012 Jan 18 [cited 2022 Nov 8];13(2):89–102. Available from: https://www.nature.com/articles/nrm3270

354. Afroze D, Kumar A. ER Stress in Skeletal Muscle Remodeling and Myopathies. FEBS J [Internet]. 2019 Jan 1 [cited 2022 Dec 20];286(2):379. Available from: /pmc/articles/PMC6002870/

355. Malhotra JD, Kaufman RJ. ER Stress and Its Functional Link to Mitochondria: Role in Cell Survival and Death. Cold Spring Harb Perspect Biol [Internet]. 2011 [cited 2022 Nov 8];3(9):1–13. Available from: /pmc/articles/PMC3181038/

356. Reed JC, Jurgensmeier JM, Matsuyama S. Bcl-2 family proteins and mitochondria. Biochimica et Biophysica Acta (BBA) - Bioenergetics. 1998 Aug 10;1366(1–2):127–37.

357. Boengler K, Kosiol M, Mayr M, Schulz R, Rohrbach S. Mitochondria and ageing: role in heart, skeletal muscle and adipose tissue. Vol. 8, Journal of Cachexia, Sarcopenia and Muscle. 2017.

358. Kaspar S, Oertlin C, Szczepanowska K, Kukat A, Senft K, Lucas C, et al. Adaptation to mitochondrial stress requires CHOP-directed tuning of ISR. Sci Adv [Internet]. 2021 May 1 [cited 2022 Nov 14];7(22):971–97. Available from: /pmc/articles/PMC8153728/

359. Anagnostou ME, Hepple RT. Mitochondrial Mechanisms of Neuromuscular Junction Degeneration with Aging. Cells [Internet]. 2020 Jan 13 [cited 2022 Nov 15];9(1). Available from: /pmc/articles/PMC7016881/

360. Lucioli S, Hoffmeier K, Carrozzo R, Tessa A, Ludwig B, Santorelli FM. Introducing a novel human mtDNA mutation into the Paracoccus denitrificans COX I gene explains functional deficits in a patient. Neurogenetics [Internet]. 2006 Mar 12 [cited 2022 Nov 15];7(1):51–7. Available from: https://link.springer.com/article/10.1007/s10048-005-0015-z

361. Liang H, Ward WF. PGC-1α: A key regulator of energy metabolism. American Journal of Physiology - Advances in Physiology Education [Internet]. 2006 [cited 2022 Nov 15];30(4):145–51. Available from: https://journals.physiology.org/doi/10.1152/advan.00052.2006

362. Chan YC, Roy S, Huang Y, Khanna S, Sen CK. The microRNA miR-199a-5p down-regulation switches on wound angiogenesis by derepressing the v-ets erythroblastosis virus E26 oncogene homolog 1-matrix metalloproteinase-1 pathway. Journal of Biological Chemistry [Internet]. 2012 Nov 30 [cited 2022 Dec 20];287(49):41032–43. Available from: http://www.jbc.org/article/S0021925820439067/fulltext

363. Dobrowolny G, Barbiera A, Sica G, Scicchitano BM. Age-Related Alterations at Neuromuscular Junction: Role of Oxidative Stress and Epigenetic Modifications. Cells [Internet]. 2021 Jun 1 [cited 2022 Dec 20];10(6). Available from: https://pubmed.ncbi.nlm.nih.gov/34074012/

364. Rodríguez Cruz PM, Cossins J, Beeson D, Vincent A. The Neuromuscular Junction in Health and Disease: Molecular Mechanisms Governing Synaptic Formation and Homeostasis. Front Mol Neurosci [Internet]. 2020 Dec 3 [cited 2022 Jul 21];13. Available from: https://pubmed.ncbi.nlm.nih.gov/33343299/

365. Gonzalez-Freire M, de Cabo R, Studenski SA, Ferrucci L. The Neuromuscular Junction: Aging at the Crossroad between Nerves and Muscle. Front Aging Neurosci [Internet]. 2014 [cited 2022 Nov 14];6(AUG). Available from: /pmc/articles/PMC4127816/

366. Holahan MR. GAP-43 in synaptic plasticity: molecular perspectives. Res Rep Biochem [Internet]. 2015 Jun 18 [cited 2022 Nov 14];5:137–46. Available from: https://www.dovepress.com/gap-43-in-synaptic-plasticity-molecular-perspectives-peer-reviewed-fulltext-article-RRBC

367. Zhang H, Wu F, Kong X, Yang J, Chen H, Deng L, et al. Nerve growth factor improves functional recovery by inhibiting endoplasmic reticulum stress-induced neuronal apoptosis in rats with spinal cord injury. J Transl Med [Internet]. 2014 May 15 [cited 2022 Jun 29];12(1):1–15. Available from: https://translational-medicine.biomedcentral.com/articles/10.1186/1479-5876-12-130

368. Guarnieri S, Morabito C, Paolini C, Boncompagni S, Pilla R. Growth Associated Protein 43 Is Expressed in Skeletal Muscle Fibers and Is Localized in Proximity of Mitochondria and Calcium Release Units. PLoS One [Internet]. 2013 [cited 2020 Feb 3];8(1):53267. Available from: www.plosone.org

369. Tang H, Goldman D. Activity-dependent gene regulation in skeletal muscle is mediated by a histone deacetylase (HDAC)-Dach2-myogenin signal transduction cascade. Proc Natl Acad Sci U S A [Internet]. 2006 Nov 7 [cited 2022 Nov 14];103(45):16977–82. Available from: https://www.pnas.org/doi/abs/10.1073/pnas.0601565103

370. Li L, Xiong WC, Mei L. Neuromuscular Junction Formation, Aging, and Disorders. https://doi.org/101146/annurev-physiol-022516-034255 [Internet]. 2018 Feb 12 [cited 2022 Aug 4];80:159–88. Available from: https://www.annualreviews.org/doi/abs/10.1146/annurev-physiol-022516-034255

371. Hunter SK, Pereira XHM, Keenan KG. The aging neuromuscular system and motor performance. J Appl Physiol [Internet]. 2016 Oct 1 [cited 2022 Nov 15];121(4):982–95. Available from: https://journals.physiology.org/doi/10.1152/japplphysiol.00475.2016

372. Piasecki J, Inns TB, Bass JJ, Scott R, Stashuk DW, Phillips BE, et al. Influence of sex on the age-related adaptations of neuromuscular function and motor unit properties in elite masters athletes. J Physiol [Internet]. 2021 Jan 1 [cited 2022 Dec 8];599(1):193–205. Available from: https://onlinelibrary.wiley.com/doi/full/10.1113/JP280679

373. Roberts BM, Lavin KM, Many GM, Thalacker-Mercer A, Merritt EK, Bickel CS, et al. Human neuromuscular aging: Sex differences revealed at the

myocellular level. Exp Gerontol [Internet]. 2018 Jun 1 [cited 2022 Dec 8];106:116. Available from: /pmc/articles/PMC6031257/

374. Li S, Overman JJ, Katsman D, Kozlov S v., Donnelly CJ, Twiss JL, et al. An age-related sprouting transcriptome provides molecular control of axonal sprouting after stroke. Nat Neurosci [Internet]. 2010 Dec [cited 2022 Dec 8];13(12):1496–506. Available from: https://pubmed.ncbi.nlm.nih.gov/21057507/

375. Riascos D, Nicholas A, Samaeekia R, Yukhnanov R, Mesulam MM, Bigio EH, et al. Alterations of Ca 2+ responsive proteins within cholinergic neurons in aging and AD. Neurobiol Aging. 2014;35(6):1325–33.

376. Mellios N, Feldman DA, Sheridan SD, Ip JPK, Kwok S, Amoah SK, et al. MeCP2-regulated miRNAs control early human neurogenesis through differential effects on ERK and AKT signaling HHS Public Access. Mol Psychiatry [Internet]. 2018 [cited 2022 Nov 15];23(4):1051–65. Available from: http://www.nature.com/authors/editorial_policies/license.html#terms

377. Zhang PX, Cheng J, Zou S, D'Souza AD, Koff JL, Lu J, et al. Pharmacological modulation of the AKT/microRNA-199a-5p/CAV1 pathway ameliorates cystic fibrosis lung hyper-inflammation. Nat Commun [Internet]. 2015 Feb 10 [cited 2022 Jul 15];6:6221. Available from: /pmc/articles/PMC4324503/

378. Bodine SC, Stitt TN, Gonzalez M, Kline WO, Stover GL, Bauerlein R, et al. Akt/mTOR pathway is a crucial regulator of skeletal muscle hypertrophy and can prevent muscle atrophy in vivo. Nature Cell Biology 2001 3:11 [Internet]. 2001 Oct 10 [cited 2022 Nov 15];3(11):1014–9. Available from: https://www.nature.com/articles/ncb1101-1014

379. Keilhoff G, Lucas B, Fansa H, Fansa H. Selected gene profiles of stressed NSC-34 cells and rat spinal cord following peripheral nerve reconstruction and minocycline treatment. Exp Ther Med [Internet]. 2016 May 1 [cited 2022 Nov 15];11(5):1685–99. Available from: http://www.spandidos-publications.com/10.3892/etm.2016.3130/abstract

380. Yadav RK, Chae SW, Kim HR, Chae HJ. Endoplasmic Reticulum Stress and Cancer. J Cancer Prev [Internet]. 2014 Jun 30 [cited 2023 Jan 17];19(2):75. Available from: /pmc/articles/PMC4204165/

381. Rossaert E, Pollari E, Jaspers T, van Helleputte L, Jarpe M, van Damme P, et al. Restoration of histone acetylation ameliorates disease and metabolic abnormalities in a FUS mouse model. Acta Neuropathol Commun [Internet]. 2019 Jul 5 [cited 2022 Dec 9];7(1):107. Available from: https://actaneurocomms.biomedcentral.com/articles/10.1186/s40478-019-0750-2

382. Hua YJ, Tang ZY, Tu K, Zhu L, Li YX, Xie L, et al. Identification and target prediction of miRNAs specifically expressed in rat neural tissue. BMC Genomics [Internet]. 2009 May 9 [cited 2022 Dec 12];10(1):1–12. Available from: https://bmcgenomics.biomedcentral.com/articles/10.1186/1471-2164-10-214

383. Liu G, Detloff MR, Miller KN, Santi L, Houlé JD. Exercise modulates microRNAs that affect the PTEN/mTOR pathway in rats after spinal cord injury. Exp Neurol. 2012 Jan 1;233(1):447–56.

384. Wang B, Huang M, Shang D, Yan X, Zhao B, Zhang X. Mitochondrial Behavior in Axon Degeneration and Regeneration. Front Aging Neurosci. 2021 Mar 8;13:103.

385. Hounoum BM, Vourc'h P, Felix R, Corcia P, Patin F, Guéguinou M, et al. NSC-34 motor neuron-like cells are unsuitable as experimental model for glutamate-mediated excitotoxicity. Front Cell Neurosci. 2016 May 9;10(MAY):118.

386. Gagliardi D, Bresolin N, Comi G pietro, Corti S. Extracellular vesicles and amyotrophic lateral sclerosis: from misfolded protein vehicles to promising clinical biomarkers. Cellular and Molecular Life Sciences [Internet]. 2021 Jan 1 [cited 2022 Nov 19];78(2):561. Available from: /pmc/articles/PMC7872995/

387. Riehl LM, Schulte JH, Mulaw MA, Dahlhaus M, Fischer M, Schramm A, et al. The mitochondrial genetic landscape in neuroblastoma from tumor initiation to

relapse. Oncotarget [Internet]. 2016 Feb 2 [cited 2022 Dec 9];7(6):6620. Available from: /pmc/articles/PMC4872737/

388. Kim T, Croce CM. MicroRNA and ER stress in cancer. Semin Cancer Biol. 2021 Oct 1;75:3–14.

389. Leiva-Rodríguez T, Romeo-Guitart D, Herrando-Grabulosa M, Muñoz-Guardiola P, Polo M, Bañuls C, et al. Grp78 overexpression triggers pink1-ip3 r-mediated neuroprotective mitophagy. Biomedicines. 2021 Aug 1;9(8).

390. Kumar Bhat R, Acharjee S, Ellestad KK. Neuroinflammation and Endoplasmic Reticulum Stress Are Coregulated by Crocin To Prevent Demyelination and Neurodegeneration Mesenchymal Stem Cell Based Therapy in Acute Pancreatitis View project Caspase-6 and Alzheimer disease View project. Article in The Journal of Immunology [Internet]. 2011 [cited 2022 Nov 19]; Available from: www.jimmunol.org/cgi/doi/10.4049/jimmunol.1004111

391. Li F, Liang J, Tong H, Zhu S, Tang D. Inhibition of microRNA-199a-5p ameliorates oxygen-glucose deprivation/reoxygenation-induced apoptosis and oxidative stress in HT22 neurons by targeting Brg1 to activate Nrf2/HO-1 signalling. Clin Exp Pharmacol Physiol [Internet]. 2020 Jun 1 [cited 2022 Nov 21];47(6):1020–9. Available from: https://onlinelibrary.wiley.com/doi/full/10.1111/1440-1681.13265

392. Kitaoka Y, Tamura Y, Takahashi K, Takeda K, Takemasa T, Hatta H. Effects of Nrf2 deficiency on mitochondrial oxidative stress in aged skeletal muscle. Physiol Rep. 2019 Feb 1;7(3).

393. Lv H ran. lncRNA-Map2k4 sequesters miR-199a to promote FGF1 expression and spinal cord neuron growth. Biochem Biophys Res Commun. 2017 Aug 26;490(3):948–54.

394. microRNA-199a-5p mediates high glucose-induced reactive oxygen species production and apoptosis in INS-1 pancreatic β-cells by targeting SIRT1 [Internet]. [cited 2022 Nov 21]. Available from: https://www.europeanreview.org/article/12333

395. Rane S, He M, Sayed D, Vashistha H, Malhotra A, Sadoshima J, et al. Downregulation of MiR-199a Derepresses Hypoxia-Inducible Factor-1α and Sirtuin 1 and Recapitulates Hypoxia Preconditioning in Cardiac Myocytes. Circ Res [Internet]. 2009 Apr 10 [cited 2022 Nov 21];104(7):879–86. Available from: https://www.ahajournals.org/doi/abs/10.1161/CIRCRESAHA.108.193102

396. Zhou Y, Jia WK, Jian Z, Zhao L, Liu CC, Wang Y, et al. Downregulation of microRNA-199a-5p protects cardiomyocytes in cyanotic congenital heart disease by attenuating endoplasmic reticulum stress. Mol Med Rep [Internet]. 2017 Sep 1 [cited 2022 Jul 22];16(3):2992–3000. Available from: http://www.spandidos-publications.com/10.3892/mmr.2017.6934/abstract

397. Avalle L, Camporeale A, Morciano G, Caroccia N, Ghetti E, Orecchia V, et al. STAT3 localizes to the ER, acting as a gatekeeper for ER-mitochondrion Ca 2+ fluxes and apoptotic responses. Cell Death Differ [Internet]. 2019 May 1 [cited 2022 Aug 10];26(5):932–42. Available from: https://pubmed.ncbi.nlm.nih.gov/30042492/

398. Franco-Iborra S, Cuadros T, Parent A, Romero-Gimenez J, Vila M, Perier C. Defective mitochondrial protein import contributes to complex I-induced mitochondrial dysfunction and neurodegeneration in Parkinson's disease. Cell Death Dis [Internet]. 2018 Nov 1 [cited 2020 Oct 14];9(11). Available from: https://pubmed.ncbi.nlm.nih.gov/30405116/

399. Aksu-Menges E, Akkaya-Ulum YZ, Dayangac-Erden D, Balci-Peynircioglu B, Yuzbasioglu A, Topaloglu H, et al. The Common miRNA Signatures Associated with Mitochondrial Dysfunction in Different Muscular Dystrophies. American Journal of Pathology [Internet]. 2020 Oct 1 [cited 2022 Nov 21];190(10):2136–45. Available from: http://ajp.amjpathol.org/article/S0002944020303308/fulltext

400. Mattson MP, Gleichmann M, Cheng A. Mitochondria in Neuroplasticity and Neurological Disorders. Neuron [Internet]. 2008 Dec 10 [cited 2022 Nov 21];60(5):748–66. Available from: http://www.cell.com/article/S0896627308008532/fulltext

401. Norat P, Soldozy S, Sokolowski JD, Gorick CM, Kumar JS, Chae Y, et al. Mitochondrial dysfunction in neurological disorders: Exploring mitochondrial transplantation. npj Regenerative Medicine 2020 5:1 [Internet]. 2020 Nov 23 [cited 2022 Dec 12];5(1):1–9. Available from: https://www.nature.com/articles/s41536-020-00107-x

402. Harmuth T, Prell-Schicker C, Weber JJ, Gellerich F, Funke C, Drießen S, et al. Mitochondrial Morphology, Function and Homeostasis Are Impaired by Expression of an N-terminal Calpain Cleavage Fragment of Ataxin-3. Front Mol Neurosci. 2018 Oct 10;11:368.

403. Aigner L, Arber S, Kapfhammer JP, Laux T, Schneider C, Botteri F, et al. Overexpression of the neural growth-associated protein GAP-43 induces nerve sprouting in the adult nervous system of transgenic mice. Cell. 1995 Oct 20;83(2):269–78.

404. Chung D, Shum A, Caraveo G. GAP-43 and BASP1 in Axon Regeneration: Implications for the Treatment of Neurodegenerative Diseases. Front Cell Dev Biol. 2020 Sep 3;8:890.

405. Rambold AS, Lippincott-Schwartz J. Mechanisms of mitochondria and autophagy crosstalk. Cell Cycle [Internet]. 2011 Dec 12 [cited 2022 Nov 21];10(23):4032. Available from: /pmc/articles/PMC3272286/

406. Rambold AS, Lippincott-Schwartz J. Mechanisms of mitochondria and autophagy crosstalk. Cell Cycle [Internet]. 2011 Dec 12 [cited 2022 Nov 22];10(23):4032. Available from: /pmc/articles/PMC3272286/

407. Tanida I, Waguri S. Measurement of autophagy in cells and tissues. Methods in Molecular Biology [Internet]. 2010 [cited 2022 Dec 12];648:193–214. Available from: https://link.springer.com/protocol/10.1007/978-1-60761-756-3_13

408. von Haehling S, Morley JE, Anker SD. An overview of sarcopenia: facts and numbers on prevalence and clinical impact. J Cachexia Sarcopenia Muscle [Internet]. 2010 [cited 2023 Jan 4];1(2):129. Available from: /pmc/articles/PMC3060646/

409. Miller RA. “Accelerated aging”: a primrose path to insight? Aging Cell [Internet]. 2004 Apr [cited 2023 Jan 4];3(2):47–51. Available from: https://pubmed.ncbi.nlm.nih.gov/15038817/

410. Pradat PF, Barani A, Wanschitz J, Dubourg O, Lombès A, Bigot A, et al. Abnormalities of satellite cells function in amyotrophic lateral sclerosis. Amyotroph Lateral Scler [Internet]. 2011 Jul [cited 2023 Jan 4];12(4):264–71. Available from: https://pubmed.ncbi.nlm.nih.gov/21473708/

411. Xu J, Wan CS, Ktoris K, Reijnierse EM, Maier AB. Sarcopenia Is Associated with Mortality in Adults: A Systematic Review and Meta-Analysis. Gerontology [Internet]. 2022 May 1 [cited 2023 Jan 4];68(4):361–76. Available from: https://www.karger.com/Article/FullText/517099

412. Xie W qing, He M, Yu D jie, Wu Y xiang, Wang X hua, Lv S, et al. Mouse models of sarcopenia: classification and evaluation. J Cachexia Sarcopenia Muscle [Internet]. 2021 Jun 1 [cited 2022 Dec 22];12(3):538. Available from: /pmc/articles/PMC8200444/

413. Christian CJ, Benian GM. Animal models of sarcopenia. Aging Cell [Internet]. 2020 Oct 1 [cited 2022 Dec 22];19(10):e13223. Available from: https://onlinelibrary.wiley.com/doi/full/10.1111/acel.13223

414. Yin J, Qian Z, Chen Y, Li Y, Zhou X. MicroRNA regulatory networks in the pathogenesis of sarcopenia. J Cell Mol Med [Internet]. 2020 May 1 [cited 2022 Jun 28];24(9):4900–12. Available from: https://pubmed.ncbi.nlm.nih.gov/32281300/

415. Connolly M, Paul R, Farre-Garros R, Natanek SA, Bloch S, Lee J, et al. miR-424-5p reduces ribosomal RNA and protein synthesis in muscle wasting. J Cachexia Sarcopenia Muscle. 2018;9(2).

416. Shorter E, Sannicandro AJAJ, Poulet B, Goljanek-Whysall K. Skeletal Muscle Wasting and Its Relationship With Osteoarthritis: a Mini-Review of Mechanisms and Current Interventions. 2019 Jun 15 [cited 2019 Jul 18];21(8):40. Available from: http://www.ncbi.nlm.nih.gov/pubmed/31203463

417. Lamon S, Zacharewicz E, Butchart LC, Orellana L, Mikovic J, Grounds MD, et al. MicroRNA expression patterns in post-natal mouse skeletal muscle development. BMC Genomics [Internet]. 2017 Jan 7 [cited 2022 Dec 22];18(1). Available from: /pmc/articles/PMC5219731/

418. Wang D, Li Z, Zhang Y, Wang G, Wei M, Hu Y, et al. Targeting of microRNA-199a-5p protects against pilocarpine-induced status epilepticus and seizure damage via SIRT1-p53 cascade. Epilepsia [Internet]. 2016 May 1 [cited 2022 Dec 22];57(5):706–16. Available from: https://pubmed.ncbi.nlm.nih.gov/26945677/

419. Sakellariou GK, Pearson T, Lightfoot AP, Nye GA, Wells N, Giakoumaki II, et al. Mitochondrial ROS regulate oxidative damage and mitophagy but not age-related muscle fiber atrophy. Scientific Reports 2016 6:1 [Internet]. 2016 Sep 29 [cited 2022 Jun 29];6(1):1–15. Available from: https://www.nature.com/articles/srep33944

420. Judith Dubach-Powell A, Erb M, van Putten M, Barton E, Grounds M, Rüegg Biozentrum MA. Quantitative determination of muscle fiber diameter (minimal Feret's diameter) and percentage of centralized nuclei SOP (ID) Number DMD_M.1.2.001 Version 2.0. 2008;

421. Holmström KM, Kostov R v., Dinkova-Kostova AT. The multifaceted role of Nrf2 in mitochondrial function. Curr Opin Toxicol [Internet]. 2016 Dec 1 [cited 2023 Jan 17];1:80. Available from: /pmc/articles/PMC5193490/

422. Gureev AP, Shaforostova EA, Popov VN. Regulation of mitochondrial biogenesis as a way for active longevity: Interaction between the Nrf2 and PGC-1α signaling pathways. Front Genet. 2019 May 14;10(MAY):435.

423. Ye X, Zhou XJ, Zhang H. Exploring the role of autophagy-related gene 5 (ATG5ATG5) yields important insights into autophagy in autoimmune/autoinflammatory diseases. Front Immunol. 2018 Oct 17;9(OCT):2334.

424. Rossi AP, Rubele S, Zamboni M. Sarcopenic Obesity. Nutrition and Skeletal Muscle. 2019 Jan 1;83–92.

425. Huang X, Jiang J, Xu J. Denervation-Related Neuromuscular Junction Changes: From Degeneration to Regeneration. Front Mol Neurosci [Internet]. 2021 Feb 24 [cited 2023 Jan 9];14. Available from: /pmc/articles/PMC8908450/

426. Taetzsch T, Valdez G. NMJ maintenance and repair in aging. Curr Opin Physiol [Internet]. 2018 Aug 1 [cited 2022 Dec 27];4:57. Available from: /pmc/articles/PMC6294463/

427. Hughes DC, Marcotte GR, Marshall AG, West DWD, Baehr LM, Wallace MA, et al. Age-related Differences in Dystrophin: Impact on Force Transfer Proteins, Membrane Integrity, and Neuromuscular Junction Stability. J Gerontol A Biol Sci Med Sci [Internet]. 2017 [cited 2023 Jan 9];72(5):640. Available from: /pmc/articles/PMC5861877/

428. Payne AM, Zheng Z, Messi ML, Milligan CE, González E, Delbono O. Motor neurone targeting of IGF-1 prevents specific force decline in ageing mouse muscle. J Physiol [Internet]. 2006 Jan 1 [cited 2023 Jan 9];570(Pt 2):283. Available from: /pmc/articles/PMC1464304/

429. Uddin MS, Yu WS, Lim LW. Exploring ER stress response in cellular aging and neuroinflammation in Alzheimer's disease. Ageing Res Rev. 2021 Sep 1;70:101417.

430. Chalil S, Pierre N, Bakker AD, Manders RJ, Pletsers A, Francaux M, et al. Aging related ER stress is not responsible for anabolic resistance in mouse skeletal muscle. Biochem Biophys Res Commun. 2015 Dec 25;468(4):702–7.

431. Galehdar Z, Swan P, Fuerth B, Callaghan SM, Park DS, Cregan SP. Neuronal Apoptosis Induced by Endoplasmic Reticulum Stress Is Regulated by ATF4–CHOP-Mediated Induction of the Bcl-2 Homology 3-Only Member PUMA. The Journal of Neuroscience [Internet]. 2010 Dec 12 [cited 2023 Jan 9];30(50):16938. Available from: /pmc/articles/PMC6634926/

432. Oyadomari S, Mori M. Roles of CHOP/GADD153 in endoplasmic reticulum stress. Cell Death & Differentiation 2004 11:4 [Internet]. 2003 Dec 19 [cited 2023 Jan 9];11(4):381–9. Available from: https://www.nature.com/articles/4401373

433. Wilson EL, Metzakopian E. ER-mitochondria contact sites in neurodegeneration: genetic screening approaches to investigate novel disease mechanisms. Cell Death & Differentiation 2020 28:6 [Internet]. 2020 Dec 17 [cited 2023 Jan 9];28(6):1804–21. Available from: https://www.nature.com/articles/s41418-020-00705-8

434. Yamamoto H, Itoh N, Kawano S, Yatsukawa YI, Momose T, Makio T, et al. Dual role of the receptor Tom20 in specificity and efficiency of protein import into mitochondria. Proc Natl Acad Sci U S A [Internet]. 2011 Jan 4 [cited 2022 Dec 28];108(1):91–6. Available from: /pmc/articles/PMC3017135/

435. Yang S, Loro E, Wada S, Kim B, Tseng WJ, Li K, et al. Functional effects of muscle PGC-1alpha in aged animals. Skelet Muscle [Internet]. 2020 May 6 [cited 2020 Oct 14];10(1):14. Available from: https://skeletalmusclejournal.biomedcentral.com/articles/10.1186/s13395-020-00231-8

436. Dang C, Han B, Li Q, Han R, Hao J. Up-regulation of PGC-1α in neurons protects against experimental autoimmune encephalomyelitis. The FASEB Journal [Internet]. 2019 Dec 1 [cited 2022 Nov 21];33(12):14811–24. Available from: https://onlinelibrary.wiley.com/doi/full/10.1096/fj.201901149RR

437. Dillon LM, Rebelo AP, Moraes CT. The role of PGC-1 coactivators in aging skeletal muscle and heart. IUBMB Life [Internet]. 2012 Mar 1 [cited 2022 Dec 28];64(3):231–41. Available from: https://onlinelibrary.wiley.com/doi/full/10.1002/iub.608

438. Liu WJ, Ye L, Huang WF, Guo LJ, Xu ZG, Wu HL, et al. p62 links the autophagy pathway and the ubiqutin-proteasome system upon ubiquitinated protein degradation. Cell Mol Biol Lett [Internet]. 2016 Dec 13 [cited 2022 Dec 28];21(1):1–14. Available from: https://cmbl.biomedcentral.com/articles/10.1186/s11658-016-0031-z

439. Bjørkøy G, Lamark T, Pankiv S, Øvervatn A, Brech A, Johansen T. Chapter 12 Monitoring Autophagic Degradation of p62/SQSTM1. Methods Enzymol. 2009 Jan 1;452(C):181–97.

440. Liu H, Dai C, Fan Y, Guo B, Ren K, Sun T, et al. From autophagy to mitophagy: the roles of P62 in neurodegenerative diseases. J Bioenerg Biomembr [Internet]. 2017 Oct 1 [cited 2022 Dec 28];49(5):413–22. Available from: https://link.springer.com/article/10.1007/s10863-017-9727-7

441. Salminen A, Kaarniranta K, Haapasalo A, Hiltunen M, Soininen H, Alafuzoff I. Emerging role of p62/sequestosome-1 in the pathogenesis of Alzheimer's disease. Prog Neurobiol. 2012 Jan 1;96(1):87–95.

442. Teyssou E, Takeda T, Lebon V, Boillée S, Doukouré B, Bataillon G, et al. Mutations in SQSTM1 encoding p62 in amyotrophic lateral sclerosis: Genetics and neuropathology. Acta Neuropathol [Internet]. 2013 Apr 17 [cited 2022 Dec 28];125(4):511–22. Available from: https://link.springer.com/article/10.1007/s00401-013-1090-0

443. Schläfli AM, Adams O, Galván JA, Gugger M, Savic S, Bubendorf L, et al. Prognostic value of the autophagy markers LC3 and p62/SQSTM1 in early-stage non-small cell lung cancer. Oncotarget [Internet]. 2016 Jun 6 [cited 2023 Jan 16];7(26):39544. Available from: /pmc/articles/PMC5129952/

444. Klionsky DJ, Abdelmohsen K, Abe A, Abedin MJ, Abeliovich H, Arozena AA, et al. Guidelines for the use and interpretation of assays for monitoring autophagy (3rd edition). Autophagy [Internet]. 2016 Jan 21 [cited 2023 Jan 16];12(1):1. Available from: /pmc/articles/PMC4835977/

445. Ma S, Attarwala IY, Xie XQ. SQSTM1/p62: A Potential Target for Neurodegenerative Disease. ACS Chem Neurosci [Internet]. 2019 May 5 [cited 2023 Jan 16];10(5):2094. Available from: /pmc/articles/PMC6712989/

446. Allegra Mascaro AL, Cesare P, Sacconi L, Grasselli G, Mandolesi G, MacO B, et al. In vivo single branch axotomy induces GAP-43-dependent sprouting and synaptic remodeling in cerebellar cortex. Proc Natl Acad Sci U S A [Internet]. 2013 Jun 25 [cited 2023 Jan 10];110(26):10824–9. Available from: /pmc/articles/PMC3696745/

447. Grasselli G, Mandolesi G, Strata P, Cesare P. Impaired Sprouting and Axonal Atrophy in Cerebellar Climbing Fibres following In Vivo Silencing of the

Growth-Associated Protein GAP-43. PLoS One [Internet]. 2011 [cited 2023 Jan 10];6(6):20791. Available from: /pmc/articles/PMC3112224/

448. Zhang YJ, Yao Y, Zhang PD, Li ZH, Zhang P, Li FR, et al. Association of regular aerobic exercises and neuromuscular junction variants with incidence of frailty: an analysis of the Chinese Longitudinal Health and Longevity Survey. J Cachexia Sarcopenia Muscle [Internet]. 2021 Apr 1 [cited 2022 Dec 28];12(2):350–7. Available from: https://onlinelibrary.wiley.com/doi/full/10.1002/jcsm.12658

449. Comfort N, Gade M, Strait M, Merwin SJ, Antoniou D, Memou A, et al. Transcriptomic analysis of aging mouse sciatic nerve reveals early pathways leading to sarcopenia. bioRxiv [Internet]. 2022 Feb 3 [cited 2022 Dec 28];2022.02.01.478571. Available from: https://www.biorxiv.org/content/10.1101/2022.02.01.478571v1

450. Gomez-sanchez JA, Patel N, Martirena F, Fazal S v., Mutschler C, Cabedo H. Emerging Role of HDACs in Regeneration and Ageing in the Peripheral Nervous System: Repair Schwann Cells as Pivotal Targets. International Journal of Molecular Sciences 2022, Vol 23, Page 2996 [Internet]. 2022 Mar 10 [cited 2022 Dec 28];23(6):2996. Available from: https://www.mdpi.com/1422-0067/23/6/2996/htm

451. Figueiredo PA, Mota MP, Appell HJ, Duarte J. Ceasing of muscle function with aging: is it the consequence of intrinsic muscle degeneration or a secondary effect of neuronal impairments? European Review of Aging and Physical Activity 2006 3:2 [Internet]. 2006 Aug 22 [cited 2023 Jan 18];3(2):75–83. Available from: https://eurapa.biomedcentral.com/articles/10.1007/s11556-006-0011-9

452. Jiao J, Demontis F. Skeletal muscle autophagy and its role in sarcopenia and organismal aging. Curr Opin Pharmacol [Internet]. 2017 Jun 1 [cited 2018 Sep 11];34:1–6. Available from: https://www-sciencedirect-com.libgate.library.nuigalway.ie/science/article/pii/S1471489216300959

453. Fan J, Kou X, Jia S, Yang X, Yang Y, Chen N. Autophagy as a Potential Target for Sarcopenia. J Cell Physiol [Internet]. 2016 Jul [cited 2018 Sep

13];231(7):1450–9. Available from: http://www.ncbi.nlm.nih.gov/pubmed/26580995

454. Deschenes MR, Roby MA, Eason MK, Harris MB. Remodeling of the Neuromuscular Junction Precedes Sarcopenia Related Alterations in Myofibers. Exp Gerontol [Internet]. 2010 May [cited 2023 Jan 4];45(5):389. Available from: /pmc/articles/PMC2854317/

455. Koles K, Budnik V. Wnt Signaling in Neuromuscular Junction Development. Cold Spring Harb Perspect Biol [Internet]. 2012 Jun [cited 2022 Aug 8];4(6):1–22. Available from: /pmc/articles/PMC3367558/

456. Sampath SC, Sampath SC, Millay DP. Myoblast fusion confusion: The resolution begins. Skelet Muscle [Internet]. 2018 Jan 31 [cited 2023 Jan 18];8(1):1–10. Available from: https://skeletalmusclejournal.biomedcentral.com/articles/10.1186/s13395-017-0149-3

457. Pratt SJP, Shah SB, Ward CW, Kerr JP, Stains JP, Lovering RM. Recovery of altered neuromuscular junction morphology and muscle function in mdx mice after injury. Cellular and Molecular Life Sciences [Internet]. 2015 Jun 18 [cited 2023 Jan 18];72(1):153. Available from: /pmc/articles/PMC4282693/

458. Rajman M, Schratt G. MicroRNAs in neural development: from master regulators to fine-tuners. Development [Internet]. 2017 Jul 1 [cited 2023 Jan 18];144(13):2310–22. Available from: https://journals.biologists.com/dev/article/144/13/2310/48113/MicroRNAs-in-neural-development-from-master

459. Burden SJ, Yumoto N, Zhang W. The Role of MuSK in Synapse Formation and Neuromuscular Disease. Cold Spring Harb Perspect Biol [Internet]. 2013 May 1 [cited 2022 Jul 21];5(5):a009167. Available from: http://cshperspectives.cshlp.org/content/5/5/a009167.full

460. Iwasa K, Nambu Y, Motozaki Y, Furukawa Y, Yoshikawa H, Yamada M. Increased skeletal muscle expression of the endoplasmic reticulum chaperone GRP78 in patients with myasthenia gravis. J Neuroimmunol. 2014 Aug 15;273(1–2):72–6.

461. Jesse CM, Bushuven E, Tripathi P, Chandrasekar A, Simon CM, Drepper C, et al. ALS-Associated Endoplasmic Reticulum Proteins in Denervated Skeletal Muscle: Implications for Motor Neuron Disease Pathology. Brain Pathology [Internet]. 2017 Nov 1 [cited 2022 Dec 28];27(6):781–94. Available from: https://onlinelibrary.wiley.com/doi/full/10.1111/bpa.12453

462. Hu H, Tian M, Ding C, Yu S. The C/EBP homologous protein (CHOP) transcription factor functions in endoplasmic reticulum stress-induced apoptosis and microbial infection. Front Immunol. 2019;10(JAN):3083.

463. Casas C. GRP78 at the Centre of the Stage in Cancer and Neuroprotection. Front Neurosci [Internet]. 2017 Apr 5 [cited 2022 Jul 22];11(APR):177. Available from: /pmc/articles/PMC5380735/

464. Zhao T, Du J, Zeng H. Interplay between endoplasmic reticulum stress and non-coding RNAs in cancer. Journal of Hematology & Oncology 2020 13:1 [Internet]. 2020 Dec 2 [cited 2023 Jan 19];13(1):1–20. Available from: https://jhoonline.biomedcentral.com/articles/10.1186/s13045-020-01002-0

465. Zhu G, Lee AS. Role of the Unfolded Protein Response, GRP78 and GRP94 in Organ Homeostasis. J Cell Physiol [Internet]. 2015 Jul 1 [cited 2023 Jan 19];230(7):1413. Available from: /pmc/articles/PMC4725317/

466. Hemmings BA, Restuccia DF. PI3K-PKB/Akt Pathway. Cold Spring Harb Perspect Biol [Internet]. 2012 Sep [cited 2023 Jan 19];4(9). Available from: /pmc/articles/PMC3428770/

467. Ren H, Zhai W, Lu X, Wang G. The Cross-Links of Endoplasmic Reticulum Stress, Autophagy, and Neurodegeneration in Parkinson's Disease. Front Aging Neurosci. 2021 Jun 3;13:288.

468. López-Otín C, Blasco MA, Partridge L, Serrano M, Kroemer G. The hallmarks of aging. Cell. 2013;153(6):1194.

469. Vanderveen BN, Fix DK, Carson JA. Disrupted Skeletal Muscle Mitochondrial Dynamics, Mitophagy, and Biogenesis during Cancer Cachexia: A Role for Inflammation. Vol. 2017, Oxidative Medicine and Cellular Longevity. Hindawi Limited; 2017.

470. Glancy B, Kim Y, Katti P, Willingham TB. The Functional Impact of Mitochondrial Structure Across Subcellular Scales. Front Physiol [Internet]. 2020 Nov 11 [cited 2023 Jan 19];11. Available from: /pmc/articles/PMC7686514/

471. Calvo-Garrido J, Maffezzini C, Schober FA, Clemente P, Uhlin E, Kele M, et al. SQSTM1/p62-Directed Metabolic Reprogramming Is Essential for Normal Neurodifferentiation. Stem Cell Reports [Internet]. 2019 Apr 4 [cited 2023 Jan 19];12(4):696. Available from: /pmc/articles/PMC6449840/

472. Li S, Zhang J, Liu C, Wang Q, Yan J, Hui L, et al. The Role of Mitophagy in Regulating Cell Death. Oxid Med Cell Longev [Internet]. 2021 [cited 2023 Jan 19];2021. Available from: /pmc/articles/PMC8154277/

473. Ge P, Dawson VL, Dawson TM. PINK1 and Parkin mitochondrial quality control: a source of regional vulnerability in Parkinson's disease. Mol Neurodegener [Internet]. 2020 Mar 13 [cited 2023 Jan 20];15(1). Available from: /pmc/articles/PMC7071653/

474. Weledji EP, Assob JC. The ubiquitous neural cell adhesion molecule (N-CAM). Annals of Medicine and Surgery [Internet]. 2014 [cited 2023 Jan 20];3(3):77. Available from: /pmc/articles/PMC4284440/

475. Theriault FM, Nuthall HN, Dong Z, Lo R, Barnabe-Heider F, Miller FD, et al. Role for Runx1 in the Proliferation and Neuronal Differentiation of Selected Progenitor Cells in the Mammalian Nervous System. The Journal of Neuroscience [Internet]. 2005 Feb 2 [cited 2023 Jan 20];25(8):2050. Available from: /pmc/articles/PMC6726063/

476. Covault J, Sanes JR. Neural cell adhesion molecule (N-CAM) accumulates in denervated and paralyzed skeletal muscles. Proc Natl Acad Sci U S A [Internet]. 1985 [cited 2023 Mar 24];82(13):4544. Available from: /pmc/articles/PMC391139/?report=abstract

477. Moreira-Pais A, Ferreira R, Oliveira PA, Duarte JA. A neuromuscular perspective of sarcopenia pathogenesis: deciphering the signaling pathways involved. Geroscience [Internet]. 2022 Jun 1 [cited 2022 Dec 20];44(3):1199. Available from: /pmc/articles/PMC9213593/

478. Li Z, Liu L, Hou N, Song Y, An X, Zhang Y, et al. MiR-199-sponge transgenic mice develop physiological cardiac hypertrophy. Cardiovasc Res [Internet]. 2016 May 15 [cited 2020 Sep 30];110(2):258–67. Available from: https://academic.oup.com/cardiovascres/article/110/2/258/1744802

479. Fukuoka M, Fujita H, Numao K, Nakamura Y, Shimizu H, Sekiguchi M, et al. MiR-199-3p enhances muscle regeneration and ameliorates aged muscle and muscular dystrophy. Commun Biol [Internet]. 2021 Dec 1 [cited 2022 Jul 15];4(1). Available from: /pmc/articles/PMC8007565/

480. Wang L, Wu W, Chen J, Li Y, Xu M, Cai Y. miR-122 and miR-199 synergistically promote autophagy in oral lichen planus by targeting the Akt/mTOR pathway. Int J Mol Med [Internet]. 2019 Mar 1 [cited 2022 Nov 21];43(3):1373. Available from: /pmc/articles/PMC6365087/

Appendices

Appendix 1

Summary of miRs with roles in regulating myogenesis and muscle size and function. Adapted from (171).

miR	Chromosome/ Cluster (humans)	Function/Mechanism	Species/Cell line	Ref
Let-7	Chr22: let-7a-3, miR-4763, let-7b Chr19: miR-99b, let-7e, miR-125a	Let-7b/e upregulated during skeletal muscle ageing; possibly affecting the expression of Pax7 through the repression of cell cycle regulators, impeding satellite cell self-renewal	Human	(34)
		Promotes neuronal autophagy by repressing mTORC1. Anti-let-7 resulted in increased lean and fat mass	Primary cortical neurons from GFP-LC3 transgenic mice	(172)
		Let7-b is involved in cellular senescence. MitomiR	Mouse Embryonic Fibroblasts (MEFs), precancerous cells, Skeletal muscle cells	(173)
		Let-7e is increased after denervation	Mouse	(174)
miR-1	Chr20: miR-1-1 Chr18: miR-1-2, miR-133a-1	MyomiR	Human, mouse, Human HeLa cells	(175–177)
		Downregulated in a *in vivo* model of skeletal muscle hypertrophy (7 days of functional overload of the plantaris muscle)	Mouse	(141)
		Mature miR-1 and pri-miR-1-2 are downregulated in the young men followed anabolic stimulus, but not in the older men. At baseline,	Human	(168)

		pri-miR-1-1 and pri-miR-1-2 are upregulated in the older men compared to the younger, but not the mature miR-1 (vastus lateralis muscle)		
		Sarcomeric actin organization	Zebrafish	(178)
		Increased expression 1 hour after acute exercise in untrained individuals, but downregulated at rest after chronic exercise (vastus lateralis muscle)	Human	(170)
		Local injections of double-stranded microRNA accelerate muscle regeneration. Upregulate MyoD1, myogenin and Pax7	Rat, C2C12 murine cell line	(150)
		Induces myogenic differentiation during development by targeting Pax3	Chicken embryo, rat RuGli glioblastoma Cells	(143)
		Increased expression 3 hours after acute exercise. Remains upregulated after 10 days of endurance training (vastus lateralis muscle). Aerobic exercise training restores the levels of miR-21 in the soleus muscle of spontaneously hypertensive rats	Human, rat	(179,180)
		Downregulated by TWEAK/Fn14. TWEAK/Fn14 induces muscle mass loss	Mouse	(181)
		Targets BAF60a and BAF60b, inducing myogenic differentiation	Chicken embryo, mouse	(146,148)
		Inhibits fibro-adipogenic progenitors (FAPs)	Mouse	(146)

		phenotype by targeting BAF60a and BAF60b		
		Involved in myoblasts differentiation	Piaractus mesopotamicus	(182)
		Higher expression in the skeletal muscle of obese rats	Rat	(183)
miR-18a	Chr13: miR-18a, miR-17, miR-19a, miR-20a, miR-19b, miR-92a	Upregulated in skeletal muscle of patients with immune-mediated necrotising myopathy by RNA binding target HuR, a modulator of myoblast fusion	Human cells	(184)
miR-16	Chr13: miR-15a, miR-16-1 Chr3: miR-15b, miR-16-2	Lower expression in the skeletal muscle of obese rats. Enhances autophagy and inhibits insulin-stimulated protein synthesis	Rat	(183)
		Increased after denervation.	Mouse	(174)
miR-19b	Chr13: miR-17, miR-18a, miR-19a, miR-20a, miR-19b-1, miR-92a-1 ChrX: miR-106a, miR-18b, miR-20b, miR-19b-2, miR-92a-2, miR-363	Involved in cellular senescence and inflammageing. MitomiR. Downregulated in human ageing	Human cells	(173)
miR-20a	Chr13: miR-17, miR-18a, miR-19a, miR-20a, miR-19b-1, miR-92a-1	Involved in cellular senescence and inflammageing. MitomiR. Downregulated in human ageing	Human cells	(173)
miR-21	Chr17: miR-21	Inhibits apoptosis, is downregulated after ischemia, is a cancer biomarker and promotes fibrosis. Positive regulator of AK signalling pathway.	Mouse, cardiac myocytes, rat	(179,185)

		Aerobic exercise training restores the levels of miR-21 in the soleus muscle of spontaneously hypertensive rats		
		Markedly increased after denervation	Mouse	(90)
miR-23a	Chr19: miR-23a, miR-27a, miR-24-2	Protects muscles from atrophy by targeting MAFbx/atrogin-1 and MuRF1	Mouse, C2C12 murine cell line	(186)
		Increased expression in skeletal muscle of amyotrophic lateral sclerosis (ALS) patients. miR-23a represses the expression of PGC-1α, resulting in mitochondrial dysfunction	Human, mouse	(187)
		Decreased expression 3 hours after acute exercise (vastus lateralis muscle)	Human	(180)
		Decreased during diabetes-induced muscle atrophy. Present in exosomes released from muscle cells	Rat, C2C12 murine cell line	(188)
		Increased expression 4 hours after exercise with post-exercise protein ingestion compared to placebo ingestion (vastus lateralis muscle)	Human	(167)
		Inhibits the differentiation of PDGFRα+ progenitor cells into adipocytes by targeting ZNF423	Foetal bovine skeletal muscle	(189)
miR-27a-3p	Chr19: miR-23a, miR-27a, miR-24-2	Downregulated in skeletal muscle during ageing	Human	(34)
		Inhibits estradiol (E_2) production and promotes apoptosis by targeting Creb1	Mouse, mouse primary ganglion cells (GCs)	(190)

		Promotes myoblasts proliferation through upregulating MyoD and myogenin and by targeting myostatin	Mouse C2C12 cell line	(191)
		Inhibits satellite cell proliferation by targeting Pax3, inducing differentiation	Goat	(192,193)
		Increased after denervation	Mouse	(174)
		Increased expression in obesity and insulin resistance. miR-27a is released from adipocytes resulting in skeletal muscle insulin resistance by targeting PPARγ	Human, mouse, mouse C2C12 cell line	(194)
miR-29	Chr7: miR-29b-1, miR-29a Chr1: miR-29b-2, miR-29c	Promotes myogenesis and differentiation by targeting HDAC4, attenuating the negative effects of TGF-β in muscle differentiation	Mouse primary cells, mouse C2C12 cell line	(195)
		Increased expression of miR-29b in skeletal muscle of amyotrophic lateral sclerosis (ALS) patients	Human	(187)
		Inhibits proliferation and favours myoblasts differentiation by targeting Akt3	C2C12 cell line, mouse satellite cells and primary myoblasts	(196)
		Enhances cellular senescence, inhibits fibrosis and supresses tumor growth through the activation of p53 pathway. Increased expression in aged mice	Mouse, rat, C2C12 cell line, mouse primary myoblasts	(197–199)
		Increased expression of miR-29b after 10 days of endurance training (vastus lateralis muscle)	Human	(180)

		FGF2 induces the expression of miR-29a in fibro-adipogenic progenitors (FAPs) and myoblasts, promoting myogenic proliferation	Mouse, human	(200)
		miR-29b and miR-29c are increased after denervation	Mouse	(174)
miR-106a	ChrX: miR-106a, miR-18b, miR-20b, miR-19b-2, miR-92a-2, miR-363	Involved in cellular senescence. MitomiR. Downregulated in human ageing	Human cells	(173)
		Increased after denervation	Mouse	(174)
miR-133a	Chr18: miR-1-2, miR-133a-1 Chr20: miR-133a-2	MyomiR	Human, mouse	(175–177)
		Downregulated in a *in vivo* model of skeletal muscle hypertrophy (7 days of functional overload of the plantaris muscle)	Mouse	(141)
		Pri-miR-133a-1 and pri-miR-133a-2 are downregulated in the young men followed anabolic stimulus, but not in the older men. At baseline, pri-miR-133a-1 and pri-miR-133a-2 are upregulated in the older men compared to the younger, but not the mature miR-133a (vastus lateralis muscle)	Human	(168)
		Sarcomeric actin organization	Zebrafish	(178)
		Increased expression after acute exercise in untrained individuals, but it is	Human	(170)

		downregulated at rest after chronic exercise (vastus lateralis muscle)		
		Local injections of double-stranded microRNA accelerate muscle regeneration. Upregulate MyoD1, myogenin and Pax7	Rat, C2C12 murine cell line	(150)
		Downregulated in skeletal muscle during ageing	Human	(34)
		Increased expression 3 hours after acute exercise (vastus lateralis muscle)	Human	(180)
		Downregulated by TWEAK/Fn14. TWEAK/Fn14 induces muscle mass loss	Mouse	(201)
		Promotes slow-to-fast muscle fibre type shifting by targeting TEAD1	Mouse, C2C12 cell line	(202)
		Inhibits fibro-adipogenic progenitors (FAPs) phenotype and promotes myogenic differentiation by targeting BAF60a and BAF60b	Mouse	(146)
		Involved in myoblasts proliferation	Piaractus mesopotamicus	(182)
		Important for mitochondrial biogenesis and exercise tolerance	Mouse	(203)
		Increased after denervation	Mouse	(174)
miR-133b	Chr6: miR-206, miR-133b	MyomiR	Human, Human, mouse, HeLa cells	(175–177)
		Downregulated at rest after chronic exercise (vastus lateralis muscle)	Human	(170)
		Local injections of double-stranded microRNA	Rat, C2C12 murine cell	(150)

		accelerate muscle regeneration. Upregulate MyoD1, myogenin and Pax7	line	
		Downregulated in skeletal muscle during ageing	Human	(34)
		Increased expression 3 hours after acute exercise (vastus lateralis muscle)	Human	(180)
		Muscle regeneration and development	Mouse	(204)
		Involved in cellular senescence. MitomiR	Human skeletal primary myoblasts	(173)
		Downregulated by TWEAK/Fn14. TWEAK/Fn14 induces muscle mass loss	Mouse	(201)
		Targets BAF60a and BAF60b, inducing myogenic differentiation	Chicken embryo	(148)
		Involved in myoblasts proliferation	Piaractus mesopotamicus	(182)
		Increased expression 4 hours after exercise with post-exercise protein ingestion compared to placebo ingestion (vastus lateralis muscle)	Human	(167)
		Lower expression in the skeletal muscle of obese rats	Rat	(183)
		Increased after denervation	Mouse	(174)
miR-143	Chr5: miR-143, miR-145	Downregulated in satellite cells and primary myoblasts during ageing. Inhibits cellular senescence by targeting Igfbp5	Human, mouse	(205)
		Increased after denervation	Mouse	(174)
miR-146a	Chr5: miR-146a	Involved in cellular senescence and	Bone marrow-derived	(173)

		inflammageing. MitomiR	dendritic cells, dermal fibroblasts, 143B human cells	
miR-181a	Chr1: miR-181a-1, miR-181b-1 Chr9: miR-181a-2, miR-181b-2	Increased after 10 days of endurance training (vastus lateralis muscle)	Human	(180)
		Involved in cellular senescence and inflammageing. MitomiR	Dermal fibroblasts, CD4 T cells, Human primary myoblasts, 143B human cells, HEK293 and HeLa	(173)
		Increased expression of miR-181 4 hours after exercise with post-exercise protein ingestion compared to placebo ingestion (vastus lateralis muscle)	Human	(167)
		Regulates myotube size by targeting Sirt-1	Mouse, C2C12 cell line	(158)
miR-206	Chr6: miR-206, miR-133b	MyomiR. Skeletal muscle specific	Human, mouse, HeLa cells	(175,177,206)
		Pri-miR-206 (but not the mature miR-206) is upregulated in the young and older men followed anabolic stimulus but at different time points (vastus lateralis muscle)	Human	(168)
		Involved in myoblasts differentiation	Rat	(207)
		Delays Amyotrophic lateral sclerosis (ALS) progression. miR-206 is upregulated in a mouse model of ALS although its deficiency	Mouse	(208)

		accelerates ALS. It is needed for the regeneration of neuromuscular synapses after acute injury		
		Downregulated at rest after chronic exercise (vastus lateralis muscle)	Human	(170)
		Local injections of double-stranded microRNA accelerate muscle regeneration. Upregulate MyoD1, myogenin and Pax7	Rat, C2C12 murine cell line	(150)
		Induces myogenic differentiation by targeting Pax3 and Pax7 during development and skeletal muscle regeneration in the adult	Chicken embryo, rat RuGli glioblastoma Cells, C2C12 cell line, mouse primary myoblasts	(143,209)
		Increased expression of miR-29b in skeletal muscle of amyotrophic lateral sclerosis (ALS) patients	Human	(187)
		Downregulated by TWEAK/Fn14. TWEAK/Fn14 induces muscle mass loss	Mouse	(210)
		Enriched in slow twitch muscle fibres such as soleus	Mouse	(201)
		Fibrosis/ Duchenne	Mouse	(204)
		Promotes myogenesis and differentiation by targeting HDAC4, attenuating the negative effects of TGF-β in muscle differentiation	Piaractus mesopotamicus, mouse primary cells, mouse C2C12 cell line	(182,195)
		Targets BAF60a and BAF60b, inducing myogenic differentiation	Chicken embryo, mouse	(146,148)
		Inhibits fibro-adipogenic progenitors (FAPs) phenotype by targeting BAF60a and BAF60b	Mouse	(146)

		Markedly increased after denervation	Mouse, C2C12 murine cell line	(90,174)
miR-208b	Chr14: miR-208b	MyomiR	Mouse	(149,211)
		Enriched in slow twitch muscle fibres such as soleus. Favours slow-twitch muscle fibre conversion and increases exercise endurance. Targets Sox6. Sox6 induces a fast twitch phenotype	Rat, mouse, C2C12 cell line, mouse primary myoblasts	(149,202,207,212,213)
miR-378	Chr5: miR-378a Chr8: miR-378d-2 Chr3: miR-378b Chr10: miR-378c Chr4: miR-378d-1 Chr5: miR-378e Chr1: miR-378f Chr1: miR-378g Chr5: miR-378h Chr22: miR-378i Chr17: miR-378j	Inhibits estradiol (E_2) production by targeting aromatase	Porcine granulosa cells	(214)
		Downregulated in skeletal muscle during ageing	Human	(34)
		Delays satellite cells activation through targeting Igf1r	Mouse	(215)
		Increased after denervation	Mouse	(174)
miR-486	Chr8: miR-486-2, miR-486-1	MyomiR	Mouse	(216)
		Induces hypertrophy by targeting PTEN and FoxO1	Mouse	(216)
		Induces myoblasts differentiation by targeting Pax7	C2C12 cell line, mouse primary myoblasts	(209)
miR-499	Chr20: miR-499a, miR-499b	Muscle enriched	Zebrafis, mouse	(149,217)

		Enriched in slow twitch muscle fibres such as soleus. Favours slow-twitch muscle fibre conversion and increases exercise endurance. Targets Sox6. Sox6 induces a fast twitch phenotype	Rat, mouse, C2C12 cell line, mouse primary myoblasts, Piaractus mesopotamicus, mouse primary ganglion cells (GCs)	(149,182,202,207,212,213,218)
miR-696	*Not described in humans	Negatively affects fatty acid oxidation and mitochondrial biogenesis by targeting PGC-1α High expression in the skeletal muscle; lower expression during myoblast differentiation	Mouse, C2C12 murine cell line	(219,220)
miR-199a	Chr19: miR-199a, Chr9 miR-199b	Highly expressed in cardiac muscle and skeletal muscle Tumour promoter Targets Akt/mTOR	Human, mice	(478–480)

Mouse gene sequences

>Gap43-201 utr3:protein_coding HUMAN

ACTTTAAGAAATGGCTTTCCACGTTGCCCCCACCTGAACCCTGTCTCTCCT
GCCCTTCTCAGCTCCACTCGAAGTTTCCTCTCCTGTCCTGCTCACGTGTGT
GAGCCTGTCCTCTCCTACCTATGAGCCCTCTCTCTCTGTGTGGCAAACATT
TAAAGAAAAAAAAAAAAGCAGGAAAGATCCCAAGTCCAACAGTGTGGCTT
AAACATTTGTTTCTTGGTGTTGTTATGGCGAGTTTTTGGTAATGATGATGC
AGTCATCTTGGGAAATTCTTGCACTGTACCCCGGTTTTTTGATCTGGTGCG
TGTGGCCCTGTGGGAGTCCACTTTCCTCTCTATTTCTCTCTGTTCCAAGTG
TGTGTGTGCAATGTTCCGTTCTGAGGAGTCCAAAATATTAAGTGAATTCA
AAAACCATTTCTGTTTCCTCATTTTCAATGTGATGGAATGAACAAAAAGG
TTAAAAAATTAAAAAAAAAAACCGGTTTGTTTTAAAAATAAATAAATAA
AGCAAATGTGCCAATTAGCGTAACTTAAGGCTGTGAGGCTCCTTTTTCAA
TCTGAATATTAATAAATCATGAGAGTAATCAA

Mouse Gap43 3’UTR

TGTGGCTTAAACATTTGTTTCTTGGTGTTGTTATGGCGAGTTTTTGGTAAT
GATGATGCAGTCATCTTGGGAAATTCTTGCACTGTACCCCGGTTTTTTGAT
CTGGTGCGTGTGGCCCTGTGGGAGTCCACTTTCCTCTCTATTTCTCTCTGT
TCCAAGTGTGTGTGTGCAATGTTCCGTTCTGAGGAGTCCAAAATATTAAG
TGAATTCAAAAACCATTTCTGTTTCCTCATTTT

Mouse Grp78

AAAAAGGTGGGTCAGGGTGTGTGTTCACCTTGGATATGGTCTATTTAACA
ATTGGGTCATGCACATGTGGTGTAGGAACTTTTTTCTACCATAAGTGACA

CCAATAAATGTTTGTTATTTACACTGGTCTAATTTTTGTGAAAAGTTTGTA
ATTATATCCATCTTTTATTTTAGATAACTAAAATTTAAGACTGGATTCTCA
GGTGTGTCTTTCTTCGGTGGGCAGGGAAGTGGGGCTTG

Mouse Hdac9

AAUCGCACCAUGAGUAGGGAAACCCUUACGGAAGCUAUCCUCUGGAAC
AUUUCCUUAAUAUUCCCUUUUGGUCUGUUUGCCUUGUUGGACAGGUUU
ACUUUUGUUAUGCUAGUUAAACGUUUGCUGUCUAAAGACACAUUUAA
UAUGGAUAAUCCAAAUUGACCUAGAAUCUUCCUGAGUCUUUUCUCUAU
UAAAAUAUUUAUACUUCUUAAUCCAU-
GGUAUUUUAAGGUGUGGUAUCCUGUUUCAG

Mouse Acvr2a

AGGUGUGCUGUGUUUGGGAAAUAUUUGAAAACAUAAAGCAUGAUUUA
AAAUUUUUUAAGUGAGCUGUGACACUGGAAAGCUCUUCAUUUUUCUU
UUAAAAUAGAUUUUUUUUUCCUAUUUAUAUAUAUAAAAUGACGGUGU
AUUUCUUCUUUUCACC-
AAACAGUGUGUGGGAUAUUCUUAUCACUGUUUUAUGAUCACCUCAGGA
AGU

References

References